CARRIER PHASE RECOVERY FOR COHERENT OPTICAL TRANSMISSION SYSTEMS.

A thesis submitted to the

Faculty of Engineering of the

University of Glasgow for the Degree of

Doctor of Philosophy

by

Walter Craig Michie.

To Mrs. Janet Michie.

ACKNOWLEDGEMENTS.

I wish to express my thanks to professor J. Lamb for the use of the laboratory facilities at the Department of Electrical Engineering and for encouragement given during the course of this project.

My thanks is also given to Dr. P. Hlawiczka for his supervision and guidance throughout this project. I would also like to thank Professor R. De La Rue, Dr. J. Arnold and Dr. C.N. Ironside for taking time to read through sections of this thesis manuscript and for offering helpful advice and suggestions.

I am greatly indebted to Dr. M.A. Grant, and M.J. Fletcher for many useful hours of discussion and for their friendship throughout the course of this project.

The assistance of the technical staff of the Department, including Mr. R. Hutchins, Mr. T. Wright, Mr. P. Bower, Mr. K. Melvin, Mr S. Fairbairn, Mr H. Anderson and Mr. G. Boyle is gratefully acknowledged. Dr's H. Davie, M. Macauley and D. Muir are thanked for their generous use of computing facilities in the microprocessor laboratory. My thanks is also given to Dr. D. Halliday for the use of spectral analysis routines.

Finally I would wish to extend a special thanks to my friends and colleagues who have made the past few years so enjoyable.

TABLE OF CONTENTS.

CHAPTER 3.

The Laser Diode : A Signal Source for Coherent Transmission.

CHAPTER 4.

Coherent Reception : The Problem of Phase Synchronisation

CHAPTER 5.

The Practical Phase– locked Loop

CHAPTER 6.

The Dynamic Response of the Optical Phase Locked Loop.

CHAPTER 7.

Heterodyne System Experiments.

CHAPTER 8.

Conclusions.

SUMMARY.

This thesis presents studies concerned with the evaluation of the suitablility of an optical– phase– locked– loop (OPLL) as a component in a coherent optical transmission network.

The performance of various binary optical transmission schemes, measured by the probability of error (Bit Error Rate), is presented. The linewidths of semiconductor diode lasers are, in general, not optimally suited to coherent transmission formats and therefore an additional power penalty must be paid if such sources are to be used. This power penalty is included in the analysis of a binary PSK transmission. The performance analysis of coherent transmission schemes is extended to encompass multi– level signalling formats. It is shown that, with the use of a sufficient number of signalling levels, these schemes can provide a receiver sensitivity which is better than a shot noise limited binary PSK transmission even when subject to the effects of high laser linewidth.

A discussion on the properties of the laser diode, which are of interest in the design of a coherent optical transmission scheme (the source linewidth, modulation charateristics, wavelength tunablity and frequency and power stability), is provided. Measurements of these properties is given along with documentation of experimental attempts to reduce the linewidth of the laser emission. Linewidth reductions from between five and ten Megahertz down to tens of kilohertz were obtained.

An analysis of the performance of an OPLL, taking into consideration the effect of phase instability of the laser diode source, is given. This analysis predicts that present day laser diodes can be used in the construction of the OPLL provided that the loop bandwidth is sufficiently large to account for the laser instability, while not being excessively large such that the performance is impaired by the influence of shot noise. This analysis is extended to describe the effect which the loop transport delay will have on such a loop, as the required loop bandwidth is extended. Similar calculations are performed to evaluate the effect of the loop receiver amplifier bandwidth.

An evaluation of the OPLL response in the time domain, with the use of the Root Locus construction technique and a digital simulation, is

presented. This analysis supports the findings of the analysis described above. The simulation of the loop dynamic response is found to be in reasonable agreement with the experimental findings of a previous worker.

The components for the construction of an optical heterodyne– phase– locked– loop were assembled and attempts were made to lock both free running laser diodes and external cavity line– narrowed diodes. Reliable aquisition of lock was never achieved in any of the experiments performed despite the fact that beat notes of less than 50 kHz were achieved on a regular basis. The main factor which frustrated the succesful implenentation of the OPLL was deduced to have been mechanical disturbances, of the order of nanometers in magnitude, in the reflecting mirror of the external cavity sources. Hysteresis in the mechanical positioning equipment used to control the external reflector positioning was responsible for limiting the effectiveness of the frequency control loop. Experimentation was terminated by the deterioration of the laser sources, the suspected cause of which was the clustering of material defects within the active region of the device.

CHAPTER 1.

Introduction.

1.1 Optical Transmission: Historical Background.

The past twenty years have witnessed a dramatic increase in communications traffic which has stretched the capabilities of conventional coaxial systems to the extent that, in certain instances, their practical limitations have been reached and alternative transmission media have been necessary for some time. One of the approaches to the problem of meeting the demands for information transfer, which has been particularly successful, has been the investigation of the use of an optical carrier [1-14]. This transmission format, in particular the use of coherent signal processing techniques at optical frequencies, is the concern of this project.

Prior to the invention of a suitably low loss optically guiding medium, the pioneering experiments in optical transmission were carried out in the open air and consequently the transmission range of such experiments was limited. Goodwin reported that over an optical path length of 1000 ft there was sufficient turbulence in air to produce approximately 10% amplitude modulation on a 3.39 μm carrier [1]. The need for an alternative transmission medium was therefore an obvious one. The potential use of optical fibres to provide a reliable, wide bandwidth, transmission medium had been seen as early as 1960 [2] however, at this point in time, fibre manufacturing processes were in their infancy and accumulated losses of hundreds of dB/km were typical [3]. A significant breakthrough was made in 1970 when the Corning Glass Company realised the first optical fibre to have an attenuation of approximately 20 dB/km [4]. Fibres with losses of this magnitude, while not an optimal solution, are compatible with communications system requirements. Since 1970 manufacturing techniques have made remarkeable progress and present day fibres exhibit loss characteristics of as little as 0.2 dB/km [5], approaching the fundamental limit that may be achieved in fibre as a result of Rayleigh scattering.

The initial fibre systems, incorporating diode sources, were multi-moded schemes and operated at a transmission wavelength between 0.85 μm and 0.9 μm: GaAlAs/GaAs diodes and silicon detectors were employed [6]. Graded index fibres were developed in order to combat the effects of group dispersion [3]. However, this approach was superceded with a move to mono-mode transmission and a change in operating wavelength to 1.3 μm and 1.5 μm. At the 1.3μm wavelength the dispersion of the fibre is at a minimum, and hence the transmission bandwidth is greatest, and at 1.5 μm the attenuation characteristics are at their lowest value[3,7] and therefore the transmsission distance is potentially longer. The move to the longer wavelengths required new source and detector technology to be developed. Quaternary III-V material compounds were found to be well suited to this task [8,9]. Many of the development problems facing fibre based Intensity Modulation transmission schemes have now been overcome, and in the UK telephone networks have been equipped for some time now with 1.3μm systems operating at data rates between 8 and 565 MBits/sec [6]. In Japan, a working 400 Mbit/sec transmission system extending over a distance of some 2000 km has been in operation since 1985 [6].

The deployment of optical fibre systems has not been restricted to land based systems. Extensive evaluations carried out on a world wide scale have shown that fibres are capable of withstanding the harsh working conditions of undersea operation [10,11]. In the late 1970's development of submarine optical fibre systems commenced and the first transatlantic optical link (TAT8) was scheduled for completion in 1988 [10].

While present optical fibre tranmsission systems have experienced considerable successes, the full potential of this transmission medium has not yet been harnassed. Present day systems have made no attempt to utilise the phase, or frequency, of the optical carrier to convey their information: relying simply on the detection of optical energy at the receiver. The benefits which would be made available to a scheme employing phase or frequency sensitive detection of the transmitted signal are the concern of this project.

1.2 Coherent Optical Transmission.

Since the early sixties, with the invention of the gas laser [15], a considerable amount of interest has been shown in methods of communication which make use the temporal coherence of the laser light [1,16,17,20–45]. It has been known, since as early as 1962, that optical heterodyne (or homodyne) detection improves the signal to noise ratio of a detection system above that which is obtainable with IM/DD schemes [16]. An experimental verification of this analysis was provided in 1967 with a heterodyne transmission experiment at 3.39 μm [1]. In 1970, Delange proposed the use of frequency division multiplexing techniques which would utilise the immense transmission bandwidth of monomde optical fibres [17]. These two observations are the basis for the drive behind the development of coherent transmission systems.

Commercial interest in developing the semiconductor laser diode, primarily for IM/DD systems, has rapidly lead to the production of diodes with linewidths approaching values which would be suitable for coherent signal processing [18]. Speculation that the diode source technology was beginning to produce sources compatible with coherent transmission requirements was first reported in 1979 when an interference experiment was carried out using AlGaAs/GaAs diodes with a monomode fibre delay of 4.5 km [19]. This experiment was significant in a number of respects. Firstly, it demonstrated that the fibre manufacturing technology was sufficiently well advanced to develop a fibre which could, under laboratory conditions, maintain the polarisation state of the optical carrier over a number of kilometres of optical path. Secondly it showed that laser diodes could be manufactured with linewidths which were suitable for coherent fibre transmission systems (an estimate of 50 kHz laser linewdith was made from the interference fringe resolution). The third point of significance is related to the second observation from this experiment. The observation of a 50 kHz linewidth demonstrates clearly that optical isolation is a key component in coherent transmission schemes if misrepresentative results are to be avoided. The manufacturing processes of today are not sufficiently progressed such that diodes with linewidths of tens of kilohertz can be produced [18]. It must be

concluded therefore that in this particular experiment the source was linenarrowed as a result of backscatter from the fibre or coupling apparatus or both.

Initiated by Yamamoto in 1970 [20], a substantial amount of effort has been directed towards providing a thorough evaluation of the receiver sensitivities of various coherent optical transmission schemes [20–27]. These calculations predict that, with transmission rate of 565MBits/sec and a diode responsivity of 0.85, receiver power levels of −60.2 dBm are necessary for a Bit Error Rate (BER) performance of 10^{-9} (for a binary PSK transmission format). The realisation of a transmission system with this level of receiver sensitivity would make possible transmission over distances of around 300 km, for a 1 mW launch power at 1.5 μm. Transmission over distances of this magnitude would permit transoceanic communication without the need for undersea repeater stations using an island hopping approach. At the shorter wavelength of 850 nm the corresponding transmission distance drops to 30 km however this distance would still be suitable for local area network transmission where the benifts of the wide transmission bandwidth could be made available.

While the improvements in the spectral purity of semiconductor laser sources have been impressive, present day devices exhibit linewidths which must still be considered as sub–optimal for coherent purposes. Generally the Full Width Half Maximun (FWHM) of the emmission is in the region of 10–100 MHz [30]. Source linewidths of this magnitude could have catastrophic effects upon a coherent transmission scheme. In order to combat these high levels of phase noise in laser diodes numerous methods of linewidth reduction have been devised [28–37], and some of these approaches have met with considerable success. In particular, the coupling of the laser oscillation to an external resonator, to enhance the quality factor of the diode, has been notable in markedly reducing the operational linewidth of the diode laser sources [31,32]. However, techniques such as this remove one of the main attractions of using diode laser: their small size and compatibility with fibre systems. Moreover, the problems of providing the necessary accoustic isolation from the environment, normally associated with gas lasers, are also incurred. Line–narrowed sources,

which are sufficiently insensitive to mechanical disturbance to operate in an experimental transmission system over standard fibre networks, have been made, however no long term evaluation of the performance of such devices has yet been undertaken [45]. While the coupling of the laser diode to an external cavity is a succesful, well proven, approach to reducing the source linewidth, ultimately the production of diodes which can be used on their own is a more desireable goal. Although it is improbable that sources with the linewidths approaching those of gas lasers (typically tens of kilohertz or better) will be manufactured in the near future, it is not unreasonable to assume that future generations of diodes could be sufficiently linenarrowed to be of use in practical coherent transmission schemes. A recent publication has reported the manufacture of extremely narrow (<1MHz) DFB laser diodes [18], therefore it is reasonable to assume, that laser devices with combined free running linewidths of better than 1MHz will be produced in the not too distant future. The work contained within this thesis will show that linewidths of this magnitude could provide a significant breakthrough in the development of coherent transmission systems.

In addition to the source technolgies, large amounts of research effort has been geared towards the manufacture of the various system components for coherent transmission. The device technologies using crystals such as $LiNbO_3$ for phase and amplitude modulation, frequency shifting and spectrum analysis are well established [38]. These devices are not the particular concern of this project and therefore will not be considered in any detail.

1.2.1 Coherent Transmission: The Optical Phase– Locked– Loop.

The implementation of a coherent receiver requires that a knowledge of the transmission phase or frequency of the transmitted signal can be derived at the receiver. A technique which is widely used to perform this task in microwave systems is the phase– locked– loop (PLL). A similar receiver building block, the Optical– phase– locked– loop (OPLL), would be a desireable component in coherent optical transmission schemes. It was demonstrated in 1965 that phase locking of optical sources is possible

[39] and in 1983 a homodyne Optical Costas Loop was constructed for the first time using CO_2 lasers [40]. Also in 1983, R.C. Steele constructed the first reported OPLL using semiconductor diode lasers[41]. This experiment was repeated in 1986 using an external cavity diode laser with an intra–cavity phase modulator to implement the required phase tracking[42]. The successes of the phase–locking experiments using semiconductor lasers are significant in two accounts. The former experiment showed that phase locking could be achieved with sources of high linewidth using large loop bandwidths (the natural frequency of the loop contructed by Steele was of the order of 6 MHz) to aquire sufficient phase information for tracking to take place. The later experiment displayed that, by coupling the source to an external cavity, the instabilities in the laser could be reduced to the extent that phase locking could be achieved with a much reduced locking bandwidth of around 300 kHz. However, while these experiments have demonstrated that it is possible to construct a PLL with oscillators at optical frequencies, the incorporation of an OPLL in a practical working system is not a viable prospect for the immediate future. This is not surpising however when the magnitude of the task is put into perspective. Two fundamental physical constants, namely the second and the metre, are measured in terms of the wavelength of light. It is not difficult to appreciate therefore that phase synchronisation to within a fraction of a wavelength, with the reliabilty required by a communications network, is a formidable task.

Investigations into the feasibility of frequency multiplexing and the suitability of present day laser sources, for coherent transmission, have been carried out by a number of workers [43,44]. Two particular examples, transmitting frequency multiplexed video transmission channels sperated 1 GHz apart, are worthy of mention in that they demonstrate two different, but equally succesful, approaches. The first experiment, performed at the Heinrich Hertz Institut Berlin, made use of free running GaAlAs/GaAs diodes at 830 nm with an FM modulation format and PM modulated subcarrier to transmit 10 separate channels over a 2 km length of fibre [43]. These channels were heterodyne detected and demodulated using post detection coherent processing. An alternative transmission experiment, with a similar aim was conducted at BTRL Martlesham Heath [44]. Here the

transmission wavelength was 1.5 μm and two transmitter sources, an external cavity diode laser and a HeNe laser, modulated with an external $LiNbO_3$ modulator were employed. The local oscillator laser used was an external cavity diode laser. These experiments demonstrate that coherent technologies are sufficiently advanced that working systems are possible and both transmissions exhibited long term stability for periods of hours. The experiment using the free running diodes was however particularly impressive because it displayed a high degree of imunity to mechanical disturbance.

The elements of coherent transmission technology, which have been outlined above, are all of interest and relevance to this project; the aim of which is the investigation of the use of an Optical Phase–Locked Loop as a receiver component in a coherent transmission scheme. The OPLL is an integral part of an optical transmission scheme and as such its operation cannot be considered in isolation but must be evaluated within this context. It is necessary therefore to present first of all a certain amount of background information relating to optical transmission systems and the use of coherent signal processing techniques. This background information will be presented in the following chapter.

1.3 Contents of Thesis.

The contents of this thesis can be separated into four main catagories. In Chapter 2 a description of the communications systems is developed. This description provides an analysis of the sensitivity of an Intensity Modulation/Direct Detection (IM/DD) optical transmission scheme. The sensitivity is defined in terms of the required signal to noise ratio at the receiver for a given Bit Error Rate (BER) performance. An analytical description of the performance of the system in the fundamental (quantum limit) of operation is presented. The introduction of a local oscillator, and the effect of coherent signal processing on the receiver sensitivity, is then discussed for the case of a binary transmission scheme. This discussion is further extended to account for the fact that the linewidths of present day laser diode sources are not optimally suited to coherent signalling techniques: therefore a power penalty due to flucuations in phase synchronisation

is introduced. If the spectral purity of the transmission source cannot be improved over present day values then alternative means of realising the benifits offered by coherent signalling may have to be investigated. One possible solution, the use of Multi−level orthogonal coding (in particular M−ary FSK) transmission techniques is discussed in the final section of this chapter.

Chapter 3 provides an introduction to the properties of the semiconductor laser diode which are of relevance to the problem of designing a coherent transmission system. These properties include, the source power and frequency stability, and sensitivity to current and temperature variations, the wavelength tunability, the modulation characteristics of the laser and the laser linewidth. Documentation of the experimental evaluation of a laser source (the Hitachi HLP 1400 laser diode) for use in the experimental work program is also given in this chapter alongside a report of attempts made to improve the linewidth and frequency stability of this device. To these aims both the coupled cavity operation of the source and external cavity laser constructions were investigated.

The background knowledge for the performance evaluation of the Optical Phase Locked Loop is provided in Chapter 4. The analysis given here is based upon the work of a number of authors. The OPLL is significantly different from other types of phase−locked−loop due to the fact that the high levels of phase instabilty present in the signal sources employed necessitates the use of wide loop bandwidths. These large loop bandwidths contradict the requirements of the OPLL for an optimal shot noise performance, thus the optimum loop bandwidth is a compromised value. An evaluation of the required loop bandwidths to phase−lock typical present day sources is provided.

The analysis of Chapter 4 is extended in Chapter 5 to show how the loop tracking performance is influenced by system imperfections, such as a significant amount loop transport delay, or the fact that the receiver bandwidth is non infinite. Both of these perturbations have a significant effect when the loop bandwidths are increased to the magnitude required to lock present day sources.

A simulation of the OPLL is discussed in Chapter 6 along with a

time domain analysis of the loop behaviour. The findings of this analyisis are related to the previous discussions given in Chapters 4 and 5. A comparison of the findings with an independent experimental evaluation of the OPLL [41] is also presented. The simulation of the loop transient response is found to be in good agreement with the experimental data.

Experimental attempts to implement an OPLL are documented in Chapter 7. The loop components were designed considering the theory developed in the previous chapters and measurements of the HLP 1400 linewidth made in Chapter 3. Repeatable beat spectra between two independent sources were obtained on a number of occasions, however a condition of solid locking was never achieved. The predominant factor preventing this condition from being realised was concluded to have been accoustically induced displacements in the laser mirror position. These displacements were estimated to have been less than 5 nanometres in magnitude.

The final chapter, Chapter 8 provides a discussion of the work carried out during this project. Ideas for improving the experimental performance of the OPLL are provided alongside some suggestions for an alternative approach to the OPLL design problem. An assessment of the suitablility of the OPLL as a receiver component is provided in the final section along with a suggestion for the development of an alternative coherent signal processing scheme using free running sources should the OPLL, using such sources, prove to be an evasive goal.

References.

1. F.E. Goodwin 'A 3.39 μm Infrared Optical Heterodyne Communcations System.' IEEE Journ. Quant. Electron. QE−3(11) 1967 pp524−531.

2. K.C. Kao, G.A.Hockham 'Dielectric Fibre Surface Waveguides for Optical Frequencies.' Proc. IEEE, vol113, no.7, pp1151−1158.

3. G. Keiser 'Optical Fiber Communications.' McGraw Hill 1983.

4. Kapron *et.al.* 'Radiation Losses in Glass Optical Waveguides.' Appl. Phys. Lett. vol.17, Nov. 1970, pp423−425.

5. T. Miya *et.al.* 'Ultimate low loss single mode fibre at 1.55μm.' Electron Lett. vol.15 pp106−108, 1979.

6. M. Brain, T.P. Lee 'Optical Receivers for Lightwave Communications Systems.' Journ. Lightwave Technol. LT−3(6) Dec 1985 pp1281−1300.

7. J. Gower 'Optical Communications Systems.' Prentice Hall, London 1984.

8. J. Barnard *et.al* 'Integrated Double Heterostructure GaInAs Photoreceiver with Automatic Gain Control.' IEEE Electron Device Letters, EDL2(1) 1981 pp7−9.

9. J. Gammel, H. Ohno, J.M. Ballantyne 'High−speed Photconductive Detectors Using GaInAs.' Journ. Quant. Electron. QE−17(2) 1981 pp269−272.

10. J.E. Midwinter 'Current Status of Optical Communications Technology.' Journal Lightwave Technol. LT−3(5) OCt. 1985 pp927−930.

11. Y. Iwamoto *et.al.* 'Recent Advances in Submarine Optical Fibre Cable Transmission Systems in Japan.' Journal Lightwave Technol.

Lt−3(5) October 1985, pp1005−1016.

12. R.A. Linke *et.al.*'Coherent Lightwave Transmission over 150km fibre lengths at 400 MBits/s and 1 GBits/s data rates using Phase Modulation.' Elect. Lett 22(1) 1986 pp30−31.

13. A.H. Gnauk *et.al.* 'Coherent Lightwave Transmission at 2 GBits/s over 170 km of Optical Fibre Using Phase Modulation.' IEE Elect. Lett. 23(6) 1987 pp286−287.

14. M. Shikada *et.al.* '1.5 μm High Bit Rate Long Span Transmission Experiments Employing High Power BFD−DC−PBH Laser Diode.' 5th Int. Conf. Integrated Optics and Optical Fibre Coomun. ECOC(11) Venice, Italy, Oct 85 Post Deadline Paper.

15. A.L. Schawlow, C.H.Townes 'Infrared and Optical Masers' Phys. Rev. voll 112, 1958. pp1940−1949.

16. B.M. Oliver 'Signal to Noise Ratios in Photoelectric Mixing' Proc. IRE, vol. 49, no. 12, pp1960−1961 Dec.1961. H.A.Haus, C.H.Townes 'Comments on 'Noise in Photelectric Mixing' ' Proc. IRE, vol. 50, no.6, pp 1544−1546 1962.

17. O.E. Delange 'Wide Band Optical Communication Systems: Part 2− Frequency Division Multiplexing' Proc. IRE, vol, 58, no.10,pp1683−1690 1970.

18. Y. Kondo *et.al.* 'Extremely Narrow (1MHz) and high−power DFB lasers grown by MOVPE.' Elect. Lett. 25(3) Feb. 1989 pp175−177.

19. S. Machida *et.al* 'Interference of an AlGaAs Diode Using a 4.15km Single Mode Fibre Cable' IEEE Journ. Quantum Elect. QE−15(7) pp535−537, 1979.

20. Y. Yammamoto 'Receiver Performance Evaluation of Various Digital Optical Modulation−Demodulation Systems in the 0.5−10μm Wavelength Region.' IEEE J.Quant. Electron. 16(11) 1980. pp1251−1259.

21. K. Kikuchi *et.al.* ' Degradation of the BER in Coherent Optical Communications Due to the Spectral Spread of the Transmitter and the Local Oscillator.' J. Lightwave Technol. 2(6), 1984. pp1024－1033

22. T. Okoshi *et.al.* 'Calculation of the Bit Error Rate of Various Heterodyne and Coherent Type Optical Comminication Schemes.' J.Opt. Commun. vol. 2(3) 1983. pp89－96.

23. S. Saito, Y.Yammamoto, T.Kimura 'S/N and Error Rate Evaluation for an Optical FSK Heterodyne Detection System Using Semiconductor Laers.' IEEE J.Quant. Electron. 19(2) 1983. pp180－193.

24. L.G. Kazovsky. 'Optical Heterodyning Versus Optical Homodyning: A Comparison.' Journal of Optical Commun. vol 6(1985) no.1, pp18－24.

25. Y. Yamamoto, H. Tsuchiya 'Optical Receiver Sensitivity Improvement by a Semiconductor Laser Preamplifier.' IEE Elect. Lett. vol.16 no.6 1980 pp233－235.

26. B. Glance 'Performance of Homodyne Detection of Binary PSK Optical Signals.' J.Lightwave Technol. 4(2) 1986 pp228－235.

27. J. Franz 'Evaluation of the Probability Density Function and the Bit Error Rate in Coherent Optical Transmission Systems Including Laser Phase Noise and Gaussian Additive Noise.'J.Opt. Commun. 6(2), 1985, pp51－57.

28. F. Favre, D. LeGuen 'Emmision Frequency Stability in Single Mode Fibre Optical Feedback Controlled Semiconductor Lasers' Elect. Lett. 19(17) 1983. pp 663－ 665.

29. F. Favre, D. Leguen 'Autostabilisation Technique for Achieving Highly Stable Resonant Optical Feedback' Elect. Lett. 19(24) 1983. pp1046－1048.

30. F. Favre, D. Leguen, J.C. Simon 'Optical Feedback Effects on

Laser Diode Oscillation Field Spectrum' IEEE J.Quant. Elect, vol QE−18(10) 1982 pp1712−1717.

31. M.R. Mathews, K.H. Cameron, R. Wyatt, W.J. Devlin 'Packaged Frequency−Stable Tunable 20 kHz Linewidth 1.5 μm InGaAsP External Cavity Laser' Elect. Lett. 21(3) 1985. pp113−115.

32. R. Wyatt, W.J. Devlin '10 kHz Linewidth 1.5 μm InGaAsp with 55nm Tuning Range' Elect. Lett. 19(0) 1983 pp110−112.

33. T. Fujita *et.al.* 'Narrow Spectral Linewidth Characteristics of Monolithic Integrated Passive Cavity InGaAsP/InP Semiconductor Lasers' Elect. Lett. 21(9) 1985. pp374−376.

34. T.P. Lee *et.al.* 'Characteristics of Linewidth Narrowing of a 1.5 μm DFB Laser with a short Grin−Rod External Coupled Cavity' Elect. Lett. 21(15) 1985. pp655−656.

35. C.J. Nielson, J.H. Osmundsen 'Linewidth Stabilisation of Semiconductor Lasers in an External Cavity' J.Opt.Commun. vol. 5(2) 1984. pp42−25.

36. C.H. Henry 'Theory of Linewidth of Semiconductor Lasers' IEEE J.Quant. Elect. QE−18(2) 1982, pp259−264.

37. R.C. Steele 'Coherent Detection for Optical Fibre Communications Systems.' Ph.D. Thesis submitted to University of Glasgow, 1984.

38. R.C. Alferness 'Guided Wave Devices for Optical Communications.' Journ, Qunatum Electron. QE−17(6) 1981. pp946−959.

39. L.H. Enloe, J.L. Roddda 'Laser Phase Locked Loop.' Proc. IEEE 1965 pp165−166.

40. H.K. Phillip, A.L. Scholtz, W.R. Leeb 'Costas Loop Experiment for a 10.6 μm Reciever.' IEEE Trans. Commun. vol. COM−31 no.8. 1983 pp1000−1002.

41.R.C. Steele 'Optical Phase−Locked Loop Using Semiconductor Laser Diodes' Elect. Lett. vol. 19(2) 1983 pp67−71.

42. D. Malyon, D.W. Smith, R. Wyatt.' Semiconductor Laser Homodyne OPLL.' Electron. Lett. 22(8) 1986 pp421−422.

43. E.J. Bachus *et.al.* 'Ten Channel Coherent Optical Fibre Transmission.' Electron. Lett. 22(19) 1986 pp1002−1003.

44. D.G.T. Heatly, T.G. Hodgkinson' Video Transmission over Cabled Monomode Fibre using PFM with 2−PSK heterodyne detection.' Electron. Lett. 20 pp110−112, 1984.

45. Creaner M.J. *et.al.* 'Field Demonstration of 565 Mbit/s DPSK Transmission over 176 km of installed fibre.' Electron. Lett. vol.24(22) Oct. 1988 pp1354−1356.

Chapter 2: Optical Transmission.

2.1 Introduction.

Intensity Modulation/Direct Detection (IM/DD) Optical transmission systems are already a well established technology. Their transmission performance exceeds that of conventional coaxial cable networks and, in their use, other benifits, such as immunity to electromagnetic interference and a reduction in cable thickness, are provided. With the use of present day low loss optical fibres and avalanche photodiodes (APD), receiver sensitivities of around 700 photons per bit [1] have been achieved, at bit error rate performances (BER) of 10^{-9}. Further improvements are predicted from lower loss fibres of a fluorine composition and a shift to longer wavelengths. Although the success of optical transmission has been impressive, IM/DD systems make no attempt to utilise the coherent properties of the optical carrier. Present day state of the art laser diodes are now of sufficient temporal coherence to make the less exacting of coherent transmission techniques (*e.g.* coherent ASK) a possibility. A shift to coherent technologies would provide the benifit of enhanced receiver sensitivity and, perhaps more importantly, it would open up the possibility of utilising the immense transmission bandwidth available in mono-mode optical fibre. When it is considered that the spectral spread of an On/Off Keyed (OOK) laser diode is typically of the order of 1 THz, it is possible to argue that the success of IM/DD systems to date is due almost entirely to the low loss wide bandwidth characteristics of the fibre.

IM/DD and coherent transmission formats will be evaluated in this section, on the basis of their Bit Error Rate (BER) performances, in order that a comparison between these two technologies can be made. The bulk of this analysis, which can be found in a number of publications [2,3,4,5,6.] , is included to enable the reader to judge for himself why the drive towards coherent transmission is considered worthy of investigation. Attention will be given to the penalties that must be tolerated if the semi-conductor laser diode, with its relatively high levels of phase instability, is to be used as a source. To conclude this section, the discussion on information transfer will be

extended from binary signalling to encompass multi level transmission formats. It will be shown that these techniques provide one possible means of circumventing the degrading effects of laser phase instability.

2.2 Components for Coherent Transmission.

The essential elements of a coherent optical fibre transmission network are as illustrated in Figure 2.1. Making use of the laser emission as a signal carrier requires that some means of introducing the modulation be provided. Direct amplitude modulation (AM) or frequency modulation (FM) of the laser emission can be achieved in a semiconductor laser by manipulation of the laser injection current [7]. Phase modulation (PM) is possible but not readily achieved in this manner [8], hence an external modulator of some form will be necessary. A wide range of devices utilising the electro–optic effect of certain crystals such as $LiNbO_3$ already exist for this purpose [9]. The power losses in an external modulator may require that some additional amplification of the laser signal be provided. A substantial amount of research effort has been directed towards this aim using both travelling wave and resonant Fabry Perot type optical amplifiers [10,11,12].

A number of transmitters may be combined and multiple channels can be frequency multiplexed along the one fibre. Transmissions of this form will require that a suitably stabilised master oscillator is present to provide a steady reference signal. Frequency locking of a laser diode to a Fabry Perot transmission peak [13] or an atomic absorption peak[14] have produced stabilities of 1 in 10^{11} and 1 in 10^{14} respectively. The phase locking of the individual channels to the sidebands of a frequency comb generated from a frequency stabilised mode locked laser has been suggested as being a suitable technique for providing the required frequency separation between channels. The technological problems of such a venture are however immense.

Coherent systems are sensitive to polarisation shifts; Polarisation Shift Keying (POLSK) has in fact been shown to be a feasible form of transmission [15]. The transmission medium, the fibre, must therefore

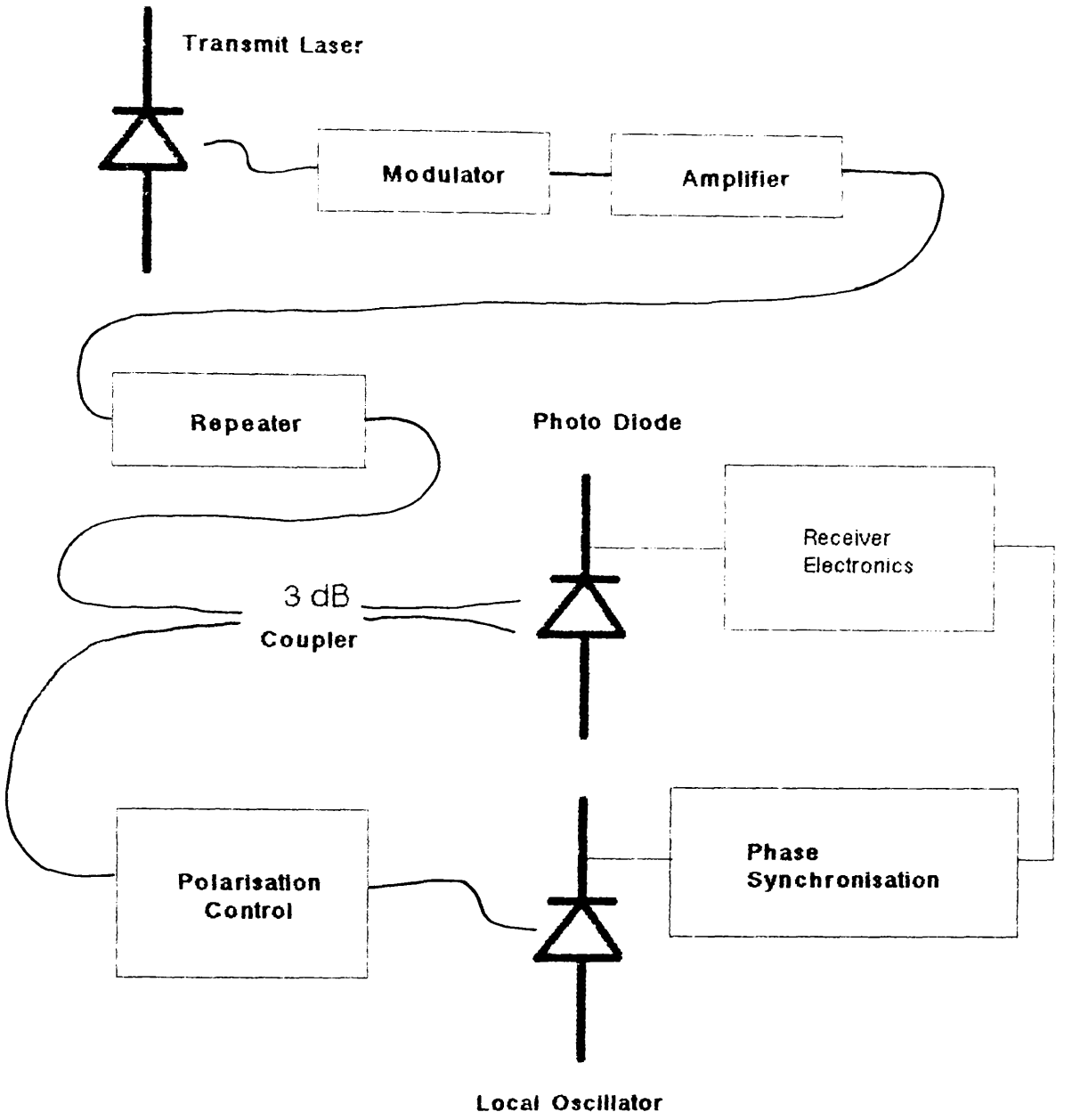

Figure 2.1 Optical Transmission Schematic.

be able to preserve the state of the signal polarisation. It is likely that additional polarisation control at the receiver will also be necessary [16].

Long haul transmissions, *eg* transoceanic links, will require that optical repeater stations are installed periodically along the transmission length. The optical amplifier, as discussed above, will be employed for this purpose.

Detection of the received signal will be made by a standard photodetector (APD, or a unity gain PIN diode). A local oscillator will be required to implement the heterodyne or homodyne detection of the selected channel. Finally, the remaining standard system components (amplification, equalisation and decision circuitry) will also be necessary.

2.3 Bit Error Rate Performance.

2.3.1 Noise in Optical Receivers: Thermal Noise.

A convenient measure of the performance of a communications receiver is the Signal to Noise Ratio (SNR) required at the receiver for a given probability of error in data reception (Bit Error Rate BER). The BER performances of the various modulation schemes will be compared in the present section.

Calculation of the BER requires that first of all the noise contributions are understood and quantified. This problem will now be addressed. It is not the aim of the present chapter to provide a complete coverage of the noise origins, the reader is referred to the following sources if a fuller examination is required [17,18,19,20].

All receivers will be subject to the limiting effects of thermal, or Johnson noise. This noise arises due to the random motion of free electrons in a conductor. The net effect is a random current which can, in general, be approximated as a Gaussian distribution [17,18] with zero mean. For an optical receiver, with a simple resistor network used to bias the photo–diode, the thermal noise contribution can be

written,

$$\overline{i^2_R} = 4kTB/R_L. \qquad (2.1)$$

where R_L is the value of the bias resistor, k Boltzmann's constant, T the temperature of the resistor (^oK) and B the bandwidth over which the noise contribution is effective. The bias resistor, R_L, may not be the dominant thermal noise source. In such an instance it will be necessary to evaluate the noise contribution of the front end amplifier. A standard front end configuration is the high impedance FET which has a noise contribution of the form [16],

$$\overline{i^2_C} = (4kT/R_L)(1 + \Gamma/g_mR_L) + 2eI_q + 4kT\Gamma(2\pi C_T)^2B^2/g_m \qquad (2.2)$$

where

g_m = transconductance of the FET,

I_q = the gate leakage current,

and C_T = the total load capacitance of the amplifier.

The factor Γ is present to allow for material variations. FETs manufactured on Silicon have a different noise performance from GaAs FETs. In Silicon devices the factor Γ commonly takes a value of around 1.2 whereas GaAs FETs exhibit a lower characteristic of around 0.7 [17].

2.3.2 Shot Noise.

Due to the quantum nature of the optical detection process a random photo–current will be associated with each of the incident optical powers. This random photo–current will have a mean square power dependent on the power of the optical signal and is known as a shot noise current. In an optical receiver shot noise currents will be associated with the signal power P_S, the level of background radiation P_B, the internal dark current of the photodetector I_D and, in the case of the heterodyne/homodyne receivers, the local oscillator power P_{LO}. These noise sources are accommodated into the calculations as equivalent noise currents of the form

$$\overline{i^2_S} = 2e(\eta e/h\nu)P_S\langle M\rangle^{2+X}B$$

$$\overline{i^2_B} = 2e(\eta e/h\nu)P_B\langle M\rangle^{2+X}.B$$

$$\overline{i^2_D} = 2e(I_m\langle M\rangle^{2+X} + I_n)B \qquad (2.3)$$

$$\overline{i^2_{LO}} = 2e(\eta e/h\nu)P_{LO}\langle M\rangle^{2+X}B$$

where,

i_S = signal photocurrent,

i_B = background light photocurrent,

i_D = dark current,

i_{LO} = local oscillator photocurrent,

η = quantum efficiency of the diode,

ν = frequency of incident radiation and

e = charge of an electron.

The use of an APD in the detector has been accounted for with the notation M (denoting the associated multiplication). If a PIN diode is used then this factor will take the value 1. The operator X, is known as the excess noise factor and describes the additional noise introduced into the system as a result of the avalanche multiplication process [21]. X usually takes a value between 0.2 and 1 [21].

The dark current, mentioned above, arises from the spontaneous recombination of hole electron pairs under the condition where no light is incident. The representation of the dark current in an APD is more complicated than for the case of a PIN diode. In an APD there is a probability that a proportion of this current will undergo further multiplication. The dark current in the APD is therefore subdivided into a component that will undergo multiplication, I_m, and a component which will not, I_n. In a PIN diode the component I_m does not exist.

Having defined each of the component noise sources, it is possible to proceed with the theoretical performance evaluation of the transmission formats.

2.3.3 IM/DD : The Gaussian Approximation.

As was stated above, the detection of an optical signal is a discrete process. The most accurate description of the receiver performance will therefore be achieved using Poisson statistics. Significant savings in the complexity of the mathematical computation can be made however, if the the Gaussian approximation is used. If a sufficient number of events is observed then the errors introduced in making this assumption will be minimal. The present section uses the Gaussian approximation to evaluate the probability of error, the BER, for an IM/DD scheme and thereby establish the datum level against which the performance of a coherent system can be gauged.

The IM/DD scheme relies on the presence or absence of a carrier at the receiver to denote a particular logic state. The present argument will employ the notation that a 'logic 1', or 'mark', is represented by the presence of the signal. The absence will convey the 'logic 0', or ' space', state. The carrier present condition will have associated with it a noise current with a variance equivalent to the sum of the individual sources, see Figure 2.2) thus,

$$\sigma^2_{DD1} = \overline{i^2}_s + \overline{i^2}_D + \overline{i^2}_B + \overline{i^2}_C \qquad (2.5)$$

A similar noise current will exist for the 'logic 0', transmission. In this instance however, the shot noise corruption due to the signal current will not be present,

$$\sigma^2_{DD0} = \overline{i^2}_D + \overline{i^2}_B + \overline{i^2}_C \qquad (2.6)$$

The probability distribution for the two logic states can be described, under the Gaussian approximation, as,

$$P_0(x) = \frac{1}{\sqrt{(2\pi\sigma^2_{DD0})}} \exp -(x^2/2\sigma^2_{DD0}) \qquad (2.7)$$

and

$$P_1(x) = \frac{1}{\sqrt{(2\pi\sigma^2_{DD1})}} \exp -((S_{DD}-x)^2/2\sigma^2_{DD1}) \qquad (2.8)$$

The notation S_{DD} is used to denote the mean value of the 'logic 1' state under direct detection conditions. D represents the threshold level for the decision on which of the logic states is present (see Figure 2.2).

The probability of the 'logic 1', condition being detected when a space is transmitted is also indicated on Figure 2.2. A similar region is indicated for the corresponding 'logic 0' error. These error conditions can be designated $P_{e0}(x)$ and $P_{e1}(x)$ respectively. The total probability of error is therefore written

$$P_D = P_{e0}(x)P_0 + P_{e1}(x)P_1 \qquad (2.9)$$

P_0 and P_1 are the probabilities of transmission of a mark and space respectively. In general, it is desirous that a communications system operates without any dc component in the transmission. A coding format will therefore be used that, on average, transmits an equal number of zeros and ones. Thus $P_0 = P_1 = {}^1/_2$. The total probability of error is therefore equal to

$$P_{DD} = \frac{1}{2}\left[\frac{1}{\sqrt{(2\pi\sigma^2_{DD_0})}}\int_D^{\infty} \exp -(x^2/2\sigma^2_{DD0}).dx + \frac{1}{\sqrt{(2\pi\sigma^2_{DD1})}}\int_{-\infty}^{D} \exp -((S_{DD}-x)^2/2\sigma^2_{DD1}).dx\right] \qquad (2.10)$$

The change of variable, $t = (S_{DD} - x)/\sigma_{DD1}$ and $t = x/\sigma_{DD0}$ can be introduced into $P_{e1}(x)$ and $P_{e0}(x)$ respectively and thus equation 2.10 can be rewritten as

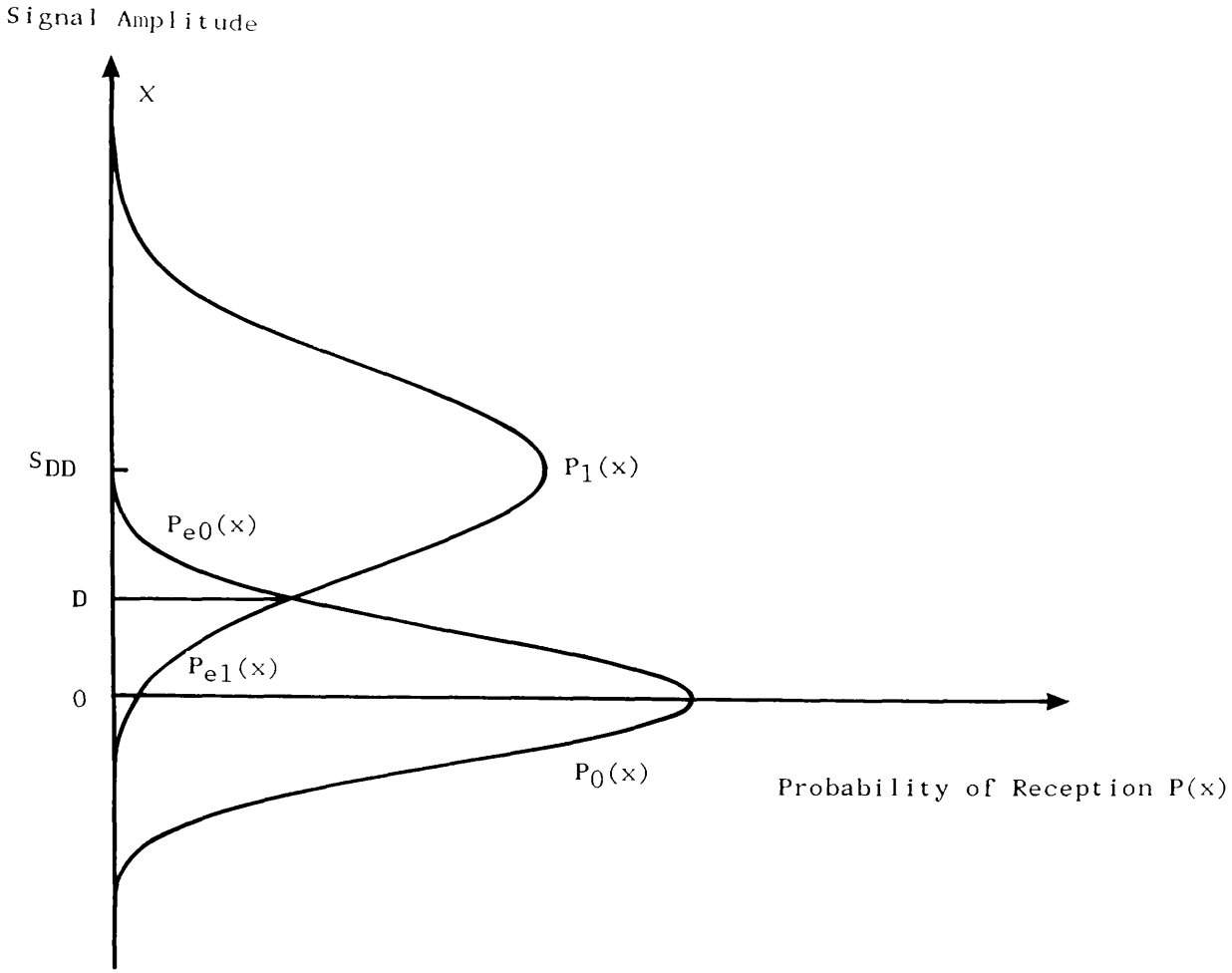

Figure 2.2

Probability Density Functions of Direct Detection.

$$P_{DD} = \frac{1}{2}\left[\frac{1}{\sqrt{(2\pi)}}\int_{D/\sigma_{DD0}}^{\infty} \exp -(t^2/2).dt + \frac{1}{\sqrt{(2\pi)}}\int_{(S_{DD}-D)/\sigma_{DD1}}^{\infty} \exp -(t^2/2).dt\right] \quad (2.11)$$

It is assumed that an equal probability of error exists for the mark or space condition. The decision limits on both of the integrals may then be equated to provide an optimum decision level,

$$\Rightarrow \qquad D_{OPT} = \frac{\sigma_{DD1} S_{DD}}{\sigma_{DD1} + \sigma_{DD0}} \qquad (2.12)$$

Substitution of equation 2.12 into equation 2.11 allows the total probability of error to be written as,

$$BER = \frac{1}{\sqrt{(2\pi)}}\int_{S_{DD}/(\sigma_{DD0} + \sigma_{DD1})}^{\infty} \exp - t^2/2 \; .dt \qquad (2.13)$$

Integrals of this form are well known as the complimentary error function as defined in reference 22, thus the BER can be written,

$$BER = \frac{1}{2} Erfc(Q) \qquad (2.14)$$

where Erfc(x) = 1 − Erf(x) and Erf(x), the error function is defined as,

$$Erf(x) = \frac{1}{\sqrt{\pi}}\int_{\infty}^{x} \exp(-u^2/2).du \quad (2.15).$$

A graphical representation of the complimentary error function is given in Figure 2.3. In this particular application attention should be drawn to the fact that the parameter Q^2 is representative of the detector signal to noise ratio (SNR). The requisite SNR for a given BER performance is therefore readily obtained as,

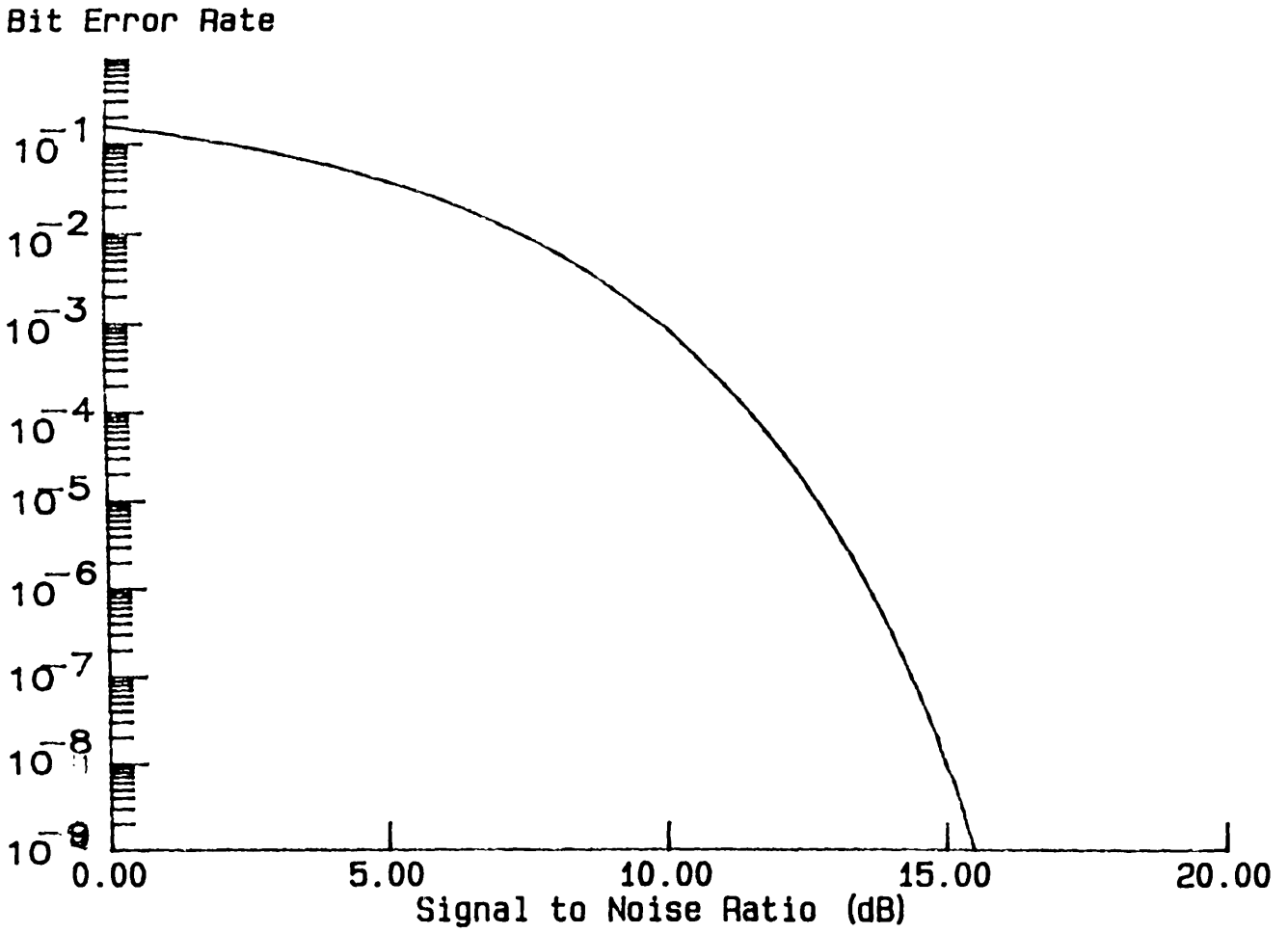

Figure 2.3

BER versus Signal to Noise Ratio

$$BER = \frac{1}{2}\ erfc(S/N)^{1/2}. \qquad (2.16)$$

The graphical representation of the complimentary error function reveals that for a BER of 10^{-9} the required value of SNR is 15.56 dB corresponding to a value of Q of approximately 6.

2.4 IM/DD : The Quantum Limit.

The quantum limit for an IM/DD limit can be defined as that situation where the stimualtion of one photo–electron constitutes the presence of a 'logic 1' received. Under ideal conditions the only noise that would be present is the shot noise generated from the incident signal power. The signal to noise ratio is therefore evaluated as follows.

Assuming a normalised receiver bais resistor and amplifier impedance of 1 Ω, the received Signal Power is simply equal to the square of the signal current thus,

$$S_{DD}^2 = R^2P_S^2.\ W. \qquad (2.18)$$

The associated noise power is (from 2.3)

$$\overline{i_{DD}}^2 = eRP_SB \qquad W. \quad (2.19)$$

The SNR at the receiver is therefore,

$$Q^2 = \frac{R^2P_S^2}{eRP_SB} = \frac{RP_S}{eB} \quad (2.19)$$

It should be noted that the right hand side of 2.19 corresponds to the average number of photons received during the transmission of one bit. It was stated earlier that the necessary value of Q for a BER of 10^{-9} was 6, thus according to 2.19, 36 photons are required at the receiver per bit. However, in quantum limited operation, it is assumed that no signal is transmitted in the 'space' condition. Therefore, since it is also assumed that an equal number of 'ones' and 'zeros' are transmitted, the average power in the transmission will be equal to one half of the value indicated above. Thus, the shot

noise limited receiver sensitivity, for a binary IM/DD transmission with a BER of 10^{-9} is equal to 18 photons/bit. Specification of the system bit rate, wavelength and quantum efficiency of the detector enables this value to be re-expressed as a necessary received power. The quantum efficiency of a diode is generally quoted by a manufacturer in terms of the diode responsivity ($R = \eta e/(h\nu)$) and a typical value for a PIN diode, with an operating wavelength of 850 nm, is $R = 0.85$. If this is taken as the desired operating wavelength and the typical value of responsivity also accepted then for a system operating at 565 Mbits/sec the minimum received power of -57.2 dBm is necessary for a BER of 10^{-9}.

2.5 IM/DD : Discussions and Conclusions.

The performance of the IM/DD system has been evaluated and the necessary receiver components outlined. The power limit for the ideal noiseless receiver (the quantum limit) has been evaluated for a specific instance. This ideal noiseless situation is obviously impossible to achieve and therefore an additional power penalty will be incurred. In practical systems this penalty is typically of the order of 7-12 dB [2,3,4,5,6].

The IM/DD method of transmission can be critiscised from the viewpoint that it monopolises almost the entire transmission bandwidth of a fibre system for what is generally a relatively low data rate transmission. In defence of these systems however it must be said that this simplistic approach is a major contributory factor to the success that IM/DD systems have enjoyed. The simplicity of the systems has ensured that they can be made to be highly reliable even in the unsympathetic field environment. This reliability cannot be underestimated. Coherent systems, with their additional complexity, would be required to perform with the same high degree of reliance; a fact which is likely to make this, more advanced, form of receiver expensive to implement. The advantages and disadvantages that a shift to coherent techniques offers must therefore be critically assessed before the decision of moving to this technology is taken. It has been suggested that a huge saving can be made in terms of more economical use of system bandwidth with coherent transmission.

Additional benifits in receiver power levels will also be made available. Immense technological problems have yet to be solved however, particulary in the area of finding a suitable source for this form of transmission. The present day laser diodes are tolerable for the less sensitive of the coherent detection formats (commonly referred to as 'weakly coherent' transmission). They remain however unsuitable for the phase sensitive transmission formats without some form of external modification. The benefits that will be received from the less sensitive formats are obviously less substantial than those which stand to be gained from the implementation of the phase sensistve transmissions. The following section will compare the performance of the IM/DD receiver to that of coherent receivers by evaluating the receiver performance of some common 'weakly coherent' systems and also that of the phase sensitive schemes.

2.6 Coherent Reception Performance Evaluation.

Shot Noise Limited Detection.

The most obvious difference between an IM/DD receiver and a coherent receiver is the presence, in the coherent case, of the local oscillator (Figure 2.4). It is within the presence of this oscillator that the performance improvement lies. The mixing of the incoming and local oscillator signals effects a multiplication of the signal power before a decision has to be made as to what logic state is present. Furthermore, the close proximity of the local oscillator enables relatively large levels of local oscillator signal to be obtained. The condition where the shot noise current due to the local oscillator power is the dominant noise source may therefore be engineered. This corresponds to the maximum possible SNR and thus provides the coherent receiver with a more sensitive form of detection. The mathematics of coherent detection that enable these assertions to be made will now be outlined.

The electric field of the transmitted signal, and that of the local oscillator can be described in the following manner,

$$\begin{aligned} E_T(t) &= \mathrm{Re}\{ \sqrt{(2P_T)}.\exp(i(\omega_T t + \varphi_T)\} \\ &= \sqrt{(2P_T)}.\ \cos(\omega_T t + \varphi_T) \quad \text{and,} \end{aligned} \tag{2.22}$$

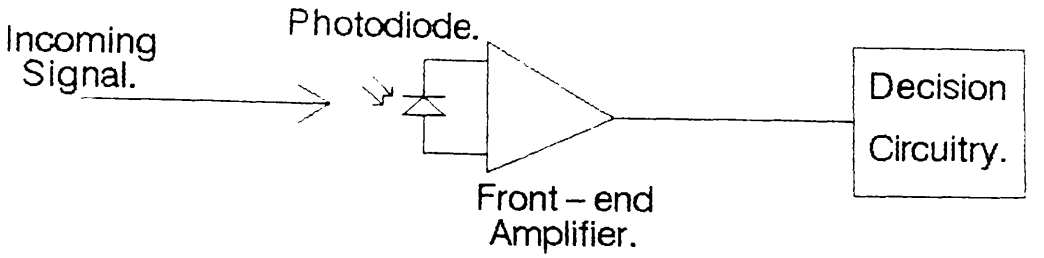

IM/DD Communications Receiver

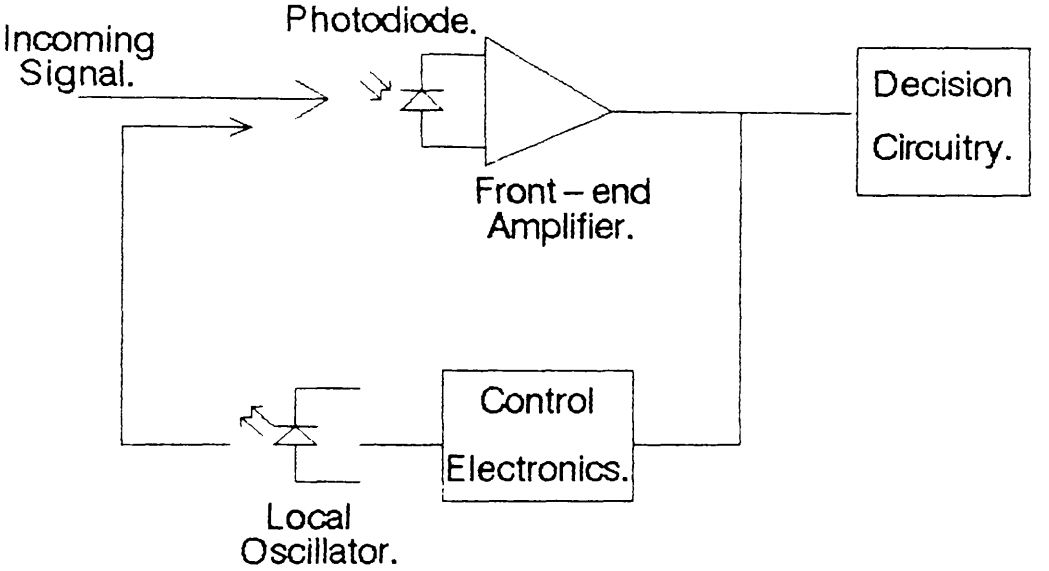

Coherent Communications Receiver.

Figure 2.4

$$E_{LO}(t) = Re\{ \sqrt{(2P_{LO})}.\exp(i(\omega_{LO}t + \varphi_{LO})\} = \sqrt{(2P_{LO})}.\ \cos(\omega_{LO}t + \varphi_{LO}) \quad (2.23)$$

The subscripts T and LO denote the transmit and local oscillator wave respectively, ω is the instantaneous angular frequency of the two waveforms and φ the instantaneous phase. Consideration of the phase instabilities of the sources due to the inherent linewidth of the devices has not been allowed for at this stage. This phase noise will be taken into account at a later point in the discussion.

Detection of the intermediary frequency (IF) between these two sources arises due to the square law property of the photodetector. The photo-current i_S, resulting from the mixing of the local and transmit oscillators, is proportional to the square of the two thus,

$$i_S = R.\{ E_T(t) + E_{LO}(t) \}^2 = R.\{ P_T + P_{LO} + \sqrt{(4P_T.P_{LO})}\cos((\omega_T - \omega_{LO})t + (\varphi_T - \varphi_{LO}))\} \quad (2.24)$$

The beat note, that exists in a heterodyne detection format, between the transmitted and local oscillator signals is described in the above equation as $\omega_T - \omega_{LO}$. The term $\varphi_T - \varphi_{LO}$ describes the instantaneous phase error between the two signals.

The photo-current terms associated with the transmit and local oscillator signals on their own convey no information. The information signal power is contained in the beat signal current and will have a mean square power of

$$\langle i_S \rangle^2 = 4P_TP_{LO}R^2. \quad (2.25)$$

The noise current will be dependent on the incident optical powers and the input circuit noise. The particular type of input stage is irrelevant in this argument and the associated noise will be designated $\langle i_{in} \rangle^2$. The shot noise photo-currents can be written

$$\langle i_{shot} \rangle^2 = 2e(P_SR + P_{LO}R + P_BR + I_D)B. \quad (2.26)$$

The signal to noise ratio is therefore given by

$$SNR = \frac{4P_T P_{LO} R^2}{2e(P_S R + P_{LO} R + P_B R + I_D)B. + \langle i_{in} \rangle^2} \qquad (2.27)$$

In the practical situation this can be further reduced to,

$$SNR = \frac{4P_S P_{LO} R^2}{2e(P_S + P_{LO})RB. + \langle i_{in} \rangle^2} \qquad (2.28)$$

Examination of the above equation quickly reveals that the local oscillator power has an influence not only over the noise contribution but over the signal power as well. As the shot noise term is increased in power, such that it dominates over the circuit noise, the SNR is improved. Further increase in local oscillator power will not result in a continued improvment in SNR. The SNR tends assymptotically to what is commonly refered to as the shot noise limit

$$SNR = 2P_S R/eB. \qquad (2.29)$$

It is much easier to come within a reasonable distance of achieving this condition as opposed to the corresponding noiseless receiver equivalent in the IM/DD situation. Hence the coherent receiver is likely to outperform the IM/DD receiver even in situations where the theoretical optimum performance may be less impressive.

2.7 Coherent Amplitude Shift Keying (ASK).

The coherent format that will be given attention first is the Amplitude Shift Keyed (ASK) system. It will be assumed, during the course of the present discussion, that the carrier amplitude will be keyed between the two discrete states of On and Off. This may be considered as the coherent equivalent to the IM/DD format and thus a useful comparison of the two formats can be made.

The noise source arising from the presence of the local oscillator is expressed as

$$i^2_{LO} = 2eRP_{LO}B_H \qquad (2.30)$$

The noise bandwidth term has been designated B_H to denote that heterodyne detection is being considered. Heterodyne ASK detection is arguably the simplest of the coherent formats to realise. The total variance for the ASK receiver is

$$\sigma^2_{H1} = \overline{i^2_{LO}} + \overline{i^2_s} + \overline{i^2_D} + \overline{i^2_B} + \overline{i^2_C}$$

and (2.31)

$$\sigma^2_{H0} = \overline{i^2_{LO}} + \overline{i^2_D} + \overline{i^2_B} + \overline{i^2_C}$$

This, and any following discussion, will assume that sufficient local oscillator power is available to enable shot noise limited detection to be carrried out. Therefore for the ASK situation

$$\sigma^2_{H1} = \sigma^2_{H0} = \sigma^2_H = i^2_{LO} \qquad (2.32),$$

and the amplitude of the detected signal component is,

$$S_H = 2R\sqrt{(P_{LO}P_T)}. \qquad (2.33)$$

Comparison of the pdf's of the received signal photo–current (Figure 2.5) reveals that the optimum decision level will be equal to one half of the transmitted level in the 'on' condition. Thus

$$D_{opt} = S_H/2. \qquad (2.34)$$

A similar argument to that previously given in the IM/DD situation reveals the coherent ASK BER performance to be specified

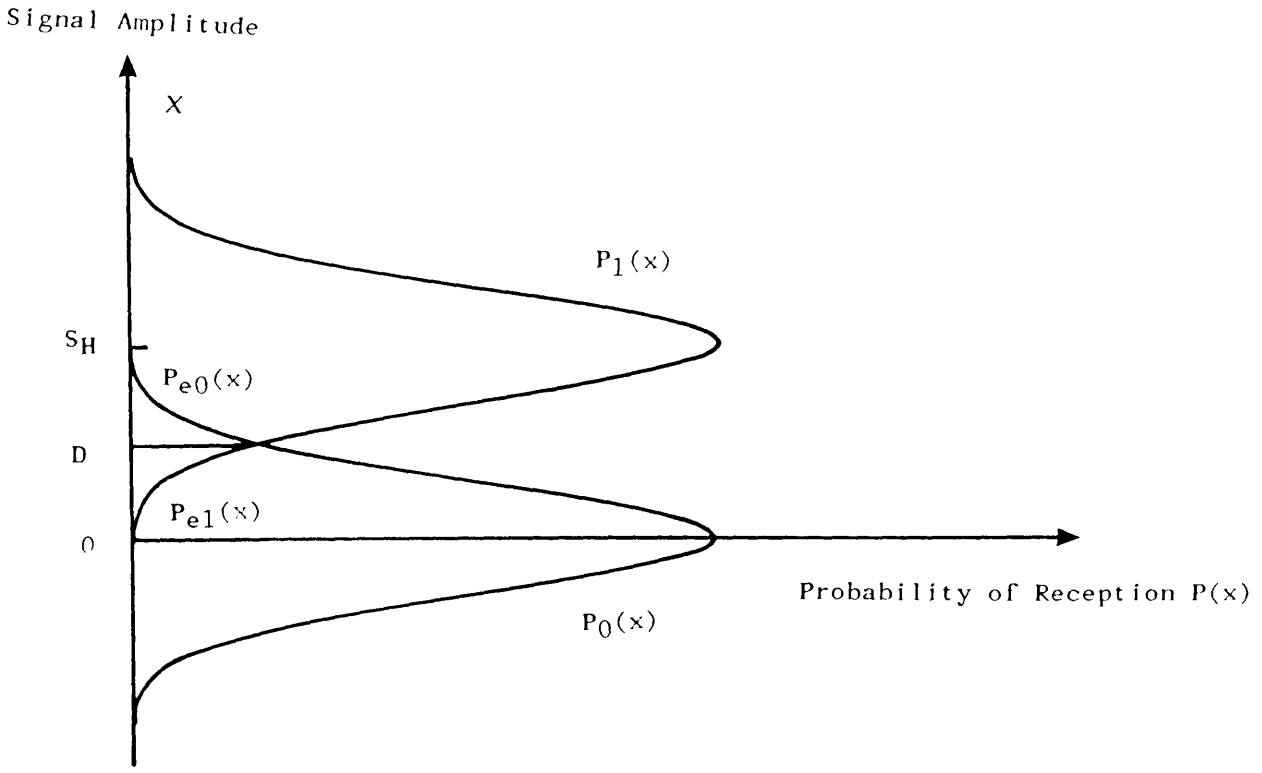

Figure 2.5
Probability Density Functions of ASK Coherent Detection.

as

$$BER_{ASK} = \frac{1}{2}\ erfc(\frac{S_H}{2\sigma_H}) \qquad (2.35)$$

The corresponding minimum receiver levels can therefore be established as

$$Q^2 = R.P_T/(2eB_H)$$

$$\Rightarrow P_T = Q^2 2eB_H/R \qquad (2.36)$$

which for similar conditions to those described in the IM/DD situation will result in a received power level of -51.2 dBm.

2.8 Frequency Shift Keying (FSK).

Coherent ASK heterodyne detection has been shown to provide a BER performance that is 6dB worse than the optimum case for the IM/DD detection. The only benefit, it would appear, from adopting this type of transmission scheme would be that the transmission bandwidth available in monomode fibre could be more effectivelty utilised. This in itself would provide a strong argument for 1: implementing the more complicated coherent receiver and 2: making the extra effort to ensure that ASK transmission is transform limited. As was explained earlier however, approaching the shot noise limit is possible and therefore in a practical situation the coherent ASK is likely to outperform the IM/DD system by some 7−12 dB. Further improvements will be available from more sophisticated receiver formats. These will now be further examined.

The use of the temporal characteristics of the carrier allow for the transmit signal to be present in both the logic 1 and logic 0 conditions. In the FSK transmission the carrier is frquency shifted between two centre frequencies, f_1 and f_2, to represent the mark and space transmission. The use of the local oscillator is again employed to beat the incoming carriers down to radio frequencies for processing. The intermediate frequency is fed into two bandpass filters of centre frequency f_1-f_{LO} and f_2 - f_{LO}. A decision is reached

regarding the particular logic state of the transmission by subtracting the output of these two filters from each other (see Figure 2.6). In computing the BER performance of such a scheme it is necessary to consider the output signals of both filters. If S_H is the received signal power then the output of filter f_1 is described (Figure 2.7),

$$P(v_1) = \frac{1}{\sqrt{(2\pi\sigma^2_{V1})}} \exp-((S_H - v_1)^2/2\sigma^2_{V1}) \qquad (2.37)$$

and the corresponding pdf of filter f_2 is

$$P(v_2) = \frac{1}{\sqrt{(2\pi\sigma^2_{V2})}} \exp-((S_H - v_2)^2/2\sigma^2_{V2}) \qquad (2.38)$$

Assuming that the frequency f_1 represents the mark transmission, an error will occur (*ie* a space will be detected) if $v_2 > v_1$. Thus the probability
of error is $P(v_1 - v_2 < 0)$.

$$P_e(v_1) = \frac{1}{\sqrt{(2\pi(\sigma^2_{V1}+\sigma^2_{V2}))}} \int_{-\infty}^{0} \exp-((\omega - S_H)^2/2(\sigma^2_{V1}+\sigma^2_{V2}) \; .d\omega$$

$$= \frac{1}{\sqrt{(2\pi\sigma^2_H)}} \int_{-\infty}^{0} \exp-((\omega - S_H)^2/4\sigma^2_H \; .d\omega \qquad (2.39)$$

which, using the change of variables $u = (\omega - S_H)/\sqrt{2}\sigma_H$, solves to

$$= \frac{1}{2} \operatorname{erfc}\left(\frac{S_H}{\sqrt{2}\sigma_H}\right) \qquad (2.40)$$

The symmetry of the detector dictates that a similar probality of error must exist in the corresponding space transmission. Therefore,

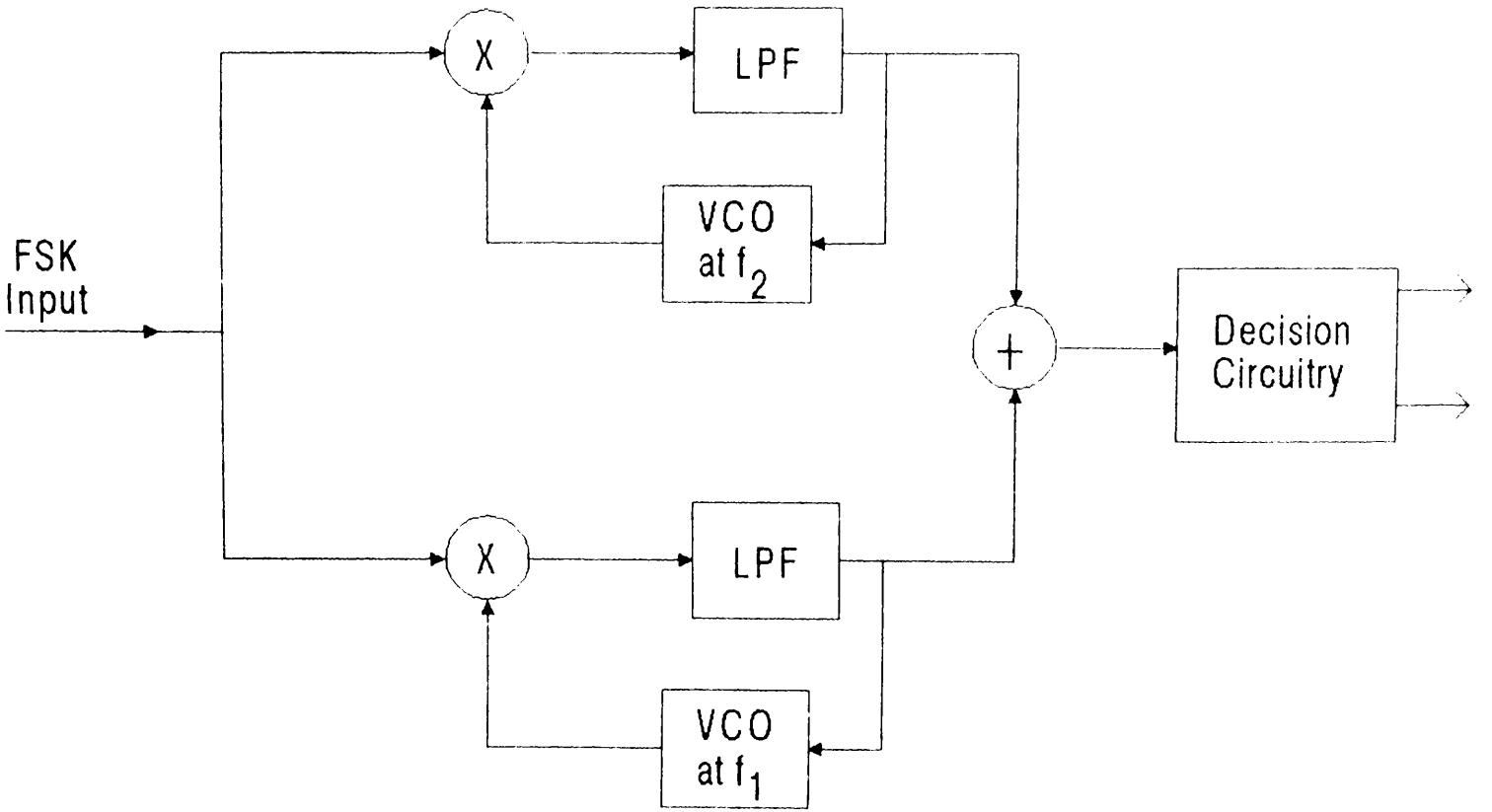

Figure 2.6 Schematic of an FSK Reciever

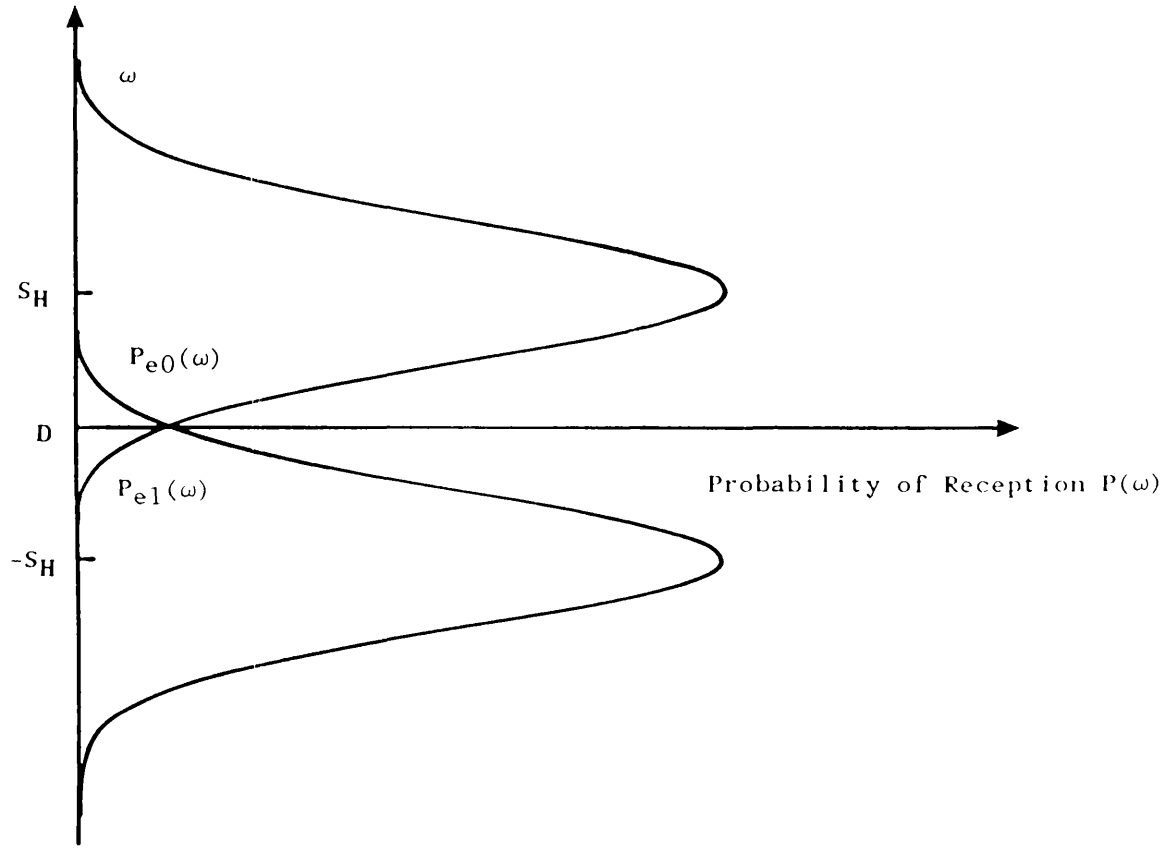

Figure 2.7
Probability Density Functions of FSK Coherent Detection.

assuming equi-probable mark and space transmissions, the overall probability of error is

$$BER = \frac{1}{2}\,erfc\left(\frac{S_H}{\sqrt{2\sigma_H}}\right). \qquad (2.41)$$

Specification of similar parameters to those used earlier yields a 3dB receiver sensitivity improvement over the coherent ASK system of -54.2 dBm

2.9 Phase Shift Keying (PSK).

The use of the instantaneous carrier phase to transmit information results in a more sensitive form of transmission. The present discussion will evaluate the required SNR for a transmission network employing such a format. In keeping with the previous analysis the case of a binary transmission will be considered and the phase of the carrier will be assumed to be keyed between two states 180° apart. This form of transmission is commonly referred to as anti-podal PSK or Phase Reverse Keying (PRK).

The electric field of the carrier under this form of modulation is written

$$E_T(t) = \sqrt{(2P_T)}\sin(\omega_T + \delta\theta p(t)) \qquad (2.42)$$

The phase modulation of the carrier is described in the term $\delta\theta$ which denotes the amount of phase deviation. p(t) is representative of the data stream which has possible states of $\mp$ 1. The phase modulation is most conveniently described with a re-definition of the modulation index[18]

$$m = \cos\,\delta\theta. \qquad (2.43)$$

The electric field description will therefore be modified to

$$E_T(t) = \sqrt{P_T}\{m.\sin\omega_T t + p(t)\sqrt{(1-m^2)}\cos\omega_T t\} \qquad (2.44)$$

The above description of the electric field shows the average power in the carrier is $P_T m^2/2$ and the data transmission power $P_T(1-m^2)/2$. The most efficient form of transmission is therefore the PRK waveform where all the power is sent in the data sidebands as $\delta\theta = \pi/2$ and $m = 0$.

In the PRK transmission, the amplitude of the received modulating signal is seen to be switched between two levels (see Figure 2.8). Continuing the analysis for the more general Bi-polar PSK transmission, where the phase shift may not necessarily be $\pi/2$, the recieved signal states will have powers described by,

$$S_H = S_H \sin\delta\theta \quad \text{'logic 1' and}$$
$$S_H = -S_H \sin\delta\theta \quad \text{'logic 0'.} \tag{2.45}$$

The signal amplitude $S_H = 2R\sqrt{(P_{LO}P_T)}$ for both instances. The probalbility of error can therefore be evaluated as

$$P_{e1}(x) = \frac{1}{\sqrt{(2\pi)}\sigma_H} \int_{-\infty}^{0} \exp-(S_H \sin\delta\theta - x)^2/2\sigma^2_H \, .dx$$

$$= \frac{1}{2} \operatorname{erfc}\left(\frac{S_H \sin\delta\theta}{\sigma_H}\right) \tag{2.46}$$

Since $P_{e1}(x) = P_{e0}(x)$, and $P_0 = P_1 = 1/2$, then the total probability of error is

$$\text{BER} = \frac{1}{2} \operatorname{erfc}\left(\frac{S_H \sin\delta\theta}{\sigma_H}\right), \tag{2.47}$$

which for the PRK transmission case reduces to

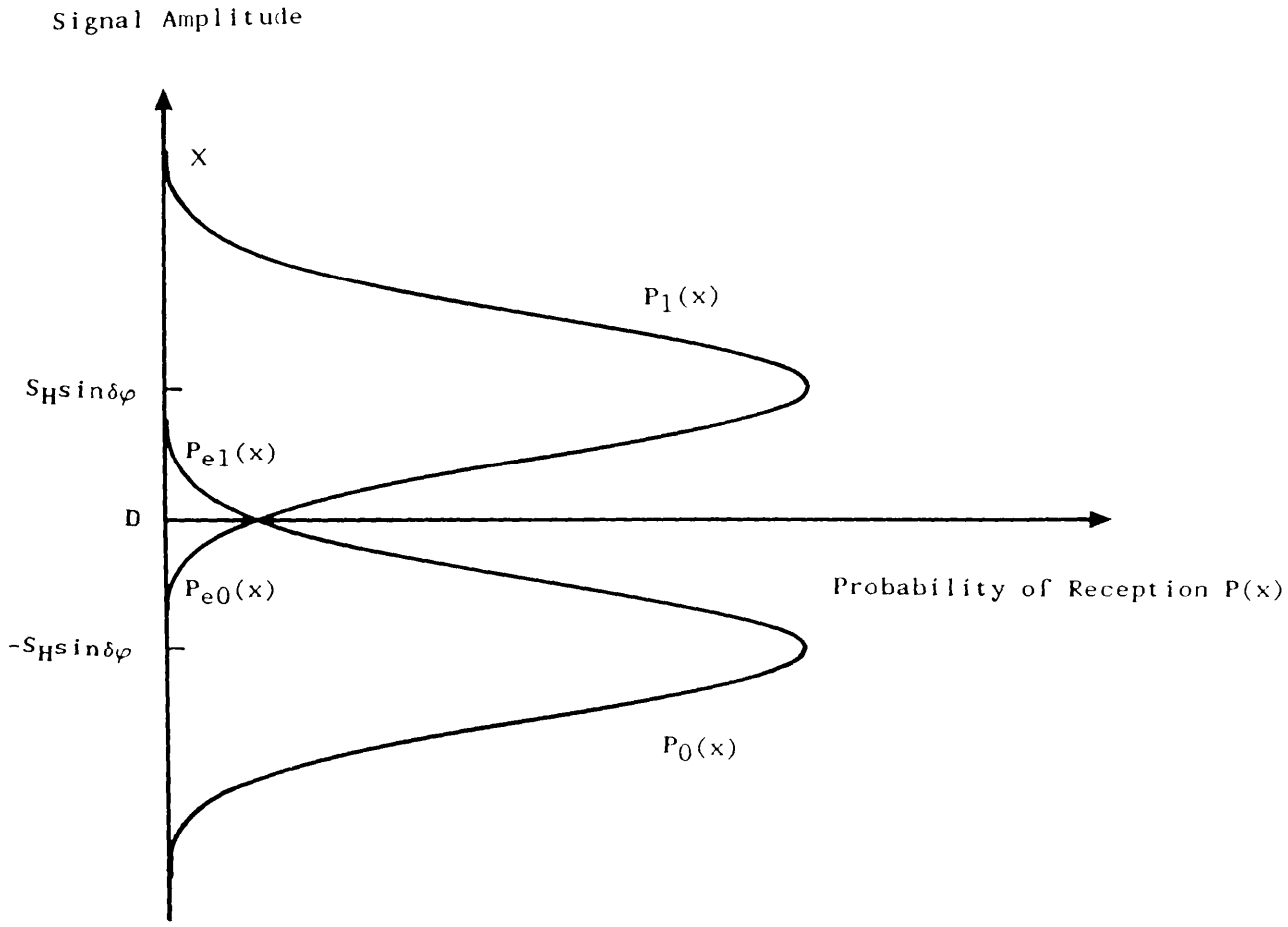

Figure 2.8
Probability Density Functions of PSK Coherent Detection.

$$BER = \frac{1}{2}\,erfc\left(\frac{S_H}{\sigma_H}\right). \qquad (2.48)$$

The PRK system thus gives an improved receiver sensitivity of 3dB over that of coherent FSK hererodyne detection, *ie* a received power of -57.2 dBm is necessary for a system operating with identical parameters to those used in earlier discussions.

2.10 Coherent Homodyne Detection.

The analyses so far have assumed that a heterodyne form of detection is employed. A further improvement, at a cost of increased receiver complexity, becomes available if the intermediate frequency of the heterodyne detection is eliminated. The modulation can be extracted by beating the incoming transmission with a frequency equal to its own and hence converting the received data directly to baseband. A reduction of front end bandwidth of exactly one half of that reqired for the heterodyne detector results in an equivalent reduction in the noise power. The SNR at the dtector is thus effectively doubled therefore a 3dB improvement in receiver sensitivity has been achieved [6].

2.11 Performance Degradation due to the Spectral Spread of the Laser Oscillator.

The theoretical performances of binary IM/DD and coherent transmission schemes have been presented. The general conclusion of the analysis is that coherent detection offers a performace improvment of up to 3 dB over the IM/DD system. When it is considered that the models used are ideal and in practice the IM/DD performance is generally some $7 - 12$ dB away from the theoretical limit then the benifits that would be gained from a move to coherent formats becomes more evident. The analysis is as yet however incomplete. The state of the art semiconductor laser devices exhibit poor performance in terms of phase stability. The effect that this instability would have on a coherent detection scheme remains to be discussed. This section will present a brief analysis of this problem as evaluated in refernces 23 and 24. The result is shown to be equivalent to calculations made

by Prabhu [25] and Lindsey [26] for microwave receivers. The PSK detection format was shown to be the most sensitive of the coherent schemes therefore attention will be limited to that area.

To carry out the analysis the problem is considered in two parts. The performance degradation for a given measure of phase tracking performance (specified as the phase error variance) in the carrier synchronisation circuitry is calculated first of all. This does not take account of the necessary carrier power to achieve this level of tracking performance. The amount of carrier power necessary to achieve a specific phase error variance must then be calculated and added to the above to complete the calculation. This carrier power is influenced by a number of factors but most importantly will be determined by the laser linewidth. In chapters 4 and 5 more attention will be given to the question of the laser linewidth influence on the phase synchronisation. For the moment therefore results that have as yet not been proven will be quoted.

Under the influence of the laser phase noise the detected photocurrent can be described as

$$i_S(t) = S_H.\cos(\varphi_e(t) + \delta\varphi_n(t)) + x(t) \quad (2.49)$$

The power spectral density of the shot noise term x(t) will remain the same as before. The received signal levels for the anti podal PSK transmission will therefore be modified thus,

$$i_S(t) = \begin{bmatrix} S_H\cos(\delta\varphi_n(t)) + x(t) \\ -S_H\cos(\delta\varphi_n(t)) + x(t) \end{bmatrix} \quad (2.50)$$

Although the phase instability of the two laser sources due to their inherent linewidth may be such that the power spectral density of the phase difference between the incoming and local oscillator laser is non white [27,28] the assumption is made that, under the phaselocked condition, the phase noise, over the bit period, may indeed be considered white [23,24]. The above equation therefore leads

to the modified expression describing the BER performance [23,24,25,26]

$$BER = \frac{1}{2}\,erfc\left[\frac{S_H \cos(\delta\varphi_n(t))}{\sigma_H}\right]. \qquad (2.51)$$

The effect of the phase noise on an anti-podal PSK transmission as described by the above has been evaluated by Prabhu and is shown graphically overleaf (Figure 2.9). The two noise corruptions that have been considered are phase fluctautions of a Gaussian distribution and those of a Tikhonov Distribution. The latter is a good approximation to the fluctuations present in a narrow band second order PLL [20,25,26]. The representation indicates the effect of the phase fluctuations on the BER performances. Predictably, as the performance requirement increases, or as the tracking becomes less precise, the required signal to noise ratio at the receiver becomes larger. It is important to observe however that distinct floors exist in the BER performance where, if a specific level of phase synchronisation is not reached, then this performance requirment will also not be met. A specific example is the BER of 10^{-9}. A system performance of this magnitude necessitates that a phase error variance of 0.03 $rads^2$ must be achieved. This is a point that will be of prime interest to a system designer. Phase synchronisation to this degree is possible but, as will be evaluated in detail in chapters 4 and 5, requires increasing amounts of carrier power as the phase instability (or linewidth) of the laser oscillator is increased. Typical semiconductor laser linewidths of state of the art sources of today would require power levels that would render this form of transmission unviable when considered against the more simple approach of heterodyne/homodyne ASK detection.

2.12 Coherent Binary Transmission : Conclusions.

The essential elements of the coherent receiver have been outlined and the performance of various binary transmission formats presented. The effect that the phase noise, due to the laser oscillator linewidth, would have on a coherent system has been briefly described for the case of a binary PSK transmission. This phase noise has been shown to have catastrophic effects on BER performances unless it is

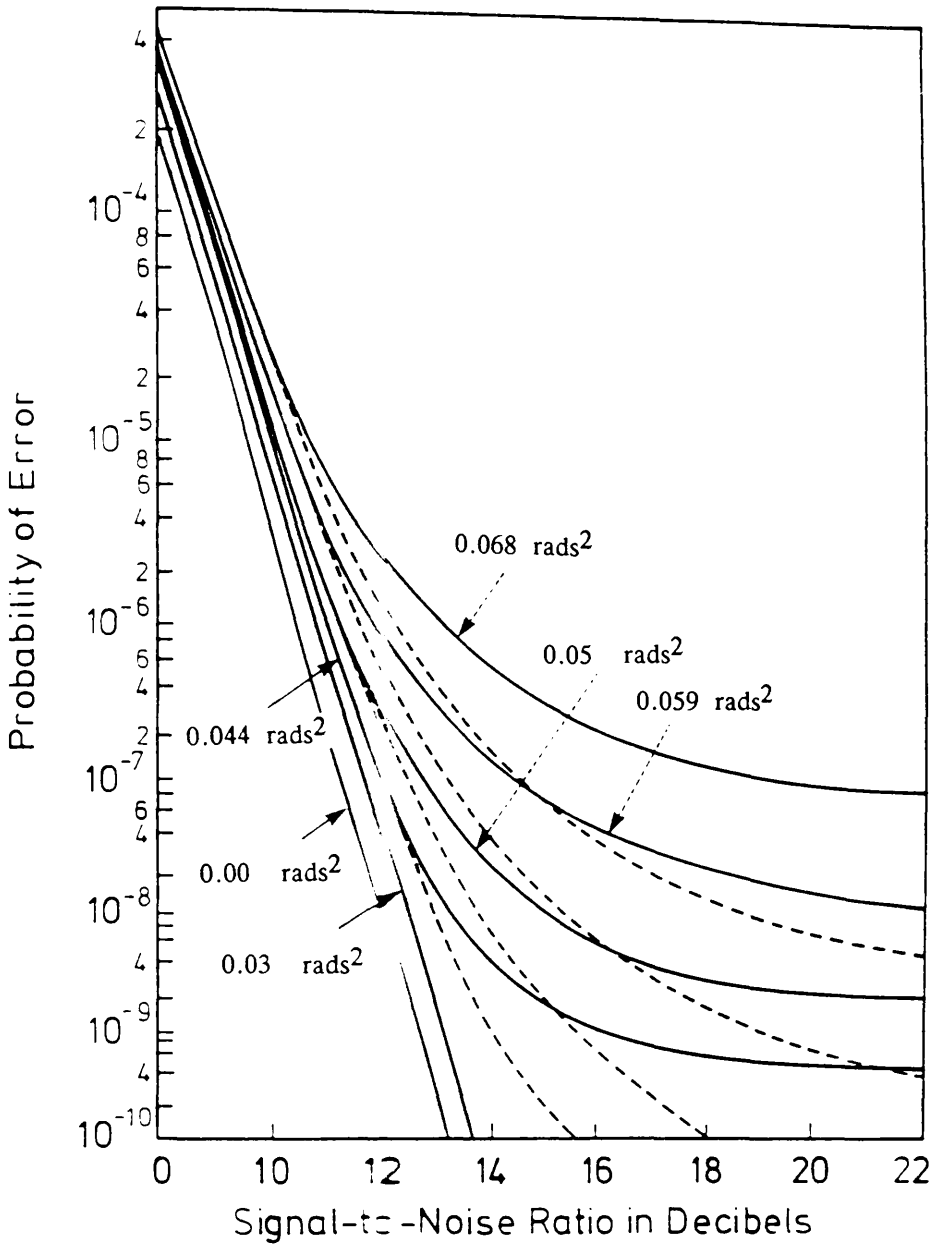

Figure 2.9

Probability of Error for Binary PSK Transmission with Imperfect Carrier Recovery [24].

Solid Lines denote Tikhonov Distribution,
Dashed Lines denote Gaussian Distribution.
Legends denote Phase Error Variance.

maintained below a given level (σ^2 = 0.047 rad^2 for a BER of 10^{-9}). Alternative coding techniques exist that outperform binary PSK in terms of receiver sensitivity. These techniques will be given some attention in the following section.

2.13 Coded Phase Coherent Transmissions.

The preceeding sections have given an evaluation of the relative efficiencies of various binary digital modulation schemes. It was shown that the most efficient of these transmission formats was the coherent detection of a PSK waveform. The effect upon the receiver sensitivity of such a scheme, that the high level of phase instability of the laser source has, was presented in graphical form. This section will provide a treatment of an alternative form of digital transmission, that is of coded phase coherent transmission formats. The use of transmission schemes such as these provides an enhanced receiver sensitivity at the expense of transmission bandwidth and increased receiver complexity.

According to the theory derived by Shannon [29] a coding technique exists which will allow error free transmission to be achieved, provided that the transmission rate is less than what he describes as the system bandwidth. Shannons hypothesis, presented graphically in Figure 2.10 [30], shows that a high transmission bandwidth to information bit rate ratio is necessary in order that the fundamental limit can be approached. That fundamental limit is evaluated as being an error free transmission with a normalised SNR (Signal Energy per bit to Noise power per unit Bandwidth ratio) of -1.6 dB. What Shannon's theorem does not state however, is how this performance can be attained. The following section will examine a particular coding technique and present an evaluation of how effective this would be in an optical transmission.

The brief discussion above suggested that any improvement in receiver power levels was likely to be accompanied by an increase in system transmission bandwidth. The use of an optical carrier opens up the possibilty of large bandwidth transmission provided that the transission medium is suitable. In general this can be assumed to be true for optical fibre systems and should present no problem for

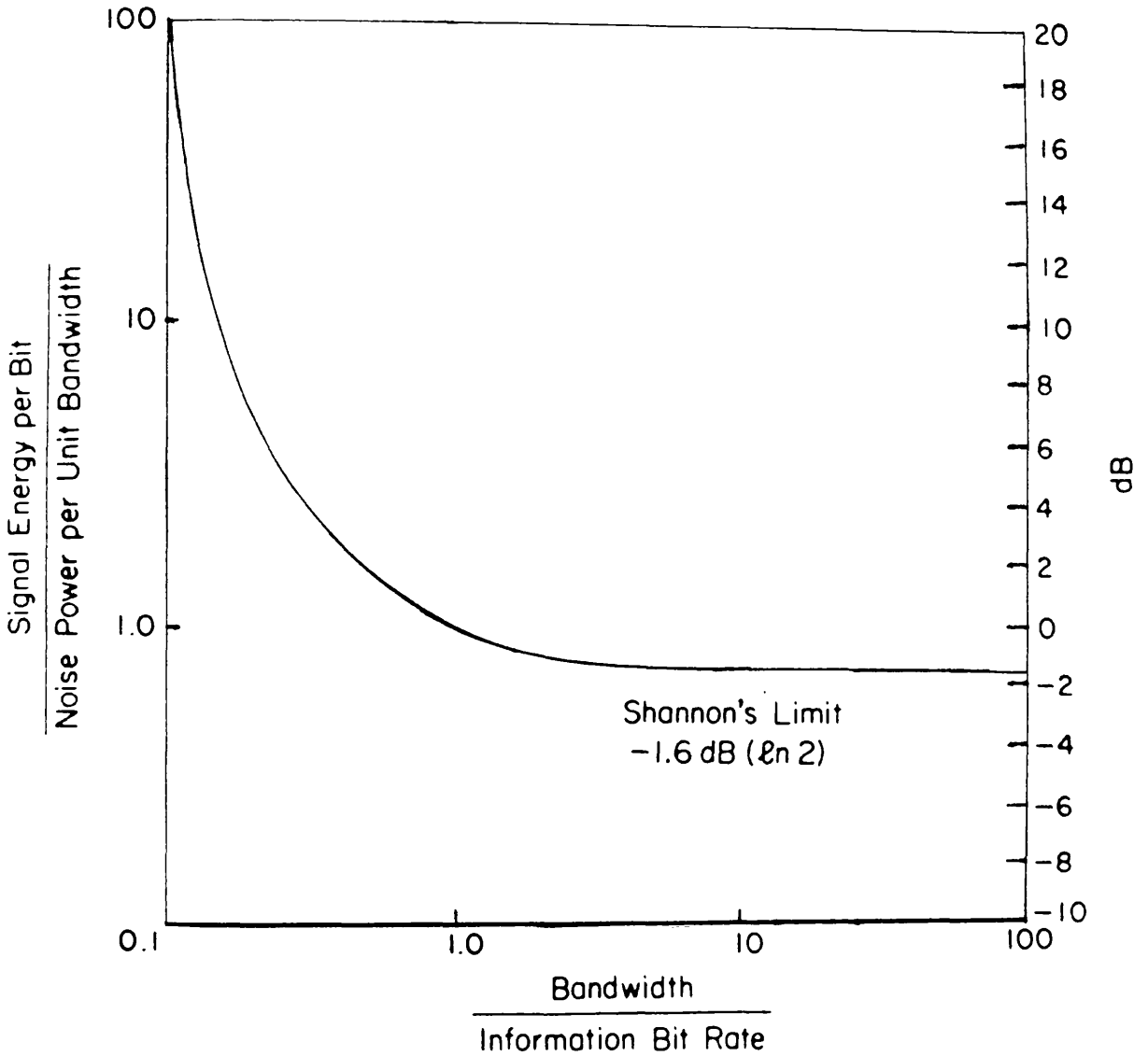

Figure 2.10

Normalised SNR versus Transmission Bandwidth to Information Bit Rate Ratio. [29].

satellite– satellite inter space links. It is therefore considered worthwhile that attention be given to the investigation of alternative coding formats that are perhaps expensive in terms of system bandwidth but more economical in the sense of transmission power for optical data transmission. In particular this section will address the problem of multilevel orthogonal signals.

2.14 The Basic Model.

In the Coded Phase Coherent Transmission format a word of a chosen length from a known set of words is transmitted to represent one data symbol. A correlation is performed at the receiver between this word and a set of locally generated words from an identical set [31,32]. In order that n bits of information may be represented, 2^n messages, or words, are required in the transmission set. Assuming that the bit time is T seconds then, over a period of nT seconds the receiver will compute the probability that a given word was transmitted. The method of this computation will now be outlined.

The principle is illustrated in Figure 2.11 with the use of a 4 level transmission schematic. Four times four bit binary code words are used to transmit blocks of two bits of information. In order that the maximum receiver sensitivity may be achieved the transmitted waveforms should be as different from each other (have the minimum cross correlation) as possible. In the preceeding section the case of an antipodal PSK transmission was discussed, this particular format corresponds to the minimum cross correlation coefficient (equal to -1) that may be achieved. The use of multi– level or coded phase coherent format does not permit this value of cross correlation to be achieved however, the signals can be chosen in such a way that all the cross products are equal to zero [30,31,32,33]. In this instance the signals are said to be orthogonal. In the following examples attention will be limited to this particular set of signals. In order to illustrate the concept it will be assumed that the blocks of words are amplitide shitfted between ±1 (equivalent to Phase Shift Keying by π radians) and are centred on a carrier frequency of ω_T radians/sec. Coherent detection of the carrier frequency and coherent demodulation of the transmission at the IF stage are assumed. Corruption of the

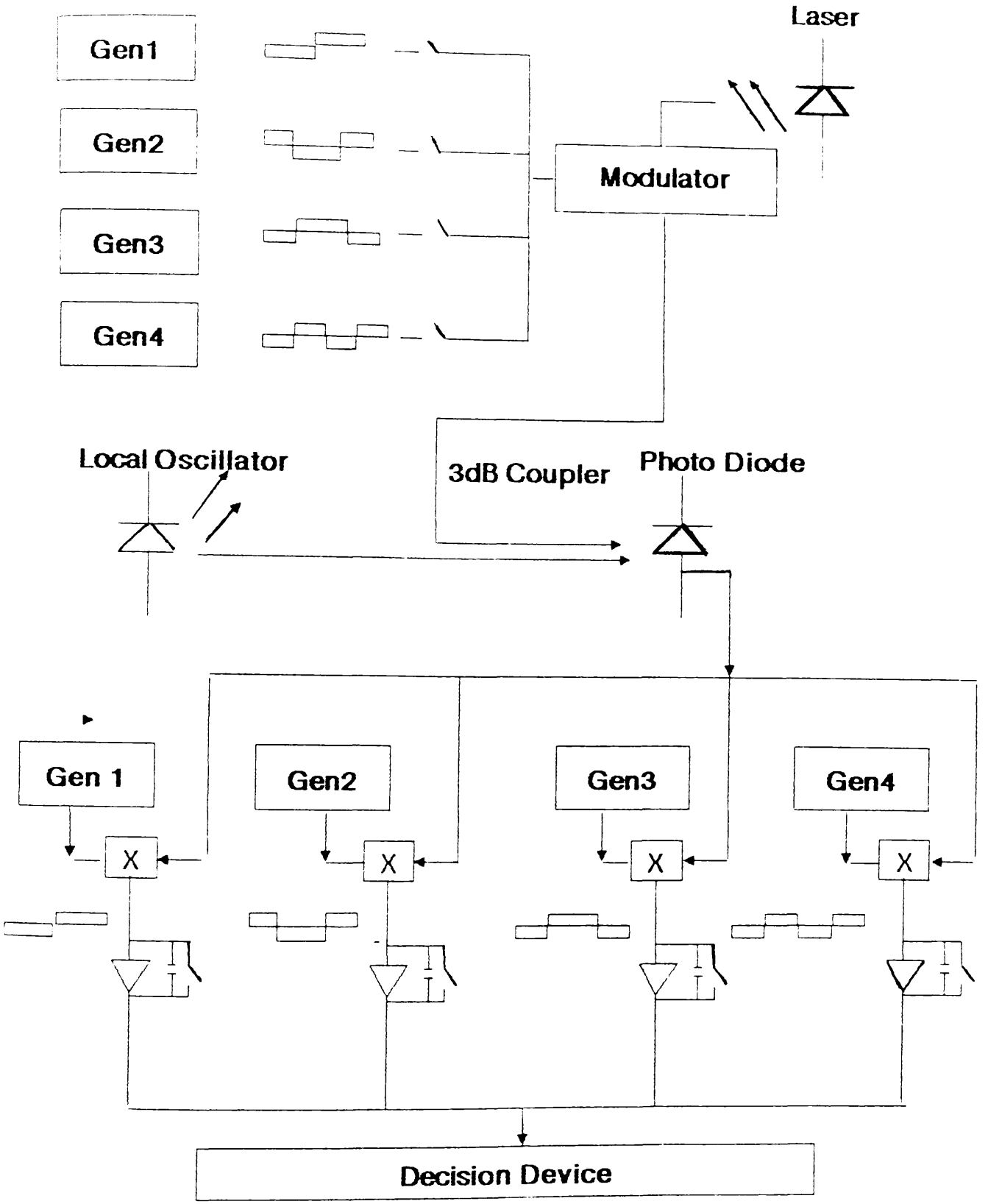

Figure 2.11 Coded Phase Coherent Transmission Schematic.

transmission will result due to the influence of the additive Gaussian noise and from the influence of the laser phase noise. For the moment attention will be restricted to the former and as in the previous analysis it will be assumed that the condition of shot noise limited detection has been reached.

The output of each of the correlators will be sampled at a time interval nT. Assuming homodyne detection the signal level at the output of the 'correct' correlator will be,

$$x_i = \frac{2\surd(P_{LO}P_T)}{nT} \int_0^{nT} \sin^2(\omega t).dt \qquad (2.52)$$

$$= 2\surd(P_{LO}P_T)R = A. \qquad (2.53)$$

Due to the orthogonality of the coding the output of all other correlators will be equal to zero (in the absence of noise). The noise outputs of each of the n correlators will be dictated by the amount of local oscillator signal power. The single sided power sectral density of the shot noise due to the local oscillator is

$$S_N = 2eRP_{LO} \quad A^2/Hz. \qquad (2.54)$$

The signal variance at the output of each of the correlators is therefore [32,33]

$$\sigma^2 = 2eRP_{LO}/nT. \qquad (2.55)$$

The ratio of the peak output signal to the noise variance can thus be written

$$\frac{(e(nT))^2}{\sigma^2} = \frac{(2\surd(P_{LO}P_T)R)^2}{2eRP_{LO}/nT} = \left[\frac{2P_TRnT}{e}\right]^{1/2} \qquad (2.56)$$

Since the noise power spectral density, S_N, can be described as the

equivalent noise power per unit bandwidth, and since P_T is the average input signal power, the above expression can be re-written as

$$\frac{e(nT)}{\sigma} = \sqrt{(2nSNR)} \qquad (2.57)$$

where the SNR is defined as the ratio of the received signal energy per bit to the noise power per unit bandwidth. In the above example this corresponds to the ratio

$$SNR = P_T R/e. \qquad (2.58)$$

The above discussion on the noise contribution at the output of each of the n correlators has ommitted to account for the fact that the noise inputs are each multiplied by the word generator. However, it may be shown[21] that the multiplication of the noise input by a series of levels of ±1 does not alter the Gaussian statistics and, provided that an equal number of both multipliers is present over the integration time, the effective variance at the output remains unchanged. Furthermore the orthogonality of the coding ensures that there is zero cross correlation of the noise outputs of the n correlators.

The probability that a particular signal set x_i was sent, given that a signal y(t) was recieved, is given by a maximum probability decision rule which is expressed, using Bayes theorem, as [22,30,31,32,33].

$$p(x_i|y) = \frac{P(x_i)P(y|x_i)}{P(y)} = \exp\int_0^{nT} x_i(t).y(t).dt \qquad (2.59)$$

The decision device shown in Figure 2.11 decides which particular message was transmitted by examining all the correlator outputs and deciding which particular output is the greatest (corresponding to the maximum probability). The probability that a word will be correctly detected is the probability that the outputs of all the other correlators will be less than that of the 'correct' one. This is expressed as,

$$P_c = \int_0^{\infty} p(x_i)dx_i P(y_2, y_3, \ldots . y_{N-1} < x_i) \quad (\text{where } N = 2^n)$$

(2.60)

$$= \int_0^{\infty} p(x_i).dx_i \prod_{i=2}^{N} P(y_i < x_i)$$

(2.61)

where $P(x_i)$ is the probability density of the output of the correct correlator and $P(y_i < x_i)$ represents the probability that each of the remaining 'incorrect' correlator outputs will in fact be less than the output of the correct correlator.

$$P(y_i < x_i) = \int_{-\infty}^{x_i} p(y_i)dy_i \qquad (2.62)$$

For a given transmission x the probability of a correct reception is

$$P_C(n) = \int_{-\infty}^{\infty} \frac{1}{\sqrt{(2\pi)}\sigma} \exp(-(x-A)^2/2\sigma^2) \cdot$$

(2.63)

$$\left[\int_{-\infty}^{x} \frac{1}{\sqrt{(2\pi)}\sigma} \exp(-y^2/2\sigma^2).dy\right]^{N-1}.dx$$

the use of the substitutions $u = (x-A)/\sigma$ and $z = y/\sigma$ yields

$$P_C(n) = \int_{-\infty}^{\infty} \frac{1}{\sqrt{(2\pi)}} \exp(-u^2/2). \qquad (2.64)$$

$$\left[\int_{-\infty}^{u + A/\sigma} \frac{1}{\sqrt{(2\pi)}} \exp(-z^2/2).dz\right]^{N-1}.dz$$

The probability of error is therefore

$$P_E(n) = 1 - \int_{-\infty}^{\infty} \frac{\exp(-u^2/2)}{\sqrt{(2\pi)}} \cdot \left[\int_{-\infty}^{u + \sqrt{(2nSNR)}} \frac{\exp(z^2/2)}{\sqrt{(2\pi)}} dz\right]^{N-1}.du$$

(2.65)

The above integral was solved numerically on an IBM System 2 personal computer in Turbo Pascal version 4 using 10 byte representation of real numbers. However, before these results are presented, it is felt that it would be instructive to relate the general principle to a specific type of orthogonal signalling, that is multi-level FSK.

Multi level, or M-ary FSK, transmission schemes are perhaps the easiest to appreciate conceptually. This format requires that an n-bit word is represented by $M = 2^n$ frequencies. That is, the set of signals can be described as

$$s_i(t) = \sqrt{2}A\sin(\pi(\omega + x)/T) \quad x = 1,2..... \qquad (2.66)$$

The multiplier x must be an integer number to ensure orthogonality of symbols. The minimum separation between any two levels is

$(\omega_n - \omega_M)_{min} = \pi/T$ where T is the transmission time for n bits of information. The minimum transmission bandwidth is therefore

$$B = M/2T \text{ Hz.} \qquad (2.67)$$

For example, if a transmission system is operating at a rate of 565 Mbits/s then the transmission bandwidth can in theory be limited to 565 MHz for a binary transmission. An M-ary system operating with an 8 bit word length a bandwidth of

$$B = 256.565/(2.8) \text{ Hz}$$
$$= 9040 \text{ MHz} \qquad (2.68)$$

The transmission bandwidth has therefore been increased by a factor of 16. One further point to note before examining the results of the BER integrals is this. In making the transition from the binary signalling condition to the multi level scheme the representaion of the BER performance in order that a comparison between the two formats can be made becomes slightly more involved. Because the M-ary representation transmits a code over a period of n bits, it is more

meaningful to compare the error performance over these n bits (or word) with the binary performance over a similar period. An M−ary system containing N signal states conveys $\log_2 N$ binry digits of information. This system can only be compared meaningfully with a binary system (or indeed an M−ary system with a different number of levels) if the energy required to transmit a given amount of information is compared as energy per bit. In order that this comparison may be made the following discussion will relate BER to the required Signal to Noise Ratio per Bit of information transfer. Furthermore since the discussion presented above evaluates the symbol, or word, error rate, it would be sensible to present the Binary PSK equivalent performance in a similar manner. That is an 8–ARY FSK should be compared against a Binary PSK tranmission Word Error Rate (WER) of word length 3. Similarly a 32−ARY FSK system should be compared against the binary WER of word length 5. The WER can be calculated from the BER as follows. If the

$$BER = \text{erfc}(S/N) \qquad (2.69)$$

$$= 1 - \text{erf}(S/N),$$

then the corresponding WER is given by

$$WER = 1 - (\text{erf}(S/N))^n,$$

where n is the number of bits in a word.

Figure 2.12 depicts the required SNR at the receiver for a given probability of error of symbol detection. The performance improvement with increasing numbers of transmission levels is clearly evident. The instance of n = 1 corresponds to the case of binary coherent FSK as desciribed earlier. 8−ary FSK (n=3) is seen to outperform binary PSK and an improvement in receiver sensitivity to approximately 5 photons per bit achieved with n = 5 (32 level transmission). It must also be noted here that these figures show improvements in receiver performance even before the PSK power level has been corrected to the WER. The PSK WER at a word length of 5 predicts a receiver sensitivity of approximately 10 photons per bit for a WER of 10^{-9}. Thus, in the absence of the phase

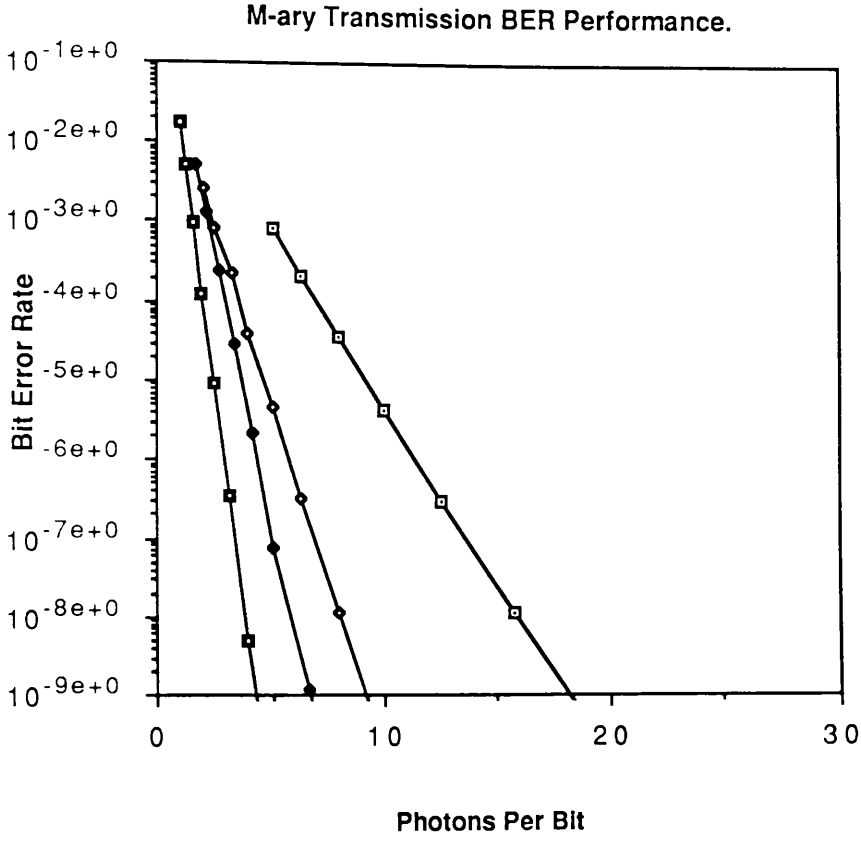

Figure 2.12

Multi Level FSK Receiver Performance.

Legends

- PSK BER
- FSK BER
- 8 – ary FSK WER
- 32 – ary FSK WER

instability, characteristic of optical sources, a performace improvement, over binary PSK, in receiver sensitivity is seen with the use of relatively low numbers of transmission levels. The effect that the laser instability will have on this performance will now be addressed.

2.15 Degradation of M−ary Signalling Due to Spectral Spread of Laser Oscillator.

It was demonstrated in the previous section that, with the use of coded phase coherent transmission formats, improvements in receiver sensitivity, over and above that obtainable with coherent PSK, can be achieved. The present discussion will extend the treatment to encompass the situation where the performance is impaired due to noisy, or imperfect, reference signal. Thus it will be made possible to compare the performance of binary and multi−level transmission formats in the presence of laser phase noise.

Similar assumptions will be made for the multi−level situation, that is it will be assumed that the phase jitter can be assumed to be Gaussian in distribution and quasi constant over the word duration. This assumption is only justified under certain conditions: a short word length, or the condition where the word length is equivalent to the bit length. It is the latter case that will be investigated as the calculations are directed toward the MFSK transmission.

The system power penalty under these conditions will be the result of a reduction in the signal−to−noise ratio due to imperfect correlation between the transmit and the reference signals. This power penalty can be described with the use of a matrix to represent the cross correlation coefficients thus [30,31,32],

$$X_{i,j} = \begin{bmatrix} \cos(\varphi) & i = j \\ 0 & i \neq j \end{bmatrix} \qquad (2.70)$$

This has the effect of modifying the effective SNR thus

$$SNR = SNR.\cos^2(\varphi). \qquad (2.71)$$

The performance of the MFSK system is therefore described by

$$P_E(n) = 1 - \int_{-\infty}^{\infty} \frac{\exp(\varphi^2/2\sigma^2)}{\sqrt{(2\pi\sigma^2)}} \cdot \int_{-\infty}^{\infty} \frac{\exp(u^2/2)}{\sqrt{(2\pi)}}$$

$$\cdot \left[\int_{-\infty}^{u + \sqrt{(2nSN)}R.\cos(\varphi)} \frac{\exp(z^2/2)}{\sqrt{(2\pi)}} dz \right]^{N-1} .du.d\varphi \qquad (2.72)$$

The above integrals were solved as previous on an IBM PS 2 using the extended representation of real variables. The results are displayed graphically in Figure 2.13–15.

For the condition of n = 1 (Figure 2.13), the equivalent of binary coherent FSK transmission, the PSK system is quite clearly seen to provide the better performance. Figure 2.14 however shows that for even a small increase in the number of transmission levels a significant performance improvement can be obtained. The performance of 8–ARY FSK is displayed against Binary PSK for the condition of 0 reference error and a mean phase error of 0.19 rads. The required signal level per bit of imformation is −60.2 dBm at 565 Mbits/sec for the ideal PSK situation. With a mean phase error of 0.19 rads the corresponding power is increased to −58.9 dBm. The required signal power for the 8–ARY FSK with a phase error of 0.19 rads can be extracted from Figure 2.14 as −60.1 dBm. Thus a performance equivalent to the ideal PSK transmission is achieved for only a small increase in the system bandwidth and a receiver design that is arguably comparible in difficulty to implement. The benefits that have been obtained here are not yet fully evaluated as the conversion has not yet been made from the Binary BER to WER. An additional power penalty to accomodate for this would be incurred. Further increase in the number of signalling levels may be of benefit up to a point. This is shown in Figure 2.15 where the BER and WER performance for ideal binary PSK is displayed against 32−ary FSK. 32–ARY FSK requires a receiver power level of −61.6 dBm which is an improvement of 1.4 dB over the ideal binary situation. The complexity of the receiver design does however increase with the number of signalling levels and will become more of a practical

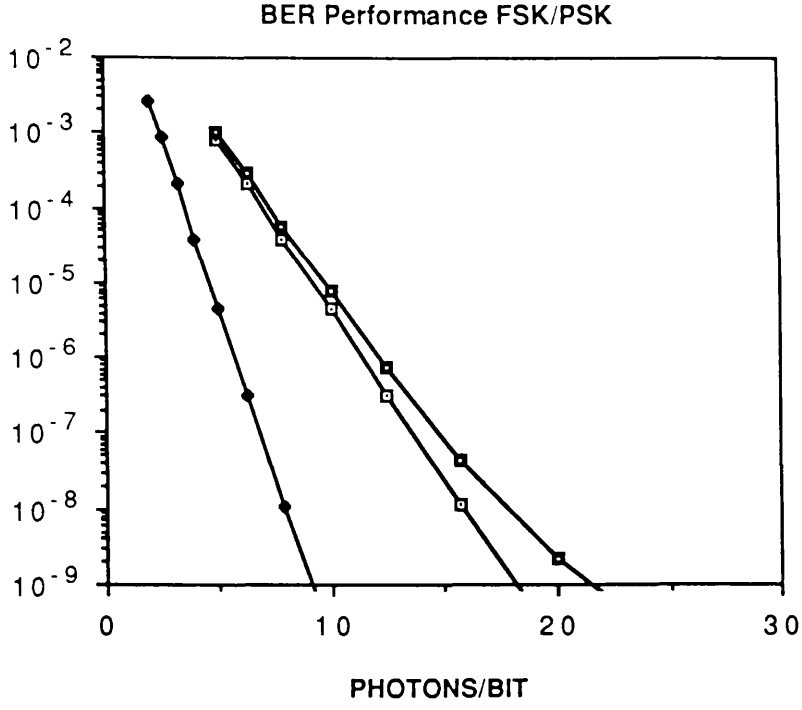

Figure 2.13

Multi Level FSK Receiver Performance.

Legends

- **PSK BER**
- **FSK BER (Ideal)**
- **FSK BER ($\sigma = 0.19$ rads)**

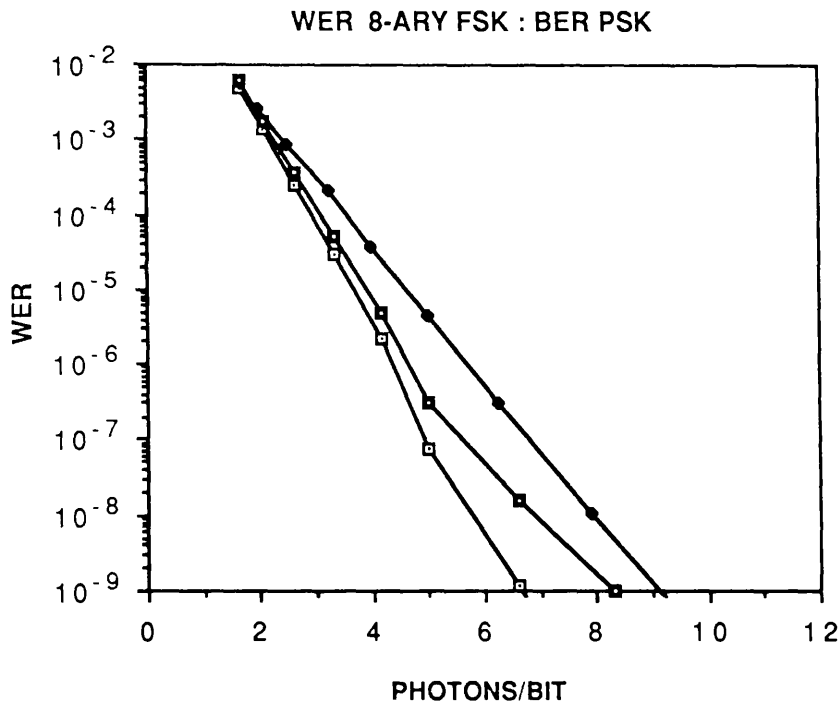

Figure 2.14

Multi Level FSK Receiver Performance.

Legends — **PSK BER**

— **8 – ary FSK BER (Ideal)**

— **8 – ary FSK BER ($\sigma = 0.19$ rads)**

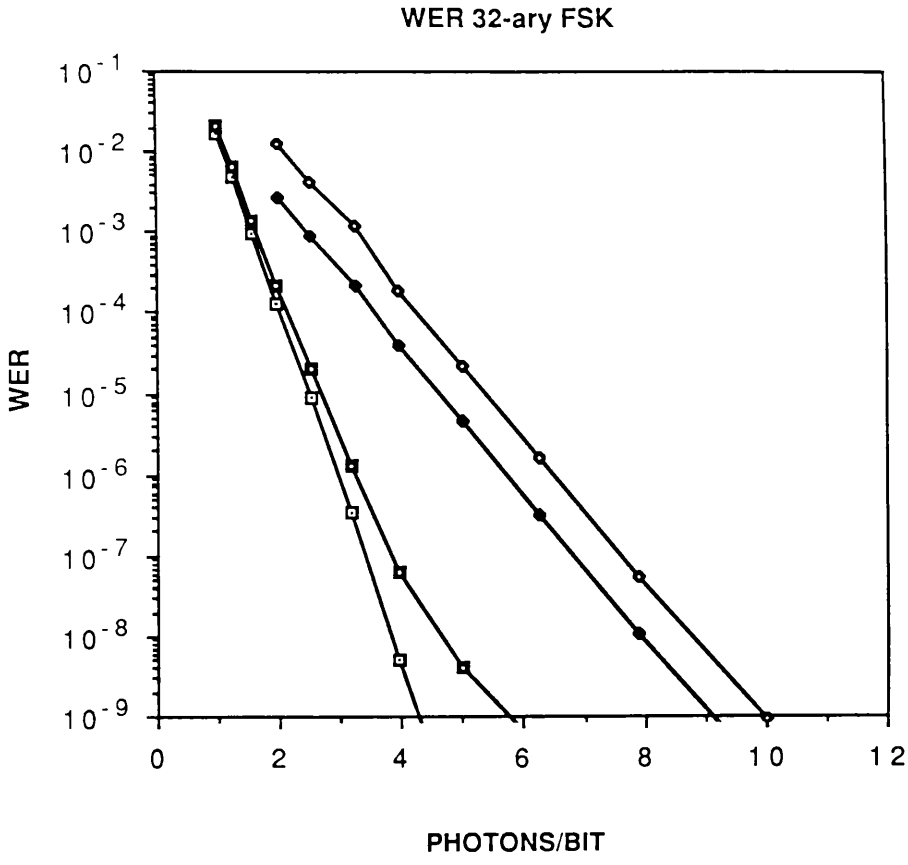

Figure 2.15

Multi Level FSK Receiver Performance.

Legends
- **PSK BER**
- **32 – ary FSK WER (Ideal)**
- **32 – ary FSK WER (σ = 0.19 rads)**
- **PSK WER (n = 5)**

challenge.

2.16 Conclusions and Discussions.

This section has presented an evaluation, in terms of the required SNR at the receiver, of the performance of a number of binary transmission formats. Coherent detection techniques have been compared against IM/DD schemes and have been found to provide a potential sensitivity improvement of 10 to 25 dB. The dominant noise contributions in an IM/DD system are receiver thermal noise and the shot noise from the signal, the background radiation and the dark current. A coherent receiver has an additional noise contribution from the local oscillator source. It is found that, if this noise source can be made to dominate the total noise input, then the condition for optimum detection sensitivity is reached. This condition is known as shot noise limited detection.

The lack of coherence of present day laser diode sources will result in a performance degradation from the above mentioned figures. The power penalty that will be incurred due to this factor can be determined by evaluating the effect of the laser linewidth on the phase synchronisation at the receiver. A datum level can thus be derived which will determine the maximum allowable laser linewidth for a given set of transmission variables (transmission scheme, data rate, allowable error *etc*). This has been outlined for the case of a binary PSK transmission by making use of a set of curves evluated for the case of a micro wave receiver using a similar detection method. It was found that a phase error variance of no greater than 0.03 $rads^2$ is tolerable for a receiver to operate within 0.5 dB of the optimum performance at a BER of 10^{-9} (provided that no other corruptions are present). If the phase tracking requirements are relaxed to a variance of greater than 0.047 $rads^2$ then the above performance cannot be reached. These values will be made use of in later chapters to specify the required performance of an optical phase locked loop.

The receiver analysis has been extended from the binary situation to encompass more sophisticated formats which provide a potential means of defeating the problems of the laser phase noise. Coded

phase coherent transmissions were examined as a possible means of circumventing the effects of laser phase instability. Such schemes were found to be advantageous in situations where a high degree of phase synchronisation was maintained. However, under such circumstances, the extra complexity of the M−ary receiver may detract from the advantages gained from moving from a binary PSK transmission format. In situations where the source linewidth would prevent good phase locking ($\sigma^2 = 0.03$ rads^2) from being achieved the majority of communications applications may be better served by 'weakly coherent' (heterodyne ASK, FSK) transmissions.

Before leaving the topic of multi−level signalling schemes it is necessary to first of all comment upon the use of incoherent detection schems which employ such receiver configurations. The present discussion has revolved around the use of coherent detection and post coherent processing of the data transmission. It is of benefit to consider this particular transmission format because it is relatively straight forward to appreciate the concept of multi−level signalling techniques using this approach. However, it must be noted that in the present example, phase sensitive detection and phase sensitive demodulation of the data stream could not be performed with out sacrifice of carrier power to provide the phase locking information. The inclusion of such a scheme has not been considered in the present work. However, the performance improvements that are gained from a move to multi−level signalling schemes are not entirely negated when this aspect of the transmission format is taken into consideration. Indeed if the number of transmission levels is sufficiently large then it can be shown that it is not necessary to perform a phase sensitive detection of the transmitted signal prior to data recovery. An analysis by Jeromin *et al* has shown that multi−level transmission scheme operating with M−ary orthogonal non−coherent detection of the data stream has a performance which approaches that of truly phase sensitive schemes provided that sufficient data bandwidth is available. It will be demonstrated in later chapters that the problem of maintaining sufficient phase synchronisation for coherent detection techniques to be viable is far from being totally resolved. Multi level signalling techniques, with incoherent signal processing schemes may therefore hold the key to future transmission developments.

References.

1. M.Shikada *et.al.* '1.5 μm High Bit Rate Long Span Transmission Experiments Employing High Power BFD−DC−PBH Laser Diode.' 5th Int. Conf. Integrated Optics and Optical Fibre Coomun. ECOC(11) Venice, Italy, Oct 85 Post Deadline Paper.

2. K.Kikuchi *et.al.* ' Degradation of the BER in Coherent Optical Communications Due to the Spectral Spread of the Transmitter and the Local Oscillator.' J. Lightwave Technol. 2(6), 1984. pp1024−1033

3. T.Okoshi *et.al.* 'Calculation of the Bit Error Rate of Various Heterodyne and Coherent Type Optical Comminication Schemes.' J.Opt. Commun. vol. 2(3) 1983. pp89−96.

4. Y.Yammamoto 'Recoever Performance Evaluation of Various Digital Optical Modulation−Demodulation Systems in the 0.5−10μm Wavelength Region.' IEEE J.Quant.Electron. 16(11) 1980. pp1251−1259.

5. S.Saito, Y.Yammamoto, T.Kimura 'S/N and Error Rate Evaluation for an Optical FSK Heterodyne Detection System Using Semiconductor Laers.' IEEE J.Quant. Electron. 19(2) 1983. pp180−193.

6. L.G.Kazovsky. 'Optical Heterodyning Versus Optical Homodyning: A Comparison.' Journal of Optical Commun. vol 6(1985) no.1, pp18−24.

7. S. Kobayashi *et.al.* 'Direct Frequency Modulation in AlGaAs Semiconductor Lasers' IEEE J.Quant.Electron. vol. QE−18(4) 1982 pp 582−595.

8. G.Wenke, S.Saito 'Stabilised PSK Transmitter with Negative Feedback to a Semiconductor Laser' IEEE Elect. Lett. Vol.21 No.15. 1985 pp653−655.

9. Alferness R.C. 'Guided Wave Devices for Optical Communications.' Journ, Qunatum Electron. QE−17(6) 1981. pp946−959.

10. G. Grosskopf *et.al.* 'Experiments on Optical Amplifiers for two Channel Transmission.' Proceedings ECOC 12. 1986 Techn. Digest Vol. 1 pp245–249.

11. I.W. Marshall, *et.al.* 'Measurements on a 206km Optical Transmission System Experiment at 1.5μm Using Two Packaged Semiconductor Laser Amplifiers as Repeaters.' Proceedings ECOC 12. 1986 Techn. Digest Vol. 1 pp245–249.

12. Y.Yamamoto, H. Tsuchiya 'Optical Receiver Sensitivity Improvement by a Semiconductor Laser Preamplifier.' IEE Elect. Lett. vol.16 no.6 1980 pp233–235.

13. C.J.Nielsen, J.H.Osmundsen 'New Approach Towards Frequency Stabilisation of Linewidth Narrowed Semiconductor Lasers.' IEE Elect. Lett. Vol.19 no.16 1983 pp 644–646.

14. S.Yamaguchi, M. Suzuki 'Frequency Stabilisation of a Diode Laser by Use of the Optogalvanic Effect.' Appl. Phys. Lett. 41(7) 1982 pp597–598.

15. E.Dietrich, B.Enning, R.Gross, H.Knupe 'Heterodyne Transmission of a 560 Mbits/s Optical Signal by Means of Polarisation Shift Keying.' Elect. Lett. vol.23 no.8 1987 pp421–422.

16. R.Noe 'Endless Polarisation Control in Coherent Optical Communications.' IEE Elect. Lett. vol.22 no.15. 1986 pp772–773.

17. S.D. Personcick 'Reciever Design For Digital Fibre Optic Communications Systems' Bell Syst. Tech. Journ. J52(1973) pp843–886

18. F.G Stremler 'Introduction to Communicatoin Systems.' 2nd Ed. Addison–Wesley, Reading, Massachusettes, 1982.

19. Carlson A.B.'Communications Systems: An Introduction to Signals and Noise in Electrical Communications.' Second Ed. New York: McGraw–Hill, 1975.

20. W.C.Lindsey. 'Sychronous Systems in Communications and Control' Englewood Cliffs, NJ: Prentice Hall, 1972.

21. Abramowitz M., Stegun A. 'Handbook of Mathematcial Functions.' Dover Publications Ltd. New York 1972.

22. B.Glance 'Performance of Homodyne Detection of Binary PSK Optical Signals.' J.Lightwave Technol. 4(2) 1986 pp228–235.

23. J.Franz 'Evaluation of the Probability Density Function and the Bit Error Rate in Coherent Optical Transmission Systems Including Laser Phase Noise and Gaussian Additive Noise.'J.Opt. Commun. 6(2), 1985, pp51–57.

24. V.K.Prabhu 'PSK Performance with Imperfect Carrier Phase Recovery.' IEEE Trans. on Aero. and Electron. Syst. vol. AES.12(2) 1976. pp275–286.

25. W.C.Lindsey 'Phase Shift Keyed Signal Detection with Noisey Reference Signals.' IEEE Trans. on Aero. and Electron. Syst. vol. AES.2(4), 1966. pp393–401.

26. J.Armor 'Phase–lock Control Considerations for Multiple Coherently Combined Lasers,' Master's Thesis, Air Force Institute of Technology, Wright–Patterson Air Force Base, OH, Rep. GEO/EE/77D–2, 1977.

27. T.Hodgkinson 'Phase–locked–loop Analysis for Pilot Carrier Coherent Optical Receivers.' Elect. Lett. vol. 21. 1985 pp1202–1203.

28. C.E.Shannon. ' The Mathematical Theory of Communication.' Bell Syst. Techn. Journ. 1948 vol.27 pp379–423,623–656.

29. W.C.Lindsey, M.K.Simon. 'Telecommunication Systems Engineering' Prentice Hall, Englewood Cilffs, New Jersey 1973.

30. J.J.Stiffler 'Theory of Synchronous Communications' Prentice Hall,

Englewood Cliffs, New Jersey,1971.

31. A.J.Viterbi 'Principles of Coherent Communications'McGraw= Hill 1966.

32. A.J.Viterbi 'On Coded Phase– Coherent Communications.' IRE Trans. on Space and Telem. March 1961 pp3– 14.

33. L.L. Jeromin, V.W.S. Chan 'M– ary FSK Performance for Coherent Optical Communications Systems Using Semiconductor Lasers.' IEEE Transactions on Communications COM– 34(4) 1986 pp275– 381.

CHAPTER 3.

The Laser Diode : A Signal Source for Coherent Transmission.

3.1 Introduction.

The success of the laser diode in direct detection systems has stimulated a considerable amount of interest in the possibility of using these diodes as a carrier source for coherent optical communications. The laser diode is well suited to optical fibre communications applications: it is small, has a high reliability, high efficiency (30%), low power drive circuitry (< 5volts at a few hundreds of mA), capability for direct current injection modulation and compatibility with fibre systems (small radiative area with beam divergence suitable for efficient launching into fibre). These properties would all be welcome in a coherent system. However, present day sources are of insufficient temporal coherence and stability to meet the stringent demands of a practical coherent environment. This is particularly true for the phase–sensitive formats. The present chapter will provide a review of the properties of the semiconductor laser that are of interest in the design of a coherent transmission system: the linewidth, modulation characteristics and stability. A qualitative approach to this topic will be adopted and suitable references listed where appropriate. Documentation of experimental characterisation of commercially available laser sources is also given in this chapter. In general, attention was restricted to Hitachi HLP 1400 laser diodes. In the free running condition these diodes were superior to other diodes available on the open market in terms of cost, stability and linewidth. They were therefore chosen as the most suitable candidates for an experimental source. Attempts to improve the linewidth of the laser emission were also carried out and details of this work are also given in this chapter.

3.2 Lasing Action In Semiconductors.

Figure 3.1 [1] shows a simplified schematic of an n^+p junction in a semiconductor material. The notation n^+ is used to indicate that the n– type semiconductor is more heavily doped then the p– type.

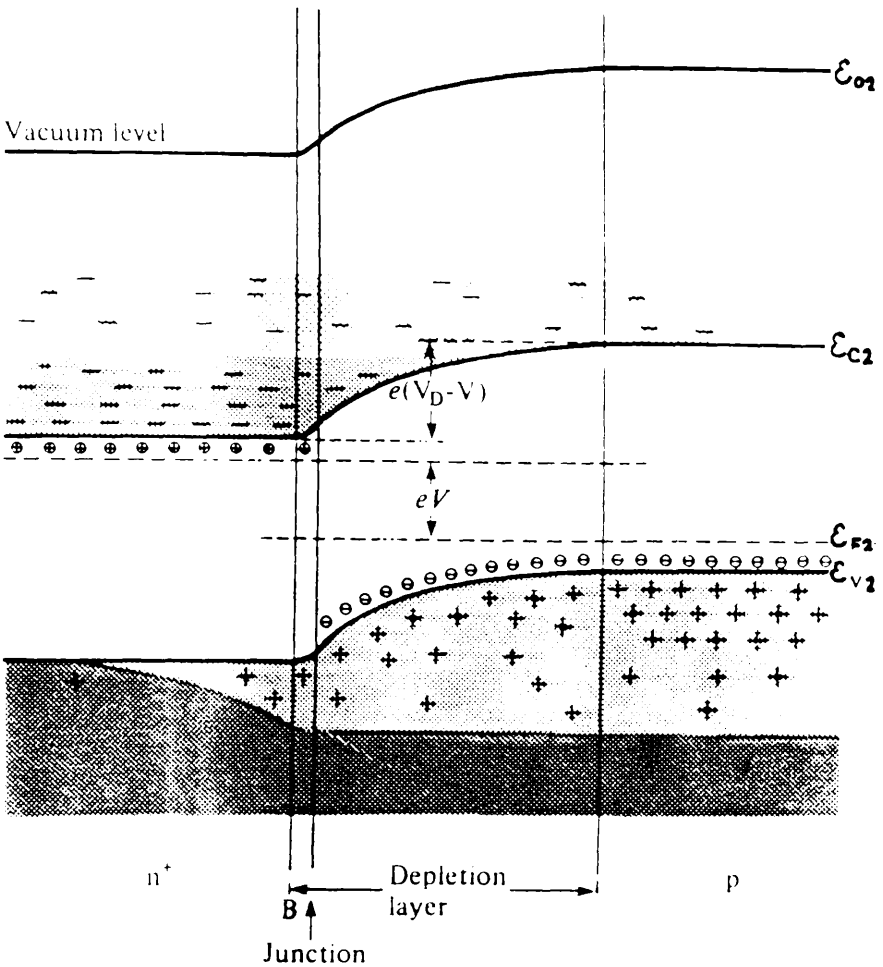

Figure 3.1
Electron Energy Levels across an N – p Homojunction forward biased [1].

The n^+p junction is as illustrated, forward biassed. Under this condition there exists, for a short distance beyond the depletion layer (generally of the order of a few μm) an area, the active region, where a large number of electrons are present in the conduction band and a similar number of holes are present in the valence band. Within the active region optical gain may be achieved. Figure 3.2 [1] shows the energy level diagram that describes the situation where the simple homojunction is replaced with a more complicated double heterostructure. The discontinuities in the energy levels at the junction boundaries provide a barrier over which the majority carriers cannot readily pass. A more uniform distribution of the gain region, shown in Figure 3.3, results. This structure also provides an optical guiding region due to the refractive index differences between the active (central) region and the side areas.

Within the active region radiative emission may take place when an electron–hole pair recombines to emit a photon of light having a free–space wavelength given by

$$\lambda = hc/\epsilon_g \qquad (3.1)$$

where h is Plancks constant and ϵ_g the energy of recombination. This radiation may cause another recombination to take place and in this instance any light emmitted will be coherent with the stimulating light (stimulated emission). Cleaving both ends of the active layer forms an abrupt junction between the semiconductor and the air boundary. At these interfaces light will be partially reflected and thus a resonant cavity can be set up between both end walls. Light propagation back and forth along this cavity can further instigate stimulated emission. If the rate of stimulated emission exceeds the rate of absorption then a population inversion exists. If the population inversion is such that sufficient stimulated emission occurs to overcome the absorption losses, then the condition of optical gain is achieved and lasing will take place.

Lasing action in the semiconductor laser is thus dependent upon the hole/electron energy distributions around the depletion layer and

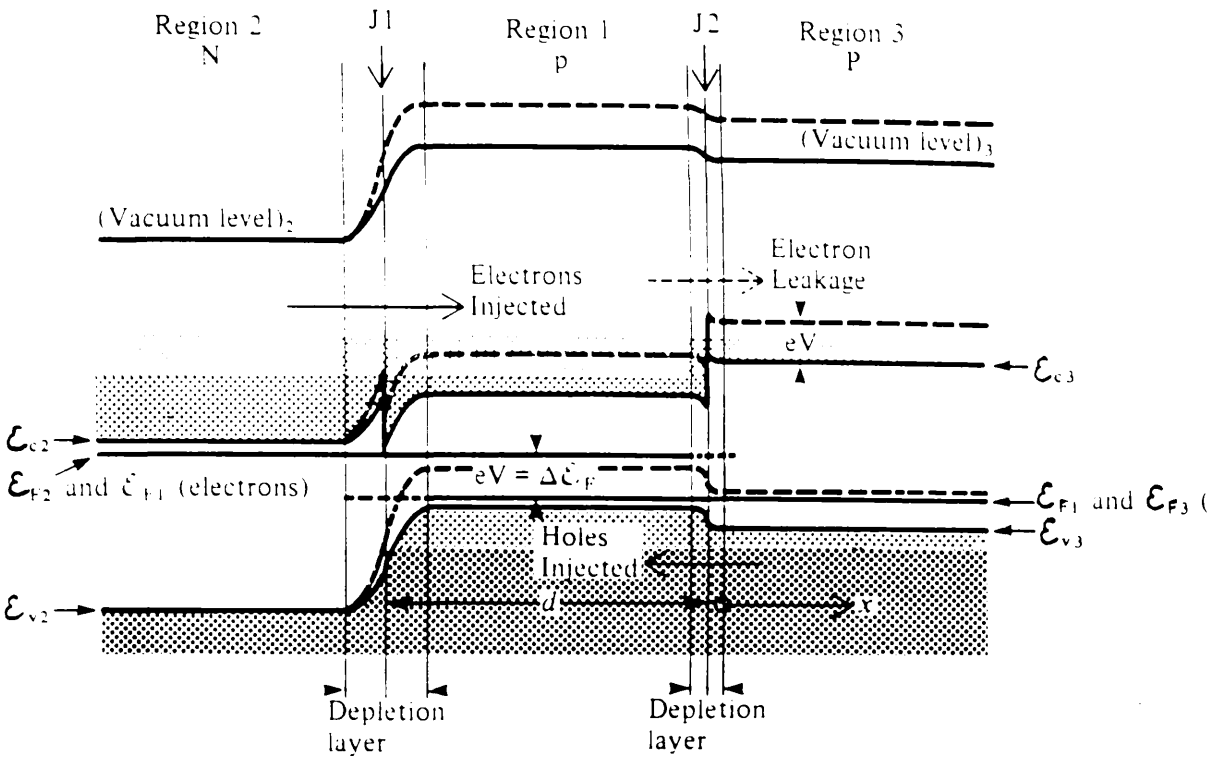

Figure 3.2
Electron Energy Levels across an NpP Double Heterojunction forward Biased [1].

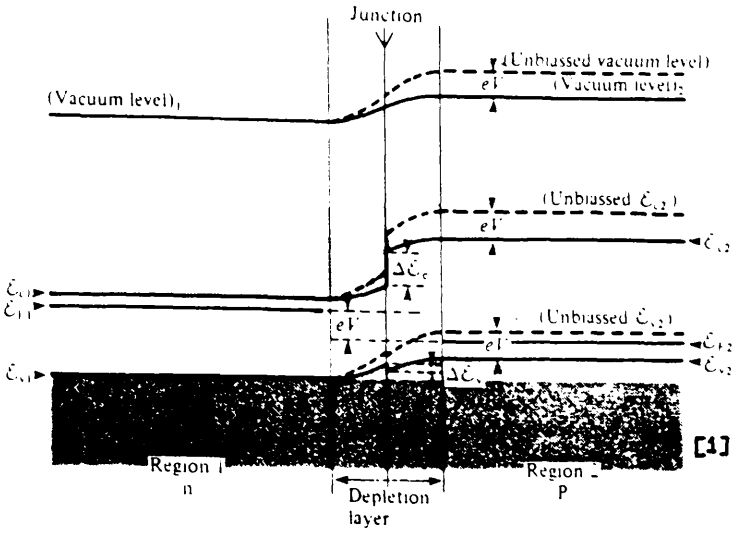

Gain Profile

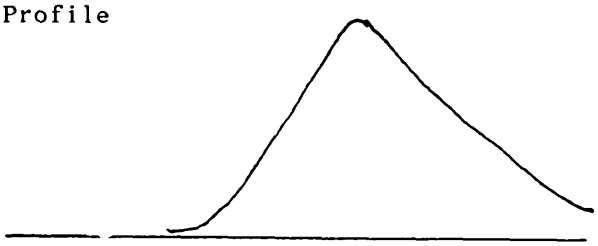

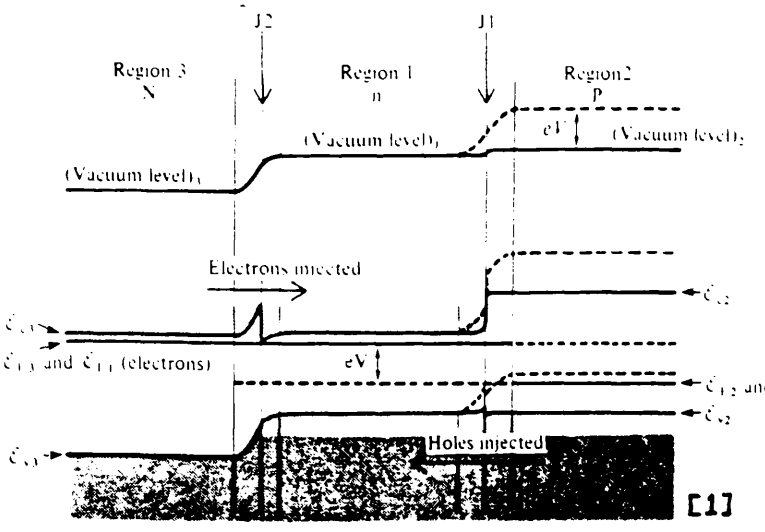

Gain Profile

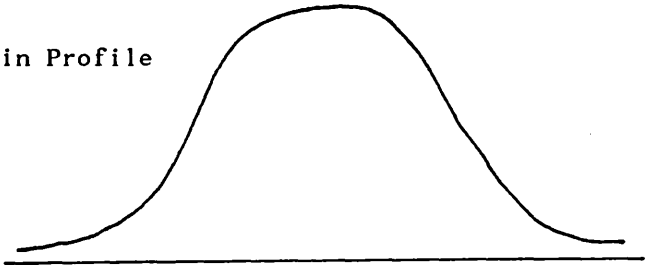

Figure 3.3 : Laser Diode Gain Profile.
a. Homostructure Device.
b. Heterostructure Device.

on the geometry of the diode structure. These features will also determine the spectral band of frequencies (linewidth) over which the diode will lase. The lineshape of the semiconductor laser may be predicted using the classical description derived by Schawlow and Townes [2]. This description does however predict that the linewidth is Lorentzian in shape. Observations of the beat spectrum linewidth between two semiconductor lasers, and of one laser correlated with a delayed portion of its own oscillation, have shown a departure from the pure Lorentzian shape [3,4]. Furthermore, this classical description of the laser lineshape also predicts a linewidth which is some 20–50 times narrower than that which is generally observed. Explanation for these departures from the classical solution has been attributed to the fact that the laser phase noise power spectral density is not flat. In particular, resonance peaks at the relaxation oscillation frequency of the diode have been pinpointed as being the root of a substantial linewidth broadening [5,6,7]. The injected carrier density undergoes a relaxation oscillation to restore the steady state field intensity after it has been perturbed from the equilibrium state by a spontaneous emission event. The result of this is a fluctuation of the the refractive index of the lasing medium and a corresponding change in lasing frequency. The semiconductor laser oscillation is thus better described by a modified version of the Schawlow–Townes expression [5,6,7].

$$\delta\nu = \frac{h\nu v_g^2 n_{sp} \ln(1/R_m)^2}{8\pi P_o \eta L^2} [1 + \alpha^2] \quad \text{Hz.} (3.2)$$

ν = Lasing frequency,
v_g = Group velocity,
n_{sp} = Spontaneous emission factor,
P_o = Output Power,
R_m = Mirror Reflectivity,
η = Quantum efficiency.
L = Cavity length.

The factor α, known as the linewidth enhancement factor, is the ratio of the imagianary to real part of the refractive index. In general α takes a value between 2 and 6 [5,6,7].

Typical linewidths for Channel Substrate Planar (CSP) laser structures are in tens of MHz. These values represent the best that has been achieved with free running sources. Sources with this magnitude of linewidth are however generally not suited to phase sensitive coherent transmission schemes.

Alternative laser structures have been developed in order to improve the frequency stability and reduce the linewidth. Particularly promising are the Distributed Feedback (DFB) [8,9] devices (see Figure 3.4). The DFB laser relies a cumulative feedback effect from an epitaxial grating adjacent to the active region to achieve sufficient gain for lasing to take place. The use of this grating also effects the selectivity of the lasing frequency. Side modes (due to the imperfect elimination of Fabry Perot resonances at the cavity ends) are typically suppressed to the order of 35 dB. Modifications of the DFB structure, such as the $\lambda/4$ shifted grating, are under investigation as they select single mode operation [10]. However DFB devices generally have broader linewidths than has been achieved to date with CSP structures (typically 10–100 [s] of MHz). The manufacturing processes are however relatively immature.

In an attempt to reduce the nonlinear effects in the FM characteristics of the laser diode (see section 3.4.3) the cleaved coupled cavity (C^3) laser diode [11] (see Figure 3.4) has been investigated. This arrangement makes use of two lasers, grown on the same substrate, separated by a small gap ($M\lambda/2$ where M is an integer). One laser is biassed above threshold to provide the lasing action. The other laser is biassed below threshold but sufficiently high that losses are minimised. Variation of the carrier density in the under–biassed section performs the frequency modulation of the diode emission. Devices with this structure have however been shown to be very sensitive to the dimensions of the gap length [11].

3.3 Line–narrowing Techniques.

Operating linewidths of tens of megahertz present considerable problems in the design of coherent transmission schemes. Numerous methods for reducing these linewidths have therefore been investigated.

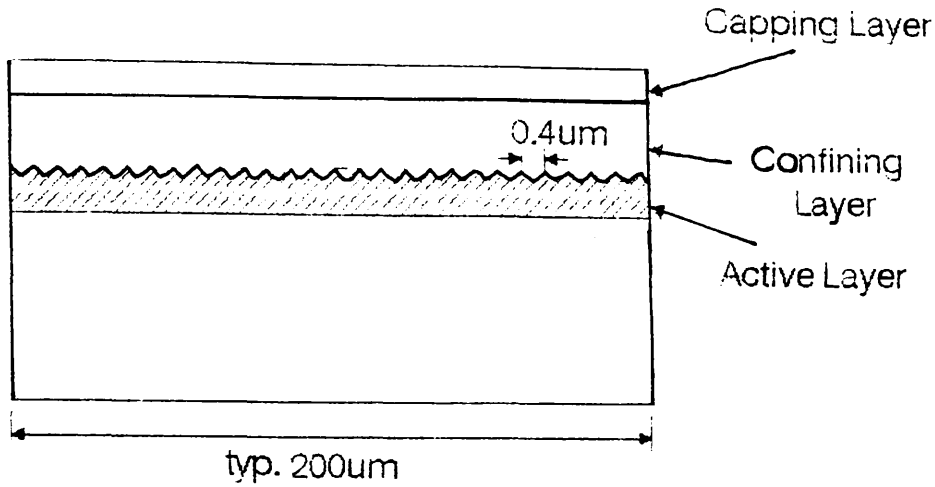

DFB Laser Diode

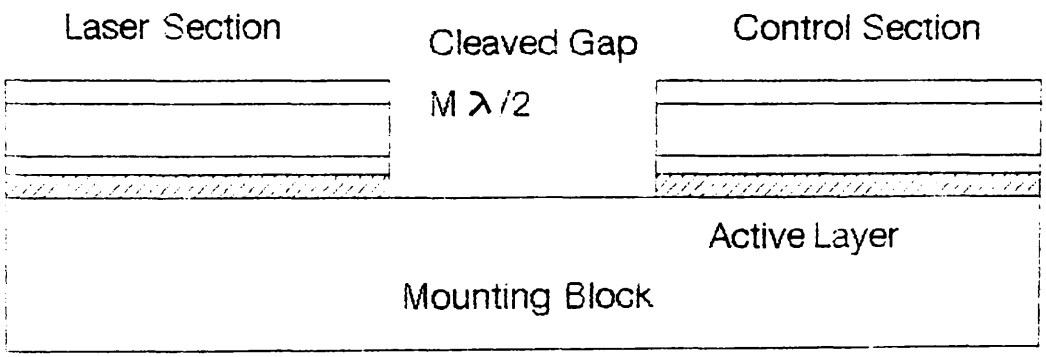

Cleaved Coupled Cavity Laser (C^3)

Figure 3.4 Alternative Laser Structures

A substantial amount of theoretical analysis, as well as experimental realisation of these techniques, has been reported [12–49]. It is the practical considerations of these techniques which are of particular interest to this project in order that a suitable source for systems experimentation may be constructed. A brief description of these techniques will now be given.

The use of negative frequency feedback methods to lock the centre–frequency of the semiconductor laser to a more stable reference *eg* a Fabry Perot discriminator or an absorption peak, are well known [12,13,14]. Such a stable reference may also be used to provide a means of extracting information relating to the relative magnitude and frequency of the phase noise components that influence the laser linewidth. Sufficient information may thus be obtained to allow a feedback signal to be applied to counter–modulate the frequency fluctuations and allow a reduction in the oscillation linewidth to be observed. The use of a Fabry Perot etalon as a discriminating element has provided some success in this area [15]. Similar schemes to this rely on heterodyning a 'noisy' laser oscillator with a narrower linewidth master oscillator to provide the necessary information for line–narrowing to be achieved. This technique has also been successful in correcting the non–linear response of a semiconductor laser under direct frequency modulation [16,17,18]. Furthermore, it provides a means whereby direct current phase modulation can be achieved (see Figure 3.5). The success of these feedback techniques depends upon the bandwidth of the feedback loop. Wider loop bandwidths should, in theory, enable more of the phase–noise components to be tracked out and hence provide a greater amount of line narrowing. The loop bandwidth will also determine the maximum modulation rates of a FM, or PM, transmitter. The limiting factor in loop bandwidth is the propagation delay [49]. It is essential therefore for systems of this nature to employ large scale integration techniques. Linewidth reductions to 1 MHz have been reported using these feedback techniques.

In addition to the standard, control type, feedback arrangements extensive research has been carried out into coupling the laser oscillation to an external cavity. Laser oscillation thus becomes

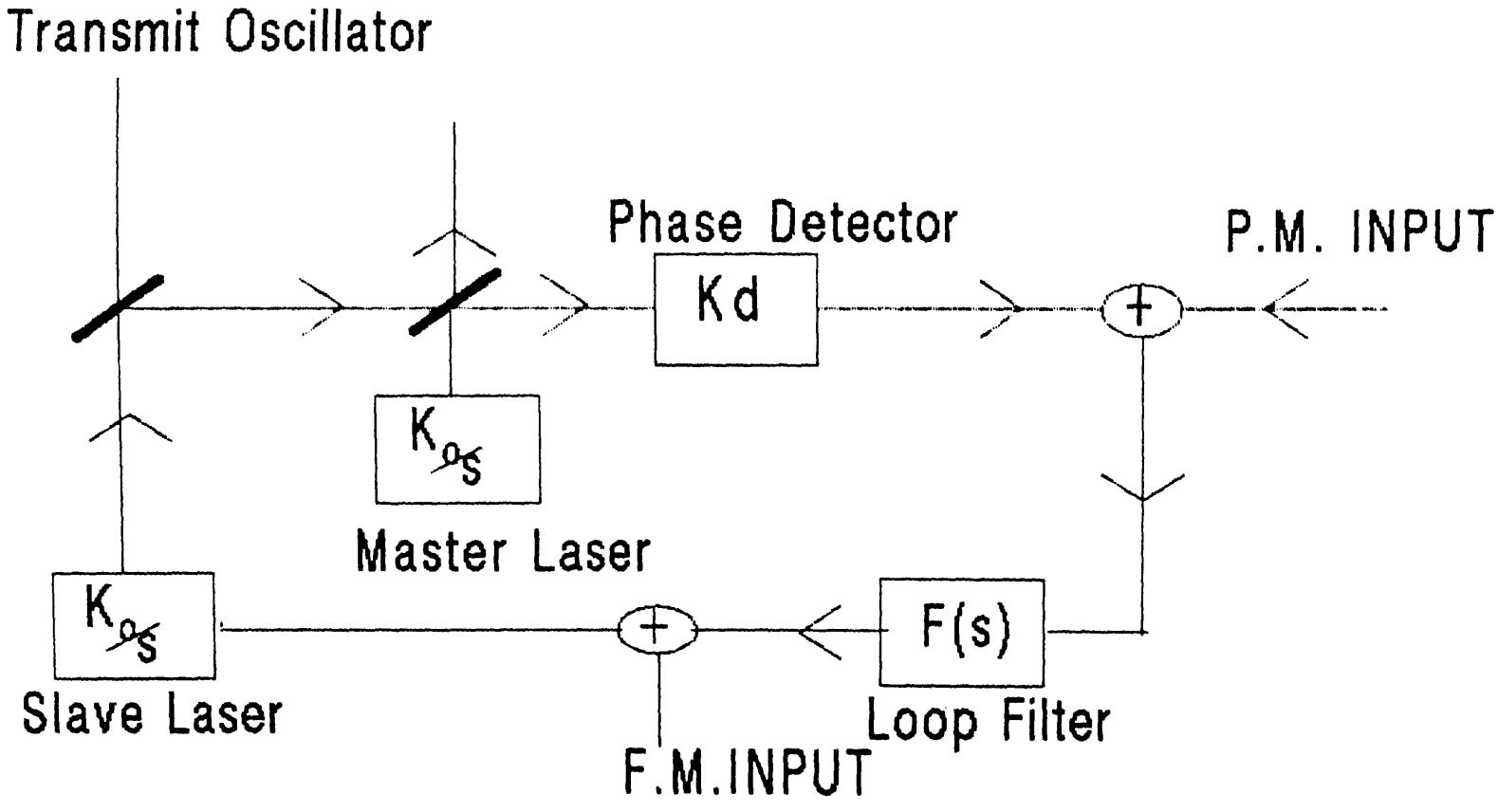

Figure 3.5
Electrical Feedback Arrangement for Linewidth Reduction, Compensation of Laser F.M. Characeristics or Direct Phase Modulation via the Injection Current.

dependent on the satisfaction of the phase conditions at the external reflection boundary. The effective cavity length is thus enlarged and the cavity finesse correspondingly increased. Lasers coupled to external resonators in this manner come under two classifactions: coupled– cavity laser diodes and external– cavity laser diodes. External– cavity oscillation requires that sufficient power is fed back from the external mirror to support lasing action without the aid of the cavity /air boundary relection. In the coupled– cavity arrangement the level of optical feedback is relatively low; lasing action is dependent upon phase matching at both the external and internal reflection boundaries. The conditions for oscillation under this type of feedback can be described thus [25].

$$\omega_0\tau = \omega\tau + X/(1 + \alpha^2)\sin(\omega\tau + \varphi) \qquad (3.3)$$

where ω_0 is the center frequency of oscillation, ω is the instantaneous frequency and τ the external cavity round trip time, α is as previously defined. The factor X is proportional to the ratio of the external to internal cavity round trip times. φ is the instantaneous random phase excursion due to a spontaneous emission event and is equal to arctan α (α is as previously defined). Coupling the laser oscillation to an external cavity results in a linewidth reduction by a factor of approximately 1 + X.

A number of experimental variations of this arrangement have been investigated. Figures 3.6 and 3.7 show some specific examples. The simplest of these makes use of the Fresnel reflection from a flat piece of glass to provide weak optical feedback. The glass mirror may be positioned at a distance of a few millimeters to tens of centimetres from the laser diode and the reflected light directed back into the active medium. Linewidths of hundreds of kilohertz have been reported using this technique [28]. However, arrangements of this nature are readily upset by accoustic disturbance. Experiments have also been executed using reflective coatings on graded index (GRIN) lenses to implement short external cavities. The GRIN lens cavity is shorter and simpler (the lens would be necessary for collimation in any case) and is therefore likely to be more reliable. Problems arise however, when the optimum distance for feedback and the optimum collimation

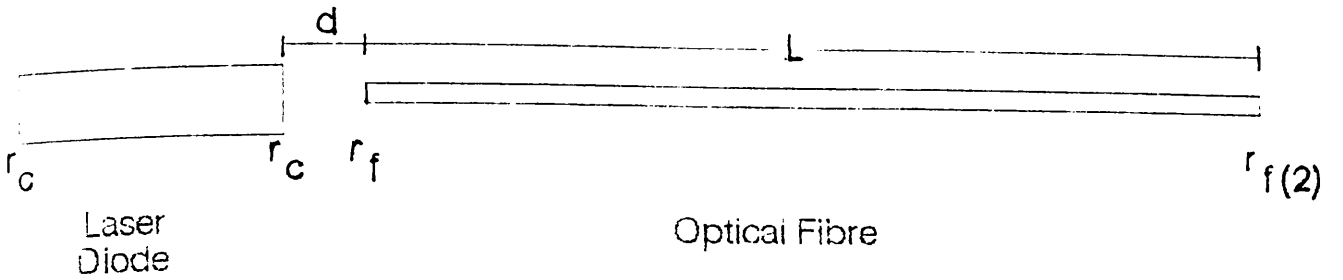

Schematic of Four Facet Fibre Cavity Laser Module.

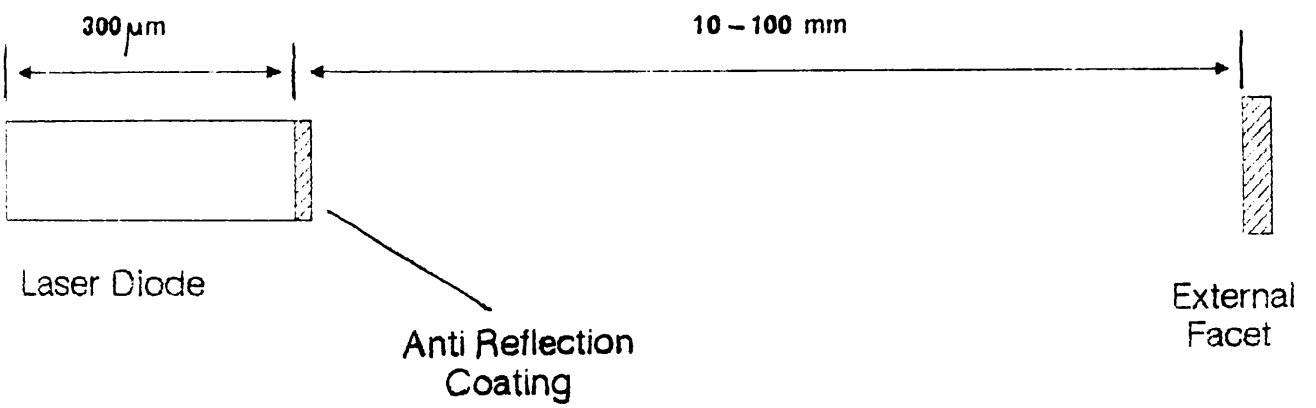

L aser Diode in External Cavity.

Figure 3.6
Laser Diode Coupled to External Cavity.

GRIN Lens cavity

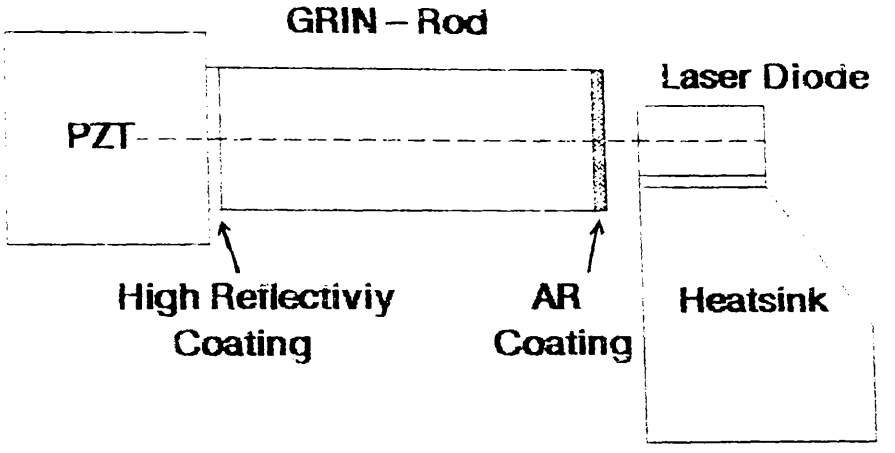

Integrated Passive Cavity

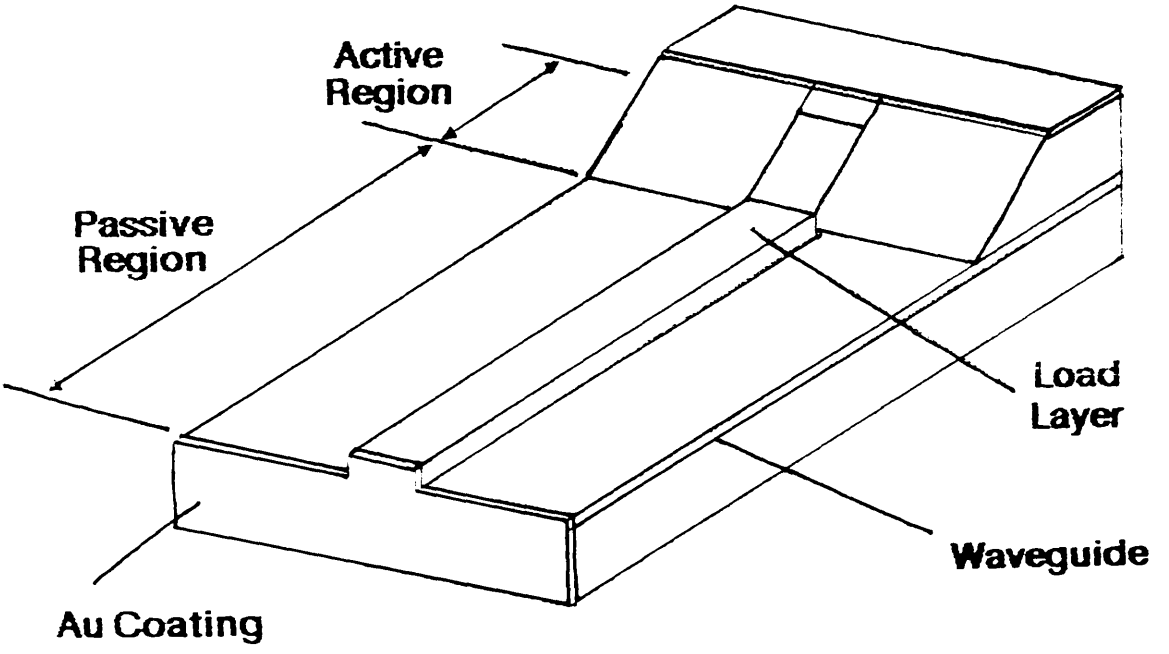

Figure 3.7 External Cavity Arrangements

distance do not exactly coincide. Submegahertz linewidths have thus far been achieved [45]. The idea of using short external cavities has been further investigated with the use of short passive cavities on the laser substrate [44]. This form of integrated structure would be expected to out perform other external arrangements in terms of tolerance of acoustic effects in the working environment. To date linewidths of 900 kHz have been reported for this configuration.

The use of coiled lengths of monomode optical fibre has shown promise as a technique which allows long cavity lengths to be obtained over short distances. Thus a compound cavity laser diode which is compact, but retains all the advantages of a long cavity length, may be manufactured. Furthermore the external cavity in fibre form can be potted for increased acoustic isolation and thermal stabilisation. Favre *et.al.* [21,22] have reported linewidths of better than 30 kHz using this approach. Further experiments have been carried at Plessey Caswell UK using fibre cavities with diffraction gratings etched into the fibre to enhance frequency selectivity yielding linewidths of narrower than 3kHz [29].

The complication of having more than two reflective boundaries in a laser arrangement can be eliminated with the use of antireflection coatings on one of the laser facets. With the reflection from one facet eliminated, the laser itself can be considered as a gain medium which provides the input power for lasing action to be achieved. A relatively high level of feedback is therefore required from the external reflector.

In a perfectly antireflection coated laser it should be possible to increase the laser drive current infinitely without lasing taking place. In practice however, sufficient gain is achieved that even with vast reductions in the facet reflectivity (to lower than 0.5%) lasing will occur at currents of the order of 1.3 times the threshold of the uncoated device. Experimental arrangements using AR coated diodes with facet reflectivities of less than five percent have produced arguably the best results to date.

In the external cavity configuration the effective linewidth is

described by [5,6,7]

$$\delta\nu = \delta\nu_o . [L_a^2 . n_{ga}^2 / l_p^2] \qquad (3.4)$$

where $\delta\nu_o$ is the free running linewidth of the diode, the subscripts p and a refer to the passive and active portions of the cavity. n_{ga} is the refractive index of the active layer. With the use of mirrors or diffraction gratings to impliment the external reflector, linewidths of less than ten kilohertz have been achieved [23,29]. The diffraction gratings have provided the additional benefit of making these external cavity diodes highly tunable over ranges exceeding 50 nm [19,20].

It is obvious, from this very brief survey of line narrowing techniques that a substantial amount of research has been carried out in this area. A number of these ideas were investigated during the course of this project. These experiments, together with experiments aimed at evaluating the source tunability and modulation characteristics, will be detailed in the following sections.

3.4 Experimental Laser Diode Source: Hitachi HLP 1400.

3.4.1 Device Description.

The choice of a suitable experimental laser diode source was influenced by a number of factors. Stable, single mode oscillation was required. In addition, it was necessary that two independant lasers be matched in wavelength to a suitable degree (< 5nm) where they could be made to beat without the need for excessive temperature and current differentials. The amount of optical power available at the front facet of the devices was not envisaged to be a particular problem as most commercially available devices were capable of delivering a few milliwatts of optical power.

The Hitachi HLP 1400 laser diode package was seen to fulfil the above requirements and, at the outset of the project, was in reasonable availability (delivery times of 3–6 months were typical). A number of these were purchased. A matched pair of Hitachi HLP 1600 laser diodes (a 1400 equivalent in a sealed package) was also

obtained. In later experiments a diode, manufactured by Sharp, provided with an AR coating on one facet was also made use of. In the main however, experiments were based around the HLP 1400. This diode is a GaAlAs/GaAs device lasing at approximately 825 nm. Although this wavelength was clearly outwith the mainstream activities, which tended to be geared toward the low loss window of 1.5 μm, it was decided that this would be the most suitable source. 1.5μm GaInAsP lasers were not as readily available, tended to support more than one longitudinal mode of oscillation and were more expensive.

The HLP 1400 GaAlAs/GaAs diode is of Channel Substrate Planar (CSP) construction. The device has dimensions of 300μm by 200μm by 100μm. It is mounted p−side down on an interface block which provides a thermal contact and an amount of stress relief between the diode and the brass heatsink mounting (see Figures 3.8−10). The active layer of the diode is approximately 4 μm from the surface of the interface block. Output coupling of light is efficiently achieved at the front facet where the diode is mounted flush with the front face of the interface block. The back facet of the diode is inset approximately 700μm from the back edge of the interface block rendering efficient coupling of light from the back facet difficult. This proved to be a major drawback in using the HLP 1400 diodes.

3.5 Characterisation of the HLP 1400 Laser Diode.

3.5.1 Current Power Characteristics.

On initial receipt of the HLP 1400 diodes the ouput was measured as a function of the laser bias current in order that the manufacturer's data could be verified. Plots of these characteristics are displayed in Figure 3.11 for a number of devices. At bias currents greater than 1.3 times the threshold current the lasing spectrum was observed to be essentially monomode (side mode suppression was typically 30 dB).

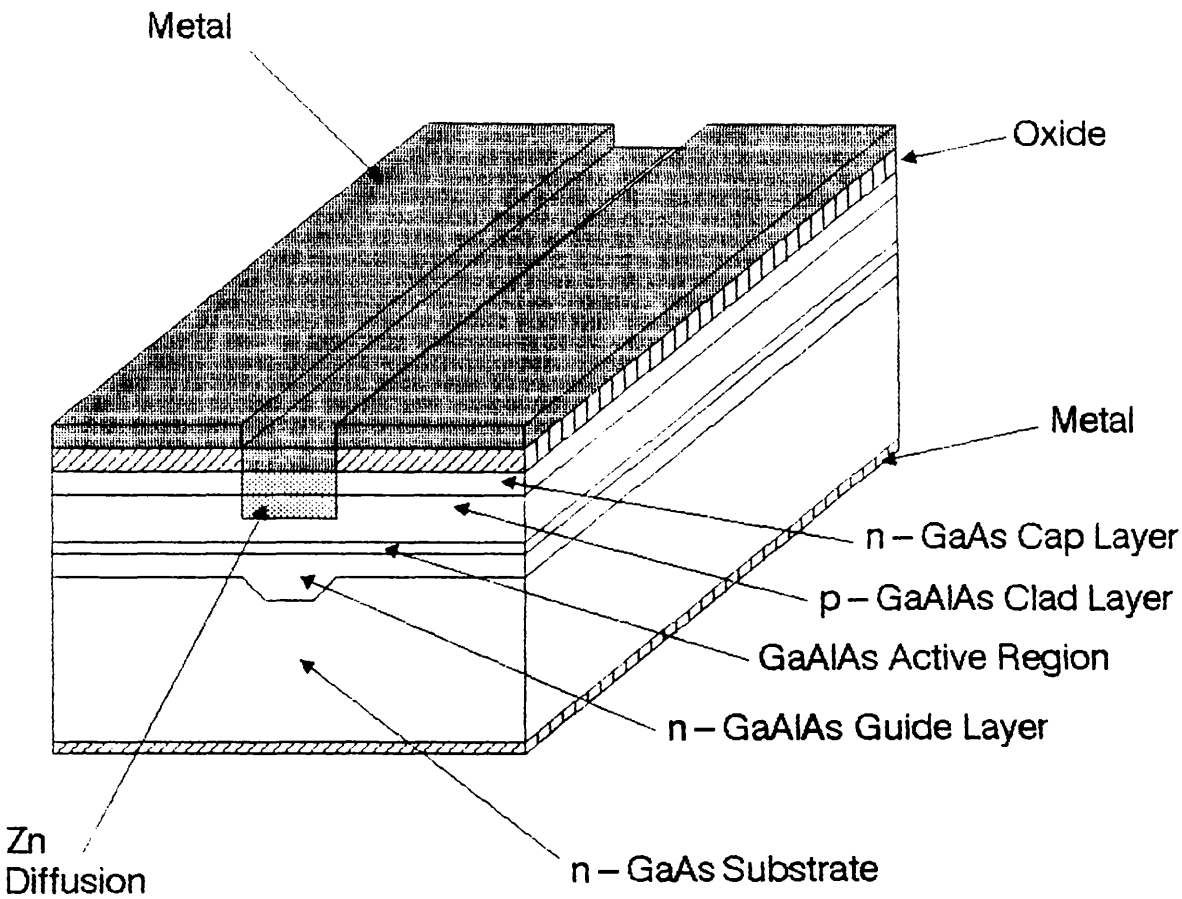

Figure 3.8

Schematic of an HLP 1400 AlGaAs Laser Diode.

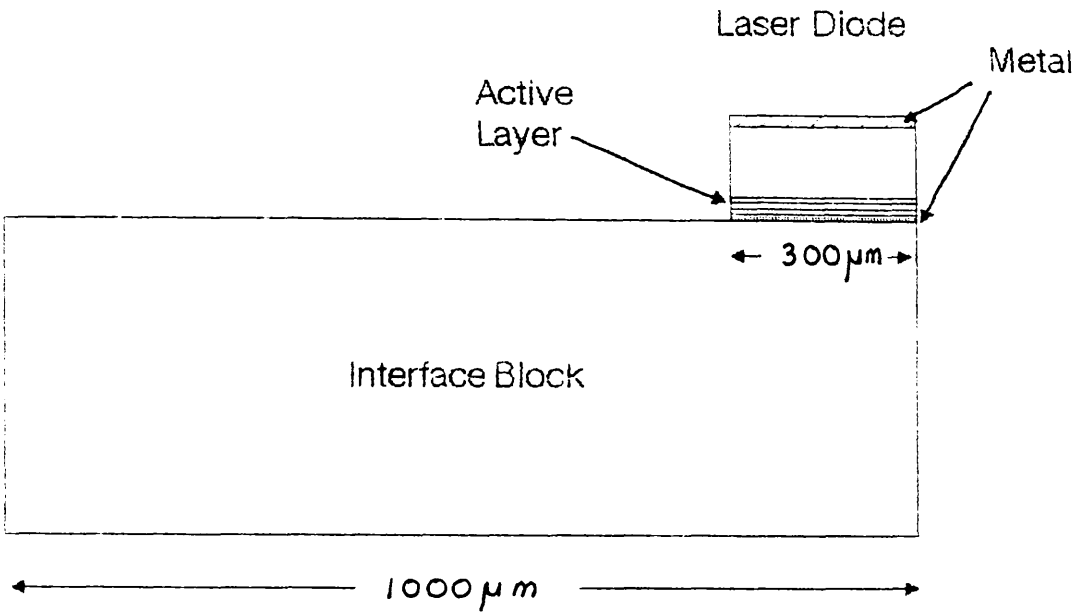

Figure 3.9
Hitatchi HLP 1400 Laser Diode Relative Dimensions.

Figure 3.10
Hitachi HLP 1400 Laser Diode
as Received from Manufacturer.

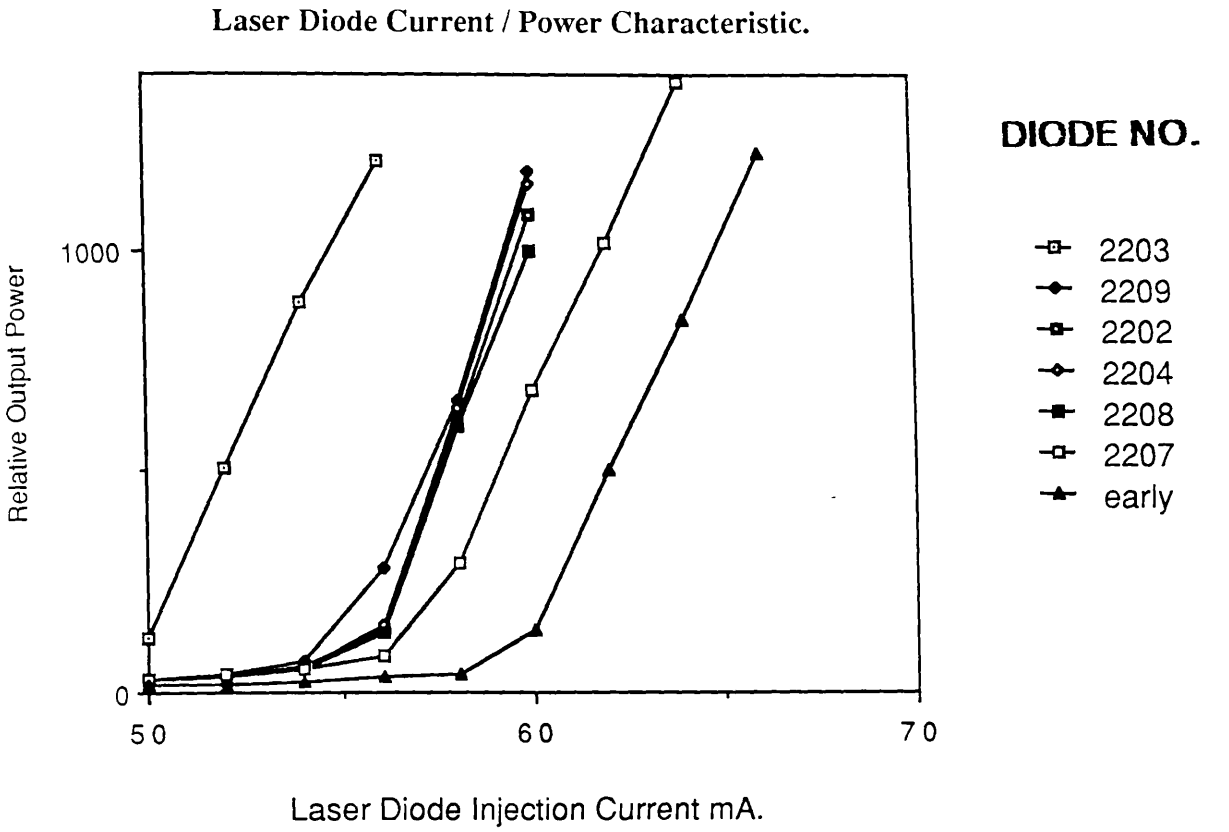

Figure 3.11
HLP 1400 Power/Current Characteristic

3.5.2 Absolute Wavelength Measurements : Current and Temperature Tunability.

The execution of any coherent experiment using two independant sources requires that an intermediate frequency beat note be obtained. It is necessary therefore to obtain an absolute measurement of the centre frequency of oscillation. Diodes which are sufficiently well matched in wavelength (within 5nm) can, in theory, be tuned through the use of current and temperature control to sufficiently close proximity that the beat note can be detected. The present section will outline the experimental arrangement used to make absolute measurements of the laser frequency of oscillation.

The lasing wavelength was measured using the arrangement shown in Figure 3.12. The laser output was coupled into a Rank Hilger Monospec 100 monochromator using a x40 microscope objective. The monochromater incorporated a diffraction grating of 1200 lines/mm and had a 2m optical path length. Focussing the laser emission down through the input slot ensured that the light was sufficiently dispersed to cover the entire grating surface (thus maximising the experimental resolution). The resolution of the setup was 0.1 A. The output of the monochromator was detected on a charge coupled array and displayed on an oscilloscope.

The scanning Fabry–Perot Interferomter (FPI) was kept in position throughout the course of the measurement to confirm that oscillation was stable. At all times during the experiment the temperature of the laser module was regulated to within $0.01^{o}K$. This was achieved with the use of a temperature control system as described in Appendix 3.1. The effects of unwanted optical feedback were gaurded against with the use of an optical isolator contructed using a polaroid film and quarter wave plate. The isolation thus achieved was found to be around 10–15 dB. If careful attention was paid to the equipment alingment then this level of isolation was found to be sufficient.

Typical distributions of the current versus wavelength characteristics of the laser diodes are given in Figures 3.13–15. Only

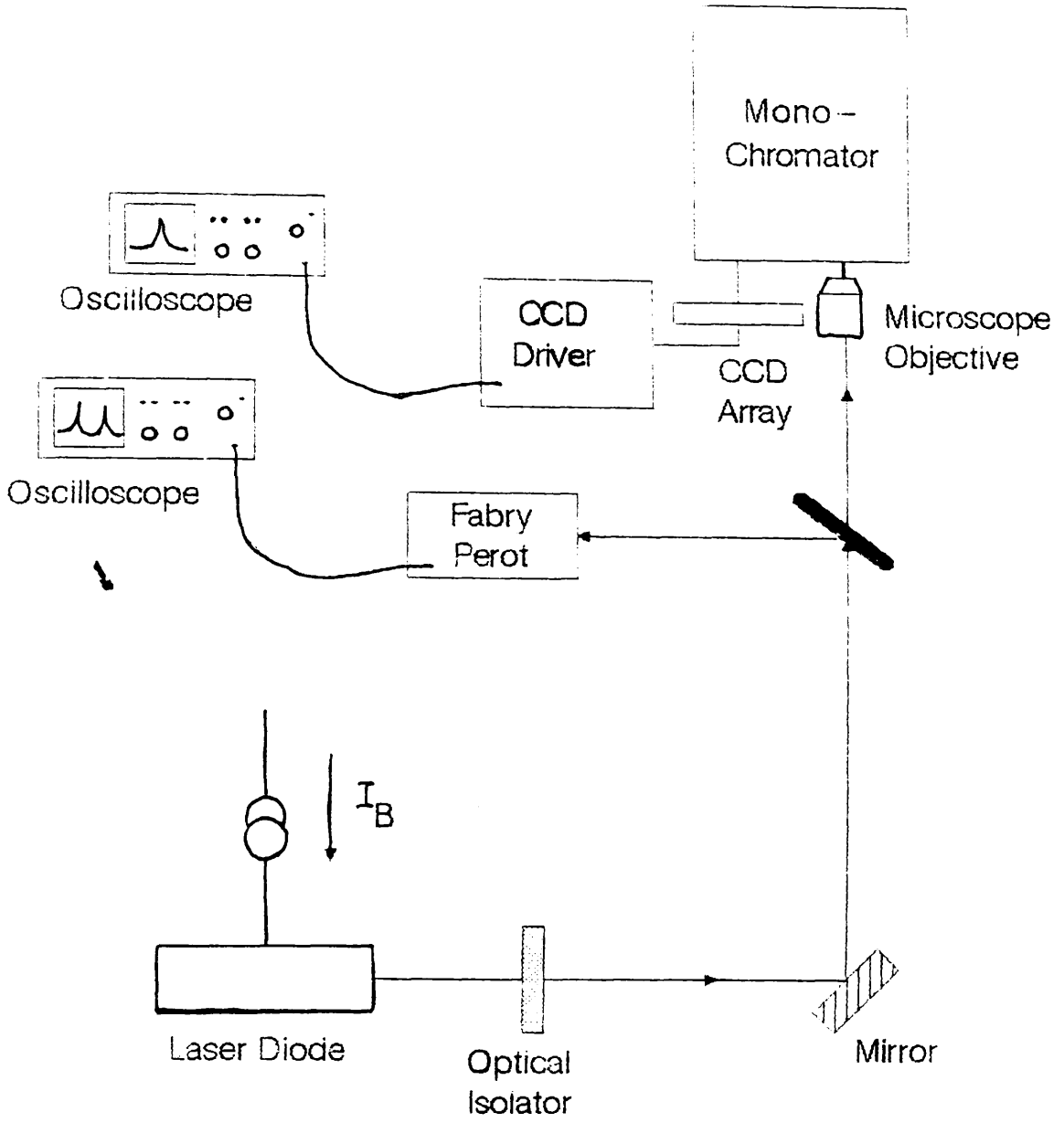

Figure 3.12
Absolute Wavelength and Modal Stability Measurement. Experimental Arrangement

one diode is seen to exhibit continuous tuning over the entire range of bias currents (see Figure 3.13). Figures 3.14 and 3.15 display a more typical response.

Lasing action was generally found to take place on one stable longitudinal mode. It was possible to tune the lasing frequency over a short range within that mode by varying the injection current. A situation of instability was then reached as the gain profile shifted and closely related modes competed for domination. Oscillation would then jump onto the most stable of these modes. All diodes measured in the above experiment were found to have particular current levels where lasing was found to be significantly more stable than at other positions.

This phenomenon of mode–hopping poses considerable problems when attempts are made to extract a beat note from two diodes. Two, apparently well matched, laser diodes can in practice be found to have stable modes of oscillation which do not overlap. The problem is compounded by the fact that a hysteresis is observed in the tuning characteristic. This hysteresis is indicated in the given figures by the arrows showing the direction of the current tuning. The diode may be seen to hop from one stable mode at a given current but may not necessarily jump either back to the mode that it came from or, if it does, may not return at the same value of current. Within the resolution of the experiment the mode–hopping was seen to occur at integral multiples of the cavity length (c/2nL).

It was observed during the course of the experiment that the characteristics were very susceptible to the influence of unwanted reflections of light into the lasing medium. Sufficient optical isolation was therefore required in order that consecutive traces were identical. Earlier modules were particularly sensitive to this form of corruption. The suspected cause of this was the GRIN lens and goniometric stage used for collimation. The goniometric lens positioner was found to have insufficient long term stability. Fractional changes in lens position, which were not sufficient to affect the overall collimation, were found influence the phase of the reflections coming from the lens modifying the modal characteristics. In later modules this problem

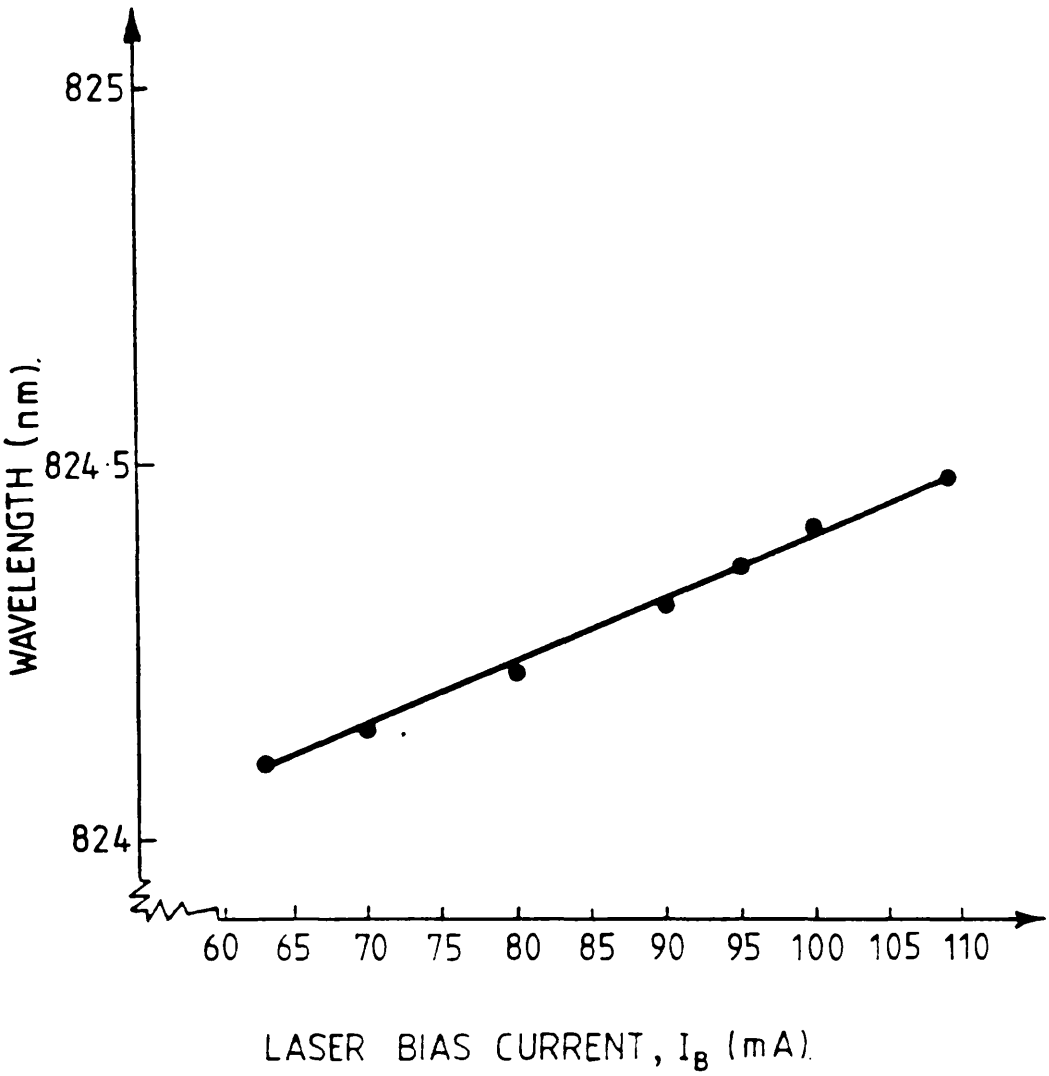

Figure 3.13
Wavelength versus Injection Current Characteristics for HLP 1400 no. 5E3072 Operating Temperature = 293.0 K.

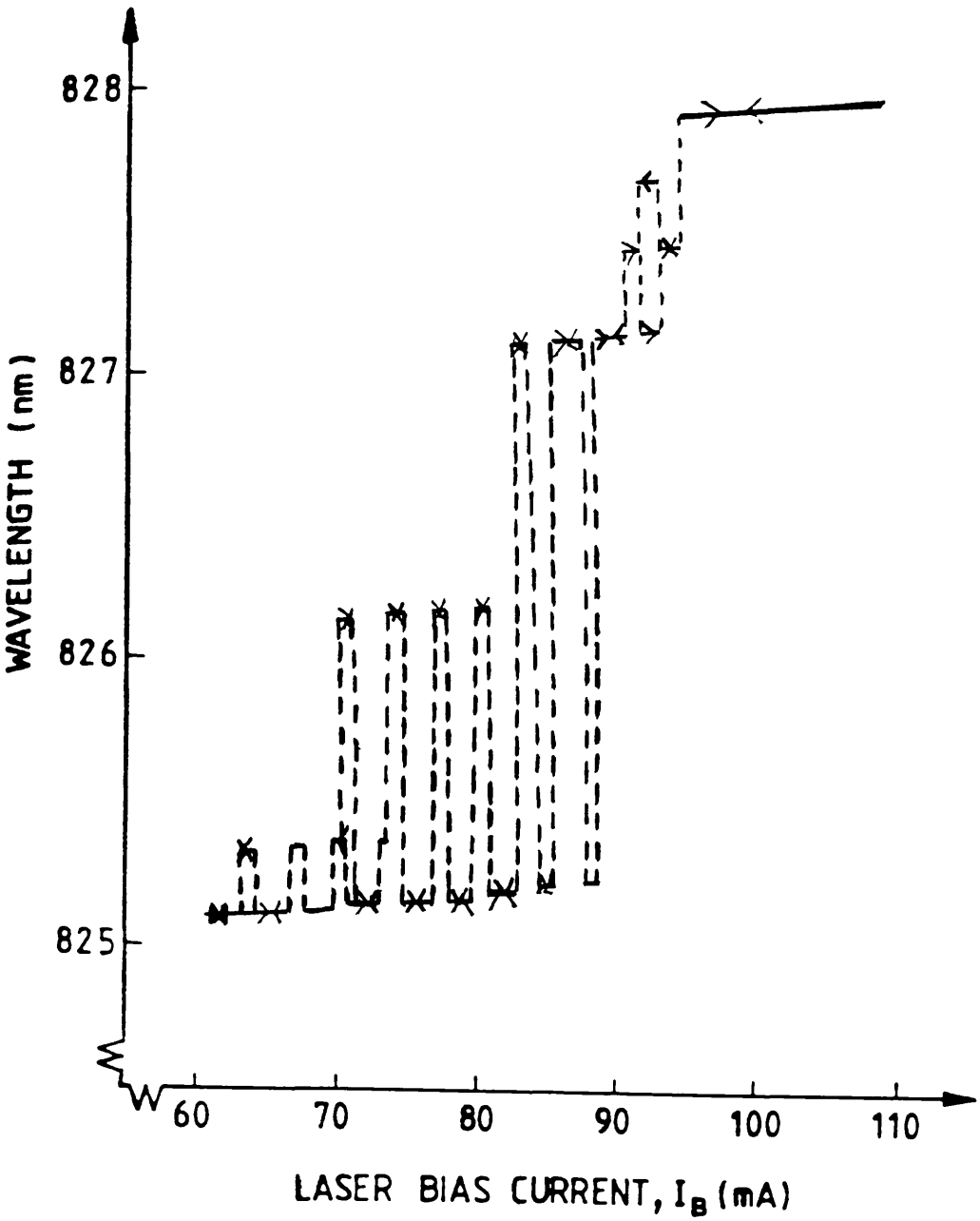

Figure 3.14
Wavelength versus Injection Current Characteristics for HLP 1400 no. 5E3070 Operating Temperature = 290.8 K.

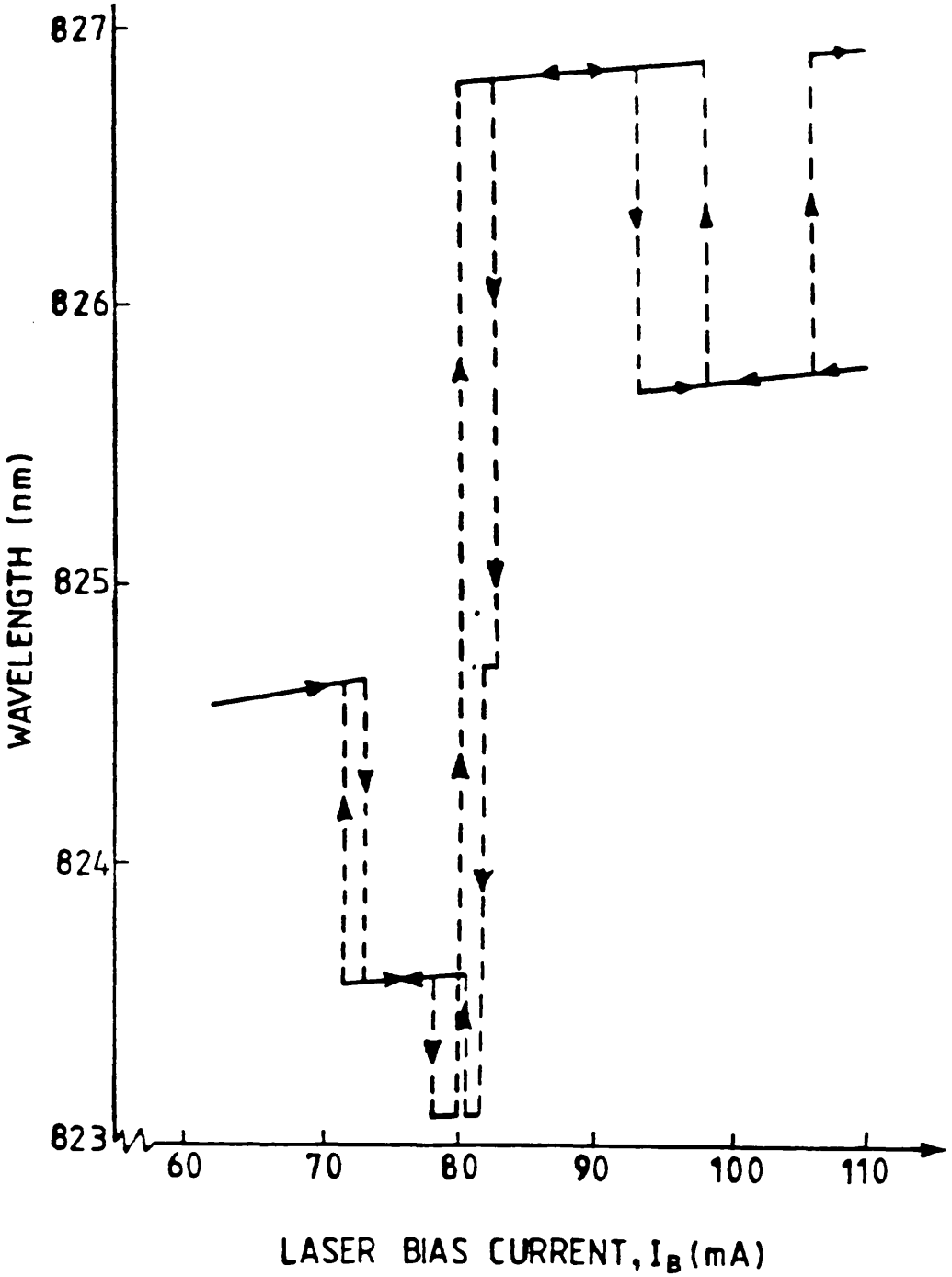

Figure 3.15
Wavelength versus Injection Current Characteristics for HLP 1400 no. 2M0861 Operating Temperature = 290.8 K.

was circumvented with the use of lenses with a more efficient anti– reflection coating.

The problems associated with tuning the diode centre frequency are clearly significant. While it is a relatively straight forward matter to tune the diode oscillation so that it approaches the frequency of another source to within a fraction of a nanometer, fine tuning beyond this point is more difficult. The substructure of the tuning range may dictate that diodes which are apparently well matched over a wide range of wavelengths do not lase on coincident stable modes. Therefore a beat note will not be detected. Despite these problems, sufficient tunability of the laser diodes was obtained with the use of temperature and current manipulation to obtain observable beats between a number of the lase sources. More details of this will be given in Chapter 7.

3.5.3 Laser Diode FM Characteristics.

To make effective use of a source in a communications experiment requires that the modulation characteristics of that source be known. In this project the major concern is the investigation of a phase locked loop using the laser diode. The FM response of the diode is therefore of particular relevance as it is used both as a transmitter and as a local oscillator. Stable construction of an Optical Phase– Locked Loop will require that any gain variation in the local oscillator with frequency is known. Details of this are given in later chapters.

Frequency modulation of the diode emission can be effected by varying the drive current directly. Two mechanisms, temperature and carrier density modulation, are involved. The overall response is a non linear modulation index variation with modulation frequency. This response has been described in detail in references 30 and 50. A brief resume of these report will now be given.

The low frequency modulation (<1MHz) behaviour is dominated by thermal considerations. Changes in the diode temperature, as a

result of a variation in the injection current, produce a cavity length expansion and a refractive index variation. Evaluation of this response requires consideration of the thermodynamics of the laser diode itself and the submount in the immediate vicinity. To a reasonable approximation the thermal response can be described by [50],

$$\frac{1}{f}\frac{df}{dt} = -\frac{1}{L}\frac{dL}{dt} - \frac{1}{n}\frac{dn}{dt} \qquad (3.5)$$

where f denotes the central oscillation frequency of the laser diode, L is the diode length and dL/dt a thermal expansion coefficient which for AlGaAs is approximately $0.6.10^{-5}$ K^{-1}. The second term on the right hand side of the equation accomodates the refractive index variation and takes the value of $0.99.10^{-4}$ K^{-1}. The combined effect of these two influences produces a frequency–temperature dependance of -38 $GHzK^{-1}$ at $\lambda = 825$ nm (this is higher than the average measured value for the Hitachi HLP 1400 diodes of -22 $GHzK^{-1}$). The thermal time constant of the laser is such that these values diminish as the frequency of operation increases. The thermal transient reponse time of the laser diode is of the order of 1 μs, giving a thermal cut–off frequency in the MHz regime.

The more complicated carrier density effect is also analysed by Kobayashi. In brief this dependance can be expressed as [50]

$$\frac{df}{dN} = \frac{f}{N}\frac{dn}{dN} \qquad (3.6)$$

where N is the carrier number density. This gives rise to a current frequency dependency of 0.05 GHz/mA. The carrier density effect on the FM characteristic is essentially flat up until the point where a resonance is observed at the relaxation oscillation frequency.

Experimental verification of these effects has been carried out using a scanning FPI and is shown in Figure 3.16. A typical trace of a measurement spectrum is shown in 3.17. The normalised modulation index is obtained from measurement of the drive current necessary to produce a modulation index of 1.5 (1st side–band equal in magnitude

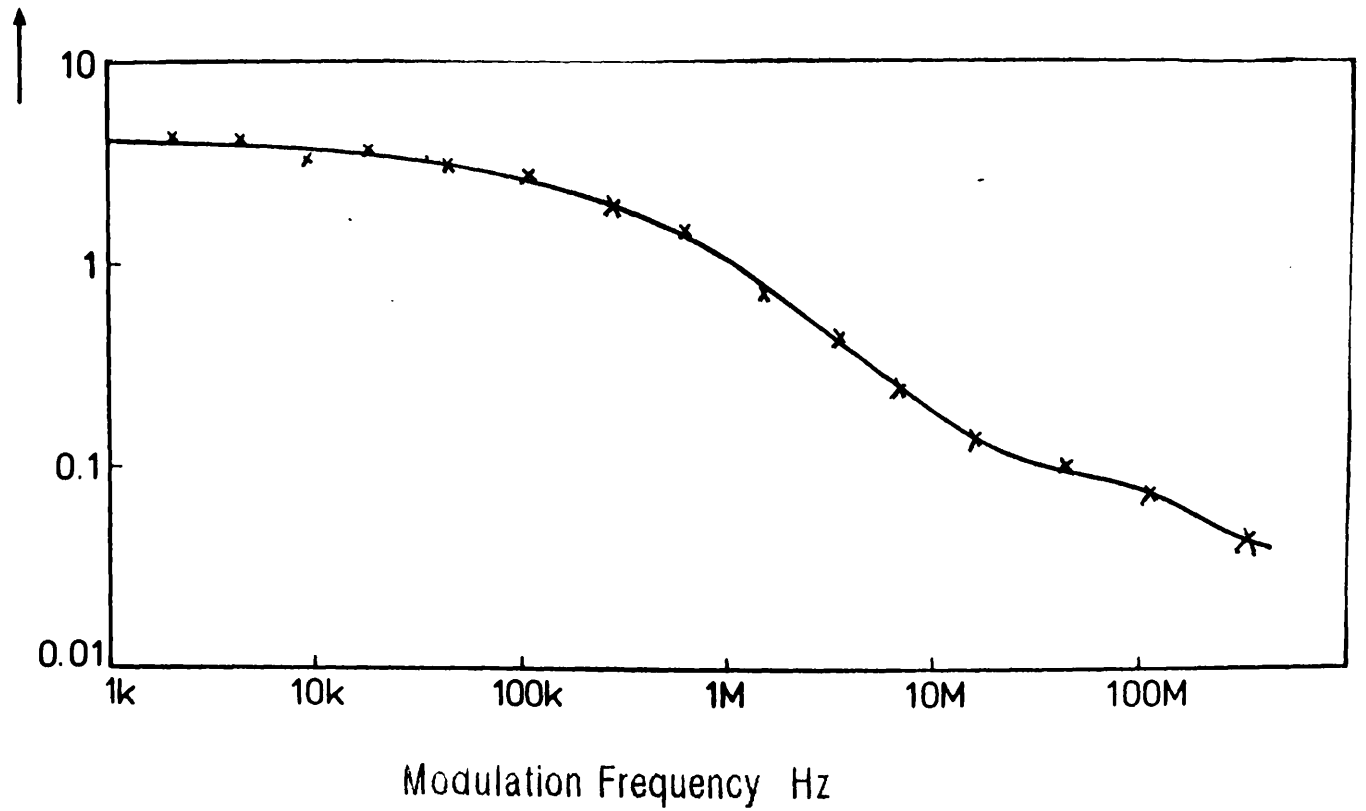

Figure 3.16 Maximum Frequency Deviation Versus Modulation Frequency for an HLP 1400 Laser Diode (5E0370)

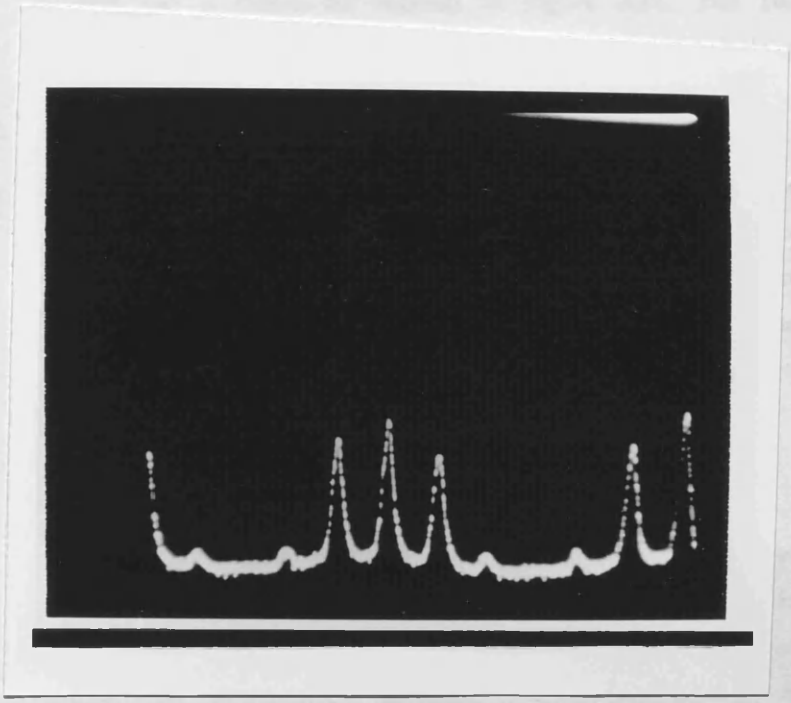

Asymmetry of
Side Band
Amplitude

FSR = 2GHz.

Carrier

Figure 3.17

FM Characteristic Measurement Example
Modulation Index = 1.5

to the carrier). The FPI trace shows an asymmetrical response in the modulation charateristc resulting from a combination of both amplitude and frequency modulation of the laser oscillation with injection current. Measurement of the FM characteristic was only possible up to a frequency of 900 MHz and therefore the resonance at the relaxation oscillation was not observed. The relaxation oscillation of the 1400 diode series was, in fact, never observed as it was outwith the bandwidth of the photo–diode response. The oscillation was observed however for the HLP 1600 diodes at low bias currents and is shown for interest in Figure 3.18. The 1600 diode is sold as being identical to the 1400 diode except that it is packaged in a sealed environment.

Figure 3.16 demonstrates the non linear characteristic of the modulation efficiency. It is important that this characteristic be considered when contructing an OPLL. The bandwidth of the loop must be restricted to below the cutoff frequency unless corrective action is taken to ensure that a more linear response is obtained.

3.5.4 Laser Linewidth Measurement.

One final property of the laser diode remains to be discussed: the emission linewidth. Measurement of the linewidth gives an indication of the magnitude of phase instabilities. Coherent detection formats are, by definition, sensitive to phase fluctuations. A knowledge of the levels of these variations in the laser oscillator is therefore required before the effect on transmission perfomance can be estimated. It is assumed that the distribution of the phase noise components in the laser oscillation is white. This assumption allows the level of phase noise, and the effect it will have on a communication system performance, to be directly deduced from measurement of the laser linewidth. It has been shown by Armor [51] that this assumption further leads to the description of the relative phase instabilities of two independent laser sources having a weighted dependency toward the low frequencies. The power spectral density of the relative phase instabilities is described by [52]

$$S_{\delta\varphi} = \delta f/2\pi f^2 \text{ rads}^2/\text{Hz}, \quad (3.7)$$

Reference Level

Marker Freq.

Horiz. Scale MHz/div

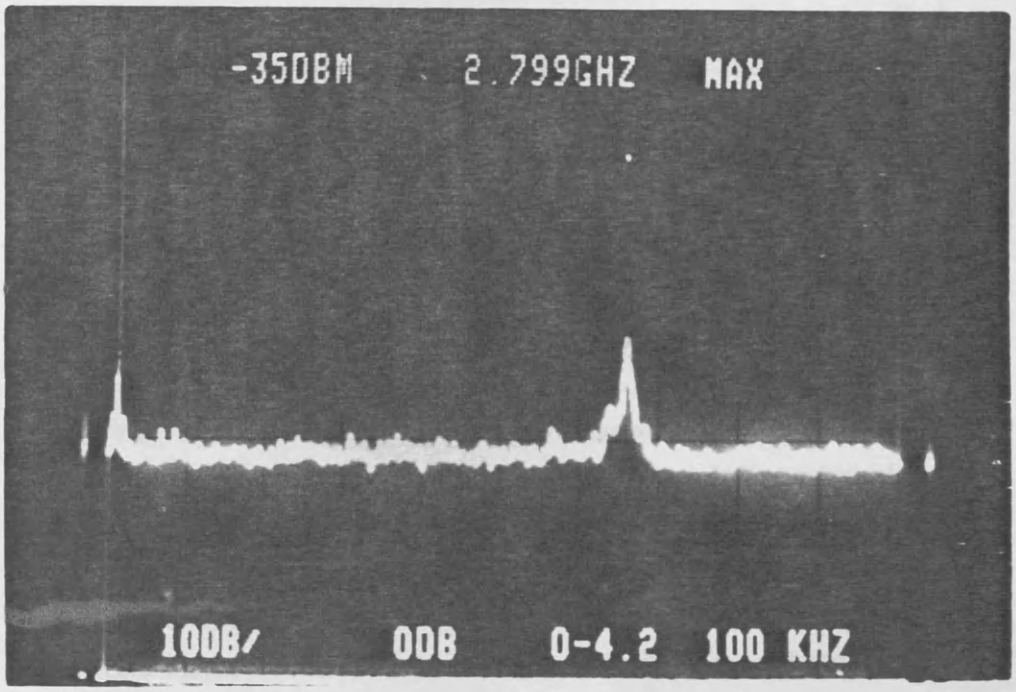

Vertical Scale dB / Div

Input Attenuation.

Freq. Span GHz

Resolution Bandwidth

Figure 3.18

HLP 1400 Laser Diode Relaxation Oscillation at 2.8 GHz.

where δf denotes the laser linewidth. Thus, if the laser linewidth is known then sufficient data will have been obtained in order that the effect of the laser phase noise on the performance of a communications system may be deduced.

Evidence has been presented by Ries *et.al.* [52] indicating that the linewidth measurement, depending on how it is performed, may conceal information such as narrow band peaks in the phase noise spectrum which may be a further source of degradation. The particular measurement technique in question is the self– heterodyne, or homodyne, as proposed by Okoshi *et.al.* [53]. It is the self– heterodyne method that was used in the experiments described below. While it is true that this method may be transparent to certain peaks in the noise spectrum (if they occur at integrals of the delay time), it was felt that these noise sources were unlikely to be present in a working system and therefore no attempt was made to account for them.

3.5.5 The Self Heterodyne Measurement Technique.

The self– heterodyne, or homodyne, technique for laser linewidth measurement is a modification of the heterodyne principal of detection. Heterodyne detection offers high resolution measurement of the frequency spectrum of a source, provided that a stable source, of known linewidth, can be found close enough in frequency to the test sourceto allow a beat frequency to be detected. Although the sensitivity of such an experiment is excellent, it is also difficult to perform and can readily be adversely affected by relatively low levels of disturbance. Poor intermediate frequency stability can degrade the experimental resolution, resulting in the beat spectrum measured appearing broader than the combination of the two linewidths. This problem may be avoided if the test source is heterodyned with a portion of its own oscillation spectrum delayed in time. It is necessary then only to evaluate the effect of the delay time to coherence– time ratio on the photo– current at the detector of a partially correlated beat spectrum. This evaluation has been carried out by Gallion *et.al* [54] and Richter *et.al.* [55]. The main body of these analyses will be discussed at a later stage. First of all however the experimental

arrangement will be outlined (Figure 3.19).

The laser output was split into two approximately equal portions using a nominally 50/50 beam splitter. One half of the beam was coupled using Newport fibre coupling equipment into a 9km (45 μs delay) length of fibre. The remaining portion of the light was coupled into a $LiNbO_3$ acousto–optic Bragg cell. The Bragg cell consisted of a planar waveguide, manufactured by proton–exchange, on a $LiNbO_3$ substrate. Aluminium electrodes were laid at either side of the optical guide. These electrodes, when driven with a suitable RF source (+26dBm at 426 MHz), set up an accoustic wave across the guide. This diffracts, and frequency shifts, light coupled in at the appropriate (Bragg) angle. The maximum diffraction efficiency obtained was approximately 30%. An additional $\lambda/4$ plate was necessary at the input to the Bragg cell in order to rotate the polarisation of the light to TE orientation, consistant with the optimum efficiency of the Bragg cell. The polarisation had therefore to be re–oriented at the output of the cell to be consistent with that emerging from the fibre. Input and output coupling from the waveguide was accomplished through the use of Rutile prisms. The frequency shifted, first order diffracted, output beam from the Bragg cell was spatially aligned on a 50/50 beam splitter with the fibre output and combined on an ac coupled BPW 128 Avalanche Photo Diode (APD). The photocurrent due to the mixing of the two sources was detected, amplified by 26 dB, and displayed on a Spectrum Analyser.

Heterodyne detection of the signal was preferred over homodyne detection because it allows the complete beat spectrum to be observed. Spectrum Analysers tend to exhibit a degraded noise performance towards the low frequency end of the spectrum due 1/f which gives a rise in the noise floor which can lead to optimistic measurements of the diode linewidth. This problem can be compounded by the fact that APDs have a tendency to exhibit a 1/f type noise corruption at high bias levels. Additional confusion can arise from making linewidth measurements in a self homodyne arrangement if an ac coupled photodetector is used. The effect of the low frequency cutoff will have to be taken into account if it is not made sufficiently low. These problems are avoided if the beat spectrum is shifted well into the pass band of the detection system with the use of the Bragg cell. The

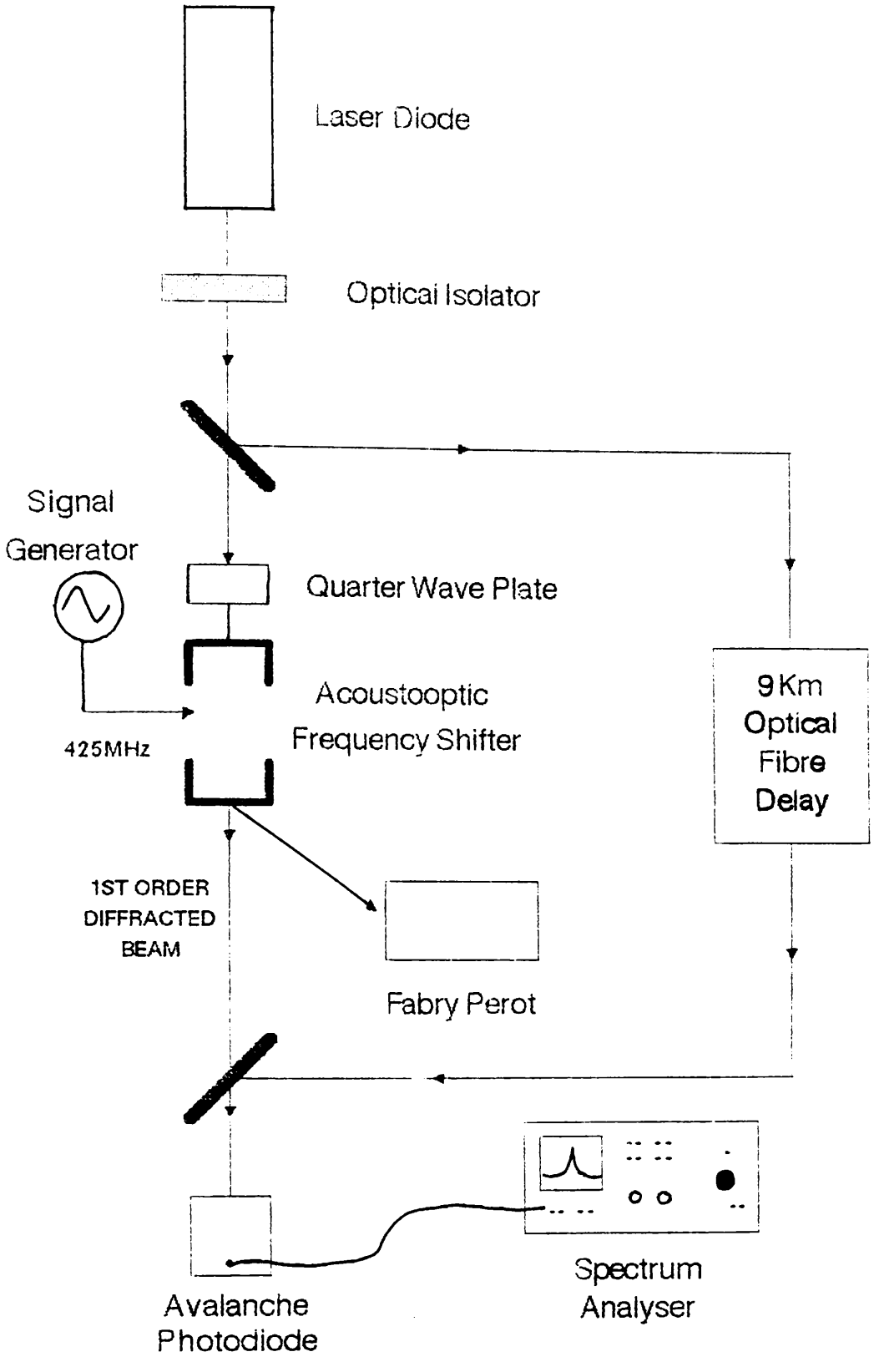

Figure 3.19 The Self Heterodyne Experiment.

drawback of using this arrangement is, however, that the necessary optical power required for each measurement is relatively high due to the inefficiency of input and output coupling of the Bragg cell. Typical insertion losses were of the order of 20–30 dB.

3.5.6 Evaluation of the Self Heterodyne Technique.

The self heterodyne correlation experiment will now be outlined. A more complete description can be found in references 55 and 56. The laser oscillation of a stable single mode laser with a non–zero linewidth can be desribed as,

$$E(t) = \mathrm{Re}\{E_o \exp[j(\omega_o t + \varphi(t))]\}, \qquad (3.8)$$

where ω_o represents the centre–frequency of oscillation and $\varphi(t)$ is a random process representing the phase and frequency–fluctuations which give rise to the finite laser linewidth. A representation of this nature leads to a Lorentzian description of the power spectral density of the laser oscillation as:

$$S_E(\omega) = \frac{E_o^2 \, \gamma/\pi}{\gamma^2 + (\omega-\omega_o)^2} \qquad (3.9)$$

where 2γ is the angular Full Width Half Maximum (FWHM) of the laser field spectrum as described by the Schawlow–Townes equation. The FWHM linewidth is also regarded as the inverse of the laser coherence time. Gallion [54] has derived an expression for the power spectral distribution of the instantaneous–photocurrent due to the combination of two partially correlated electric fields on a photodiode. The two electric fields can be considered as the composite field,

$$E_T(t) = E(t) + \rho E(t + \tau_o)\exp(j\Omega t). \qquad (3.10)$$

ρ represents the power coupling ratio between the frequency shifted field and the time delayed portion of the laser emmision. τ_o is used to denote the delay time and Ω the frequency speration between the two beams. The photocurrent spectrum is derived to be,

$$S_i(\omega) = \langle i\rangle^2\delta(\omega) + e\langle i\rangle/2\pi + \rho^2\langle i\rangle^2.\exp(-2\gamma\tau_o)\,\delta(\omega-\Omega) + \qquad (3.11)$$

$$\frac{\rho^2\langle i\rangle^2.2\gamma/\pi}{(2\gamma)^2+(\omega-\omega_0)^2}\left[1 - \frac{2\gamma\tau_o\sin(\omega-\Omega)\tau_o}{(\omega-\Omega)\tau_o} + \cos(\omega-\Omega)\tau_o\right]\exp(-2\gamma\tau_o)$$

The first two terms of 3.11 are not relevant to the determination of the laser linewidth. These represent the dc current due to the incident optical power on the diode and the corresponding random shot noise photo current. The third term in the expression describes the partial correlation which may exist between the two beams, depending on the coherence– time to delay– time ratio. The final contribution is the Lorentzian component of the spectrum. Provided that the delay time is sufficient, this part of the spectrum will be equal to twice the individual linewidths *ie* twice the linewidth of the laser source. Figure 3.20 demonstrates the effect of insufficient delay length on the observed photocurrent spectrum. From the graph it is clear that a delay time to coherence ratio of approximately 10 is necessary otherwise the Lorentzian part of the spectrum is sufficiently broadened to cause a pessimistic estimation of the laser linewidth. It was decided that the experimental measurement should be carried out using as long a delay length as possible. For this purpose 9 km of step index optical fibre was available. This fibre supprted only one mode of oscillation at 850 nm and had an attenuation of approximately 2 dB/km.

3.6 Passive Cavity Laser Mount.

Line– narrowing experiments were performed originally using the laser mount shown in Figure 3.21. A fine thread mirror– positioner was incorporated in the design to allow for fine positioning of a polished glass surface that would be used to implement external feedback. Light was collimated from the laser diode using a GRIN lens mounted on a goniometric three way positioner. Suitable collimation could be achieved in this manner however the goniometric stage was found to be sensitive to accoustic disturbance and required continuous re– alignment. Thermal stabilisation was achieved by

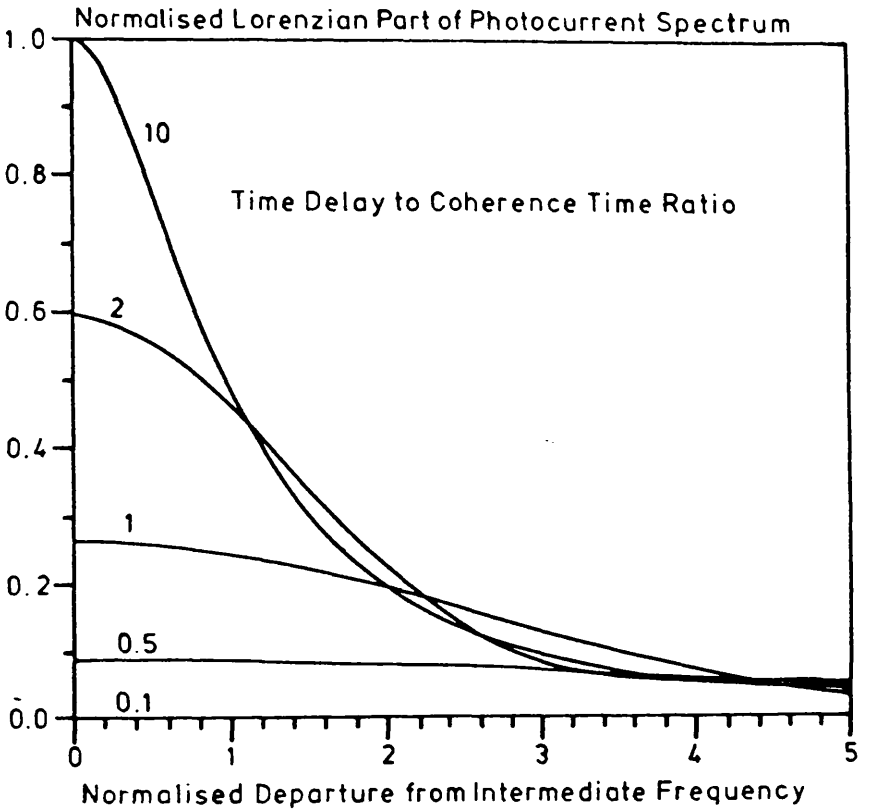

Figure 3.20

Normalised Lorentzian part of Photocurrent Spectrum as a function of normalised departure from Intermdiate Frequency $(\omega - \Omega)/2\gamma$, for several values of Delay time to Coherence ratio $2\gamma\tau_c$. [56]

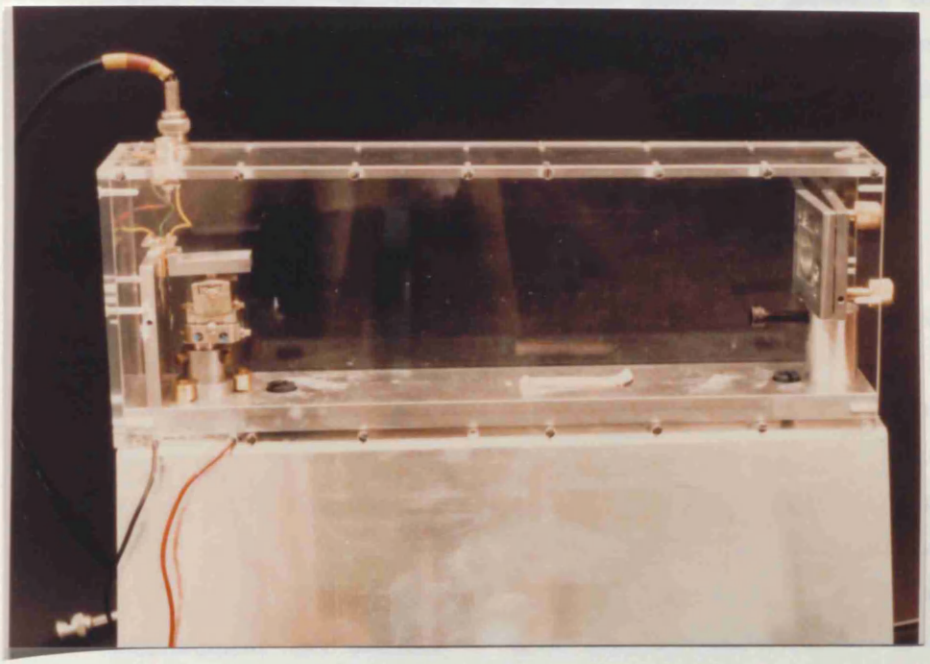

Figure 3.21
Laser Diode in Coupled Cavity Arrangement.
Cavity Length = 30 cm.

regulating the temperature of the entire mount. (This was found to be a non–optimum solution and later developments in the mount design restricted the temperature control to the vicinity of the diode itself.)

Figures 3.22 and 3.23 depict typical free–running linewidth measurements that were made using the above modules. The linewidths are clearly of the order of a number of Megahertz. Forcing a coupled cavity operation with feedback directed from the external mirror resulted in a linewidth reduction to approximately one tenth of this value, see Figure 3.24. Stability of operation in this configuration was however limited. Acoustic vibration and thermal variations would induce mutimode oscillation or at worse instigate a complete collapse of coherence. Although the line–narrowed single mode operation was, in general, recovered, a stable trace was never obtained for periods of time exceeding a few seconds.

3.6.1 Self Heterodyne Beat Lineshape.

It is interesting to note that none of the above measurements exhibit truly Lorentzian lineshapes. Gallion has predicted that rounding of the Lorentzian part of the lineshape will be observed when the delay–time to coherence–time ratio drops below a factor of approximately 10. A delay length of 9 km should however provide around 20 kHz resolution and therefore this problem should not have been encountered. The cause of this corruption in the linewidth measurement was deduced to have resulted, not from an insufficient delay time for the particular coherence–length but, from an excess delay time for the level of 1/f noise present in the laser oscillation (primarily due to inadequate temperature control). This phenomenon has been reported by other workers [56]. It was decided therefore to shorten the delay–time of the interferometer and thereby introduce a trade–off in experimental resolution between coherence effects and the low frequency noise degradation.

3.6.2 Passive–Cavity FM Characteristics.

The coupling of the laser diode to an external cavity has been seen to have a marked effect on the linewidth of the source. An

Reference Level

Marker Freq.

Horiz. Scale MHz/div

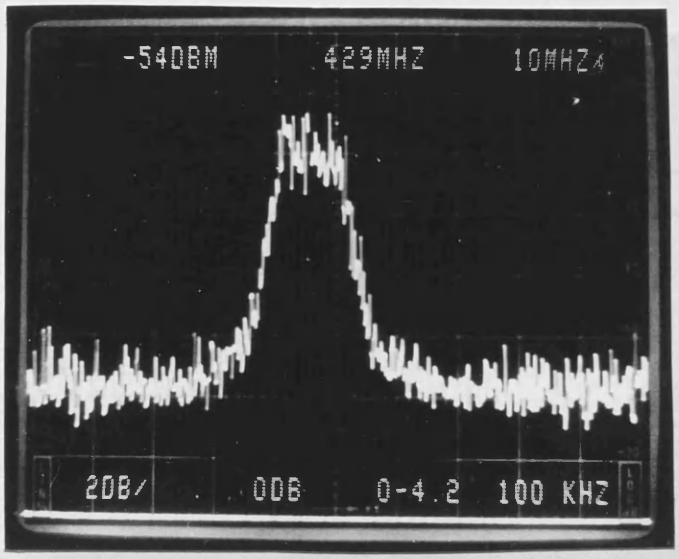

Vertical Scale dB / Div

Input Attenuation.

Freq. Span GHz

Resolution Bandwidth

Figure 3.22
Typical Linewidth Measurement of Free Running HLP 1400 Laser diode. Linewidth < 15 MHz.

Reference Level

Marker Freq.

Horiz. Scale MHz/div

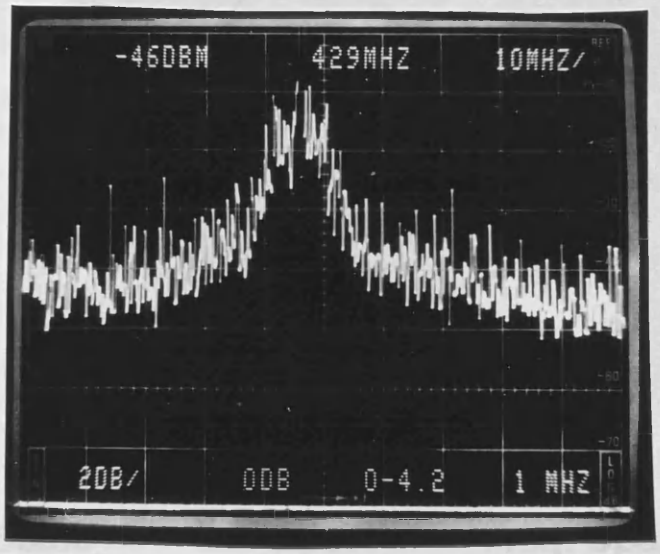

Vertical Scale dB / Div

Input Attenuation.

Freq. Span GHz

Resolution Bandwidth

Figure 3.23
Typical Linewidth Measurement of Free Running HLP 1400 Laser diode. Linewidth < 15 MHz.

Reference Level

Marker Freq.

Horiz. Scale MHz/div

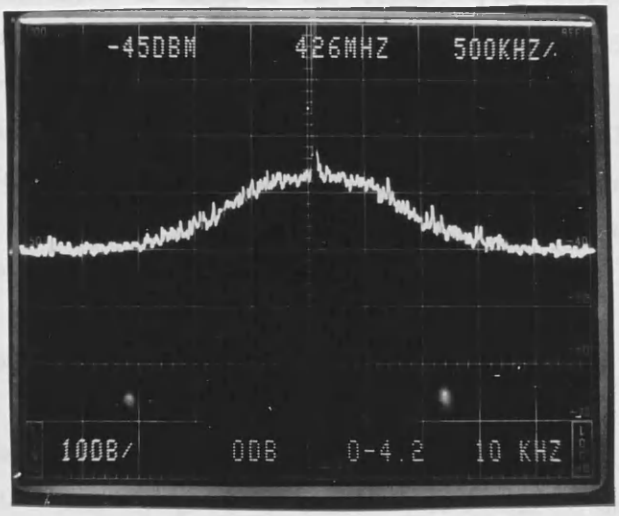

Vertical Scale dB / Div

Input Attenuation.

Freq. Span GHz

Resolution Bandwidth

Figure 3.24
Typical Linewidth Measurement of HLP 1400 Laser diode in Coupled Cavity Linewidth < 500 kHz.

effect of a similar magnitude is also predicted for the FM behaviour. The additional optical length of the coupled cavity diode modifies the FM characteristics of the laser diode. The active medium is a small percentage of the overall cavity length. Refractive index changes in the active layer are therefore not as significant as they are in the free running condition. Consequently the FM characteristics are much reduced. Figures 3.25 to 3.26 demonstrate the effect of the external feedback on the FM response. 3.25. displays the laser diode under sufficient rf drive to suppress the carrier. The effect of a small amount of feedback can be observed in Figure 3.26 where the modulation index has been significantly reduced. Further re– alignment of the mirror produces the situation shown in Figure 3.27 where the FM is alomost completely removed. The original situation can be recovered again at the expense of rf drive power (provided that the modulation frequency is within the cavity bandwidth).

3.6.3 Passive Cavity Mount: Conclusions.

A laser mount has been assembled and evaluated for use in experimental coherent optical systems. The linewidth of the mount was measured using a self– heterodyne technique and was found to be less than 500kHz. Linewidths of this magnitude are suitable for experimental phase– locking systems (see Chapter 5). The module was however found to be extremely sensitive to acoustic interference. This lack of stability prompted a redesign of the mount. Commercial companies were found at this stage who were able to place an antireflection coating on one facet of the laser diode. It was decided therefore to make an attempt to construct an external cavity laser. Experience gained in working with the goniometric stages showed them to be lacking in the necessary mechanical stability and precision for the fine alignment of the collimating lens. It was decided that future mounts would therefore be designed around Microcontrole micro– positioning stages.

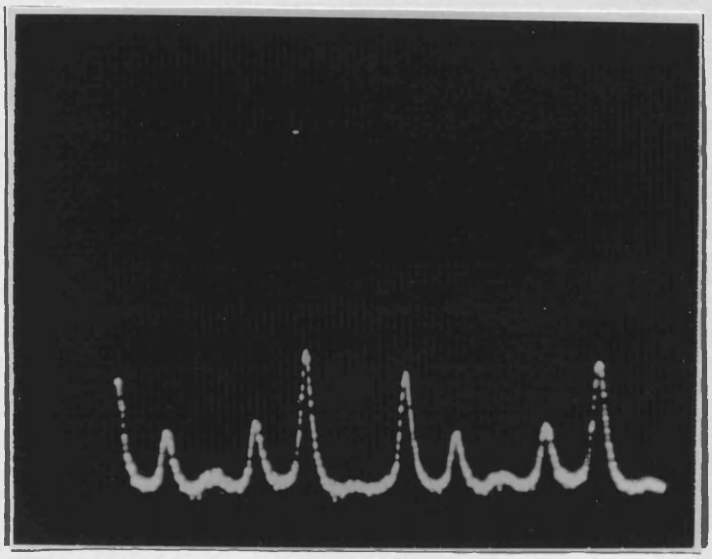

FSR = 2GHz.

Figure 3.25

Free Running Laser Diode Under Direct F.M. Modulation
Modulation Frequency = 500 MHz
Modulating Voltage = 158 mV.

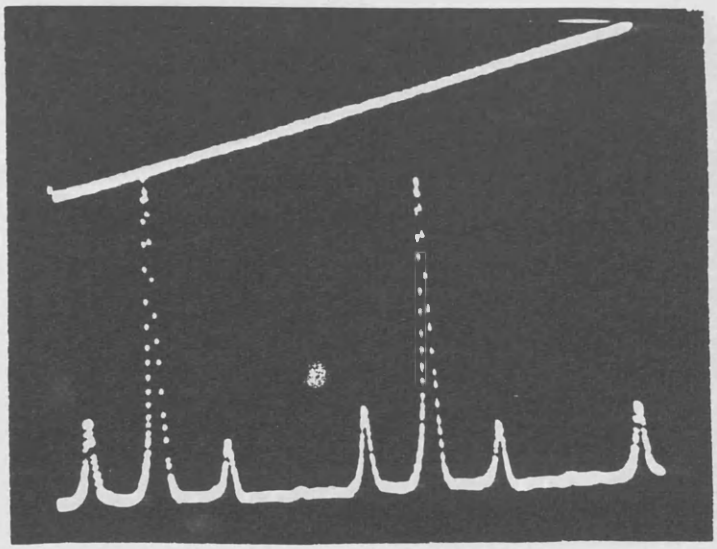

FSR = 2GHz.

Figure 3.26

Coupled Cavity Laser Diode Under Direct F.M. Modulation
Modulation Frequency = 500 MHz
Modulating Voltage = 158 mV.
Modulation Depth significantly reduced.
Non Optimum Mirror Alignment.

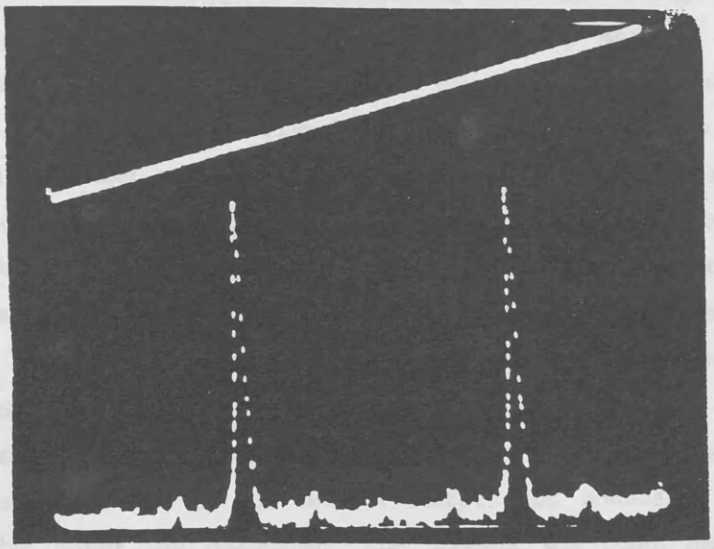

FSR = 2GHz.

Figure 3.27

Coupled Cavity Laser Diode Under Direct F.M. Modulation
Modulation Frequency = 500 MHz
Modulating Voltage = 282 mV.
Modulation Depth significantly reduced.
Optimum Mirror Alignment.

3.7 The External Cavity DIode Laser.

Considerable experimental success in obtaining stable, narrow linewidth, tunable laser sources had been achieved by various workers [12,14,19,20,29,31] using the external cavity laser approach. The greatest level of tunability had been achieved using a diffraction grating as the feedback mechanism [19,20,31]. It was considered that this tunability would be extremely beneficial to any project concerned with either heterodyning, or homodyning, of two independent laser sources and therefore the feasability of implementing such an arrangement was investigated. The main problem that was foreseen was the fact that the use of the grating relied on the user being able to access the power from both of the diode facets. The grating could then be lined up on one facet and the power from the other used as a carrier or local oscillator in system experiments. Access to the rear facet of the Hitachi HLP 1400 diode was restricted due to the geometry of the heatsink. Attempts to collimate the back facet output using GRIN lenses or microscope lenses were unsuccessful. A certain amount of success was achieved using a specifically purchased elliptical lens with a 4 mm focal length however the back facet emission was sufficiently well scattered that by the time it reached the collimating lens the available power was diminished. The decision was taken therefore to modify the laser mount by polishing the heatsink down to the thickness if the diode itself. This action was seen to be potentially hazardous to the laser itself however no alternative seemed to be available. There was no facility within the department for removing and remounting the diode on an alternative mount. In any event this operation would be likely to involve similar risks. The only other available action was to request Hitachi to mount the diodes on another type of mount. Hitachi were not co– operative.

3.7.1 Polishing the Laser Diode Mounting.

Prior to polishing, the laser diode bonding wires were moved to be in line with the front facet of the diode (see Figure 3.28) in order that they would not protrude beyond the back facet and thus be exposed to damage or interference during polishing. Conducting silver paint was then used to provide an electrical connection between the

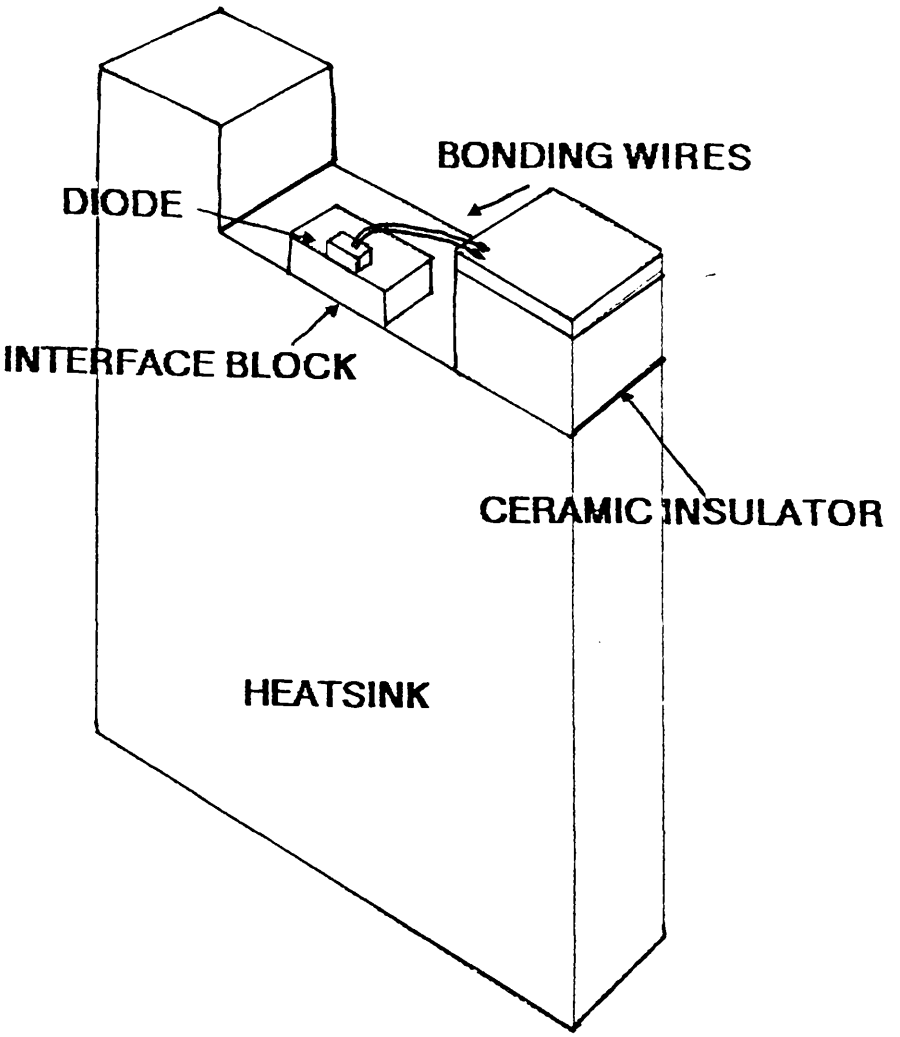

Figure 3.28

HLP 1400 DIODE

Bonding Wire Position

laser anode and cathode to prevent damage due to static build up during polishing. The diode was then mounted, front facet down, in a thin bed of Shellac (a hard wax) and the remainder of the diode coated in Shellac to protect the back facet from damage from debris during the course of the polishing. The diode mount was then ground down with the use of a fine grain abrasive agent over a period of 8 hrs. Periodic estimation of the diode thickness was made during the course of the polishing to ensure that overpolishing did not arise.

A number of diodes were polished in this manner, however the success rate was not high. One diode was destroyed during polishing although the exact cause is uncertain. At some point during the procedure the stresses were sufficient to cause a fracture of the AlGaAs wafer. This may have happened during the moving of the bonding wires and did not become evident until after the polishing. An additional diode was lost due to over–polishing. This should not have occurred but an element of careless experimental procedure allowed this to take place. The diode heatsink thickness was measured during polishing as the height (including the wax) above the polishing plate. The original diode thickness should be known and therefore the remaining thickness readily calculated from how much had been removed. The diode mount had however a variation in thickness of up to 20 μm which was not taken into account *ie* the original diode thickness was taken as 3mm and was not measured. Consequently overpolishing resulted, as is shown in Figure 3.29–31. Figure 3.29 shows the end view of the rear facet of the laser diode after polishing. The lighter shade of the interface block can be seen to have been spread over the front face of the diode thus clearly indicating that physical damage had resulted to the diode facet. A photograph of the front facet is given in Figure 3.30 for comparison. The smooth finish of the undamaged face is seen in contrast. Some localised areas of either thermal damage or damage to contact from small pieces of grit are in evidence. This amount of damage did not however inhibit laser performance. Finally an aerial view is provided in Figure 3.31 indicating that the diode heatsink has been polished to the thickness of the diode itself. Three additional diodes have been further polished in this manner and in each of these successful lasing operation was achieved. The diodes proved however to be too fragile

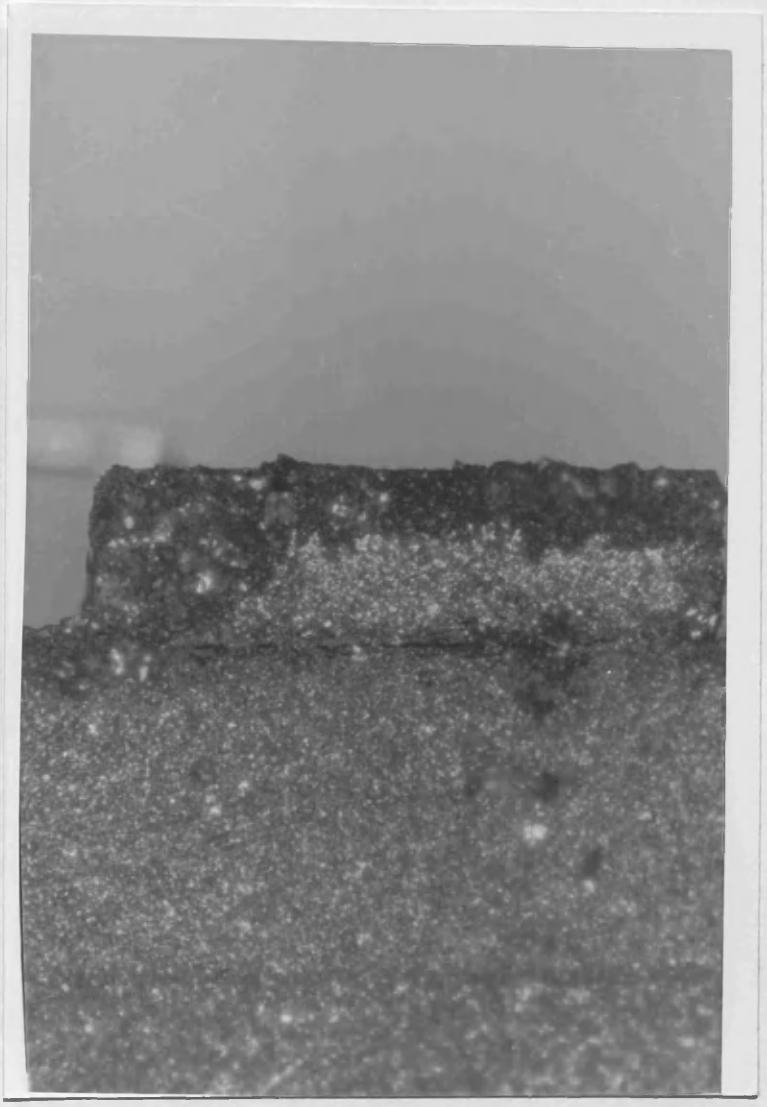

Figure 3.29
HLP 1400 : Facet Damage due to Polishing.

Figure 3.30

Undamaged HLP 1400 diode.

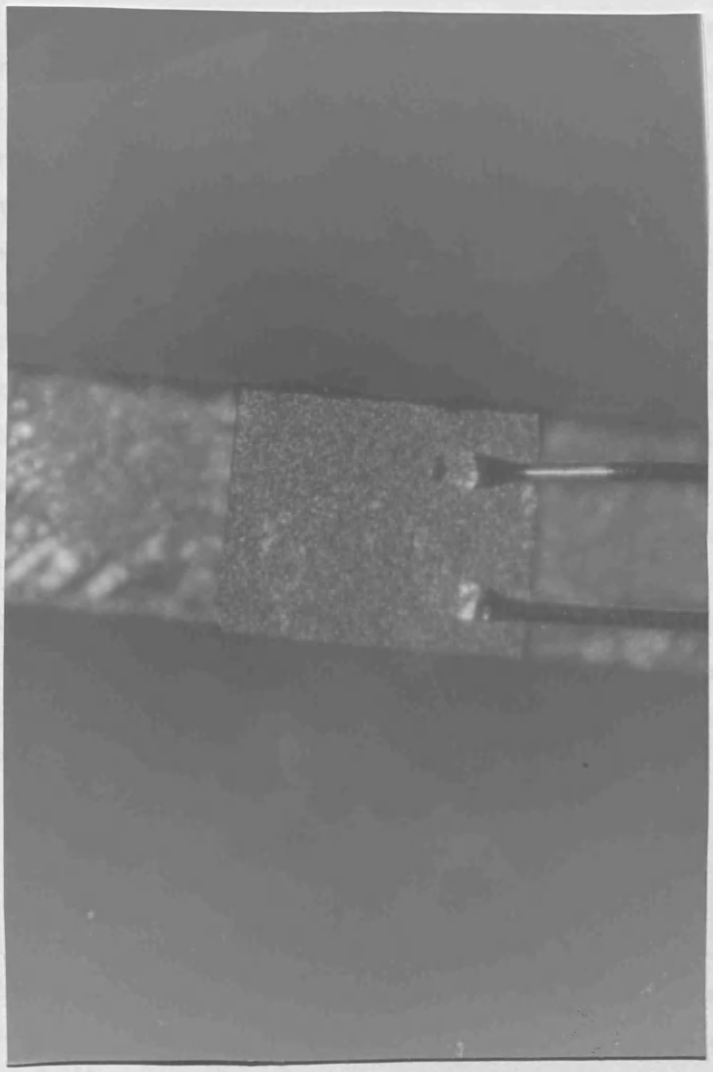

Figure 3.31
Polished Laser Diode : Aerial View.

in this condition for prolonged experimental usage and therefore this approach was abandoned.

3.7.2 Anti– Reflection Coating.

The placing of anti– reflection coating on one facet of the laser diode allows the diode then to be used simply as a pumping medium for the laser action. The lasing action is then obtained as a result of the optical gain generated over the 300μm diode length and the resonance of the laser back facet and an externally aligned reflector. Consequently the longer cavity increases the Q– factor, producing narrower linewidths. In order that this form of arrangement may be realised however, facet reflectivities have to be reduced to the order of a few percent or better. This is accomplished by the deposition of an index matching coating on the diode facet. This could not be carried out in house and therefore had to be put to tender. Two companies, Kendall and Hyde, and Optical and Electronic Coatings Ltd. agreed to perform this task. It was decided therefore one diode should be sent to each of these and the effectiveness of the AR coating assessed. The coating used by Kendall and Hyde was a multi– layer coating of undisclosed composition. The OEC coating was a single layer Titanium Oxide coating. Both coatings were assessed in the following manner.

3.7.3 Assessment of Anti– Reflection Coatings.

A simple comparison between the two coatings can be obtained from a plot of the output power versus drive current of the devices before and after the coating operation has been carried out. The diode exhibiting the greatest percentage increase in lasing threshold current has the better coating. These measurements were made (Figure 3.32) and show that the Titanium Oxide coating is the better of the two, since the lasing threshold has been raised to approximately 82 mA. To obtain a more quantitative analysis of the actual effectiveness of the coating, the following procedure was undertaken.

The lasing threshold is reached when the losses in the diode are equally balanced out by the gains. At the onset of lasing it is possible

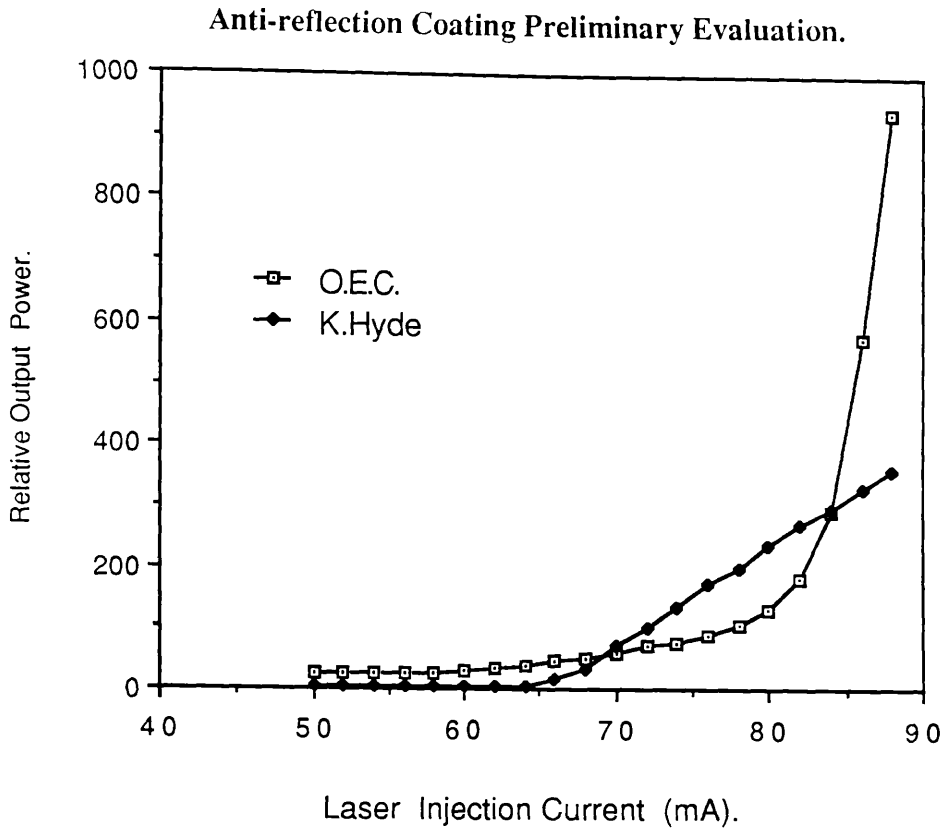

Figure 3.32
Preliminary AR Coating Assessment
Current / Power Characteristic

to define a modulation index on the spontaneous emission profile of the diode as [57]

$$m = \frac{P_{max} - P_{min}}{P_{max} + P_{min}} \quad (3.12).$$

At the onset of lasing the index will be approximately unity.

The application of an anti-reflection coating inhibits laser oscillation. At the equivalent bias current of the original (uncoated) threshold, the laser output will be similar to that of a Light Emitting Diode. The emission spectrum will be wide line (typically 5 to 10 nanometres) rising to a maximum near the original frequency of lasing. With a perfect antireflection coating this broadband emission will simply represent the spontaneous emission profile. Any residual reflectivity resulting from an imperfect index match could be expected to superimpose a Fabry-Perot modulation on the emission profile as the round trip amplification factor satisfies a periodic solution. This is the key to the effective reflectivity measurement.

The round trip amplification can be written in the form [57]

$$a = \sqrt{(R_1 R_2)}.\exp(j2\beta l)\exp((G_+ + G_-)/2) \quad (3.13)$$

G_+ and G_- represent the effective round trip gains which will be assumed constant. The remaining exponential term describes the periodic solution to the wave equation, β is the wave propagation constant. In the free running diode laser R_1 and R_2, the facet reflectivities, are assumed to be identical and equal to the Fresnel reflection coefficient of an AlGaAs/air boundary (approximately 0.32). The modulation index on the spontaneous emission profile can be related to the round trip amplification factor by [57]

$$m = 2|a|/(1+|a|^2) \quad (3.14).$$

Thus from an experimental measurement of the modulation index the reflectivity of the antifelection coated surface may be assessed.

$$R_{ar} = |a|^2 R_1 = 0.32|a|^2. \quad (3.15)$$

This measurement was conducted using the apparatus outlined in Figure 3.33. The diode emission was coupled into the monochromator which scanned over a preset range of wavelengths. The output of the monochromator was detected on a power meter and directly recorded on a chart recorder. Analysis of the traces reveals that the multi– layer coating was effective in reducing the facet reflectivity to approximately 3%. The Titanium Oxide coating was nearer to 0.3%. The Titanium Oxide coating was therefore deemed to be the most suitable. Both of these coatings are however suitable for the construction of an external cavity source. The measurement of the Titanium Oxide coating is presented in Figure 3.34.

It is interesting to note that the profile of the spectrum exhibits a definite asymmetry with an apparent enhancement of the modulation index at longer wavelengths. It was suspected that at longer wavelengths the effectiveness of the AR coating might be reduced due to the fact that the coating thickness was less well matched to $\lambda/4$.

A further three diodes were coated in this manner. However the coatings, although deposited simultaneously, differed greatly in quality from the original coating. Assessment of the diodes on immediate return from OEC revealed no observable change in the lasing threshold and a Fabry– Perot modulation index of unity on the spontaneous emission profile. It was suspected that somehow the diodes had been blanked off during coating. Recoating was attempted and recordings of the power/current characteristics made (see Figure 3.35). Estimation of the facet reflectivities was also carried out. The results of this are tabulated in Table 3.1. The measurement of Laser 2207 is shown in Figure 3.36.

The cause of the apparent wide range of performance is unknown. The HLP 1400 series diodes were known to be coated with a SiO_2 passivating layer. The quality control in the deposition of this layer is imprecise because exact thicknesses are not required. It was suspected that this might influence the quality of the anti– reflection coating, however it would not account for the fact that one diode in particular appeared unaffected by two succesive coatings. In any event,

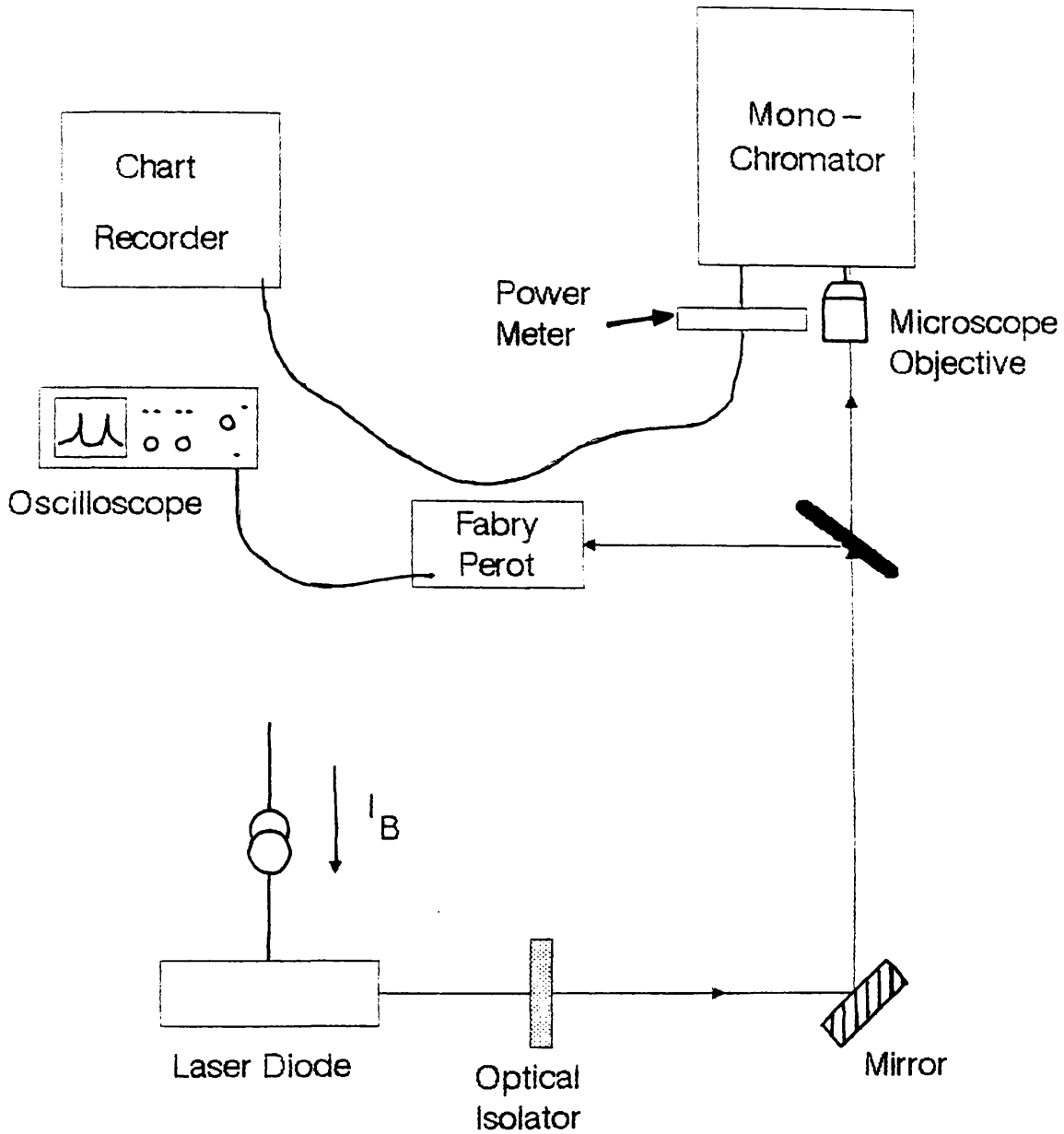

Figure 3.33

Facet Reflectivity Measurement Apparatus

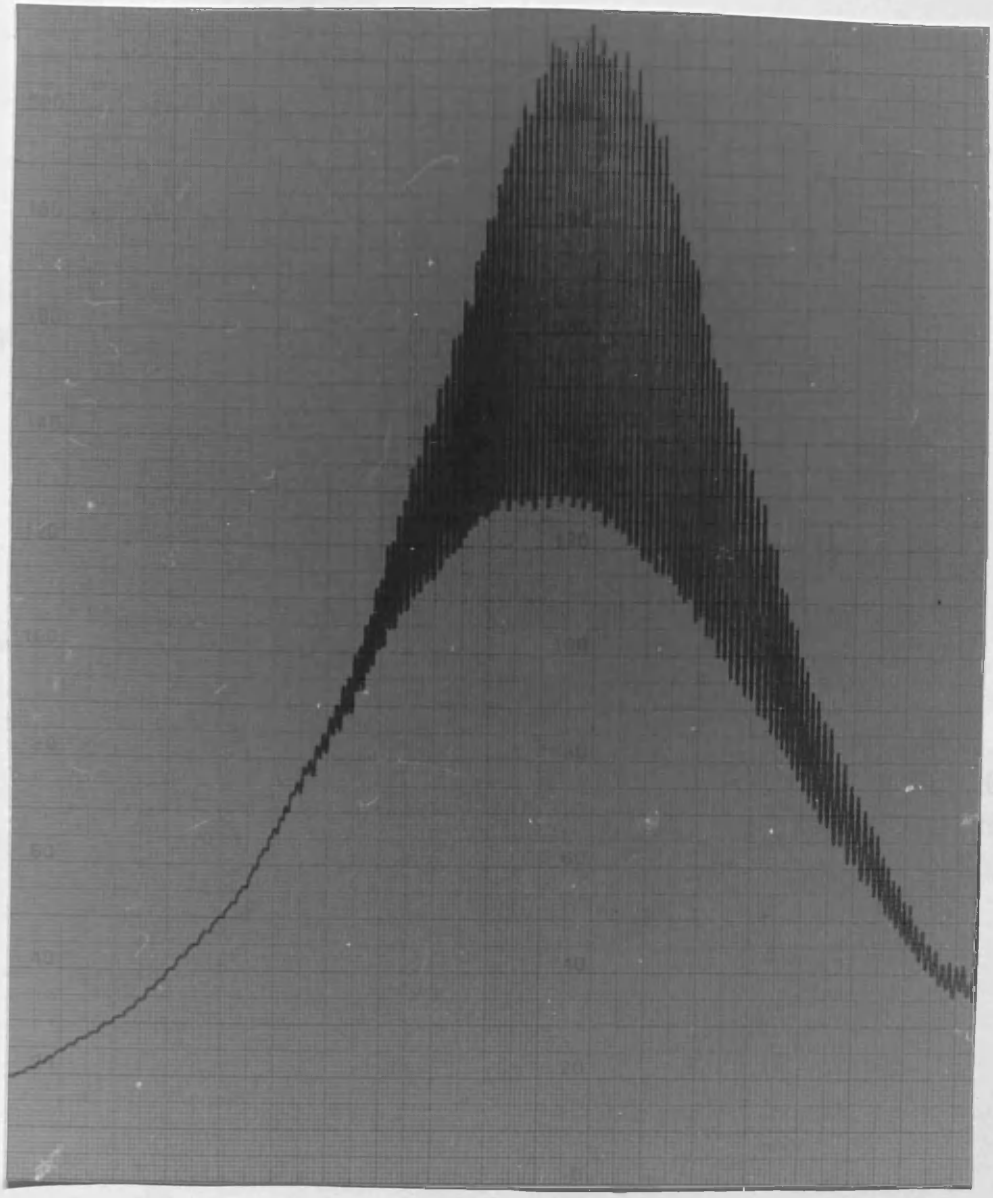

Figure 3.34

Spontaneous Emission Profile of HLP 1400 after deposition of Titanium Oxide Layer on front facet.

Facet reflectivity approximately 0.3 %

Measurement Range 800 – 852 nm.

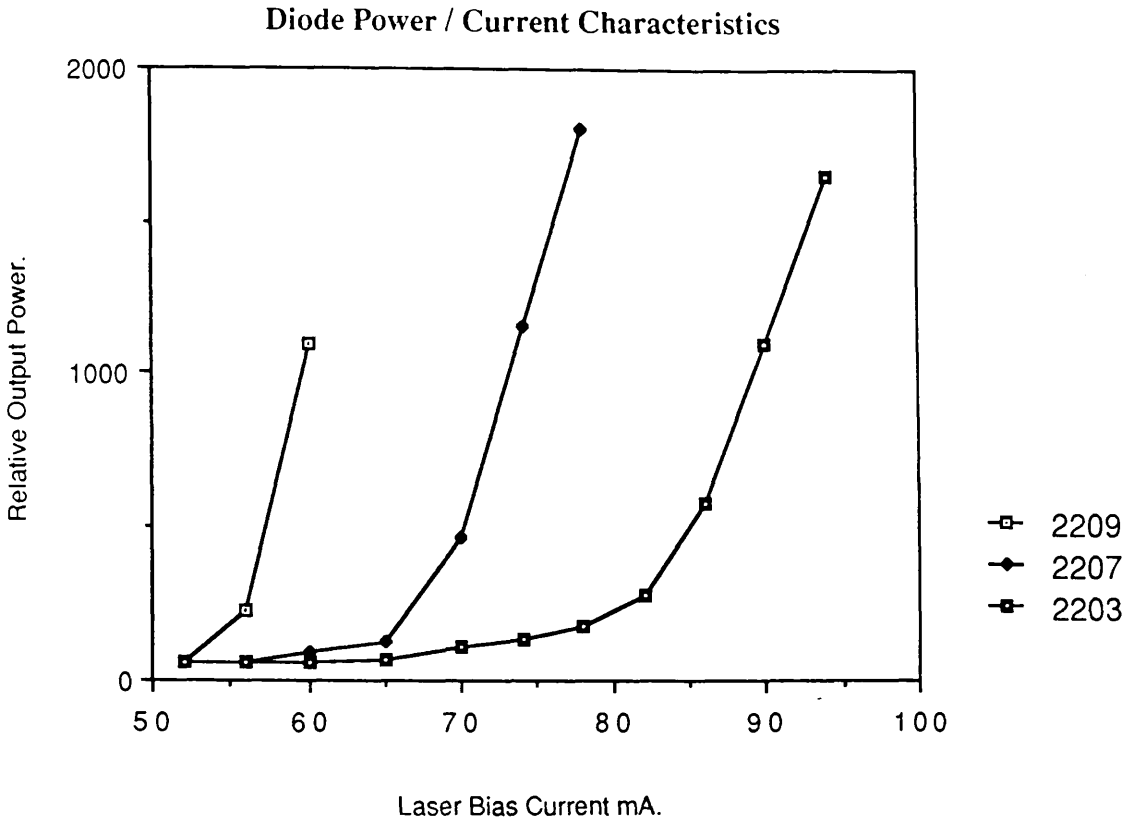

Figure 3.35

Diode Power / Current Characteristics

after deposition of TiO_2 layer (2nd Coating).

Laser Diode.	Facet Reflectivity After First Coating.	Facet Reflectivity After Second Coating.
2203	32%	0.6%
2207	32%	1.1%
2209	32%	32%

Table 3.1

Laser Diode Facet Reflectivity Measurements.

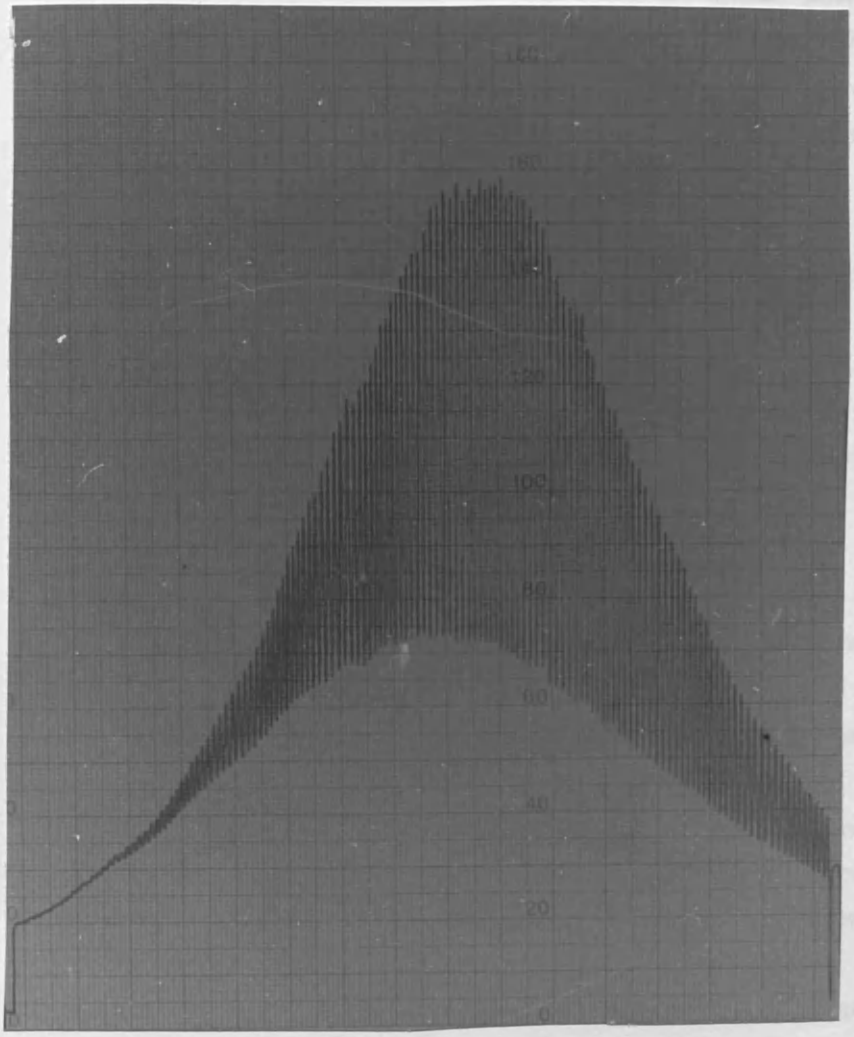

Figure 3.36

Spontaneous Emission Profile of Diode 2207.

after deposition of Titanium Oxide Layer

Facet Reflectivity Approximately 1.17%

Measurement Range 800nm to 839 nm.

Peak at 822 nm.

all diodes submitted for coating were from the same batch and therefore it would be reasonable to assume that similar coatings were applied to all three. It is possible that the Titanium Oxide layer is difficult to deposit. This may account for the range of qualities achieved. Inspection of the diode mounts under an optical microscope did not reveal any minute differences in the diode mounting or anything that might obscure the diode active region during the coating process. Investigation of the coating process itself was outwith our capabilities.

The remaining three diodes were coated and tested in this manner and again no measurable difference was detected. These diodes were therefore recleaned and sent to Kendall and Hyde for further coating. Reflectivities of 2, 5 and 32% were measured on their return. Diodes with reflectivities of better than 5% were used in the following external cavity laser experiments.

A PZT stack positioner was purchased for the alignment of the external reflector. This enabled sub– micron tuning to be implemented. The external reflectors were polished optical flats (flat to $\lambda/10$ across the entire surface) with an anti reflection coating placed on one side and a reflective coating of 4,40,60 and 95% repectively on the other. The anti– reflection coating on the remaining side substantially reduced the possibility of a compound cavity being set up between the external cavity laser and any secondary reflection from the external mirror.

The new design of laser mount was capable of accommodating both external and coupled cavity arrangements. While the first three diodes were being coated, the remainder were experimented with in a coupled– cavity configuration in order that a comparison in stability between the old and the new mount could be obtained. The linewidth measurements made on these sources are displayed alongside the external cavity results.

A selection of the typical linewidth measurements is given in Figures 3.37 to 3.39). The optical path length for this set of experiments was reduced from the previous 9 km delay to 2km. The accousto– optic frequency shifter was removed to minimise the

Reference Level

Marker Freq.

Horiz. Scale MHz/div

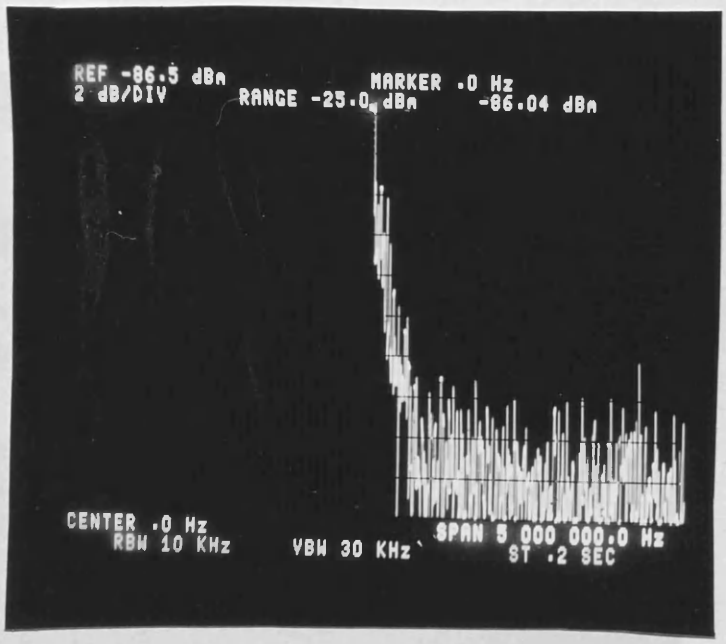

dB / Div

Input Attenuation.

Freq. Span GHz

Resolution Bandwidth

Figure 3.37

Linewidth Measurement of Coupled Cavity Laser Diode. Diode no. 2206

Linewidth = 235 kHz.

Reference Level

Marker Freq.

Horiz. Scale MHz/div

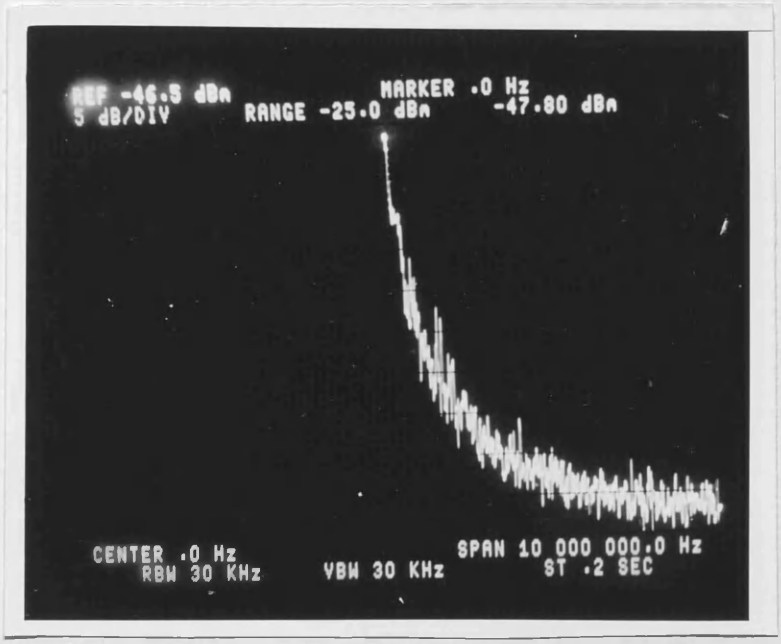

Vertical Scale dB / Div

Input Attenuation.

Freq. Span GHz

Resolution Bandwidth

Figure 3.38

Linewidth Measurement of External Cavity Laser Diode. Diode no. 2207

Linewidth = 90 kHz.

Reference Level

Marker Freq.

Horiz. Scale MHz/div

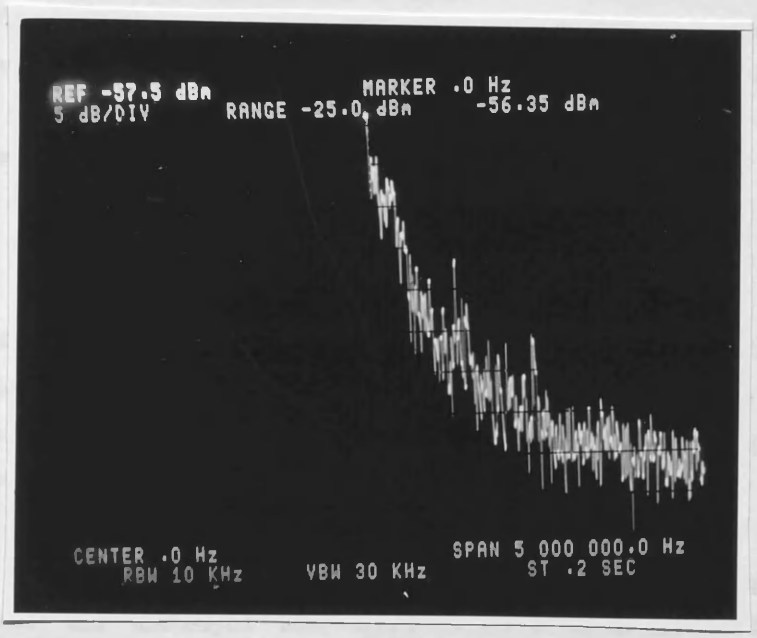

Vertical Scale dB / Div

Input Attenuation.

Freq. Span GHz

Resolution Bandwidth

Figure 3.39

Linewidth Measurement of External Cavity Laser Diode. Diode no. 2203

Linewidth = 60 kHz.

necessary power for the measurement. This enabled measurements to be made on external cavity lasers operating below the new free-running lasing threshold. In this situation the power output was significantly diminished from its previous value, making the use of long lengths of fibre delay impractical.

Rearranging equation 3.9 allows estimation of the linewidth displayed in Figures 3.37-39 to be made from extrapolation from the 20 dB power point (or which ever power value presented itself as being the most convenient). The 3dB linewidth can be deduced from a measurement of the linewidth at any other point in the distribution using the expression

$$2.f^2/(\Gamma-1) = \delta f^2 \qquad (3.16)$$

where Γ is the ratio of the peak amplitude, of the Lorentzian part of the self-homodyne beat, to the amplitude at the point in frequency where the measurement is made: f is the width of the spectrum at this point.

Figure 3.37 displays a typical measurement of a coupled cavity laser self-homodyne beat spectrum. The particular diode in this instance was laser 2206. The beat spectrum was estimated to be 10 dB down in power at a frequency of approximately 500 kHz. This predicts a laser linewidth of 235 kHz. This is comparible with results from other workers investigating coupled cavity sources. The spectrum displayed in Figure 3.38 is that of an external cavity laser diode. The measurement predicts a linewidth of around 90 kHz (30 dB power drop at 3 MHz). Finally Figure 3.39 shows a spectrum with an estimated linewidth of around 60 kHz (37 dB down at 3MHz).

The estimation of a 90 kHz 3 dB linewidth is higher than would be expected for an external cavity laser diode. However it must be made clear that the experimental measurements are difficult to make accurately due to the level of background noise. Furthermore, since the experimental programme was geared towards the implementation of an optical phase locked loop, it was felt that it would be better to design the loop around pessimistic values of linewidth rather than

restrict the loop bandwidth prematurely. The beat linewidth observed here may well have been better than 90 kHz. In this region it must also be noted that accurate measurement of the linewidth becomes impractical due to the effect of insufficient ratio of the fibre delay length to the coherence length of the source under test. This weakness of the measurement technique is further demonstrated in Figure 3.39 where the beat linewidth is estimated to be around 60 kHz. Examination of Figure 3.40 reveals that this number represents what could be considered as a reasonable limit of experimental resolution under noisy conditions. Extrapolation of the linewidth from structure observed in the spectrum must be employed if predictions of linewidth are to be made beyond this value. In order to gain an insight into the magnitude and shape of the structure likely to be encountered, the following traces (Figures 3.41−3.44) were prepared. These indicate that, with the levels of noise present in the experiment, it would be unlikely for sufficient evidence of structure to be observed to enable an accurate prediction of linewidth to be made, for linewidths of greater than 10 kHz. It must be concluded therefore that the linewidth of Figure 3.39 lies between 10 and 60 kHz, which is in good agreement with theory and with experiments performed elsewhere.

Linewidth measurements made upon external cavity laser using Sharp laser diodes were made and these did exhibit sufficient evidence of structure that linewidths of narrower than 10 kHz were estimated. These diodes did not however survive for more than a few hours of experimentation. The suspected cause of failure was material defects.

Linewidth measurements, as shown above, were made with both the 40% and 60% reflectivity mirrors in place. The 95% reflectivity limited the amount of output power available rendering the linewidth measurement impractical. The 40% and 60 % reflectivity mirrors did not produce measurable differences in performance. The linewidth of the external cavity laser was found to be highly dependent upon the alignment of the external mirror. Since it could not be determined whether or not one laser was or was not better aligned than the other no conclusive evidence could be obtained to suggest that either mirror performed better than the other. It was found however that all diodes performed best, in the external cavity mode of operation, when the

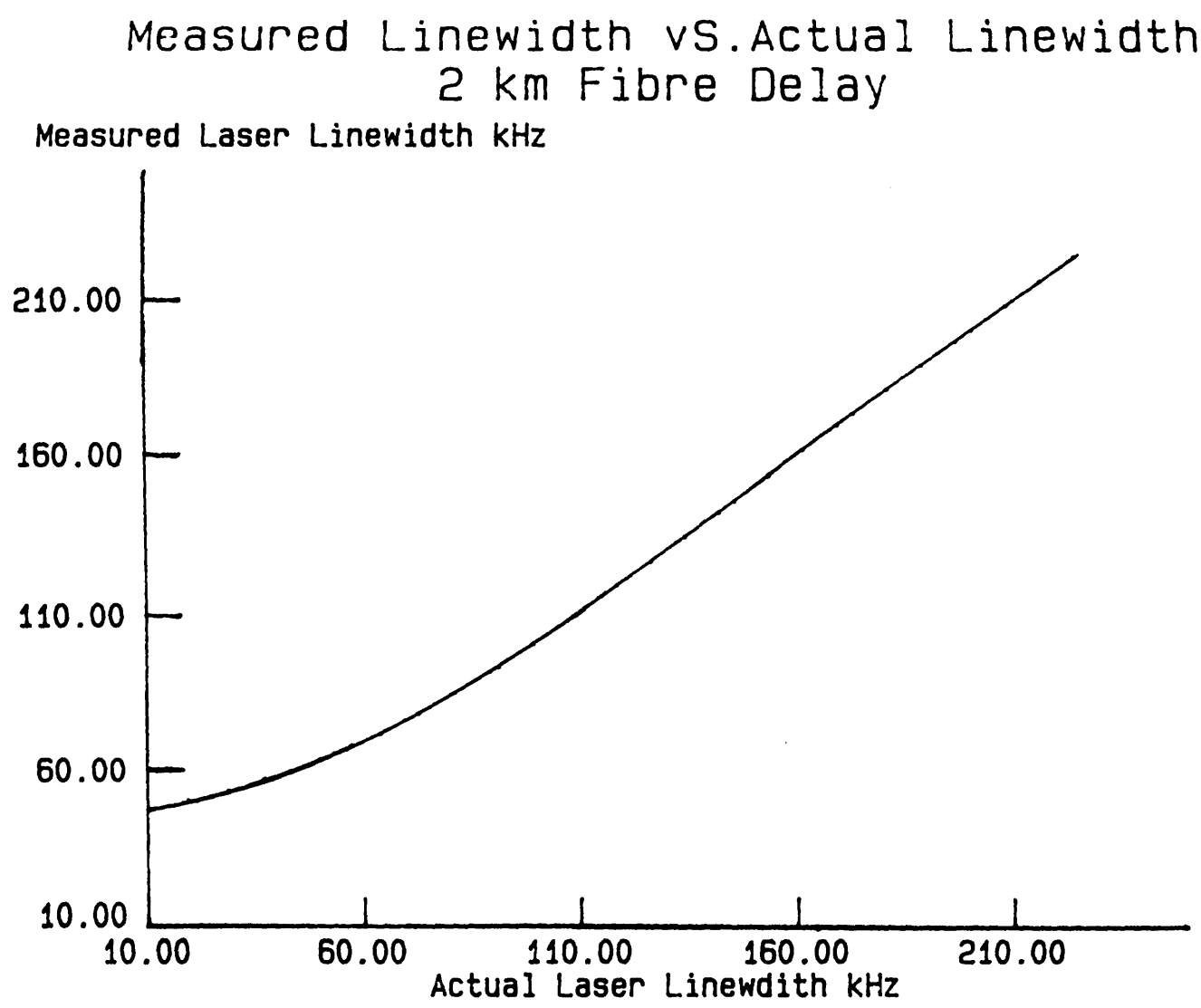

Figure 3.40

Linewidth Measurement Correction Factor.

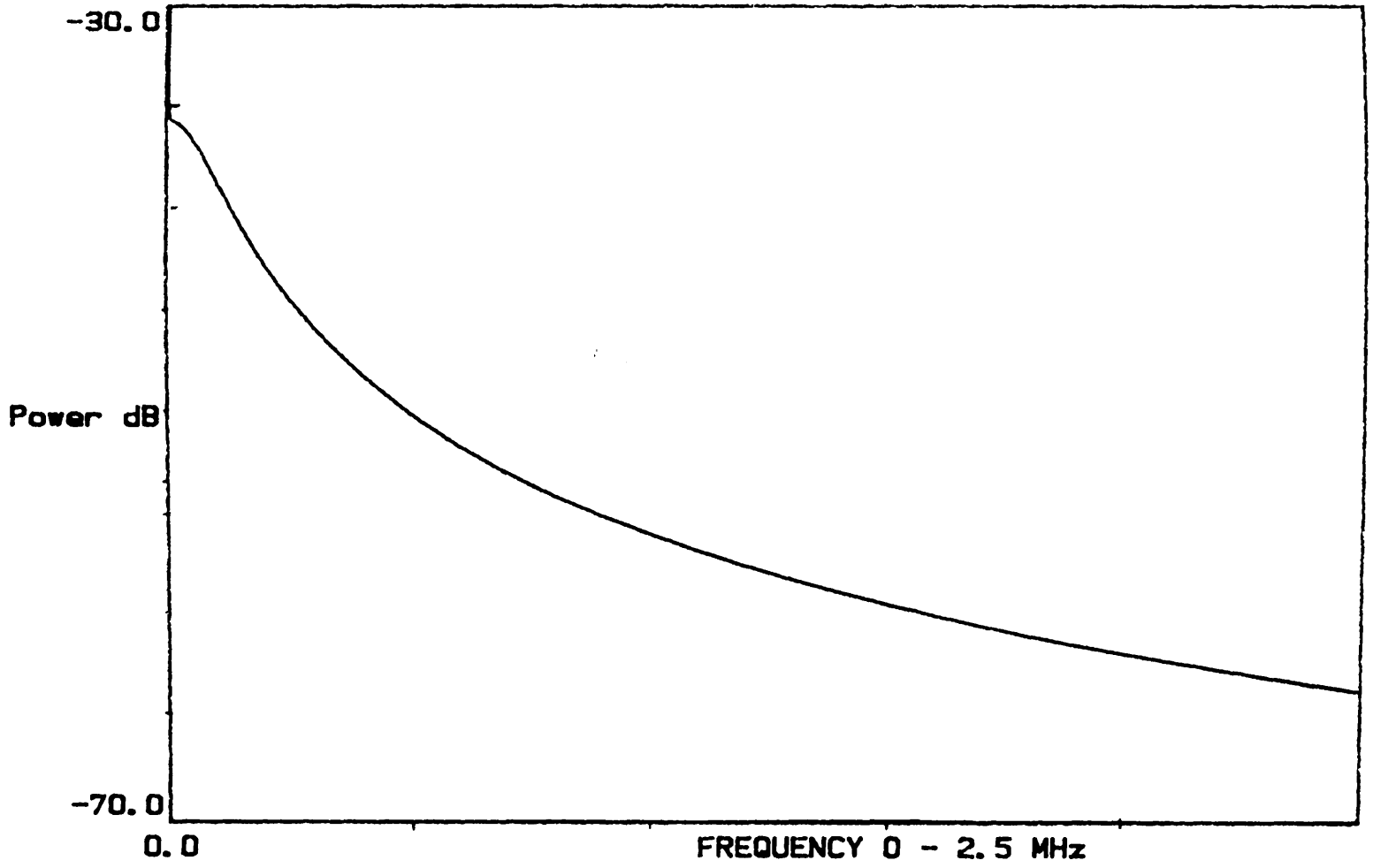

Figure 3.41
Simulated Linewdith Measurement:
Laser Linewidth = 100 kHz, 2km Fibre Delay.

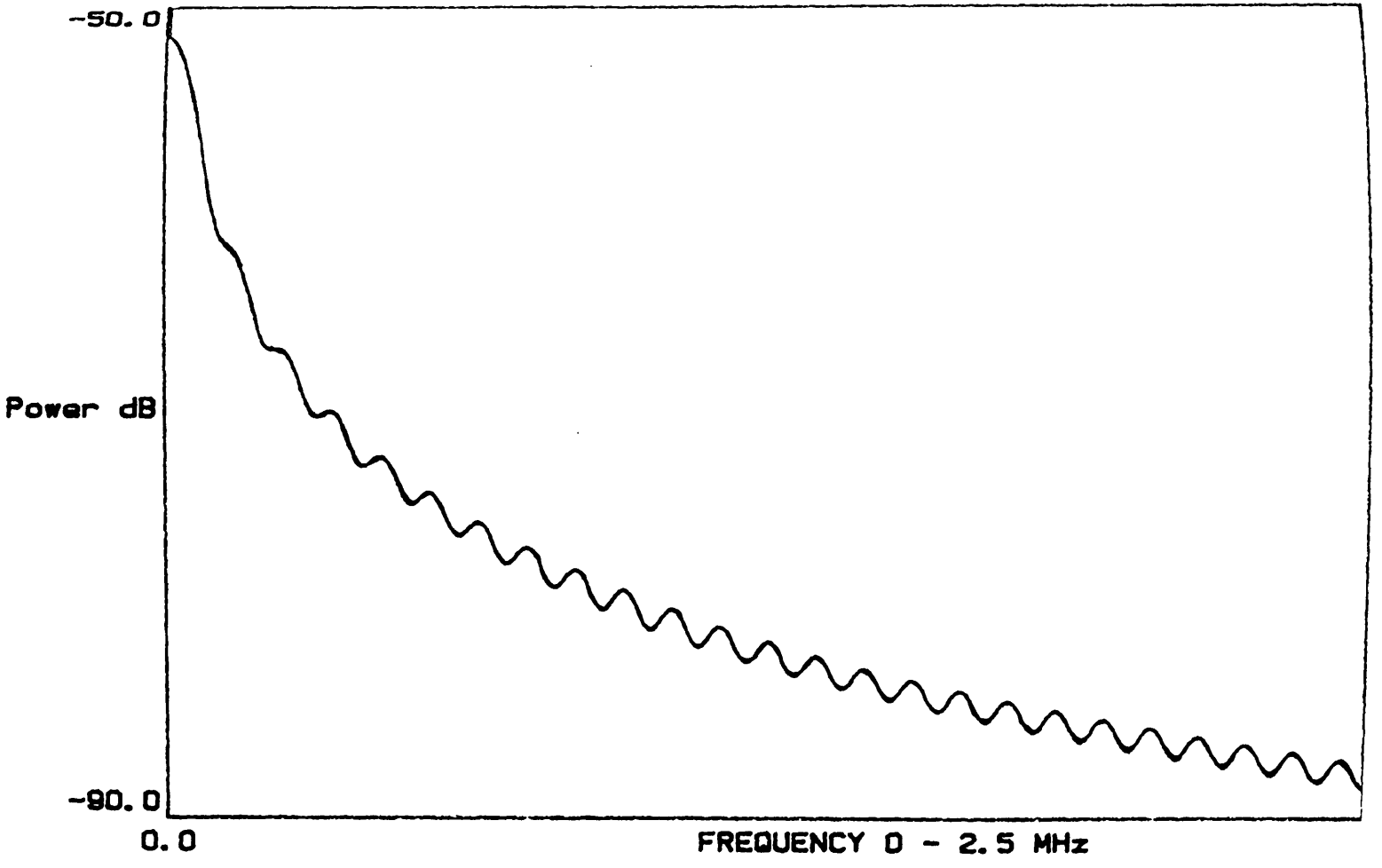

Figure 3.42
Simulated Linewdith Measurement:
Laser Linewidth = 30 kHz, 2km Fibre Delay.

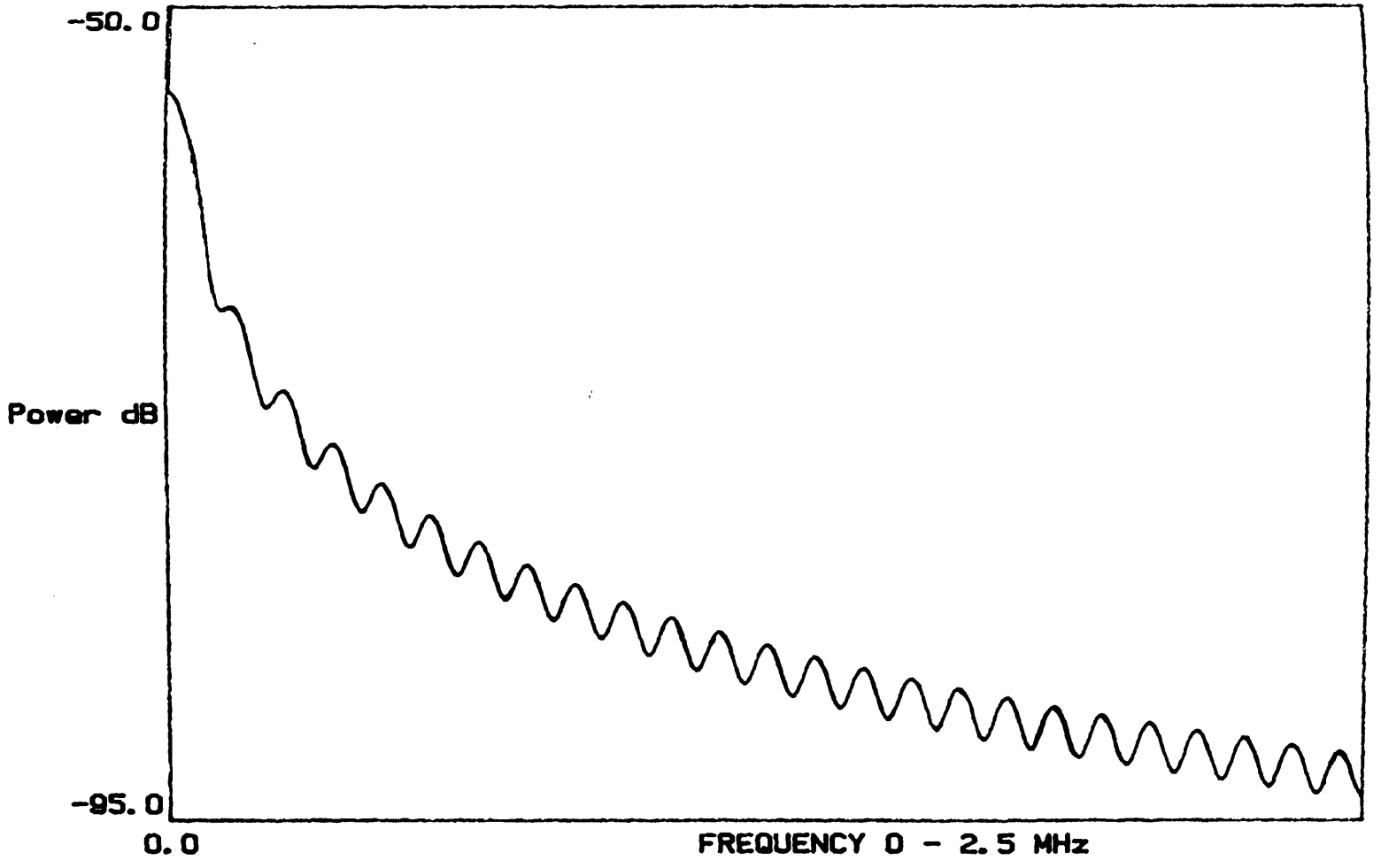

Figure 3.43
Simulated Linewdith Measurement:
Laser Linewidth = 20 kHz, 2km Fibre Delay.

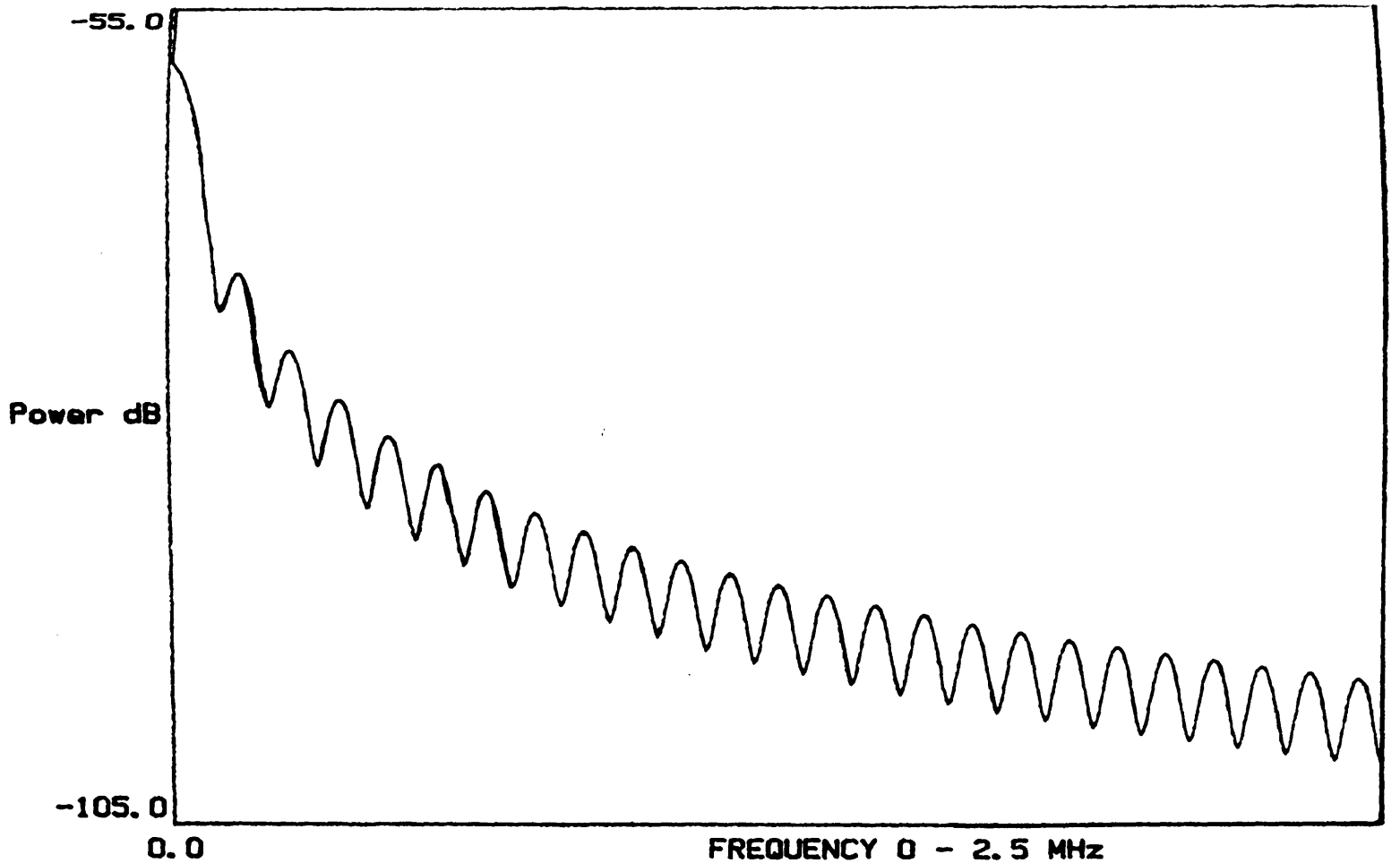

Figure 3.44

Simulated Linewdith Measurement:
Laser Linewidth = 10 kHz, 2km Fibre Delay.

optical output from the diode was focussed on the external reflector. It was expected that this would be the case, or that the optimum position would be the perfectly collimated beam. In practice the focussed beam outperformed the collimated beam. An additional lens was brought into the experimental arrangement to recollimate the beam. This lens was never found to exert any influence on the lasing spectrum due to optical feedback.

Figures 3.45–48 show the effect of improper alignment on the spectrum of the external cavity diodes. With the mirror sufficiently well aligned the side–modes are not visible. Fractional misalignment is reflected by the presence of a small mode at the external cavity frequency. Sufficient misalignment with high levels of feedback can produce the condition of total coherence collapse [58], see Figure 3.48 (more attention will be given to this area in Chapter 7). Diodes aligned to exhibit minimal evidence of side modes showed a typical increase in output power of 13 dB over the free running condition. All measurements performed upon the external cavity laser diodes were made when side mode suppression was better than 30 dB.

It is interesting to note that the above spectra, measured using the shorter length of delay, have a distinctly more Lorentzian appearance than the measurements made previously. This supports the assumption that low frequency noise was causing a rounding of the observed beat spectrum.

3.7.4. Susceptibility of Linewidth Measurement to Unwanted Reflections.

At all times during the measurement of the diode linewidth great care was taken to isolate the device from stray reflections. Figure 3.49 shows the effect of reflections from the scanning FPI on the laser spectrum. The apparent frequency jitter was eliminated with the use of an optical isolator. The feedback obtained from the FPI was relatively strong. Instability in the lasing spectrum was therefore readily induced. In practice it was found that this phenomenum could be made good use of. If the Fabry Perot was perfectly aligned, and the

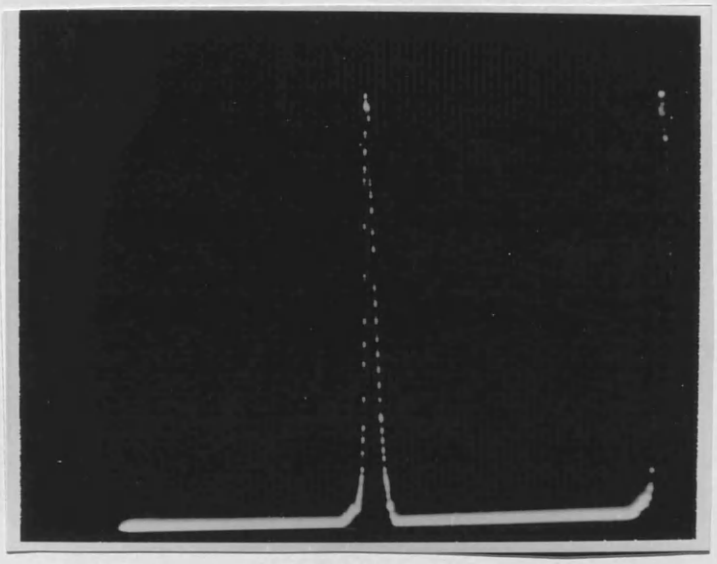

FSR = 2 GHz.

Figure 3.45

Perfect Alignment of External Cavity Diode Laser.
Side – mode Suppression > 35 dB.

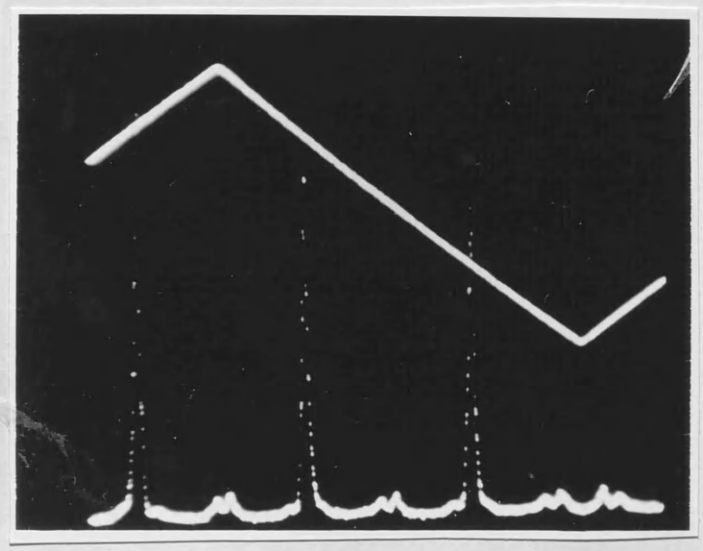

FSR = 2 GHz.

Figure 3.46

Imperfect Alignment of External Cavity Diode Laser.
Side – modes Visible.

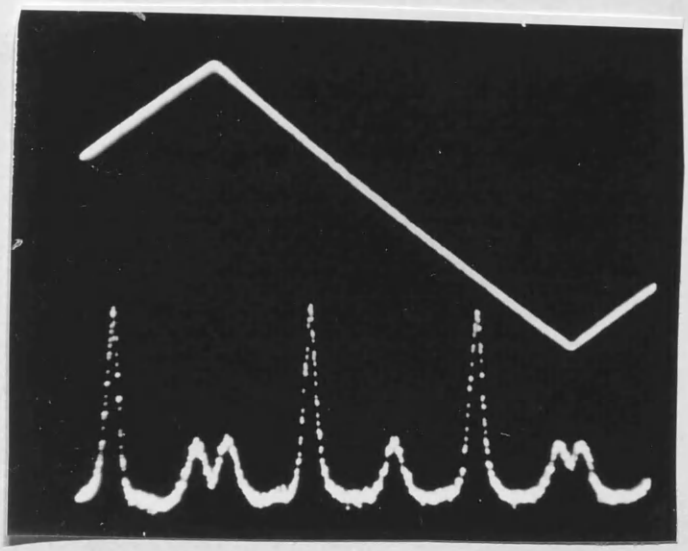

FSR = 2 GHz.

Figure 3.47

Improper Alignment of External Cavity Laser Diode.
Multi – mode Operation

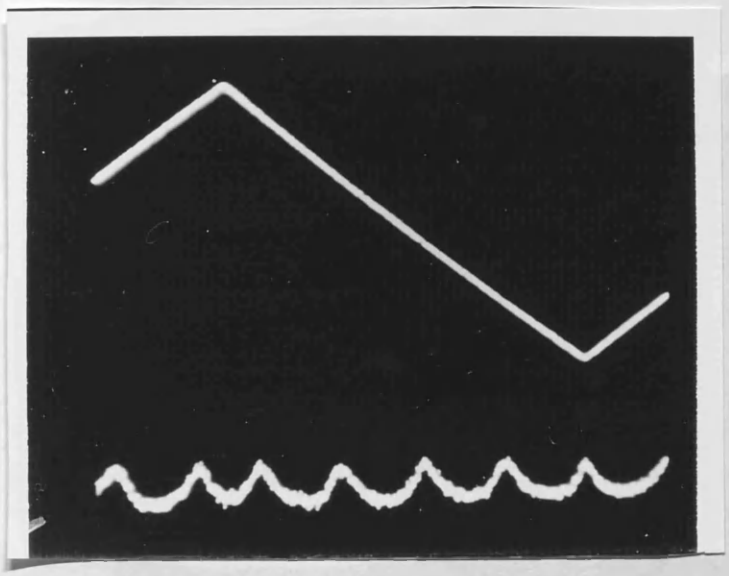

FSR = 2 GHz.

Figure 3.48

Improper Alignment of External Cavity Laser Diode.

Complete Coherence Collapse.

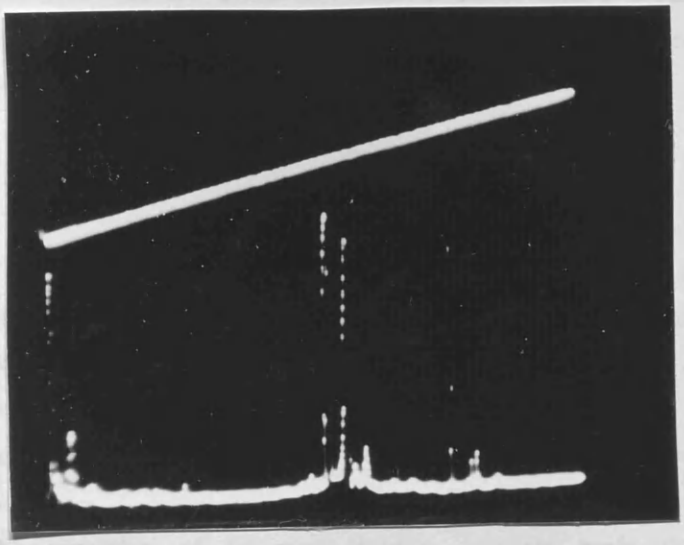

Figure 3.49
equency Instability Induced by Feedback from
Scanning Fabry Perot Interferometer.

optical isolation removed, then the condition of total coherence collapse could be initiated. Careful adjustment of the isolator allowed normal lasing conditions to be recovered. Thus the maximum isolation attainable with the λ/4 plate and polaroid sheet (about 20 dB) could be achieved. A slight misalignment of the FPI would then prevent the condition of feedback effects causing problems arising while giving excellent resolution in the FPI trace.

Feedback from the input coupling stage to the delay fibre was not as strong as from the FPI and the effect observed was more subtle. Figure 3.50 shows a measurement of a free running laser diode with no optical isolation from the fibre input. The measurement indicates that the diode linewidth is better that 1 MHz. The following figure (FIgure 3.51) shows the true linewidth as measured with the isolator in position.

3.7.5 Stability and Tunability.

Absolute wavelength measurements were made on the external cavity modules. This revealed that lasing in the external cavity was achieved over a wide, but unpredictable, range of wavelengths. Lasing on any stable mode was governed in practice by the aligment of the reflecting mirror. Current and temperature variations had only a limited effect. External cavity length adjustment was seen to provide the capability of frequency tuning, however again this was effective only within the stable mode of oscillation. While a mode jump could be provoked with the mirror alignment, no effective method of predicting to where the jump would go could be found. Neither could stability of the resulting oscillation be gauranteed. Although all lasers used in external cavities were matched to better than 0.2nm prior to coating and exhibited peaks in the coated gain profile consistent with this matching, no two diodes were found to lase on coincident wavelengths in external cavities.

Practical experimentation with the external cavity diode laser showed the arrangement to be, when well lined up, generally more stable and less susceptable to external acoustic influence than the coupled cavuty arrangement. Once aligned on a stable mode, the

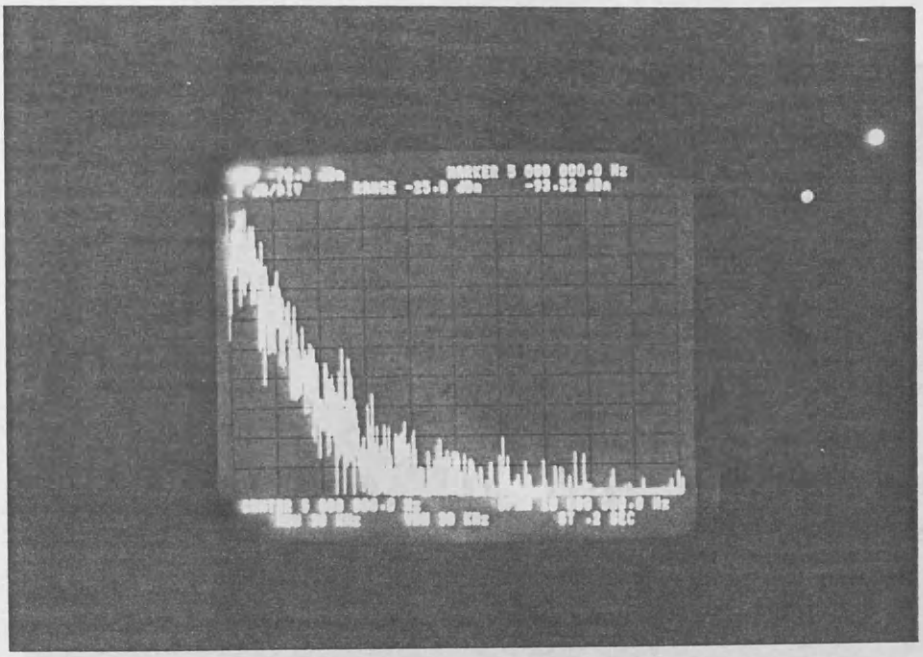

Figure 3.50

Linewidth Measurement : Free Running HLP 1400

No Optical Isolation from Fibre Input Coupling Jig.
Linewidth < 1 MHz.

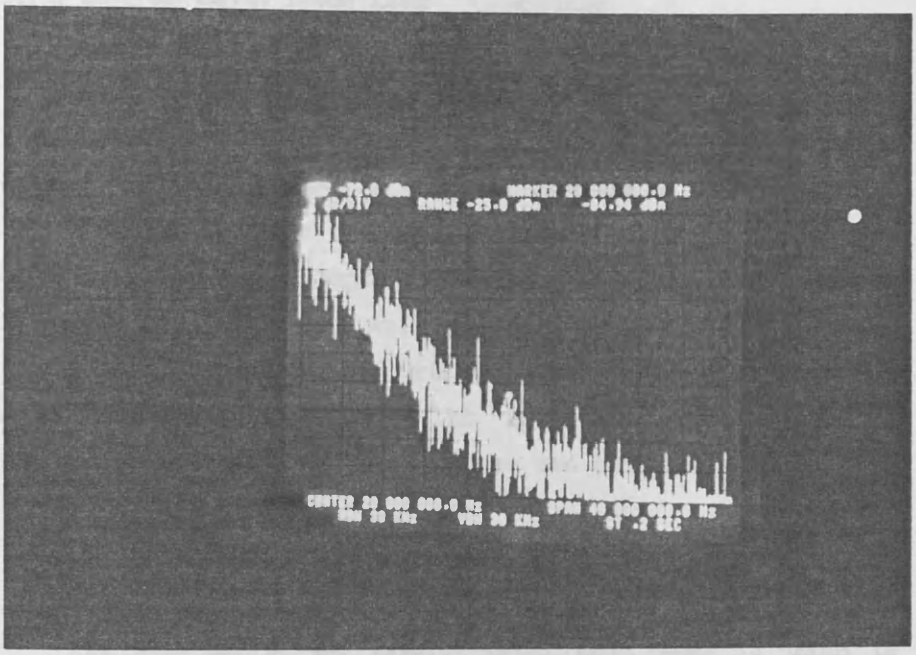

Figure 3.51

Linewidth Measurement : Free Running HLP 1400

Optical Isolation In Position.

Linewdith Approximately 6 MHz.

diode could be left for extensive periods of time (from days to weeks) and lasing in an external cavity would be achievable on power up. It must be stressed however that this performance was highly dependent upon the quality of the anti–reflection coating. One diode (coated to less than 1% reflectivity) obviously outperformed other diodes in external cavities in terms of stability. At the early stages of the diode life the diode could be subjected to fairly major mechanical disturbances (physical shaking of the bench) and still recover the lasing condition.

3.7.6 External Cavity Diode Laser : Conclusions.

The external cavity diode laser has been implemented and measurements indicate that linewidths in tens of kHz were achieved. Such a range is suitable for coherent experiments. The stability of the device was found to be markedly superior to the coupled–cavity arrangement when an adequate anti–reflection coating was deposited. However, the tunability was completely erratic. No consistent experimental procedure for selecting a particular frequency of oscillation was ever effected. This exaggerated the problems of obtaining a heterodyne beat note between two individual diodes.

3.8 Diffraction Grating Loaded External Cavity Laser.

The successes of the external cavity diode laser in terms of stability and linewidth reduction were, to a large extent, offset by the lack of tunability of the devices. Extensive experimental attempts to obtain a reproducible beat spectrum between two sources were unsuccessful. It was decided therefore to construct an external cavity laser using a diffraction grating to influence the oscillation frequency. Lenses, specifically designed for laser diodes, had at this point become available and it was therefore decided to attempt to use one of these with 4.3 mm focal length. This lens proved to be a more suited to collimating the rear facet beam, being aided to a certain degree by the fact that the laser diode mounts were imprecisely engineered and certain of the more recently purchased diodes would permit almost perfect collimation from the rear facet. With these diodes the external cavity arrangement was set up (Figure 3.52).

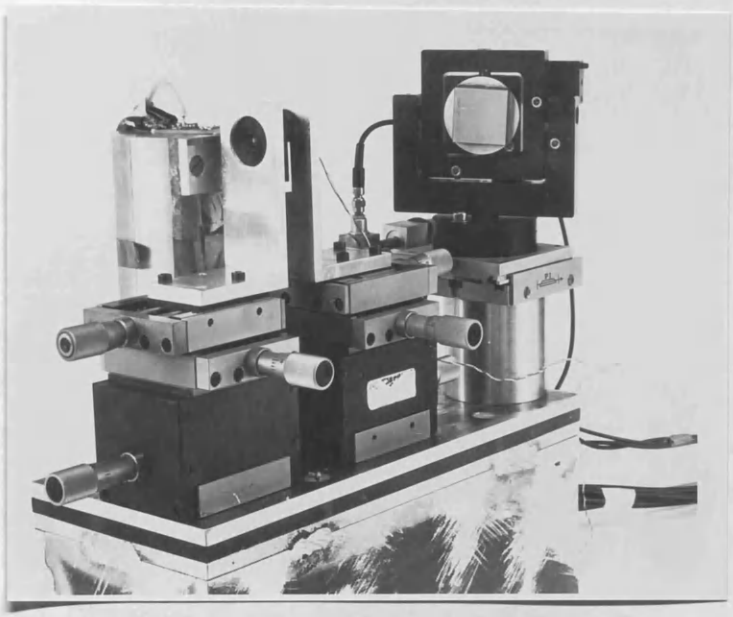

Figure 3.52
External Cavity Laser Mount
with Diffraction Grating Reflector.

The effect of the grating on the tunability can be readily observed in Figure 3.53. Tuning can be seen to take place in integral multiples of the cavity free spectral range over some 16 nm, for the best device. The reason for the apparent difference in tuning ranges for different lasers was attributed to the fact that the coating were of differing qualities. It must be noted that all the above measurements were made over the ranges where tuning could be achieved without realignment of the feedback. With readjustment of the focal position the above tuning ranges could be extended marginally. Tuning ranges in excess of 50 nm have been reported using this technique [19]. The reason for the difference in performance between this experiment and that carried out in the work described in reference 19 is the length of the cavity. The diodes used in reference 19 were 60 μm in length while the Hitachi diodes of the present work are 300μm. The longer length, while offering a higher Q factor in the free–running state, limits the spread of the gain profile and hence reduces the tuning range in the external cavity arrangement.

Due to the inefficiency of the output coupling from the rear facet of the laser diode, no attempt was made to measure the grating–loaded laser linewidth. There was no reason to suspect however that this would be different from the original external cavity laser mounts. Measurements of the linewidths of beat spectra indicate the individual linewidth to be in the order of tens of kilohertz.

3.8.1 Diffraction Grating Loaded External Cavity Laser : Conclusions.

The implementation of the external cavity laser diode using a diffraction grating to provide the external feedback proved to be successful in that the tunability of the device was greatly enhanced. Tuning was achieved onver a range of some 16 nm. The stability of the diode in the grating loaded external cavity arrangement appeared to be better than cavities using a simple mirror. However alignment of the grating loaded diode was generally found to be more critical than the plane mirror cavity. The improvement in stability of the grating loaded cavities was attributed to the fact that the grating would provide a certain amount of frequency selectivity in the feedback power. Thus mode competion was less likely to arise. The alignment

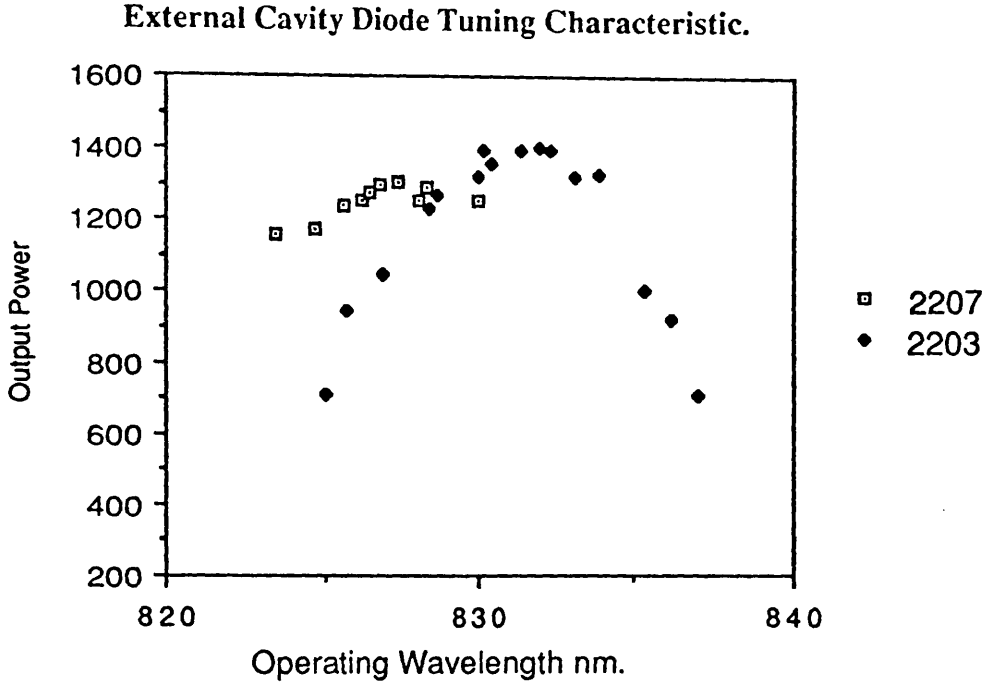

Figure 3.53

Tuning Characterisitcs of External Cavity Laser Diode

of the grating was however more exacting before lasing would take place. It is thought that the angle of the blaze in the grating was responsible for this phenomenum. Power was only efficiently fed back when the alignment was precise. External cavity devices using the mirror arrangement were found to produce an unstable oscillation with less critical alignment however required considerable fine tuning before a stable emmision was achieved.

A number of diodes (in total 8) were AR coated and set up in an external cavity arrangement. Of these however only two were found to be sufficiently well coated, and close enough in operating wavelength, for heterodyne system experiments to be carried out.

3.9 External Cavity Stabilisation.

In order to improve the frequency stability of the external cavity lasers during heterodyne system experiments, it was decided to lock the transmit laser onto the peak of a Fabry Perot discrimination curve. This was achieved with the use of the arrangement shown in Figure 3.54. The laser emission was coupled into the FPI and the output detected using a pin diode. The rear mirror of the FPI was driven with a sinusoidal 5 kHz dither signal. The output of the FPI was then mixed with the dither drive signal in order that the low frequency component, representative of the laser emission centre frequency, could be extracted. This signal was then filtered and fed back to provide the required control signal to correct the laser drift.

A typical ouptut trace from the FPI is shown in Figure 3.56. This shows the modulating dither signal and the corresponding error signal while the laser is held on the transmission peak. The assymetry of the waveform increases as the emission is detuned from the Fabry Perot transmission peak, thus providing a greater dc component to feedback to counteract large frequency drifts.

The arrangement described above was found to maintain a stable centre frequency of oscillation for minutes at a time. Short term stability did not however appear to be significantly improved.

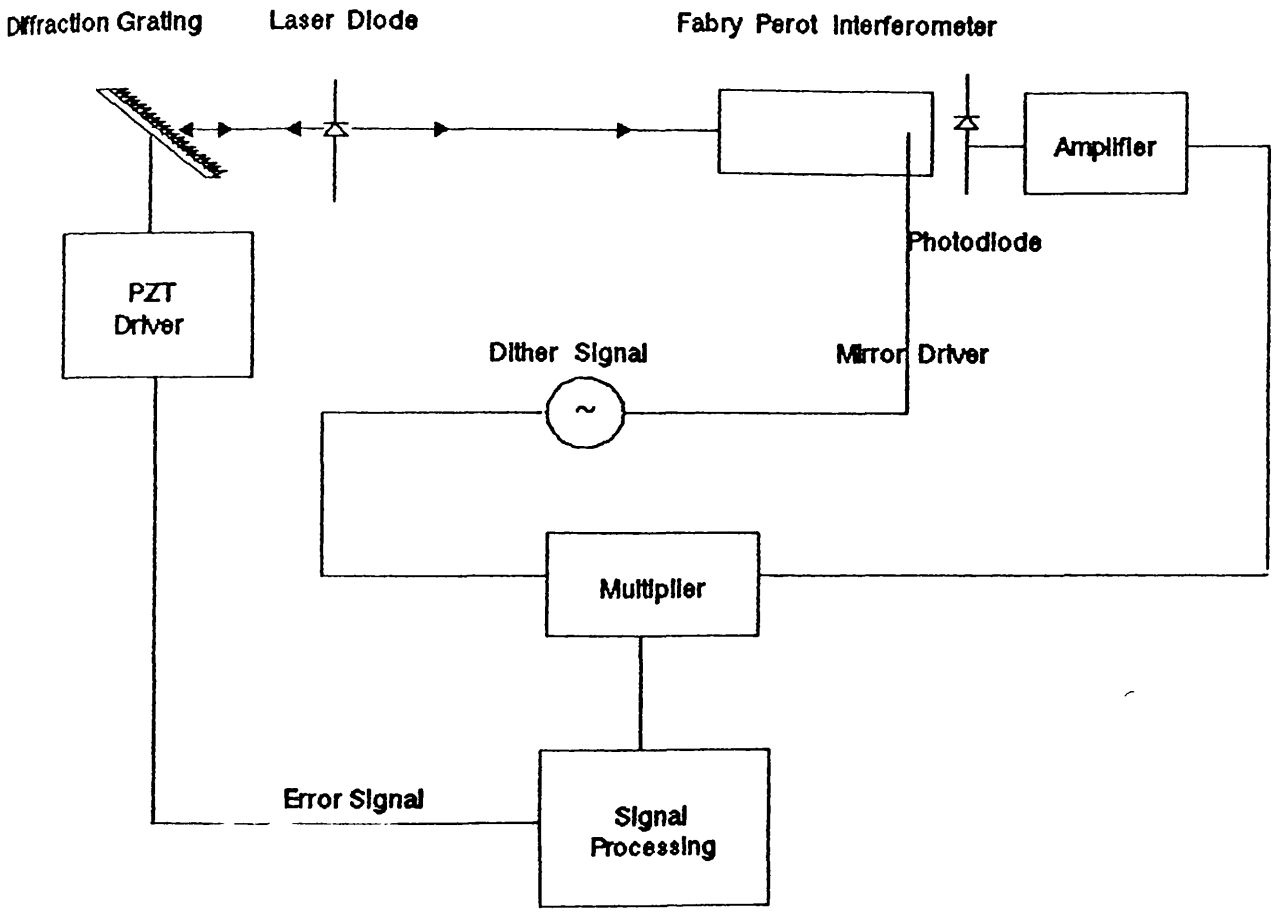

Figure 3.54

Schematic of Fabry Perot Stabilisation Circuitry.

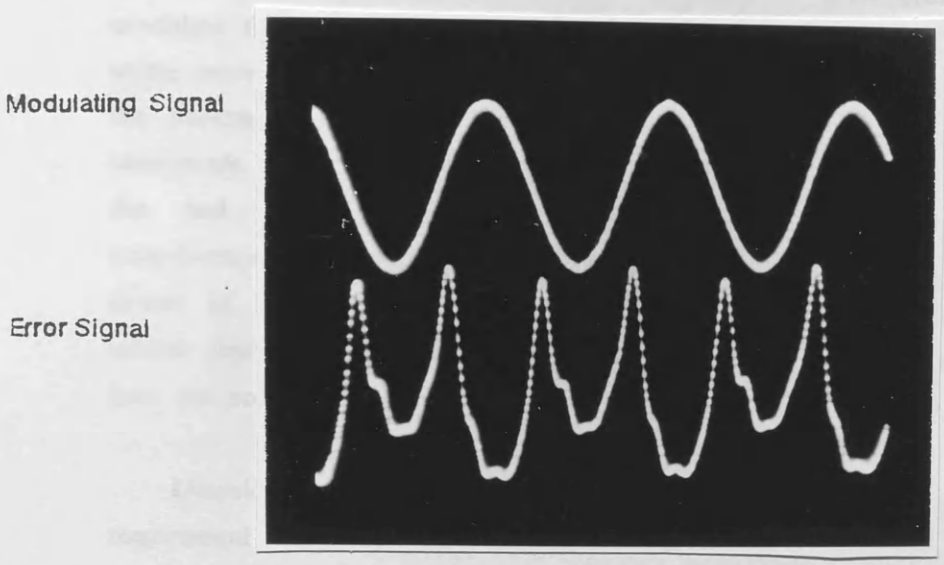

Figure 3.55

Control Signal From FPI Stabilisation Circuitry.

Frequency jitter of the order of 10 MHz was observed. The suspected cause of this was backlash in the mechanical couplings in the laser mount. Further details on this area will be given in Chapter 7..

3.10 Conclusions.

This chapter has provided a description of the properties of a laser diode which are of interest to the designer of a coherent communications network. A brief comparison of the characteristics (tunability, stability, linewidth and modulation behaviour) of various types of laser source has been given. Arguably the most promising candidate for coherent systems is the DFB laser. This device has a stable centre frequency due to the fact that it relies on a grating on the substrate to provide the optical feedback necessary for lasing. Monomode oscillation is thus achieved if the residual reflection from the end facets can be sufficiently reduced. Techniques for manufacturing DFB lasers have not however been refined to the same extent as those for the CSP devices. Consequently, DFB sources exhibit linewidths that are in general an order of magnitude poorer than the commercially available CSP sources.

Linewidth reduction has been shownto be a pre-requisite requirement for the further investigation of coherent systems. A large amount of attention has therefore been directed to this area. A description of some of the techniques developed has also been given in this chapter. The most successful of these ideas involved coupling the laser oscillation to an external cavity. Such coupling has also provided the additional benefit of flattening the laser modulation characteristics.

The Hitachi HLP 1400 laser diode was investigated as a potential source for coherent systems experiments and was found to be tunable, using current and temperature control, over a range of approximately 4-5 nm. The tuning characteristics were however found to be nonuniform and extremely sensitive to unintentional optical feedback. The linewidth of the HLP 1400 diodes was measured and was found to be less than 15 MHz. A linewidth of this magnitude would make phase-locking of laser diodes very difficult (see Chapter 6), and

therefore attempts were made to reduce it by coupling the source to an external cavity. Initial experiments provided linewidths of less than 500 kHz. However the external cavity arrangement was found to be sensitive to acoustic disturbance and was inadequately controlled in temperature. The laser mounts were then redesigned and a true external cavity arrangement implemented. The construction of such an external cavity laser required that one facet of the laser diode be antireflection coated. A multi–layer coating of unknown composition and a Titanium Oxide quarter wavelength layer were investigated for this purpose. Both coatings were sucessful in reducing the reflectivity to better than 5%. The Titanium Oxide layer achieved the best result, reducing the reflectivity to better than 0.5% in one case. The application of the coating was however found to be problematic and the reliability, for a small number of sources, was poor. Diodes coated in the same run were found to have facet reflectivities ranging from 1% to 32%. The cause of this wide range of performances is not known but it was not possible to investigate the coating procedure. Diodes coated to give reflectivities of less than 5% were used in the construction of external cavity lasers. These lasers exhibited tuning ranges of some 16 nm and showed measured linewidths estimated between 20 and 60 kHz. These sources were also found to be more stable and less sensitive to acoustic disturbance. Further stabilisation was achieved by locking the emission centre frequency to the peak of a FPI discrimination curve. This was successful in eliminating a large amount of the low frequency drifts due to temperature cycling, however no significant desensitisation with respect to acoustic fluctuations was observed. The acoustic fluctuations were more difficult to remove because they resulted from very small vibrations (in nanometres) in the mirrors positioning equipment. Fluctuations of this magnitude would be comparible with hysteresis in the mechanical coupling and would therefore not be tracked out. More attention will be given to this subject in Chapter 7.

The investigations of the laser diode have revealed that, in the free running condition, the HLP 1400 laser diode is a suitable signal source for the less exacting of the coherent formats (ASK, FSK). The concern of this project is the investigation of the Optical Phase–Locked Loop. For this application the HLP 1400 diode does

not meet the requirments in the free running state. However the linewidth and tunability characteristics of the external cavity diode would be well suited to this application (see Chapter 5).

APPENDIX 3.1: Laser Temperature Controller.

The temperature of the laser diode was regulated with the use of the arrangement depicted in Figure 3A.1. A platinum resistance thermometer was used, in a balanced bridge circuit, to measure the temperature of the laser mount. The output from the bridge circuit was amplified and fed into an analogue three term controller, the output of which was used to drive a Peltier element heat exchanger. Short term temperature stability of 0.001 K was achieved using this arrangement.

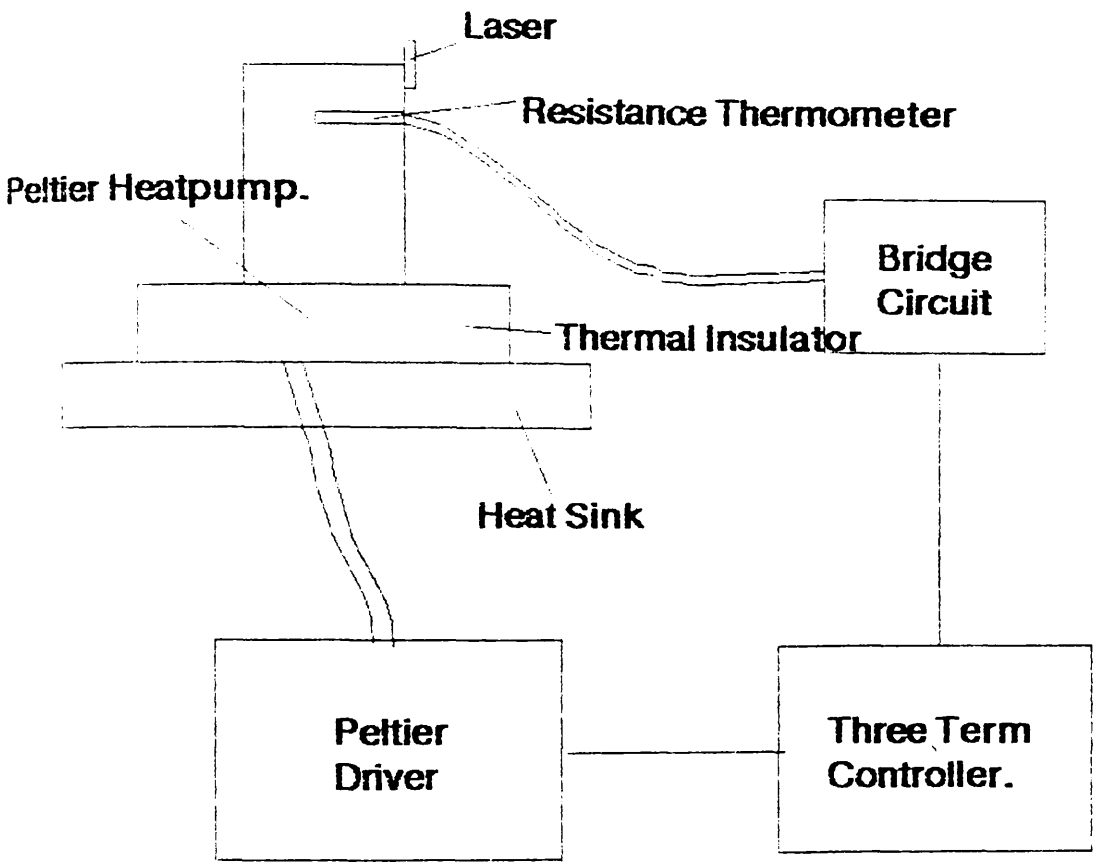

Figure 3A.1

Laser Diode Temperature Controller Schematic.

References.

1. J.Gower 'Optical Communications Systems.' Prentice Hall, London 1984.

2. A.L.Schawlow, C.H.Townes 'Infrared and Optical Masers' Phys. Rev. voll 112, 1958. pp1940–1949.

3. B.Daino *et.al.* 'Phase Noise and Spectral Lineshape in Semiconductor Lasers' IEEE J.Quant. Elect. QE–19(3) 1983. pp266–270.

4. P.Spano *et.al.* 'Phase Noise in Semiconductor Lasers: A Theoretical Approach' IEEE J.Quant. Elect. QE–19(4) 1983. pp136–137.

5. C.H.Henry 'Theory of Linewidth of Semiconductor Lasers' IEEE J.Quant. Elect. QE–18(2) 1982, pp259–264.

6. C.H.Henry 'Theory of the Phase Noise and Power Spectrum of a Single Mode Injection Laser' IEEE J.Quant. Elect. QE–19(9) 1983. pp1391–1397.

7. C.H.Henry 'Phase Noise in Semiconductor Lasers' J.Lightwave Technol. LT–4(3) 1986, pp289–311.

8. Streifer W, *et.al.* 'Coupled Wave Analysis of DFB and DBR Lasers.' IEEE Journ. Quantum Elect. QE–13(4) 1977 pp134–141.

9. P.J.Kuindersma *et.al.* 'Fabrication and Performance of 1.55μm DFB Laser Devices, Based on PB–DCPBH Diodes with First Order Gratings in InP.' Technical Digest ECOC12 1986 pp25–29.

10. F.Favre 'Sensitivity to Optical Feedback for Quarter wave Shifted DFB Lasers.' Technical Digest ECOC12 1986 pp33–37.

11. Lee, T.P. *et.al.* 'Measured Spectral Linewidth of Variable Gap Cleaved Coupled Cavity Laser.' Electron. Lett. 21(2) 1985 pp53–54.

12. C.J.Nielson, J.H.Osmundsen 'Linewidth Stabilisation of Semiconductor Lasers in an External Cavity' J.Opt.Commun. vol. 5(2) 1984. pp42–25.

13. S.Yamaguchi, M.Suzuki 'Frequency Stabilisation of a Diode Laser by Use of the Optogalvanic Effect.'Appl. Phys. Lett.41(7) 1982 pp597–598.

14. C.J.Nielsen, J.H.Osmundsen 'New Approach Towards Frequency Stabilisation of Linewidth Narrowed Semiconductor Lasers.'
IEE Elect. Lett. Vol.19 no.16 1983 pp 644–646.

15. M. Ohtsu, S. Kotajima 'Linewidth Reduction of a Semiconductor Laser by Electrical Feedback.' IEEE Journ. Quant. Elect. QE–21(12) 1985 pp1905–1912.

16. S.Saito, *et.al.* 'Frequency Modulation Noise and Linewidth Reduction in a Semiconductor Laser by means of Negative Frequency Feedback Technique.' Appl. Phys. Lett.46(1)1985 pp3–5.

17. S.Saito *et.al.* 'Coherent FSK Transmitter Using a Negative Feedback Stabilised Semiconductor Laser.' IEE Elect. Lett. vol.20 no.17 1984 pp703–704.

18. Y.Yamamoto *et.al.* 'AM and FM Quantum Noise in Semiconductor Lasers–Part 2: Comparison of Theoretical and Experimental Results for AlGaAs Lasers.' IEEE Jour. Quant. Elect. QE–19(1) 1983 pp47–58.

19. R.Wyatt, W.J.Devlin '10 kHz Linewidth 1.5 μm InGaAsP Laser with 55nm Tuning Range' Elect. Lett. 19(0) 1983 pp110–112.

20. M.R.Mathews, K.H.Cameron, R.Wyatt, W.J.Devlin 'Packaged Frequency–Stable Tunable 20 kHz Linewidth 1.5 μm InGaAsP External Cavity Laser' Elect. Lett. 21(3) 1985. pp113–115.

21. F.Favre, D.LeGuen 'Emission Frequency Stability in Single Mode Fibre Optical Feedback Controlled Semiconductor Lasers' Elect. Lett. 19(17) 1983. pp 663– 665.

22. F.Favre, D.leguen, J.C.Simon 'Optical Feedback Effects on Laser Diode Oscillation Field Spectrum' IEEE J.Quant. Elect, vol QE−18(10) 1982 pp1712−1717.

23. F.Favre, D.Leguen 'Autostabilisation Technique for Achieving Highly Stable Resonant Optical Feedback' Elect. Lett. 19(24) 1983. pp1046−1048.

24. H.Olesen *et.al* 'Solitary Spectral Linewidth and its Reduction with External Grating Feedback for a 1.55μm InGaAsP BH Laser.' Jap. Journ. Appl. Phys. vol.22 no.10 1983 pp L664−L666.

25. J.H.Osmundsen *et.al.* 'Experimental Investigation of Stability Properties for a Semiconductor Laser with Optical Feedback.' IEE Elect. Lett. vol.19 no.25 pp1068−1070 1983.

26. E.Patzak *et.al.* 'Semiconductor Laser Linewidth in Optical Feedback Configurations.' IEE Elect.Lett. 1983 vol.19 no.24.

27. E.Patzak *et.al* 'Spectral Linewidth Reduction in Semiconductor Lasers by an External Cavity with Optical Feedback' Elect. Lett. 19(22) 1983. pp938−040.

28. R.Lang, K.Kobayashi 'External Optical Feedback Effects on Semiconductor Injection Laser Properties' IEEE J.Quant. Elect. QE−16(3) 1980. pp347−355.

29. C.Park *et.al.* 'Single Mode Behaviour of a Multimode 1.55μm Laser with a Fibre Grating External Cavity'. IEE Elect. Lett 22(21), pp1132−1134 1986.

30. Saito S. *et.al.* 'Oscillation Centre Frequency Tuning, Quantum FM Noise, and Direct Frequency Modulation Characteristics in External Gating Loaded Semiconductor Lasers' IEEE Journ. Quant. Elect. QE−18(6). June 1982. pp961−971.

31. K.Kikuchi, T.P.Lee 'Spectral Analysis of Weakly Coupled External Cavity Semiconductor Lasers.' Journ. Lightwave. Techn. LT−5(9) 1987

pp1269–1272.

31. F.Favre *et.al.* 'External Cavity Semiconductor Laser with 15nm Continuous Tuning Range.' IEE Elect. Lett. 1986 vol.22 no.15 pp795–796.

33. F.Favre, D.Le Guen'FM Noise Reduction in Semiconductor Laser Weakly Coupled to a Single–mode Fibre Resonator.' IEE Elect. Lett. vol.21. no.11. 1985 pp467–466.

34. K.Kikuchi *et.al.* 'Measurement of Linewidth and FM Noise Spectrum of 1.52μm InGaAsP Lasers.' IEE Elect.Lett. vol.20. no.13 pp535–536.

35. H.Sato *et.al.* 'Theoretical Analysis of Longditudinal Mode Coupling in External Cavity Semiconductor Lasers.' IEEE JOurn. Quant. Elect. QE–21(4)1985 pp284–291.

36. L.A.Glasser 'A Linearised Theory for a Diode Laser in an External Cavity.' IEEE Journ. Quant. Elect. QE–16(5) 1980 pp525–531.

37. K.Kikuchi, T.Okoshi 'Simple Formula Giving Spectrum Narrowing Ratio of Semiconductor Laser Output Obtained by Optical Feedback.'IEE Elect. Lett. vol. 18 no.1. 1982 pp10–12.

38. H.Olesen *et.al.* 'Nonlinear Dynamics and Spectral Behaviour for an External Cavity Laser.' IEEE Journ. Quant. Electron. QE–22(6) 1986 pp762–773.

39. Chie–Yu Huo, J.P. van der Ziel 'Linewidth Reduction of 1.5μm Grating Loaded External Cavity Semiconductor Laser by Geometric Reconfiguration.' Appl. Phys. Lett. 48(14) 1986 pp885–887.

40. H.Sato, Jun Ohya 'Theory of Linewidth of External Cavity Semiconductor Lasers.' IEEE Journ. Quant. Elect. QE–22(7) 1986 pp1060–1063.

41. M.Tamburrini, P.Spano, S.Piazzolla 'Influence of an External Cavity on Semiconductor Laser Phase Noise' Appl. Phys. Lett. vol.43(5) 1983 pp410–412.

42. H.Sato, J.Ohya 'Theory of Spectral Linewidth of External Cavity Semiconductor Lasers' IEEE J.Quant. Elect. QE–22(7) 1986. pp1060–1063.

43. P.Spano *et.al.* 'Theory of Noise in Semiconductor Lasers in the Presence of Optical Feedback' IEEE J.Quant. Elect QE–20(4) 1984. pp350–357.

44. T.Fujita *et.al.* 'Narrow Spectral Linewidth Characteristics of Monolithic Integrated Passive Cavity InGaAsP/InP Semiconductor Lasers' Elect. Lett. 21(9) 1985. pp374–376.

45. T.P.Lee *et.al.* 'Characteristics of Linewidth Narrowing of a 1.5 μm DFB Laser with a short Grin–Rod External Coupled Cavity' Elect. Lett. 21(15) 1985. pp655–656.

46. S.Piazzolla *et.al.* 'Characterisation of Phase Noise in Semiconductor Lasers.' Appl. Phys. Lett. 41(8) 1982 pp695–696.

47. L.Goldberg *et.al.* 'Noise Characteristics in Line Narrowed Semiconductor Lasers with Optical Feedback.' IEE Elect. Lett. vol.17 no.19 1981 pp677–678.

48. C.Henry, R.Kazarinov 'Instability of Semiconductor Lasers Due to Optical Feedback from Distant Reflectors.' IEEE Journ. Quant. Elect. QE–22(2) 1986 pp294–301.

49.. M.A.Grant, W.C.Michie, M.Fletcher 'The Performance of Optical Phase–Locked Loops in the Presence of Nonnegligible Loop Propagation Delay' Journ. Lightwave Technol. vol LT–5, no.4 1987 pp 592–597.

50. S.Kobayahi *et.al.* 'Modulation Frequency Characteristics of Directly Modulated AlGaAs Semiconductor Laser.' IEE Elect. Lett. vol.17

no.10 1981 pp 350–351.

51. J.Armor 'Phase–lock Control Considerations for Multiple Coherently Combined Lasers,' Master's Thesis, Air Force Institute of Technology, Wright–Patterson Air Force Base, OH, Rep. GEO/EE/77D–2, 1977.

52. Ries *et.al.* 'Influence of Extrinsic F.M. Noise on Laser Diode Linewidth Measured by Self Heterodyning' Optical Comms. vol.57(4). March 1986. pp 269–273.

53. T.Okoshi *et.al.* 'A novel Method for High Resolution Measurement of Laser Output Spectrum'Electronics Lett. vol.16(16). July 1980 pp630–631.

54. Gallion, P. *et.al.* 'Single Frequency Lase Phase–noise Limitation in Single–mode Optical Fibre Coherent–detection Systems With Correlated Fields.' Journ. Opt. Soc. Amer. Vol. 72(9) 1982 pp1167–1170.

55. L.E. Richter *et.al.* 'Linewidth Determination From Self Heterodyne Measurements with Subcoherence Delay Times.' IEEE Journ. Quant. Elect. QE–22(11) 1986 pp270–275.

56. K.Kikuchi, T.Okoshi 'Dependance of Semiconductor Laser Linewidth on Measurement Time: Evidence of Predominance of 1/f Noise.' IEE Elect. Lett. 1985 vol.21. no.22. pp1011–1012.

57. I.P.Kaminow 'Measurement of the Modal Reflectivity of an Anti–reflection Coating on a Super Luminescent Diode' Journ. Quant. Elect. QE(4). April 83.

58. R.W. Tkach, A.R. Chraplyvy 'Regiemes of Feedback in 1.5 μm DFB Lasers.' Journ. Lightwave Technol. LT–4(11) 1986 pp1655–1661.

CHAPTER 4.

Coherent Reception : The Problem of Phase Synchronisation

4.1 Inroduction.

The benefits that may be obtained from the use of coherent techniques in the optical regime have been established. There remain, however, considerable technical problems that must first be overcome if these gains are to be realised. The practical difficulties involved in the implementation of these more complicated receivers require a considerable amount of attention. Not least of these problems is the need for frequency or phase synchronisation between the local oscillator and the transmit signal. A substantial amount of work has been directed towards this target ranging from methods of direct phase synchronisation, for example the phase locked loop [1-13], to configurations which aim to, with a certain amount of frequency control, implement phase insensitive coherent receivers using the balanced receiver technique [14,15]. The area of immediate interest to this project is the phase locked loop.

4.2 The Phase-locked Loop : PLL

The phase locked loop is a technique that has been employed in microwave systems for a number of years. Its behaviour is both well understood and well documented [16,19]. It is directly applicable to optical communications although the transition from microwave frequencies to the optical domain has associated with it additional problems arising from the relative spectral impurity of the optical sources. This is particularly true in the case of the semiconductor laser source which is spectrally inferior to its gas counterpart, exhibiting linewidths typically of the order of tens of megahertz.

The present chapter reviews the ground work necessary to facilitate an understanding of the optical phase locked loop. The discussion given here will be centred around the Costas Loop. Before considering the OPLL, it is useful to revise the simpler electrical

equivalent, in order that the general loop parameters may be introduced into the discussion. The basic loop model, given in Figure 4.1, can be found in any of the standard texts mentioned above [15–18]. The analysis is simplified for the moment, by assuming that the loop is in lock and the phase detector is linear.

The output of the phase detector is a voltage, v_d, representative of the phase difference between the incoming and local oscillator signals, or phase error $\theta_i - \theta_{lo}$.

$$v_d = K_d(\theta_i - \theta_{lo}) \qquad (4.1)$$

K_d represents the detector gain. Thus a control voltage $v_C(s)$ is returned to the local oscillator equal to

$$v_C(s) = F(s)v_d(s) \qquad (4.2)$$

The control voltage $v_c(s)$ will modulate the frequency of the local oscillator. Since frequency is the derivative of phase the change in the local oscillator laser output may be described by

$$d\theta_o/dt = K_o v_c. \qquad (4.3)$$

The Laplace transform of this yields

$$s\theta_o(s) = K_o v_c(s), \qquad (4.4)$$

and therefore

$$\theta_o(s) = K_o(s)v_c(s)/s \qquad (4.5)$$

where K_o is the gain of the laser diode in Hz/mA. The local oscillator phase is therefore described

$$\theta_{lo}(s) = K_o v_c(s)/s. \qquad (4.6)$$

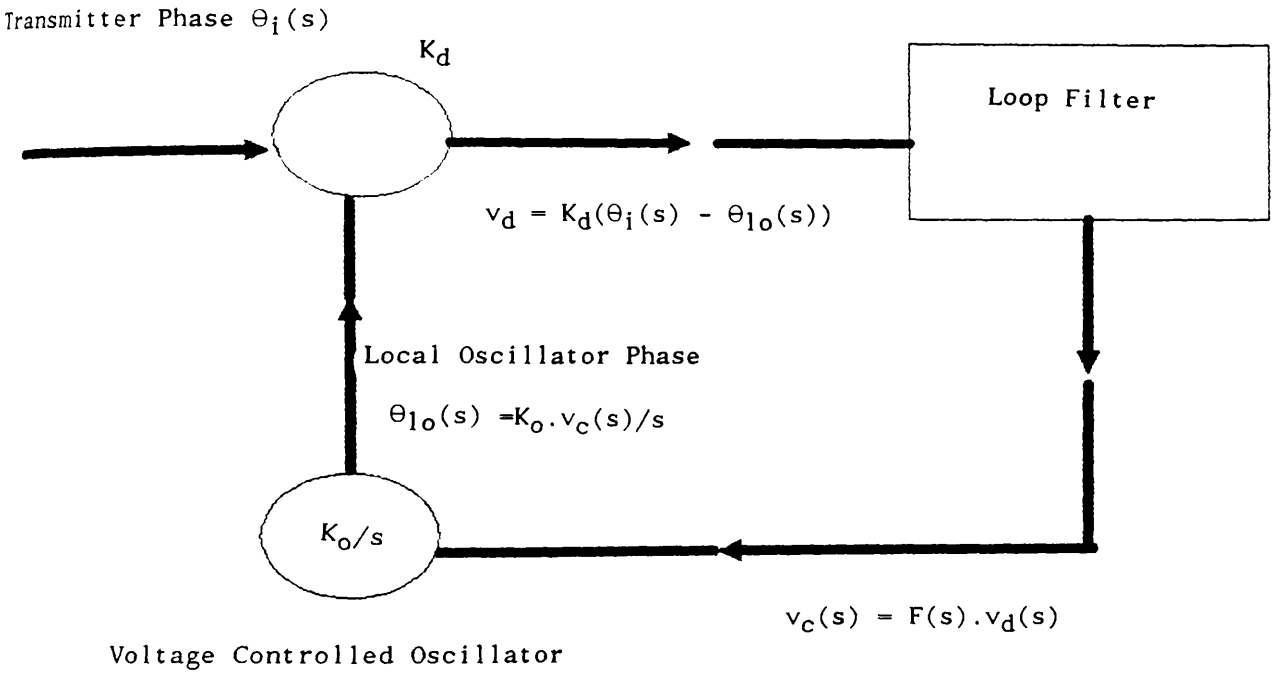

Figure 4.1

The Phase Locked Loop.

The notation F(s) is used to indicate the presence of some filtering used to tailor the loop response. The PLL transfer function H(s) may therefore be defined as

$$H(s) = \frac{\theta_{lo}}{\theta_i} = \frac{K_o K_d F(s)}{s + K_o K_d F(s)} \quad .(4.7)$$

The ratio of the phase error to the incoming signal phase is commonly referred to as the loop error function

$$\frac{\theta_i - \theta_{lo}}{\theta_i} = \frac{s}{s + K_o K_d F(s)} = 1 - H(s) \quad .(4.8)$$

In common with other closed loop systems, the performance of a PLL is described by the system natural frequency and its damping factor. These two attributes are in turn specified by the gain of the loop and the choice of loop filter. In the above example the loop gain is simply the product of the detector and local oscillator gains ($K_o.K_d$). Throughout this and subsequent discussions on the PLL the use of an active loop filter configuration, as shown in Figure 4.2, will always be assumed. The transfer fuction of a filter of this configuration is

$$F(s) = (1 + s\tau_2)/s\tau_1. \quad (4.9)$$

The time constants τ_1 and τ_2 are as defined in Figure 4.2. Assuming this choice of filter, the loop transfer function is a standard second order function and may be rewritten,

$$H(s) = \frac{2\zeta\omega_n^2 + \omega_n^2}{s^2 + 2\zeta\omega_n s + \omega_n^2} \quad (4.10)$$

where ω_n, the loop natural frequency, is given by,

$$\omega_n = (K_o K_d)^{1/2}/\tau_1 \quad (4.11)$$

and the damping factor ζ,

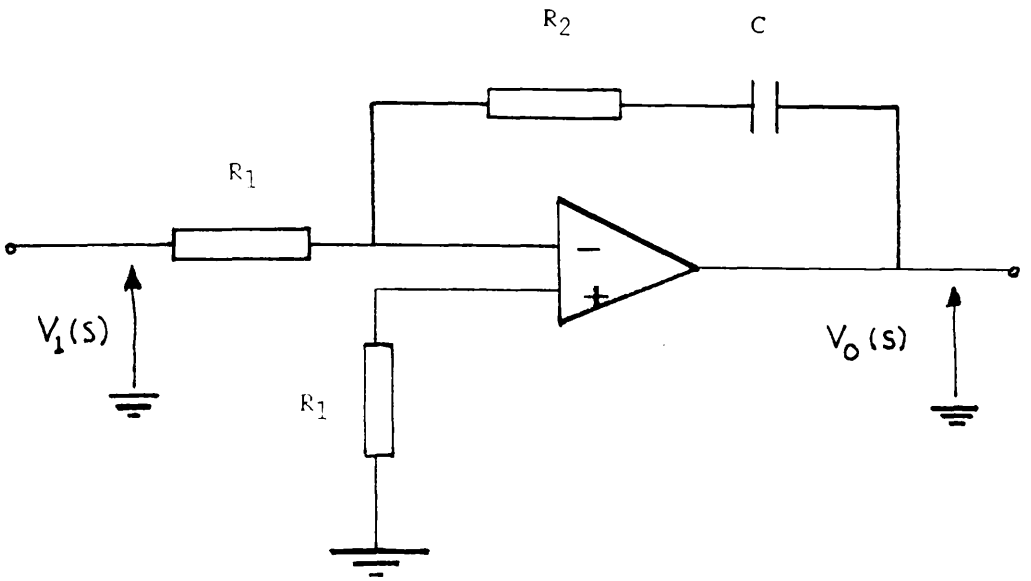

$$\frac{v_o(s)}{v_i(s)} = \frac{1 + s\tau_1}{s\tau_2} = F(s)$$

$$\tau_2 = R_2C \qquad \tau_1 = (R_1 + R_2)C$$

Figure 4.2

Active Filter Configuration.

$$\zeta = \tau_2\omega_n/2. \qquad (4.12)$$

Thus, through careful choice of the filter time constants τ_1 and τ_2, and the loop gain, the loop damping factor and natural fequency may be independantly controlled.

4.3 The Optical Phase–locked Loop : OPLL

The above discussion will now be extended to describe the PLL at optical frequencies, the OPLL. The analysis will be carried out for the case of a Costas Loop and include all noise sources. The Costas Loop has been chosen because of its excellent phase demodulation properties and because it has the advantage of being implemented as a homodyne PLL without the need for a dc coupled photodetector. This can be of considerable benefit when it is considered that reverse bias voltages of around 50 Volts are typical for standard pin diodes.

A model of a Costas Loop, as standard to any of the common review papers [4,8], is given in Figure 4.3. The generation of the 90 degrees phase shift in the quadrature arm may be accomplished through the use of a phase shifter or by means of a 90 degrees optical hybrid [20]. The particular method of generation is not relevant at this stage; it is sufficient to assume that the shift is accomplished and that some means of regulating the percentage of signal and local oscillator power allocated to each arm of the loop is provided. The relative amounts of power allocated in this manner will be quantified in the following argument with the use of the coupling ratio of the combiner α.

The incoming optical signal has an electric field $E_s(t)$ which can be described as

$$E_s(t) = m(t)(2P_s)^{1/2}\sin(\omega_c t + \theta_i + \varphi_i) \; . \qquad (4.13)$$

P_s denotes the signal power, ω_c the angular frequency of the supressed carrier, θ_i the instantaneous phase of the incoming signal

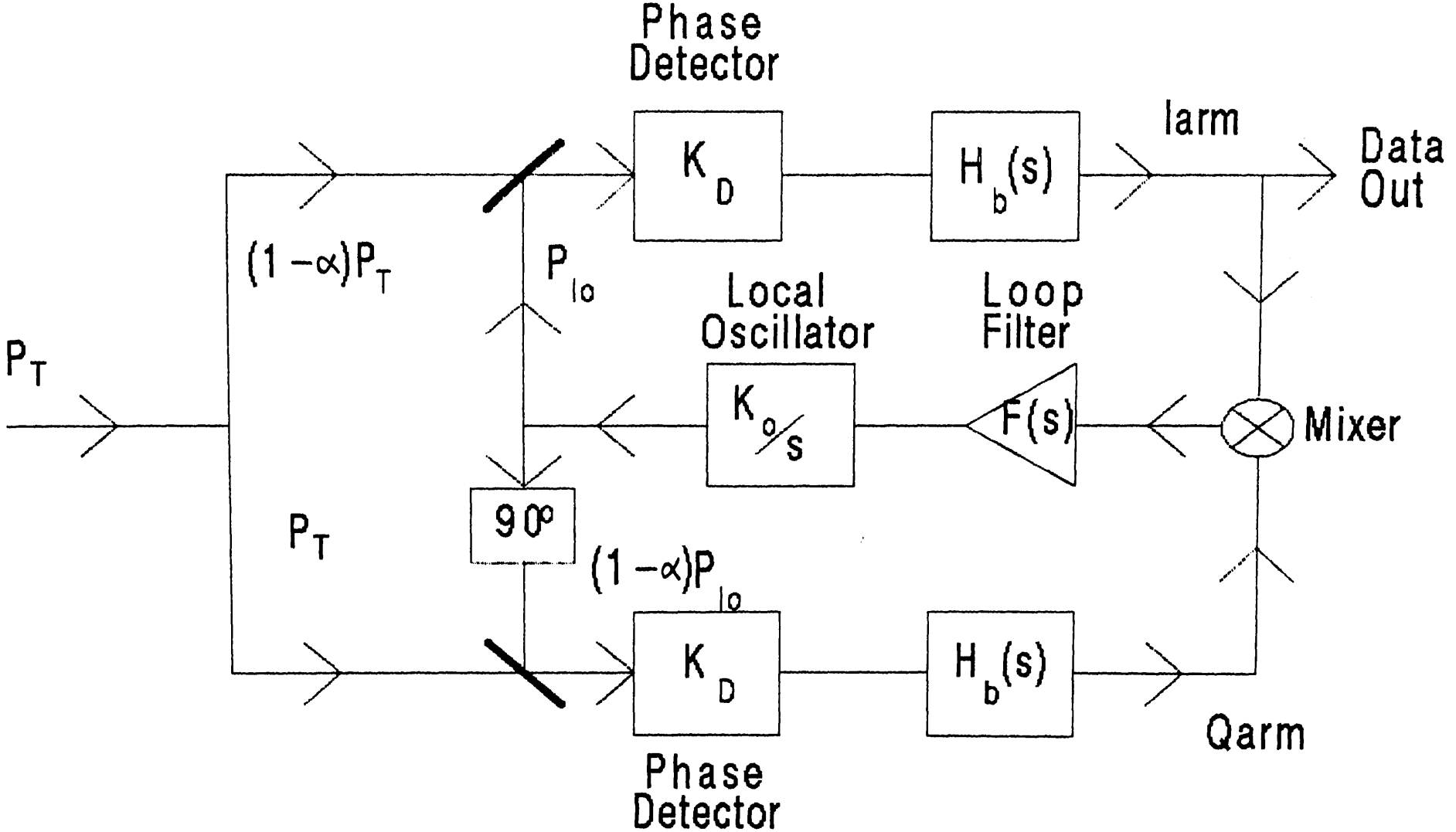

Figure 4.3 Schematic of Optical Costas Loop.

and φ_i the transmitter oscillator phase instabilities (representative of the laser linewidth). The modulation is denoted by m(t). For the moment it will be assumed that this modulation is anti-podal PSK therfore m(t) will take the values $\mp$ 1. A similar expression for the local oscillator field can be written,

$$E_{lo}(t) = (2P_{lo})^{1/2}\sin(\omega_{lo}t + \Theta_{lo} + \varphi_{lo}). \quad (4.14)$$

The photodetector is modelled as an ideal multiplier with no repsonse at the summation frequency of the two input signals, hence the outputs of the hybrid coupler may be described as,

$$e_1(t) = m(t)(2P_s(1-\alpha))^{1/2}\sin(\omega_c t + \Theta_i + \varphi_i) \quad (4.15)$$

$$e_2(t) = m(t)(2P_s\alpha)^{1/2}\sin(\omega_c t + \Theta_i + \varphi_i) \quad (4.16)$$

$$e_3(t) = (2P_{lo}\alpha)^{1/2}\sin(\omega_{lo}t + \Theta_{lo} + \varphi_{lo}) \quad (4.17)$$

$$e_4(t) = (2P_{lo}(1-\alpha))^{1/2}\cos(\omega_{lo}t + \Theta_{lo} + \varphi_{lo}). \quad (4.18)$$

The output of the photodetector is therefore,

$$e_5(t) = (P_sP_{lo}\alpha(1-\alpha))^{1/2}m(t)R\cos(\delta\Theta + \delta\varphi), \quad (4.19)$$

in the case of the, 'in phase', arm and

$$e_6(t) = (P_sP_{lo}\alpha(1-\alpha))^{1/2}m(t)R\sin(\delta\Theta + \delta\varphi), \quad (4.20)$$

in the case of the, 'quadrature', arm. It is assumed that the PLL is locked therefore the difference frequency $\omega_c-\omega_{lo}$ has been omitted. The notation $\delta\Theta$ and $\delta\varphi$ are used to denote the instantaneous phase difference between the two signals and the resultant phase noise arising from the combination of the two noisey laser sources. R is the responsivity of the photodetector diode. The algebraic manipulation of these expression may be simplified if the detector gain K_d is defined as

$$K_d = (4P_sP_{lo}\alpha(1-\alpha))^{1/2}Rm(t). \quad (4.21)$$

The discussion will be continued in the Laplace domain in order that the unneccessary complication of evaluating convolution integrals in the time domain may be avoided. Hence 4.19 and 4.20 may be rewritten as

$$e_5(s) = K_d(s)\cos(\delta\Theta + \delta\varphi)/2 \qquad (4.22)$$

and,

$$e_6(s) = K_d(s)\sin(\delta\Theta + \delta\varphi)/2. \qquad (4.23)$$

At this point it is appropriate to introduce the random noise noise voltages that are present in both arms as a result of the quantum nature of the detection process. Thus

$$e_7(s) = K_d(s)\cos(\delta\Theta + \delta\varphi)/2 + N_I(s) \qquad (4.24)$$

and,

$$e_8(s) = K_d(s)\sin(\delta\Theta + \delta\varphi)/2 + N_Q(s) \qquad (4.25)$$

where $N_I(s)$ and $N_Q(s)$ are the shot noise voltages in the in phase and quadrature arm respectively. The front end cut off frequency of the photodetector is now included. This will have the effect of filtering the e_7 and e_8 in the following manner.

$$e_9(s) = K_d(s)\cos(\delta\Theta + \delta\varphi)H_b(s)/2 + N_I(s)H_b(s) \qquad (4.26)$$

$$e_{10}(s) = K_d(s)\sin(\delta\Theta + \delta\varphi)H_b(s)/2 + N_Q(s)H_b(s) \qquad (4.27)$$

If the mixer used to extract the phase error signal from these two voltages is assumed to have a conversion efficiency K_m then feedback voltage v_m may be written

$$v_m(s) = K_m K_d^2(s)H_b^2(s)\sin(2\delta\Theta + 2\delta\varphi) + N_{tot}(s). \qquad (4.28)$$

$N_{tot}(s)$ is the total noise contribution and comprises of three separate

parts N_1,N_2,N_3 where,

$$N_1(s) = K_m K_d H_b^2(s)\sin(2\delta\Theta + 2\delta\varphi)N_I(s)/2, \quad (4.29)$$

$$N_2(s) = K_m K_d H_b^2(s)\cos(2\delta\Theta + 2\delta\varphi)N_Q(s)/2, \quad (4.30)$$

$$N_3(s) = K_m N_I N_Q H_b^2(s). \quad (4.31)$$

While the loop is in lock the linearisation $\sin(\alpha) = \alpha$ may be applied. This simplifies the description of the noise components (for small $\delta\Theta$ it is assumed that $N_1(s)$ is zero). The noise analysis may be further simplified when it is considered that, in a practical situation, the contribution $N_3(s)$ will have insufficient power to activate the mixer (the individual noise voltage will not be sufficient to forward bias a diode) and therefore will not be present at the mixer output. The only noise source of any appreciable level will therefore be the contribution from the quadrature arm. Thus

$$v_m(s) = K_m K_d^2(s) H_b^2(s)[2\delta\Theta + 2\delta\varphi]/8 + K_m K_d H_b^2(s) N_Q(s)/2 \quad (4.32)$$

and the control voltage, fed to the local oscillator laser will be

$$v_c(s) = K_m K_d^2(s) H_b^2(s) F(s)[2\delta\Theta + 2\delta\varphi]/8 + K_m K_d H_b^2(s) N_Q(s) F(s)/2. \quad (4.33)$$

The Costas Loop has now been effectively linearised and its description is equivalent to a standard phase locked loop, with certain modifications to the filtering terms. A block diagram of the linearised model is shown in Figure 4.4. The local oscillator phase is described as

$$\Theta_o(s) = K_o K_m K_d^2(s) H_b^2(s).F(s)[2\delta\Theta + 2\delta\varphi]/8s + K_o K_m K_d H_b^2(s) N_Q(s) F(s)/2s. \quad (4.34)$$

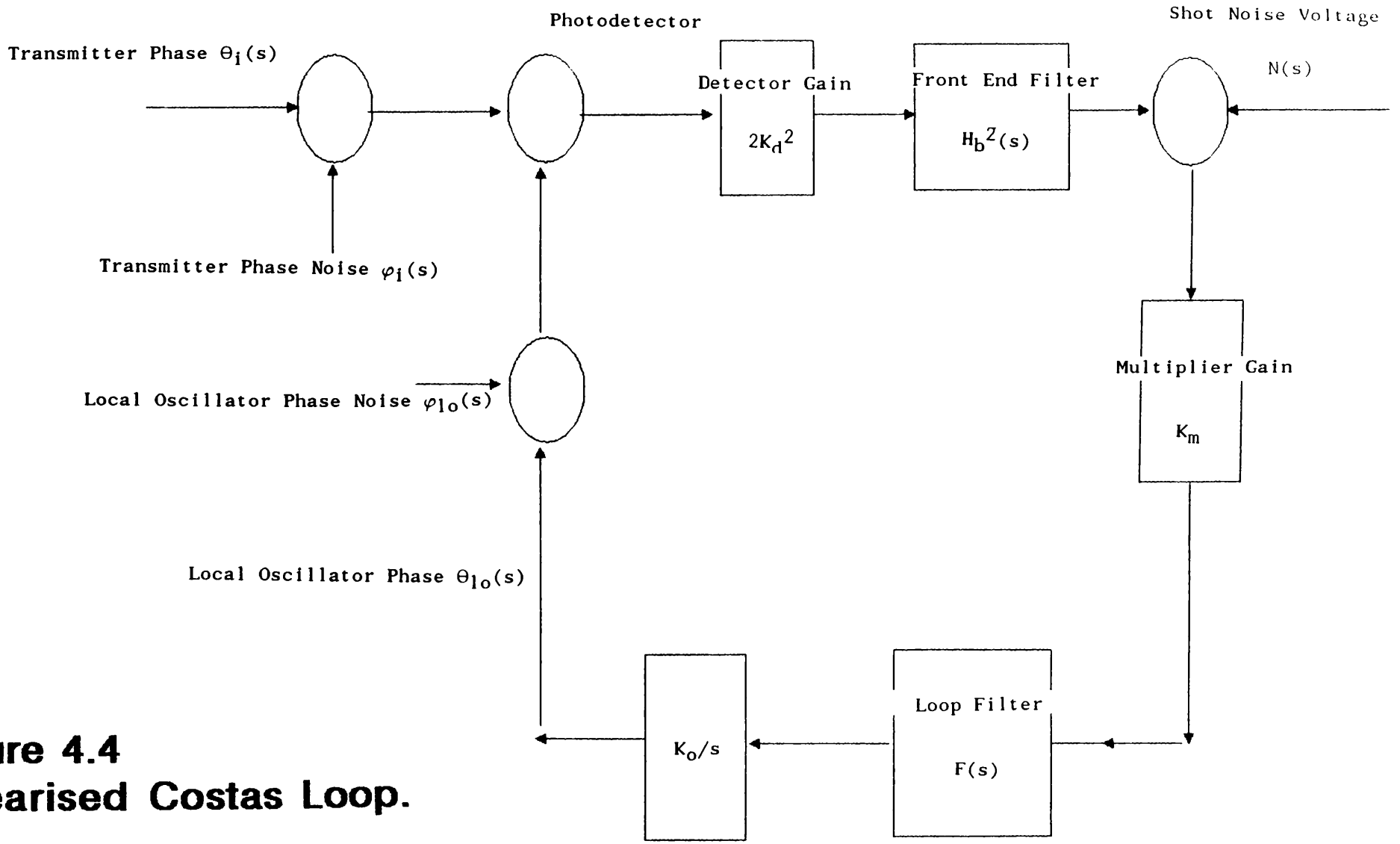

Figure 4.4
Linearised Costas Loop.

It is now possible to obtain a complete description of the PLL. The phase error at the detector is defined as

$$\Phi_d(s) = \Theta_i(s) + \varphi_i(s) - [\Theta_o(s) + \varphi_o(s)] \quad (4.35)$$

If the total loop gain $K_oK_mK_d$ is written as K then the phase difference, $\Phi_d(s)$, is

$$\Phi_d(s) = \Theta_i(s) + \delta\varphi - [KH_b^2(s)F(s)(2\delta\varphi_d + 2\delta\Theta)/8s + KH_b^2(s)F(s)N_Q(s)/2s] \quad (4.36)$$

or

$$\Phi_d(s) = \Theta_i(s) + \delta\varphi - [KH_b^2(s)F(s)(2\Phi_d)/8s + KH_b^2(s)F(s)N_Q(s)/2s] \quad (4.37)$$

This can be rearanged to

$$\Phi_d(s) = \frac{s\Theta_i(s)}{s + KH_b^2(s)F(s)/4} + \frac{s\delta\varphi(s)}{s + KH_b^2(s)F(s)/4} + \frac{KH_b^2(s)F(s)N_Q(s)/8}{s + KH_b^2(s)F(s)/4} \quad (4.37)$$

The loop transfer function can now be defined as,

$$H(s) = \frac{KH_b^2(s)F(s)/4}{s + KH_b^2(s)F(s)/4} \quad (4.38)$$

and 4.37 rewritten as

$$\Phi_d(s) = [1-H(s)][\Theta_i(s) + \delta\varphi(s)] + N_Q(s)H(s)/K_d \quad (4.39)$$

Thus an expression for the effective phase error has been

derived. There are three contributions however it is only two of these that are relevant. The incoming phase $\Theta_i(s)$ is assumed to be stationary since this is not a modulation tracking loop. The remaining two sources of error are the noise corruptions $\delta\varphi$, the laser phase noise, N_Q the shot noise. It is the quantification of the effect of these noises which is of prime interest. These two disturbances produce random fluctuations of the phase difference between the local oscillator and transmit laser. The random nature of these fluctuations dictate that recourse to statistical methods is necessary to quantify their effect. A suitable measure of the random nauture of the phase difference is the phase error variance, σ_Φ^2. Assuming both noise sources to be ergodic in nature, the phase error variance is evaulated as the expectation function of the phase error which is in turn equivalent to the autocorrelation function evaluated at $\tau = 0$. Before this can be evaluated however, it is necessary that the above expression for the phase error be written in terms of the power spectral densities of the two noise sources.

The power spectral density PSD of the phase instabilities is related to the corresponding beat linewidth of the two sources and may be written [7,8,9,13],

$$S_{\delta\varphi} = \delta f_{tot}/(2\pi f^2), \qquad (4.40)$$

where δf_{tot} denotes the full width half maximum beat linewidth of the laser sources. The corresponding expression for the shot noise contribution is,

$$S_{NQ} = eRP_{lo}(1-\alpha) \qquad (4.41)$$

Thus the phase error variance may be expressed in terms of the autocorrelation function as,

$$\sigma_\Phi^2 = S_{\delta\varphi} \int_{-\infty}^{\infty} |1-H(s)|^2 . df + S_{NQ} \int_{-\infty}^{\infty} |H(s)/K_d|^2 . df \qquad (4.42)$$

$$= (\delta f_{tot}/2\pi) \int_{-\infty}^{\infty} |1-H(s)/f|^2 . df +$$

$$(e/4P_s R\alpha) \int_{-\infty}^{\infty} |H(s)|^2 . df \qquad (4.43)$$

Evaluation of the above integrals, commonly refered to as the noise bandwidth integrals, allows the phase error variance to be expressed in terms of the bandwith of the loop transfer function. Assuming, as stated earlier, a second order loop with an active filter 4.43 can be expressed,

$$\sigma_\Phi^2 = \frac{\pi \delta f_{tot}}{2\xi\omega_n} + \frac{\omega_n e(1 + 4\xi^2)}{16RP_s\alpha^2} . \qquad (4.44)$$

It is immediately obvious from examination of equation 4.44 that the constituent noise sources have conflicting loop bandwidth requirements. An optimum solution must therefore exist, as is indicated by the plot of σ^2_Φ versus ω_n in figure 4.5. This optimum bandwidth will be evaluated in the following section.

4.4 Optimisation of an OPLL.

The following discussion will outline the process by which the optimum loop natural frequency is derived considering the effect of the two noise sources with conflicting bandwidth requirements. The analysis will be concerned at this stage purely with the ideal situation. The propagation delay around the loop will be considered negligible and also the front end bandwidth $H_b(s)$ will be considered to be large enough to be approximated as infinite. The loop transfer function is therefore as represented in equation 4.7.

$$H(s) = \frac{2\zeta\omega_n^2 + \omega_n^2}{s^2 + 2\zeta\omega_n s + \omega_n^2} \qquad (4.45)$$

where the loop natural frequency $\omega_n = (K/\tau_1)^{1/2}$, and K the total loop gain is $K_o.K_d.K_m/4$. The damping factor ζ is as previously defined,

$$\zeta = \tau_2\omega_n/2. \qquad (4.46)$$

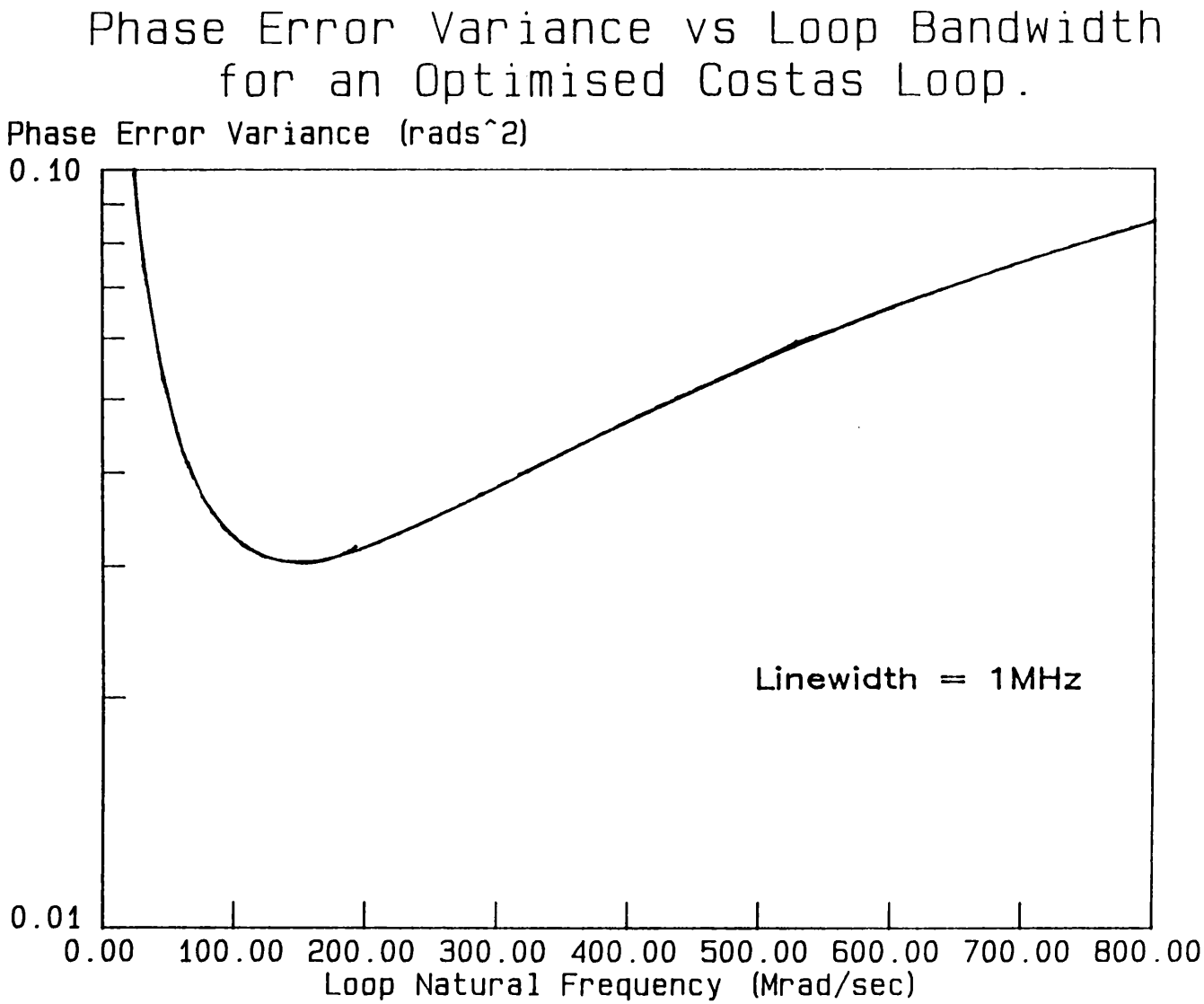
Phase Error Variance vs Loop Bandwidth
for an Optimised Costas Loop.
Phase Error Variance (rads^2)
0.10
0.01
Linewidth = 1MHz
0.00
100.00
200.00
300.00
400.00
500.00
600.00
700.00
800.00
Loop Natural Frequency (Mrad/sec)

Figure 4.5

The choice of the system parameters is not simply dependant on the tracking performace of the PLL. Obviously the final overall system performance, in terms of BER, will influence to a large extent how much attention is paid to achieving a PLL with a minimal phase error variance. The questions that will arise when considering the total problem will for the time being be avoided in order that the issue of the PLL may be given greater attention without the added complication of consideration of the system as a whole. It is assumed that the PLL is designed to fit into a system operating at 565 Mbit/sec and at a BER 10^{-9}. A value of responsivity for the photo diodes of 0.85 will also be specified.

According to the theory developed in Chapter 2, the minimum received optical power, for a binary PSK system with the above set of constraints and a BER of 10^{-9}, is $P_{th} = -60.2$dBm. This power represents the actual theoretical minimum receiver power in the ideal shot noise limited condition. There is likely to be, in a practical environment, an additional penalty to be paid. This additional penalty will arise from various sources. Initially attention will be given to imperfect phase synchronisation: the allowable penalty at the data detector for this corruption will be set at 0.5dB. Imperfect phase syschronisation can be readily quantified in terms of the phase error variance. For a BER of 10^{-9} the phase error corresponding to 0.5 dB power penalty is $\sigma_{\Phi}^2 = 0.03$ rads^2.

Other sources of corruption, such as polarisation mismatch and imperfect decision circuitry, will be allocated a similar amount of additional power. Thus the total amount of power required at the data arm is $P_{data} = -59.2$ dBm.

Having determined the required data power, the necessary carrier power to provide the phase synchronisation information must now be evaluated. In the case of the Cosatas Loop the effective carrier power is determined by the coupling ration α between the 'in phase', and 'quadrature', components of the detector. Since the data power is known to be (see Figure 4.3) equal to the fraction $(1-\alpha)$ of P_t then the total transmit power is readily determind as

$$P_t = P_{data}/(1-\alpha) \qquad (4.47)$$

The evaluation of the coupling ratio will be influenced by the choice of the remaining loop parameters. As was stated earlier, a conflict exists within the operation of the loop between obtaining an optimum shot noise performance and an optimum phase noise performance. Considering the shot noise performance, the best thing to do would be to disconnect the loop entirely, however this is not a practical solution as far as the phase synchronisation is concerned. The optimum bandwidth, in the compromised situation, is obtained by differentiating 4.44 with respect to ω_n and equating the resultant to zero to indicate the turning point. Thus

$$\omega_{nopt} = [8RP_t\alpha\pi\delta f_{tot}/e(1 + 4\zeta^2)]^{1/2}. \qquad (4.48)$$

The correspondig minimum phase error variance may be obtained by substituting this value back into 4.44,

$$\sigma_\Phi{}^2{}_{min} = [\pi\delta f_{tot}e(1+4\zeta^2)/8RP_t\alpha\zeta^2]^{1/2}. \qquad (4.49)$$

Thus an expression for the desired coupling ratio for a specific performance is obtained

$$\alpha = \frac{\pi\delta f_{tot}e(1 + 4\zeta^2)}{8\zeta^2RP_{data}\sigma_{\Phi min}{}^4 + \pi\delta f_{tot}e(1 + 4\zeta^2)} \qquad (4.50)$$

Hence, for a given beat linewidth and data power, the corresponding value of α may be evaluated. This in turn may be used in conjunction with 4.48 to evaluate the optimum natural frequency ω_n for a system. Thus the various system parameters will be evaluated.

The corresponding values of α, P_t, ω_{nopt} and total system power penalty are evaluated for three specific instances in Table 4.1. These specific values give a clear indication of how the influence of the laser phase noise degrades the system performance. The model predicts that near shot noise limited performance may be obtained for linewidths of up to 15 MHz. The required loop bandwidth at figures of this magnitude however are unlikely to be realistic. Bandwidths of

Linewidth	f_{TOT}= 20kHz	f_{TOT}= 1MHz	f_{TOT}= 15MHz
P_{DATA}	-59.2 dBm	-59.2 dBm	-59.2 dBm
α	8.13×10^{-3}	0.29	0.86
P_T	-59.16dBm	-57.7dBm	-50.7dBm
$W_{n\ opt}$	2.96Mrad/sec	148 Mrad/sec	2.22 Grad/sec
Total System Power Penalty	1.04 dB	2.5 dB	9.5 dB

Table 4.1. Optimum Loop Parameters For Three Given Beat Linewidths

BER = 10^{-9}, f_B = 565 MBits/sec, σ_E^2 = 0.03rad^2, R = 0.85, ζ = 0.707.

this magnitude would be difficult to engineer without degrading the effects from other system time constants (*eg* propagation delay) being observed. Furthermore peaks in the laser phase noise at the relaxation oscillation frequency would be encompassed by a loop bandwidth of nature and it is likely that so too would be the data. The model is however vaild for the lower values of the beat linewidth and is useful in that it provides a working understanding of the operation of the OPLL.

The above discuusion has ommitted to make clear the fact that the effect of the laser phase noise is subject to the frequency of the transmitted data. That is, for higher data rates the the effective phase error at the decision circuitry will be lower over any given bit period. This point will be taken into consideration in future discussions of the OPLL but has been ommitted for the present in order that a simple view of the loop functioning under a specific set of conditions may be obtained. To indicate the effect of the data rate to linewidth ratio the loop coupling ratio α and effective carrier power penalty have been plotted in Figures 4.6 & 4,7 as functions of this variable. The extreme cases, that is for the low ratio insatances, for either of these curves cannot be justified. In the instance of low data rate the loop natural frequency will be of the same order as the data rate and hence data to phase lock cross talk is likely to exist. These instances are however extremely unlikely to be considered in a practical situation.

4.5 OPLL : Discussion and conclusions.

A model of an optical phase locked loop has been presented. In this particular instance the loop under analysis has been the Costas Loop. The general conclusion drawn from the analysis of this type of loop are however directly applicable to any other type of OPLL. The effect of the laser phase instabilities is seen to be such that a definite optimum loop bandwidth exists. This differs from the case of the microwave PLL in that the large linewidths of laser sources dictate the use of large loop bandwidths. The analysis presented suggests that lasers with a beat linewidth of the order of 1 MHz may be phase locked to a degree of accuracy where near

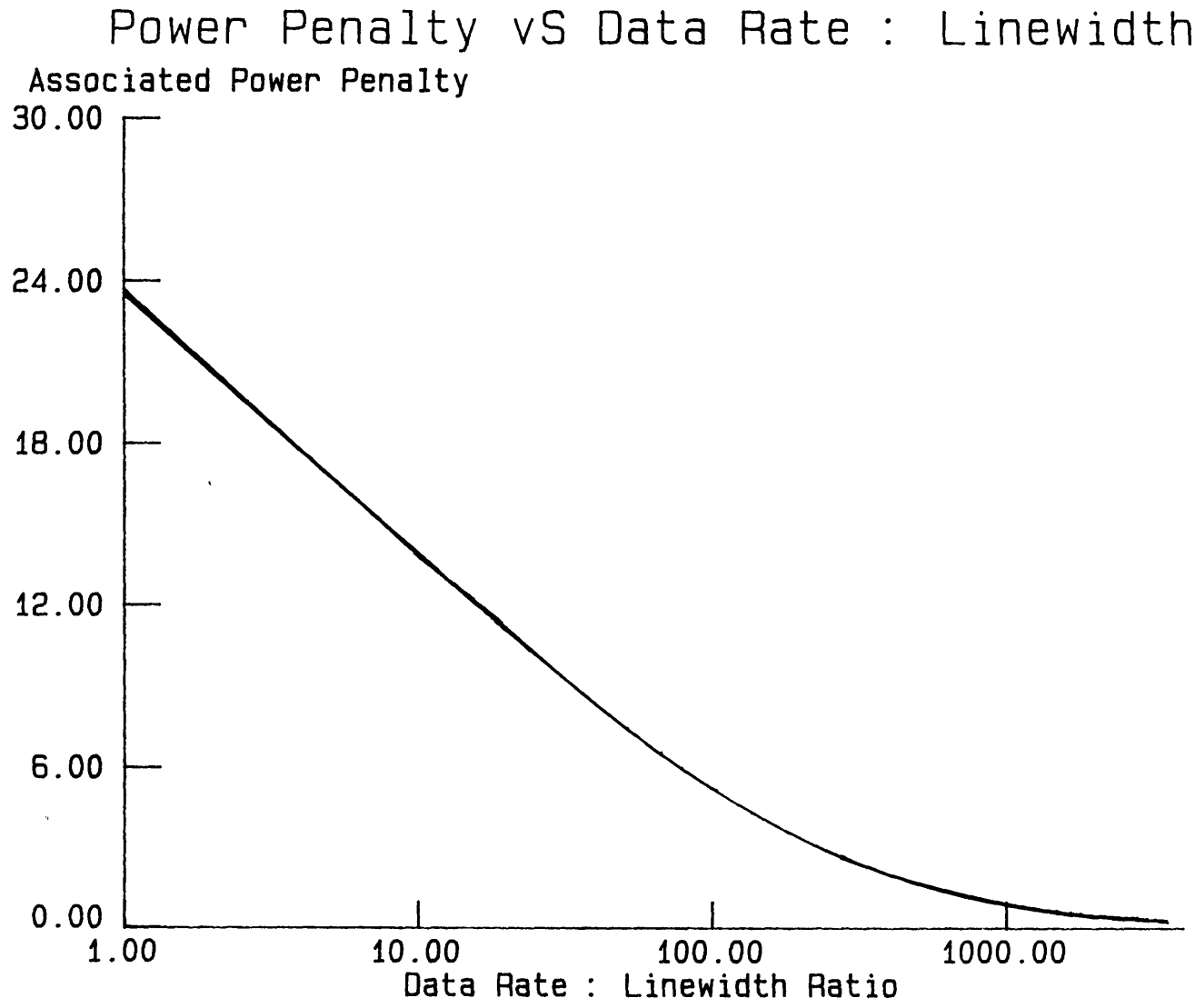
Power Penalty vS Data Rate : Linewidth
Associated Power Penalty
30.00
24.00
18.00
12.00
6.00
0.00
1.00
10.00
100.00
1000.00
Data Rate : Linewidth Ratio

Figure 4.6

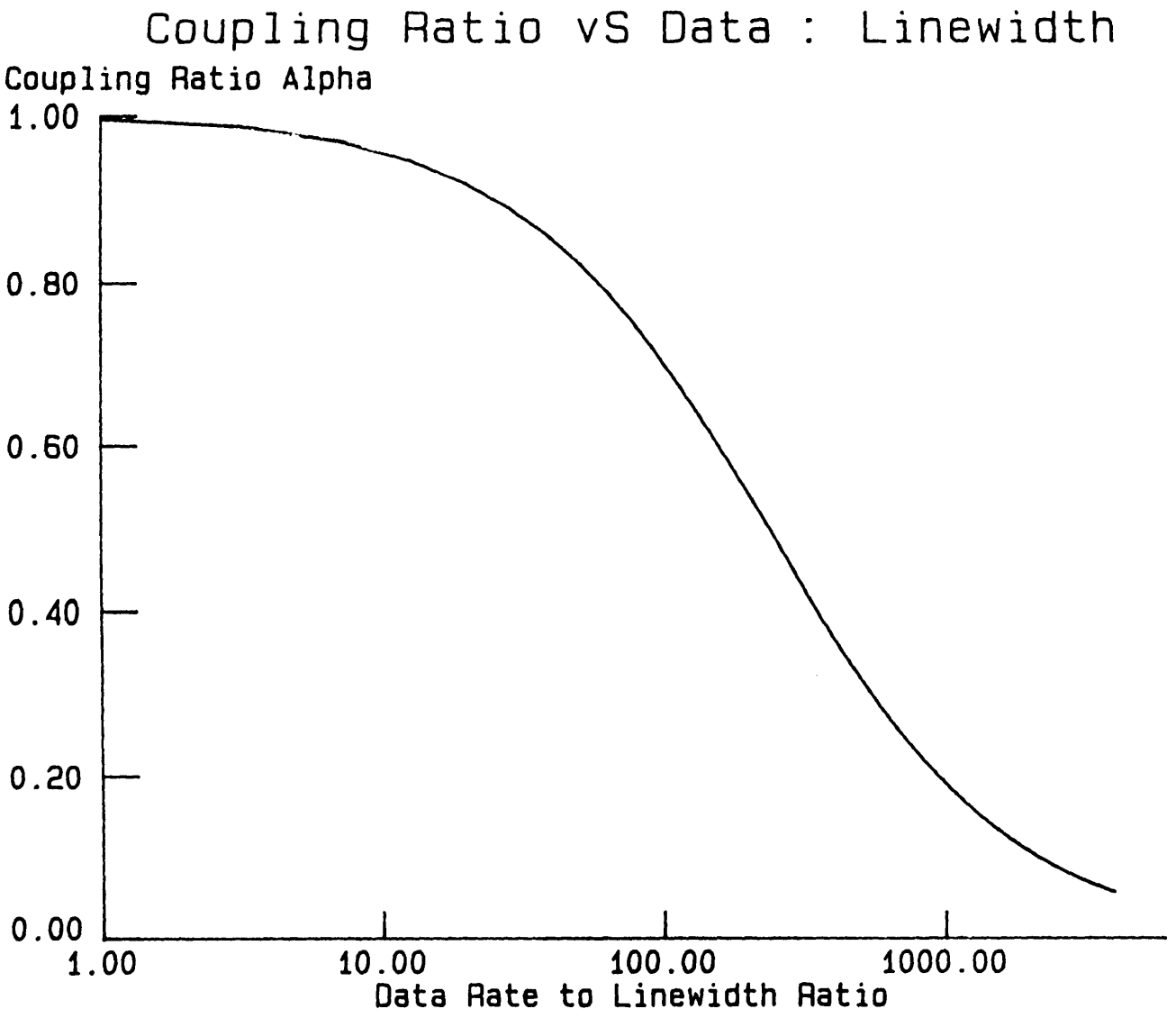
Coupling Ratio vS Data : Linewidth
Coupling Ratio Alpha
1.00
0.80
0.60
0.40
0.20
0.00
1.00
10.00
100.00
1000.00
Data Rate to Linewidth Ratio

Figure 4.7

quantum limit sensitivity may be achieved at the detector. However, this requires the use of a large (148 Mrads/s) loop bandwidth. Bandwidths of this magnitude are likely to pose their own problems; loop propagation delay is likely to become a significant factor. No account has been made as yet to account for this possibility, a further degradation in the phase tracking performance would be expected. It is arguable that a minimum phase error variance of 0.03 $rads^2$ is necessary in a practical system to achieve a BER of 10^{-9}. Solid phase locking can be achieved with a phase variance of up to 0.15 $rads^2$. Thus the possibility of phase locking lasers of even larger linewidths should not be excluded. Table 1 suugest that with a beat linewidth of 15 MHz a phase error variance of 0.03 $rads^2$ may be obtained with natural frequency of 2.22 Grads/sec. This does however begin to stretch the bounds of credibility of the model. A loop bandwidth of such a magnitude is likely to encompass the peaks in the laser phase noise spectrum, due to the relaxation oscillation, as well as the data. The excessively high coupling ratio of 0.86 renders some of the assumptions made about the shot noise being dominated by the local oscillator equally invalid. However in the general case the model is sufficient to give an understanding of the working of an OPLL. The analysis of the phase noise corruption can be assumed to be accurate over a reasonable range of values (linewidths up a few MHz). The model should certainly be accurate in cases where the beat linewidth is below 100 kHz and near quantum limit detection should be possible in these instances. Although the modelling of the effect of the phase noise may be valid up to linewidths of < 10 MHz, at linewidths of $>$ 500kHz the effect of other system time constants (propagation delay, front end cut off frequency) is likely to render the overall model inaccurate. These particular instances will be considered in the following chapter.

References.

1. W.R.Leeb *et.al.* 'Frequency Synchronisation and Phase Locking of CO_2 lasers'. Appl. Phys. Lett. 47(7) pp 592–599 Oct 82.

2. H.K.Phillip *et.al.*'Costas Loop Experiments for a 10.6 μm Communications Reciever '. IEEE Trans. Commun. COM 31(8) pp. 1000–1002 Aug 83.

3. Mengalli 'Tracking Properties of Optical Phase Locked Loops in Optical Communications Systems'. COM 26 Dec 78 1811–1818.

4. L.G.Kazovsky 'Balanced Phase Locked Loops for OPtical Homodyne Recievers: Performance Analysis, Design Considerations, and Laser Linewidth Requirement Analysis.' J. Lightwave Tech. LT–4(2) pp182–194 1982.

5. L.G.Kazovsky 'Decision–Driven Phase–Locked Loops for Optical Homodyne Recievers: Performance Analysis and Laser Linewidth Requirements.' J.Lightwave Tech. LT3(6) pp 1238–1247 1985.

6. D.J.Malyon 'Digital Fibre Transmission using Optical Homodyne Detection.' Elect. Lett. vol. 20(7) 1984. pp281–283

7. T.G Hodgkinson 'Costas Loops Analysis for Optical Recievers' Elect. Lett. vol. 22(7) 1986. pp394–396.

8. T.G.Hodgkinson 'Phase–Locked Loop Analysis for Pilot Carrier Coherent Optical Recievers' Elect. Lett. vol 21 1985 pp1202–1203.

9. B.Glance 'Mininum Power Required for Carrier Recovery at Optical Frequencies.' Journal Lightwave Technology LT–4(3) 1986, pp249–255.

10. B.Glance 'Performance Requirements of Homodyne Detection of Binary PSK Optical Signals.' J.Lightwave Tech. LT–3(6) 1985. pp228–235.

11. R.C. Steele 'Optical Phase–Locked LoopUsing Semiconductor Laser Diodes' Elect. Lett.19(2) 1983. pp69–70.

12. W.Liddell 'Optical Phase–Locked Loop.'IEE Colloquim on Advances in Coherent Optic Devices and Technologies, Savoy Place, London GB, March 1985.

13. J.B.Armor, S.R.Robinson 'Phase–lock Control Considerations for Coherently Combined Lasers.' Applied Optics vol.18,No.18, 1979 pp 3165–3175.

14. A.Davis, S.Wright 'A Phase Insensitive Optical Homodyne Reciever.'IEE Colloquim on Advances in Coherent Optic Devices and Technologies, Savoy Place, London GB, March 1985.

15. A.W.Davis *et.al.* 'Coherent Optical Reciever for 680 Mbit/s Using Phase Diversity,' Elect. Lett., 2nd Jan. 1986, vol.22,no. 1, pp9–11.

16. F.M. Gardner 'Phaselock Techniques' New York: Wiley, 1979.

17. A.Blanchard 'Phase–Locked Loops. Application to Coherent Reciever Design.' New York: Wiley, 1976.

18. W.C.Lindsey 'Synchronous Systems in Communication and Control' Englewood Cliffs, NJ:Prentice Hall,1972.

19. J.J.Stiffler 'Theory of Synchronous Communications.' Englewood Cliffs, NJ: Prentice Hall,1971.

20. W.R.Leeb 'Realization of 90^0 and 180^0 Hybrids for Optical Frequencies' Electron. Commun. AEU vol. 37 May–June 1983. pp203–206.

CHAPTER 5.

The Practical Phase– locked Loop

5.1 Introduction.

In the previous chapter a description of the optical phase– locked loop was given. The performance of the loop, under conditions of significant phase and shot noise, was evaluated and it was concluded that the OPLL requires large loop bandwidths to counteract the effects of the source phase instability. As a direct consequence of these large bandwidths, the OPLL is more sensitive to slight variations in time constants that are of little relevance to the standard rf PLL. In particular, the phase shift introduced by the front end amplifier cut off frequency and the loop propagation delay must be given careful consideration. The present chapter addresses this aspect of PLL design and demonstrates that small variations in these time constants will have a significant effect.

5.2 The Optimisation of a Communications system.

Optimisation of a communication system is not a trivial problem. The various system components, the detector, the phase synchronisation mechanism and the decision circuitry can all be individually designed and tuned to operate over a wide range of conditions. The performance of the complete system must at all times be borne in mind. In the first instance a decision must be made concerning what is demanded of the system. A computer data link may, for example, require a BER of 10^{-9} or 10^{-10} wheras a digital audio transmission may tolerate a higher percentage error, say 10^{-8} BER. An over– specification of the performance requirements can be costly in terms of data or carrier power as the following section will indicate. In order that the present analysis is consistent with the work in Chapter 4 it will be assumed that a transmission reliability of 10^{-9} BER is required and that 0.5 dB power penalty is allocated to account for lack of phase synchronisation. Thus the phase tracking circuitry must maintain a phase error variance of 0.03 rads^2

or better[1].

5.3 The Pilot Carrier Transmission Format.

In Chapter 4, the performance of the PLL was evaluated for the case of a Costas Loop construction. On first inspection, the Costas Loop appears to be the obvious choice for an optical homodyne receiver. It enables homodyne reception to be achieved without the complication of dc coupling of the photo–detector, thus relaxing the design requirements of the detector circuitry and furthermore, since no vestigial component of the carrier is transmitted, it would also appear to be the most efficient of transmission formats. This second apparent 'advantage' however, must be examined more closely. Although no carrier is transmitted, the receiver relies on the effective regeneration of the carrier for its' phase synchronisation information and thus the effective carrier power allocation may not be necessarily less than that of a vestigial carrier transmission.

In the present situation, where the construction of a wide bandwidth loop is considered, the main concern is that the loop performance is not degraded by unintentional phase shifts. It is likely that the extra complexity of the Costas Loop receiver electronics will make it more susceptible than the pilot carrier tracking loop to this source of error. For this reason, and for the sake of completeness, the PLL analysis will continue in this section assuming a carrier tracking design. Under ideal conditions, the performance of the carrier tracking loop and the Costas loop can be assumed to be equivalent. In order that this assumption may be verified for the case under consideration, the basic design procedures will be briefly reviewed.

The vestigial transmission (Figure 5.1) may be described in the following manner [2],

$$P_t = K_s.(1 + K_c).P_{data} \cdot \qquad \begin{matrix} K_s > 1 \\ K_c >= 0 \end{matrix} \qquad (5.1)$$

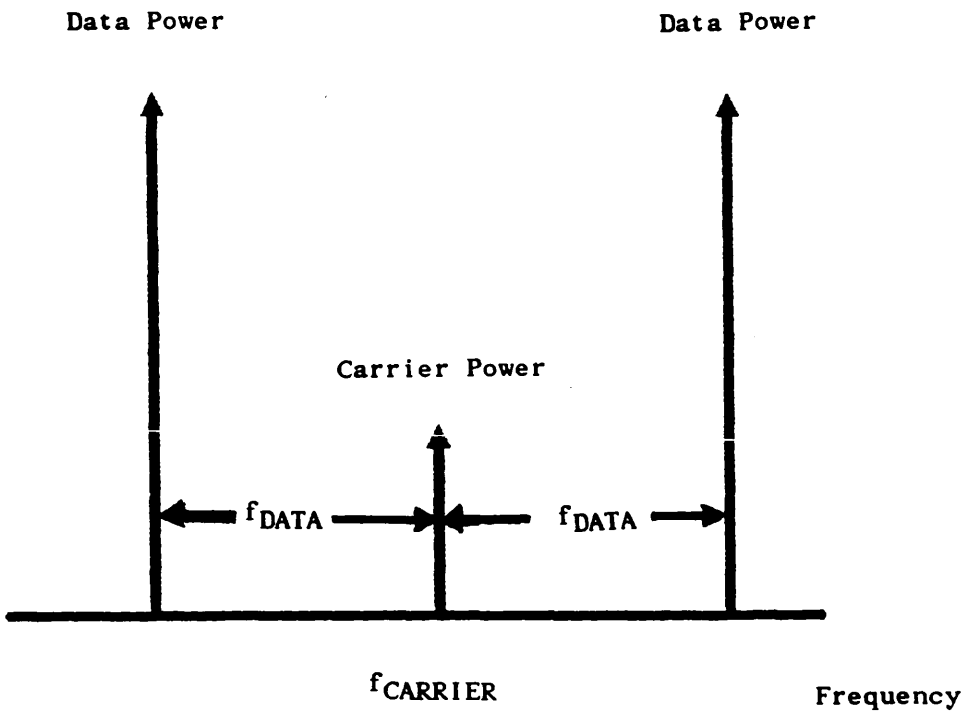

Figure 5.1
Pilot Carrier Transmission Representation.

P_{data} represents the theoretical minimum power required at the receiver to achieve a BER of 10^{-9}. For the anti-podal PSK transmission format it has already been shown (see Chapter 2) that this corresponds to 9 photons/bit or a power of -60.2 dBm (assuming a responsivity of 0.85 at the receiver and 565 Mbits transmission rate). The multiplying factor, K_S, accounts for imperfections over the transmission length such as polarisation mismatch and imperfect carrier tracking. Similar power penalties to those allowed in the Costas Loop analysis will be allocated, that is 0.5 dB is given to account for polarisation mismatch etc. and 0.5 dB accommodates for imperfect carrier tracking. The factor K_c accounts for the power penalty associated with the vestigial carrier transmission, ie it gives a measure of the carrier power.

The loop model, Fig 5.2, is adapted from the standard models [2-9]. The incoming signal has complex amplitude

$$E_i = (2P_T)^{1/2}\exp(j\varphi_T) \qquad (5.2).$$

where P_T and φ_T represent the transmitted power and phase. Similarly the local oscillator is represented

$$E_{LO} = (2P_{LO})^{1/2}\exp(j\varphi_{LO}). \qquad (5.3).$$

φ_T, the transmitter phase term incorporates the instantaneous unmodulated transmitter phase, φ_i, the transmitted phase modulation, φ_d, and the transmitted phase noise, φ_{nt}.

$$\varphi_T(t) = \varphi_d(t) + \varphi_i(t) + \varphi_{nt}(t) \qquad (5.4).$$

The power spectral density of the phase noise φ_{nt} is described as previously. The power available for phase locking is the carrier

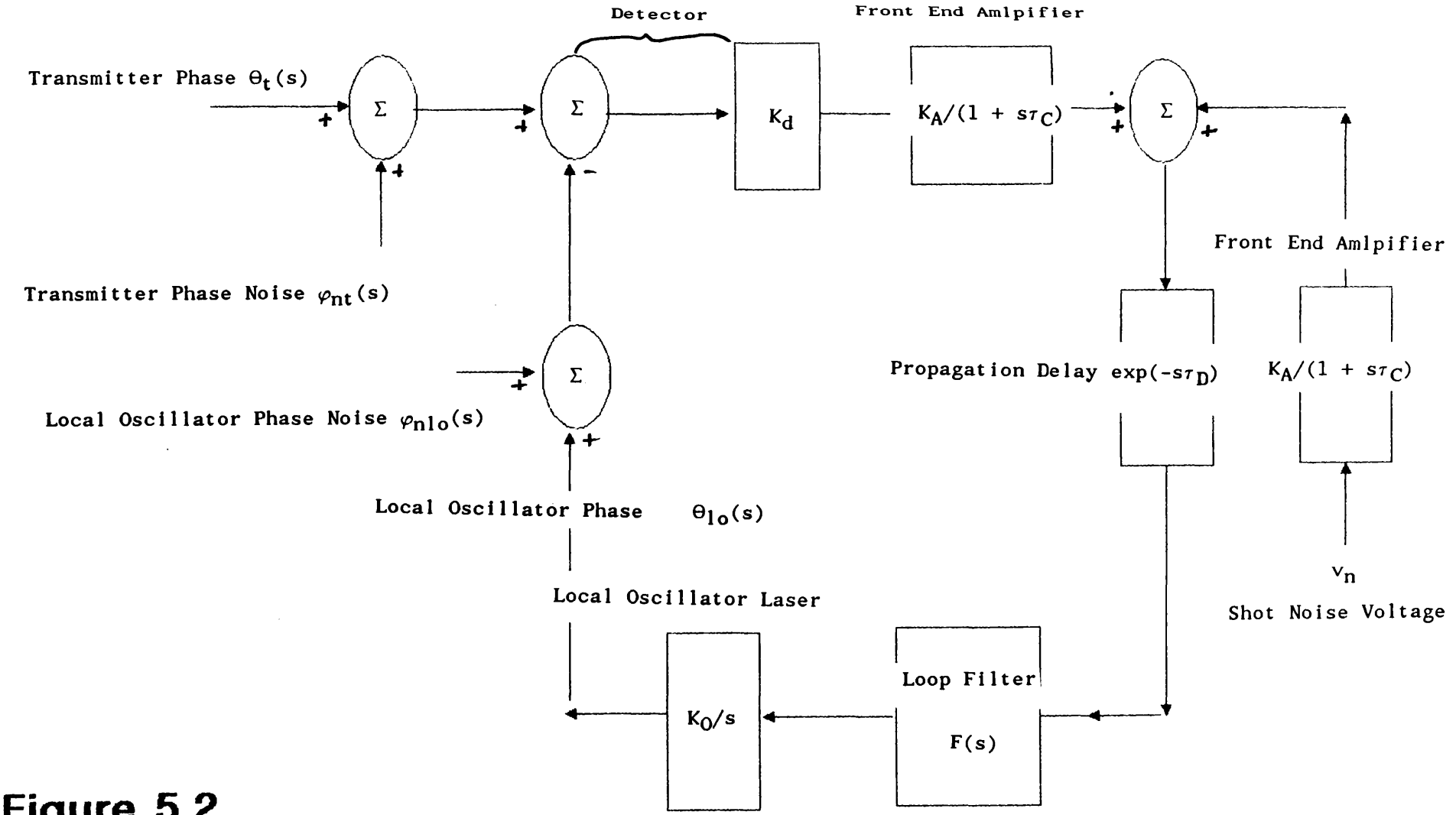

Figure 5.2
Optical Phase Locked Loop
Schematic Diagram.

power

$$P_c = K_s K_c P_{data} = P_t K_c/(1 + K_c) \qquad (5.5)$$

Equation 2. must therefore be modified to

$$E_i = (2P_c)^{1/2} \exp(j\varphi_t(t)) \qquad (5.6).$$

The assumption that data–to–phaselock crosstalk may be neglected is continued in this analysis therefore, it is convenient to remove the phase modulation term from the expression describing the transmitter phase. Thus

$$E_i = (2P_c)^{1/2} \exp(j(\varphi_{nt}(t) + \varphi_i(t))) \qquad (5.7).$$

Having made these definitions, to account for the differences between the carrier tracking and the Costas Loop, the remainder of the analysis is common to them both. The solution to the expression describing the phase error may therefore be asserted if the following definition of the loop transfer function H(s) is made

$$H(s) = \frac{\dfrac{KF(s)\exp(-s\tau_D)}{s(1 + s\tau_C)}}{s + \dfrac{KF(s)\exp(-s\tau_D)}{s(1 + s\tau_C)}} \qquad (5.8)$$

The phase error is therefore described as

$$\varphi_D(s) = (\varphi_D(s) + \delta\varphi)(1 - H(s)) + H(s)N_S(s)/K_D \qquad (5.9).$$

The phase error contributions can now be evaluated. To underpin the similarity between the two loops this will be carried out for the optimum case of zero propagation delay and infinite front end bandwidth. Under these conditions, and again assumung an active configuration for the loop filter, the phase error variance is described as,

$$\sigma_\varphi^2 = \left[\frac{e}{4RP_C} \quad \frac{\omega_n(1 + 4\zeta^2)}{4\zeta} + \frac{\delta f_{tot}}{2\zeta\omega_n} \right]$$

(5.9)

The optimum loop bandwidth for a given beat linewidth is

$$\omega_{nopt} = \left[\frac{8RP_C\delta f_{tot}}{e(1 + 4\zeta^2)} \right]^{1/2} \quad (5.10)$$

giving

$$\sigma_\varphi^2{}_{min} = \left[\frac{\pi\delta f_{tot}e(1 + 4\zeta^2)}{8RP_C\zeta^2} \right]^{1/2} \quad (5.11)$$

Thus, for an equivalent set of operating conditions to those specified for the Costas loop, the necessary carrier power is calculated as

$$P_C = 0.49356 \text{ nW.} \quad (5.12)$$

This gives a value of the carrier coefficient K_C as

$$K_C = P_C/K_SP_{data} = 0.49356 \text{ (nW)}/1.2022 \text{ (nW)} \quad (5.13)$$

$$K_C = 0.41083. \quad (5.14)$$

The total transmitted power is then given simply by the sum of the data and carrier power ,

$$P_T = 0.49356 + 1.2022 \text{ nW} = 1.69576 \text{ nW}$$
$$= -57.7 \text{ dBm.} \quad (5.15)$$

Comparing these values for those calculated for the Costas Loop operating (Chapter 4) shows that the performance of the two loops is identical in both cases.

5.4 The effect of Loop Propagation Delay.

The problems relating to the construction of wide bandwidth PLL's will now be addressed. It is the authors opinion that the greatest problem that will be faced in this area, is the reduction of the round trip delay from the detector to the local oscillator. For this reason, attention will be given to this area first of all.

The introduction of the propagation delay into the loop description requires that the transfer function is re-written thus,

$$H(s) = \frac{KF(s)\exp(-s\tau_d)}{s + KF(s)\exp(-s\tau_d t)}. \qquad (5.16)$$

The complex exponential term makes the loop bandwidth integrals more difficult to solve than previously; therefore, a numerical solution to the problem was sought. Prior to performing these calculations, the integrands were checked for continuity and stability. Both $|H(s)|^2$ and $|1-H(s)|^2$ were found to be monotonic and continuous with ω. The limits of the loop stability were evaluated using traditional Nyquist techniques as follows.

Writing the open loop transfer function of the PLL as,

$$G(s) = \omega_n^2(1 + s\tau_2)\exp(-s\tau_d)/s^2 \qquad (5.17)$$

the critical point for the overall loop stability is established as the point where

$$\omega\tau_d = \arctan(\omega\tau_2), \qquad (5.18)$$

and

$$\omega_n^2/(1 + (\omega\tau_2)^2)/\omega^2 < 1 \qquad (5.19)$$

The solution to this reveals the condition for absolute stability as the point where

$$\omega_n\tau_d < \frac{\arctan(2\zeta/(2\zeta^2 + /(1 + 4\zeta^4)))}{/((2\zeta^2 + /(1 + 4\zeta^4))} \qquad (5.20)$$

where the principal value of the arctan function is taken. In the case under consideration the damping factor ζ is assumed to be $1/\sqrt{2}$. Thus the condition for stability is

$$\omega_n \tau_d < 0.736. \qquad (5.21).$$

The loop noise bandwidth integrals were evaluated on an IBM PC AT microprocessor using the 8087 maths co-processor for speed of evaluation. The limits of integration were established as 0 and $100.\omega_n$. At this value of frequency the integrand was found to be less than 10^{-6} of the original value. The results of these calculations have been represented graphically in Figure 5.3 and 5.4.

The effect of the propagation delay is clearly seen to be significant. As the delay value is increased, the characteristic minimum in the phase error variance rises from the original 'datum' level of 0.03 rads^2. For relatively small values of delay, a substantial increase in the phase error variance is observed. In addition to this, the apparrent optimum loop natural frequency is seen to decrease in magnitude. This is more visibly demonstrated in Figures 5.5 and 5.6. Figure 5.5 depicts the locus of the optimum loop natural frequencies against a variation in propagation delay, for the specific instance of a beat linewidth of 1 MHz. Figure 5.6 displays the corresponding minimum in the phase error variance for these conditions. The significance of these results is made more obvious if the PLL is again considered as part of a communications network.

The analysis of Chapter 4 predicted that, with sources of beat linewidth 1 MHz, phase locking to a phase error variance of 0.03 rads^2 could be achieved with a carrier power penalty of 2.5 dB. Such phase synchronisation would increase the required data power by 0.5 dB from the quantum limit in a binary PSK transmission operating with a 10^{-9} BER. The analysis presented here shows that the introduction of a relatively small propagation delay severely compromises this performance. A PLL maintaining the phase synchronisation between the carrier and the local oscillator in such a system would be required to have a loop bandwidth of 148 Mrads/sec (23.5 MHz). It is not immediately obvious that a feedback system with such a bandwidth would be significantly affected by a propagation delay of the order of nano-seconds. However, the analysis presented here shows that a propagation delay

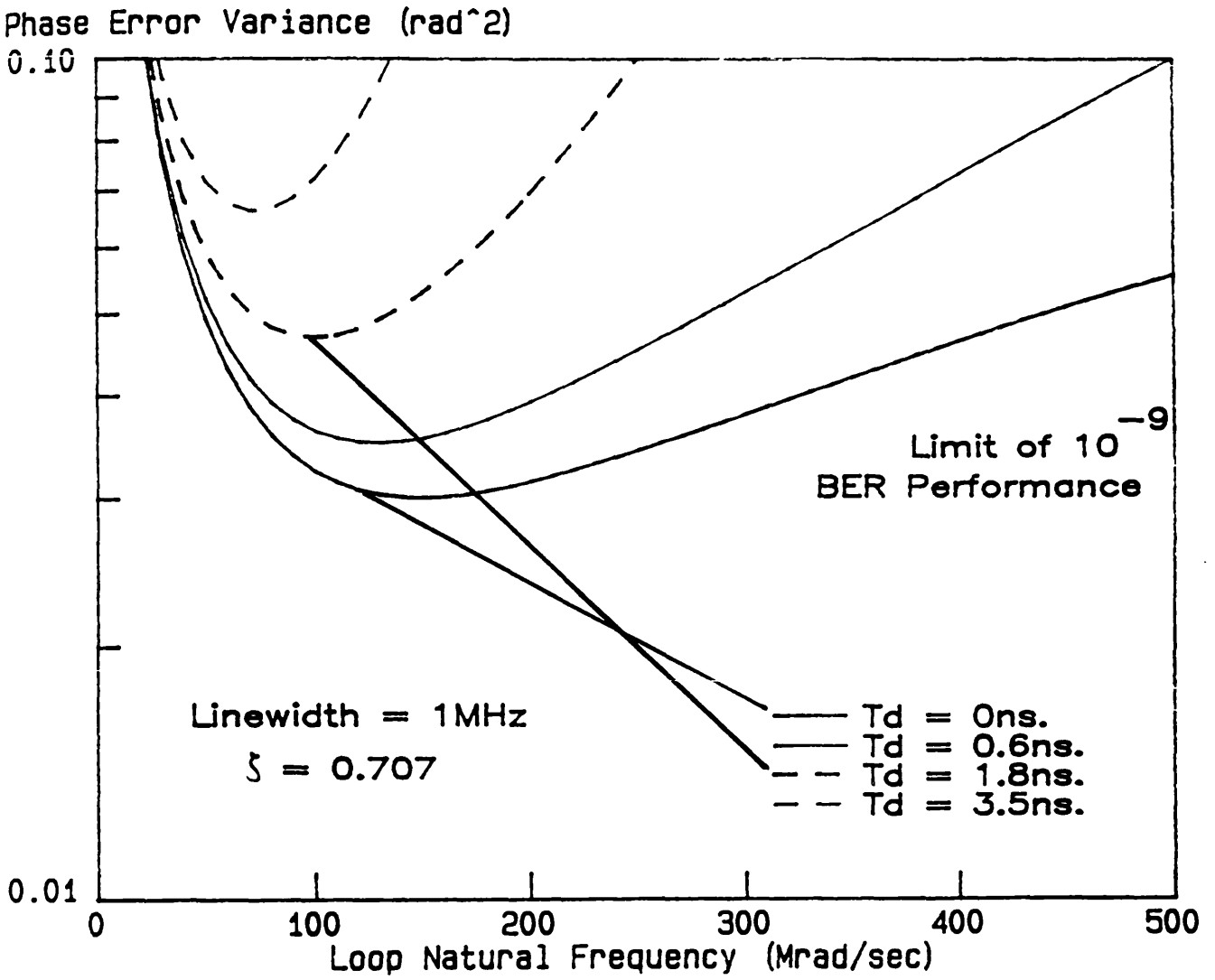

Figure 5.3
The Effect of Propagation Delay on OPLL Performance.

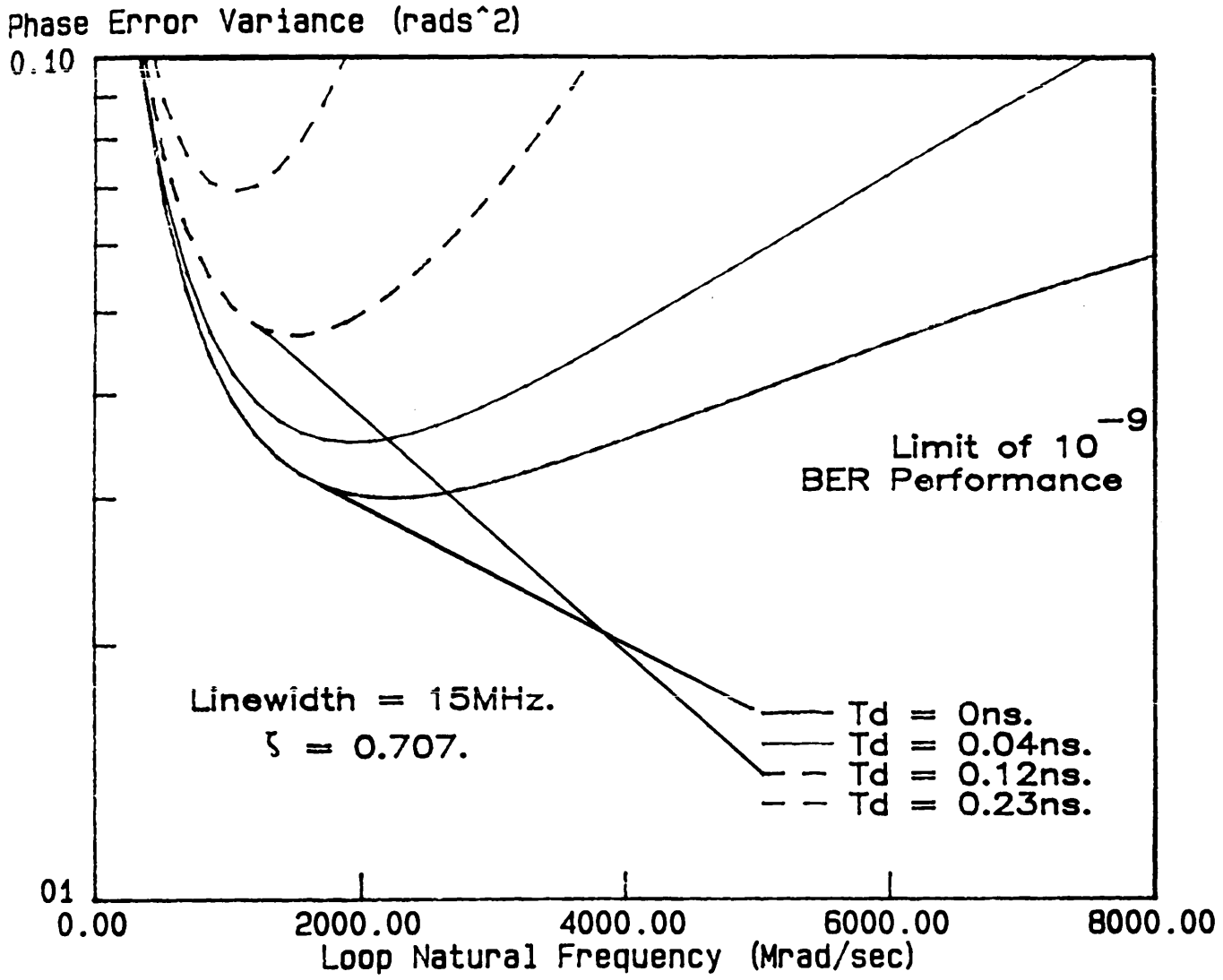

Figure 5.4
The Effect of Propagation Delay on OPLL Performance.

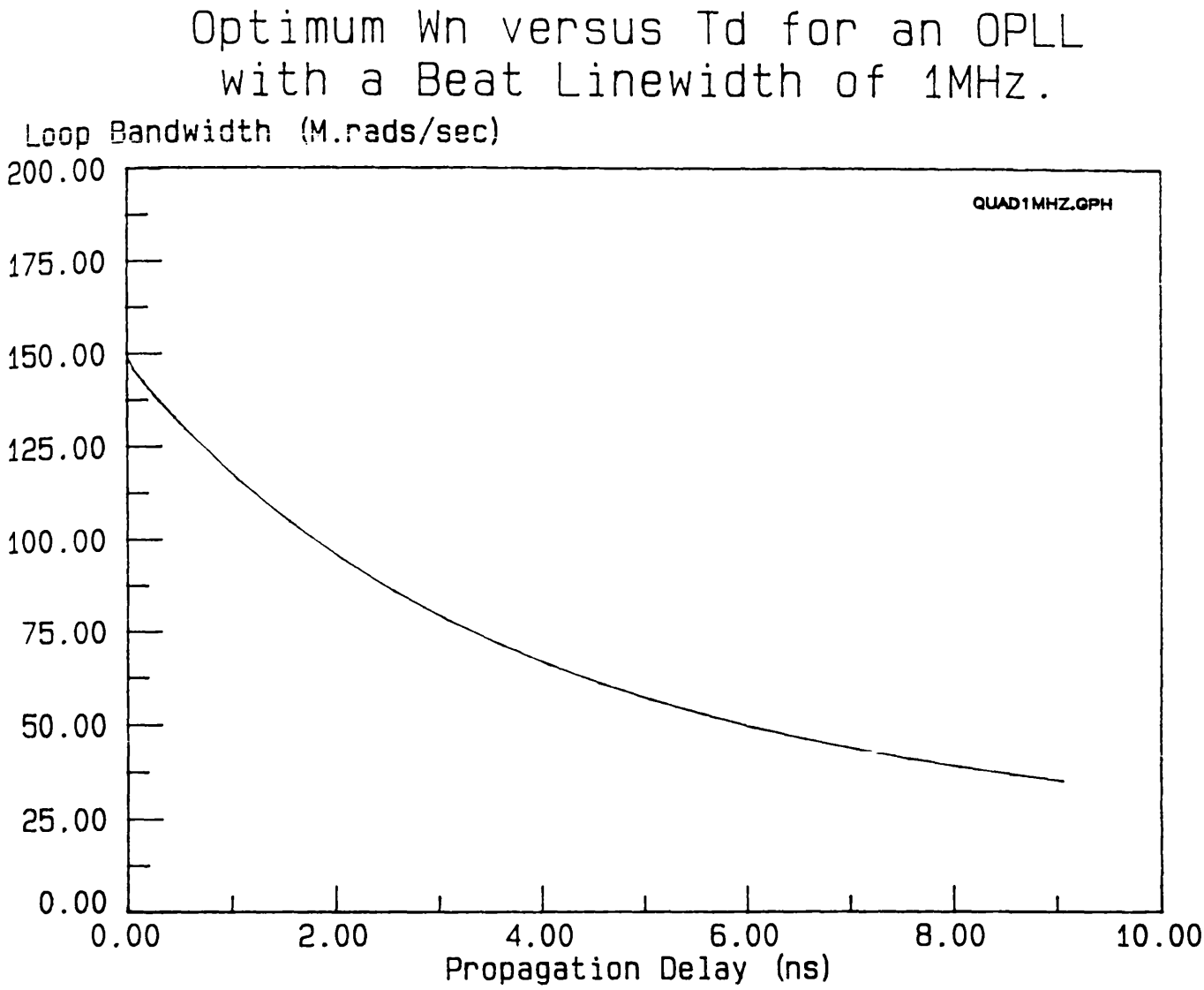

Figure 5.5

Optimum Loop Natural Frequency variation with Propagation Delay for an OPLL constructed with sources of 1MHz Beat Linewidth.

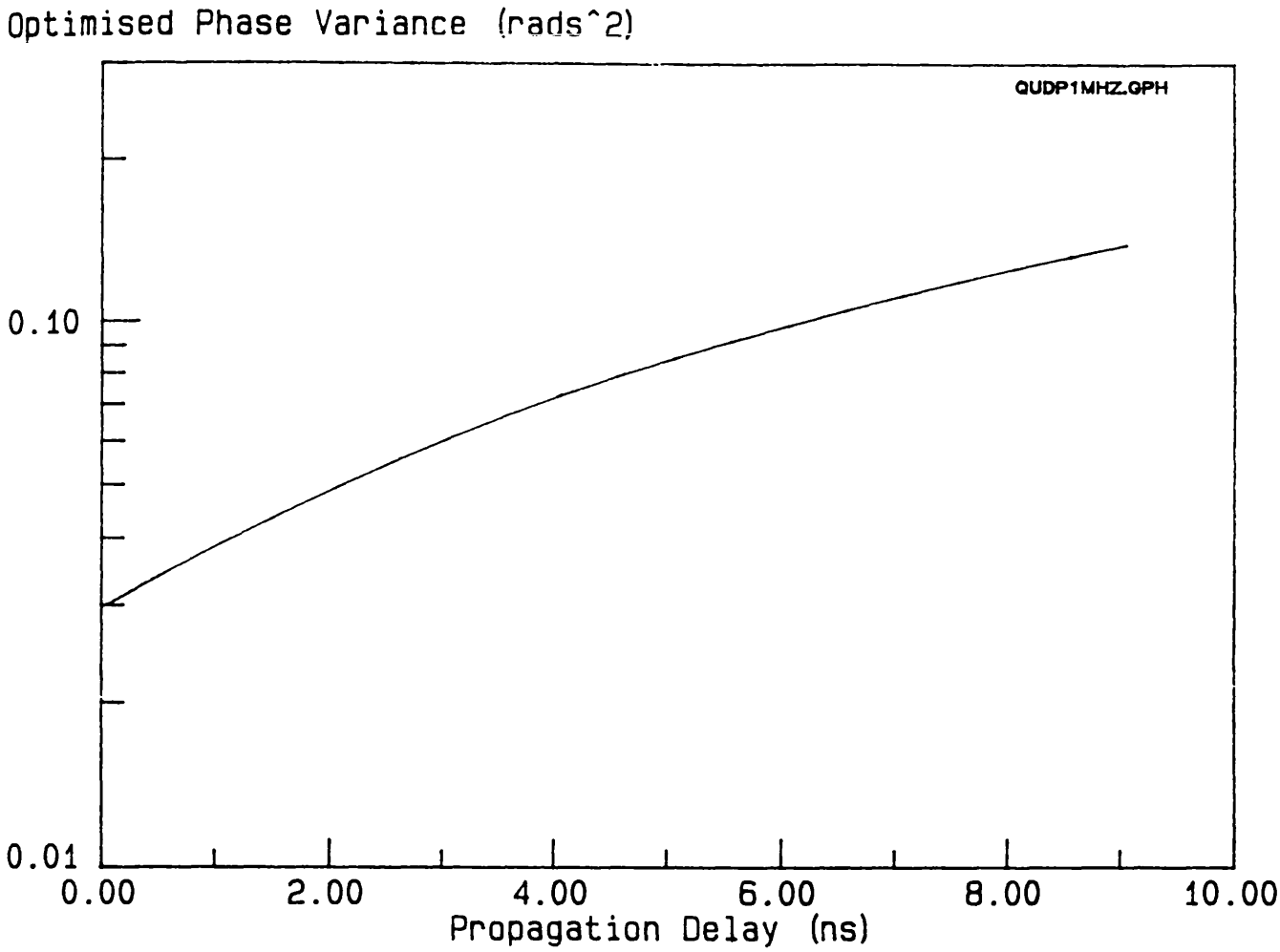

Figure 5.6

Optimum Phase Tracking Performance versus Propagation Delay for an OPLL constructed with sources of 1MHz Beat Linewidth.

of only 1.8 ns would be sufficient to degrade the tracking performance to the extent that a phase error variance of 0.047 rads^2 is more likely to be achieved. With the phase synchronisation reduced to this extent it is not possible for a BER of 10^{-9} to be achieved, irrespective of the data power [1]. This small delay value has therefore had a considerable influence on the overall system performance. If the source beat linewidth is further increased then the situation becomes correspondingly more acute. A beat linewidth of 15 MHz, which is not an unreasonable value given present day source technology, would require a loop bandwidth of approximately 340 MHz and would tolerate a maximum delay value of 0.12 ns for the above performance stipulation. When it is considered that this is equivalent to approximately 2.4 cm optical path length in fibre, then the severity of the problem is put into perspective.

While the curves presented here are useful in that they provide a clear description of the effect of the propagation delay, it is more beneficial to present these results in a more general form, in order that a more ready means of deriving the effect of the propagation delay may be provided. For this purpose, a set of normalised degradation curves has been evaluated and are displayed in Figure 5.7. These curves depict the normalised variance degradation as a multiple of the designed variance (designed without considering the delay). This degradation is plotted as a function of the loop delay– bandwidth product. If the estimated loop delay is multiplied by the designed bandwidth, then a measure of the loop delay bandwidth product can be attained. This can be used to determine a value of the performance penalty. For example, in the system considered earlier the loop bandwidth was 148 M Rads/sec and the propagation delay was 1.8 ns. This corresponds to a delay bandwidth product of approximately 0.27. The average performance degradation value for this value is approximately 1.6 which, in a system with an in built variance of 0.03 rads^2, would result in a phase error variance of 0.048 rads^2. It must be noted here that this method of calculation is only approximate. It does not take into account the fact that the optimum loop bandwidth will be reduced from the zero propagation delay case. The new estimation of the phase error variance can be used in conjunction with a graph such as that evaluated by Prabhu in

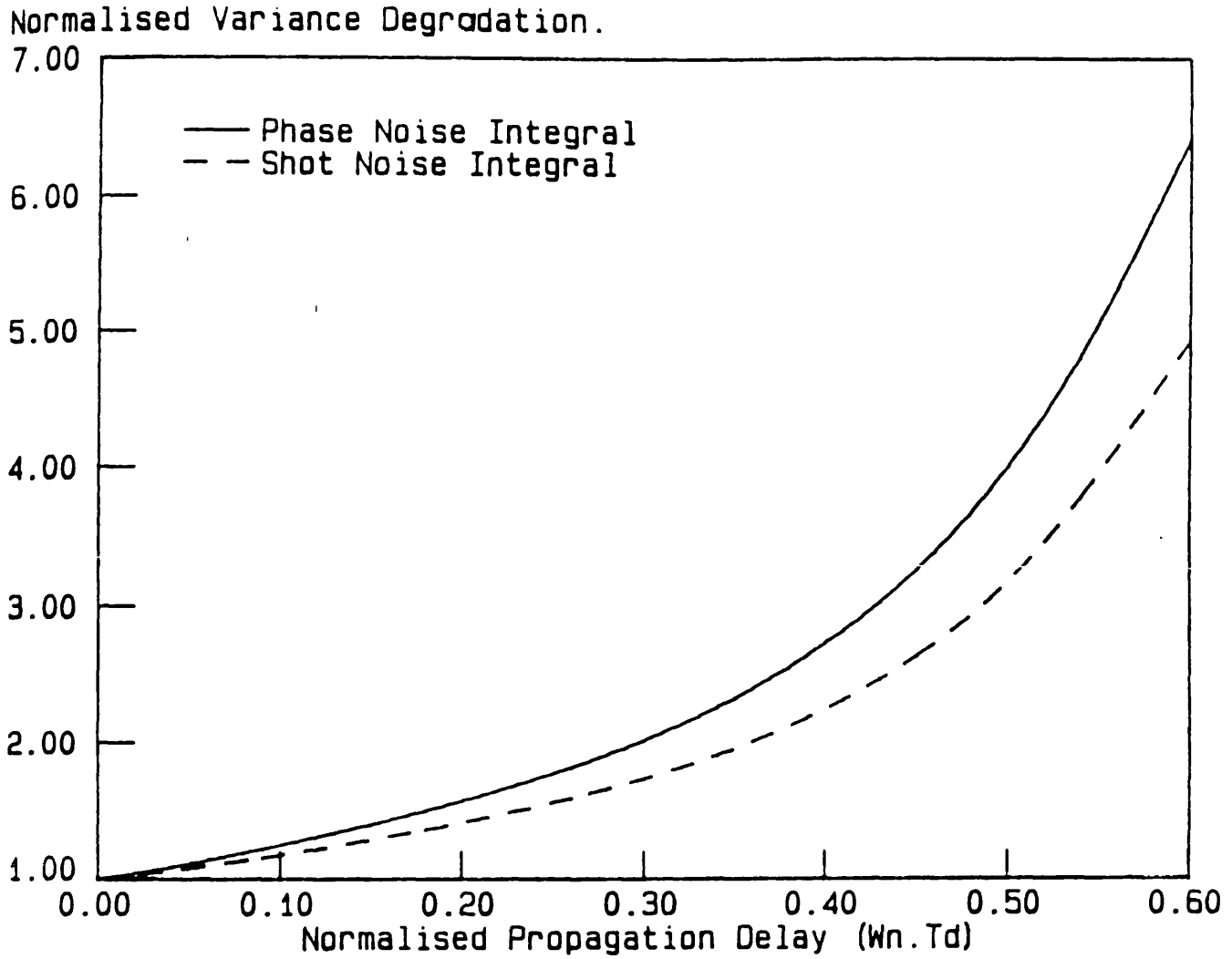

Figure 5.7

**OPLL with significant Propagtion Delay.
Normalised Performance Degradation versus
Delay Bandwidth Product.**

reference 1 (see Figure 5.8) to obtain an estimate of the overall power penalty in terms of the additional amount of data power required for a given performance. In the situation under consideration it is obvious that a performance of 10^{-9} is not possible with this new phase variance: the required data power tends to infinity.

5.4.1 Conclusions.

The analysis of the OPLL has been extended to account for the condition where the phase shift introduced by the propagation delay is significant. This investigation has been centred around the case of a pilot carrier tracking loop design. The analysis has been presented in a manner which allows the effect of the propagation delay, in a system designed without taking this into consideration, to be readily evaluated from a normalised performance degradation curve. Loop construction with sources with a beat linewidth of 1 MHz is possible however, a linewidth of this magnitude requires sufficient loop bandwidth that a propagation delay of 1.8 ns will be sufficient to prevent a BER of 10^{-9} from being attained. If the source beat linewidth is extended to 15 MHz then the allowable propagation delay is reduced to 0.12 ns.

5.5 The OPLL with a Finite Front End Bandwidth.

The effect of the front end amplifier cut off frequency will now be addressed. It is useful to investigate this time constant independantly from the propagation delay for two reasons. In the first instance it is reasonable to assume that the phase shift introduced by the amplifier will be of a comparible magnitude to that caused by the propagation delay. It is likely therefore that the effect of the amplifier will be similar to that of the delay. The solution to the loop bandwidth integrals are less complicated without the complex exponential term, an analytical solution can therefore be derived which may be used as an approximate model for the effect of the propagation delay. In the second instance, the width of the amplifier bandwidth is commonly assumed to be equivalent to the data rate. At low data rates, limiting the front end bandwidth may significantly effect on the phase tracking performance. It must be established

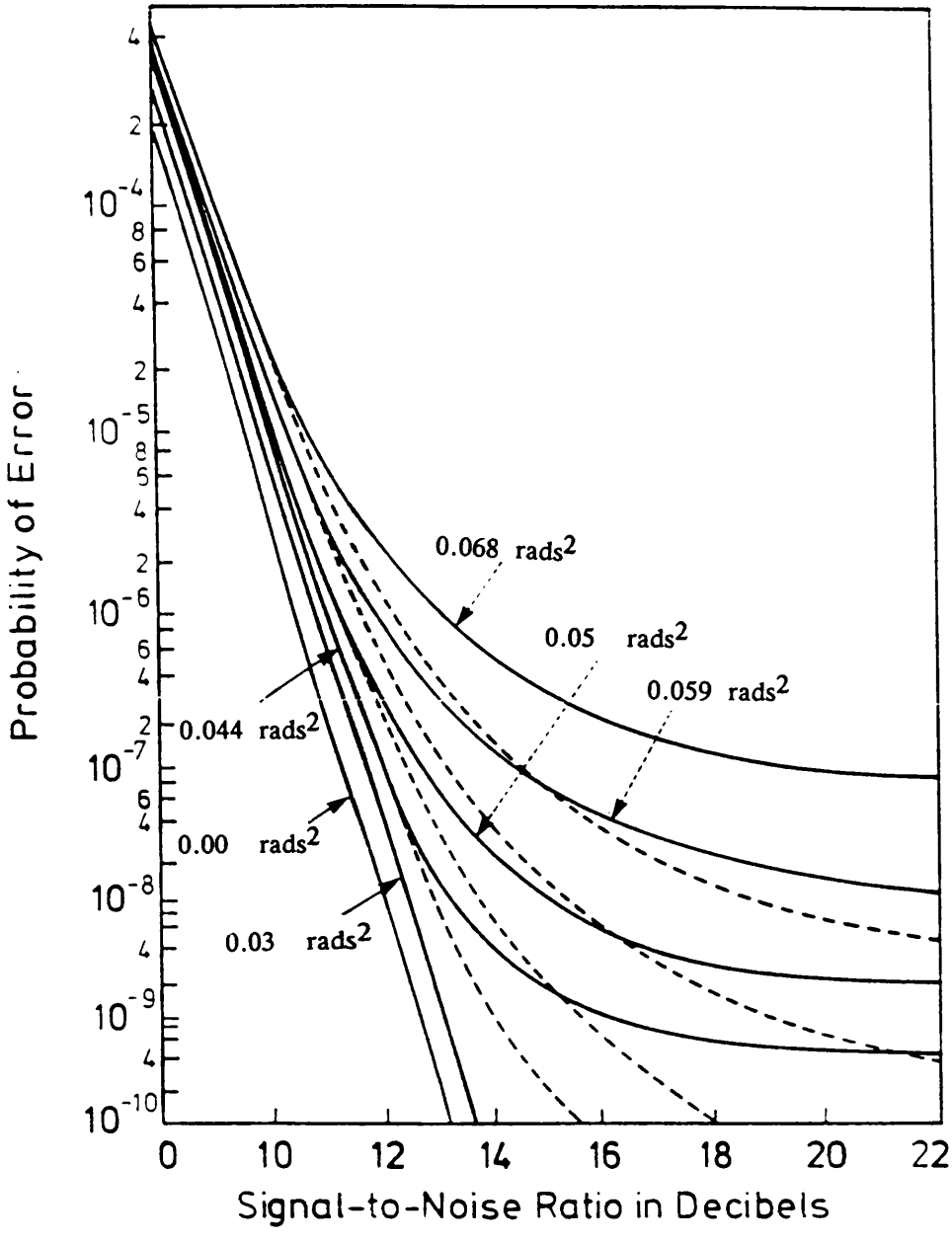

Figure 5.8

Probability of Error For Binary PSK Transmission [1].
Solid Lines Denote Tikhonov Distribution.
Dashed Lines Denote Gaussian Distribution.
Legends Denote Phase Error Variance.

therefore, where it is fair to assume that the amplifier bandwidth is set by the data transmission rate.

In the present analysis, the amplifier will be modelled as a a simple one pole filter with a transfer function $K_A/(1 + s\tau_C)$. The loop transfer function can therefore be written as,

$$H(s) = \frac{K(1 + s\tau_2)}{s^2\tau_1(1 + s\tau_c) + K(1 + s\tau_2)} \qquad (5.22).$$

The solution to the loop bandwidth integrals is readily obtained with the use of a set of standard tabulated integrals[22] as,

$$\sigma^2_{min} = \frac{e}{4RP_C}\left[\frac{\zeta\omega_n\tau_2}{\tau_2 - \tau_c} + \frac{1}{2(\tau_2 - \tau_C)}\right] + \delta f_{tot}\left[\frac{2\zeta\tau_c}{\omega_n(\tau_2 - \tau_c)} + \frac{1}{\omega_n^2(\tau_2 - \tau_c)}\right] \qquad (5.23)$$

Verification of this solution is obtained by setting $\tau_c = 0.0$. Equation 5.23 then reduces to 5.9 as would be expected.

In order that this expression can be more readily interpreted it is convenient to re-arrange the result and relate the amplifier bandwidth to the loop natural frequency. The substitution

$$\tau_c = 1/(X\omega_n) \qquad (5.24),$$

(where X is simply a multiplying factor), is introduced therefore allowing equation 5.23 to be written as

$$X = \frac{\sigma^2_\varphi\omega_n + 2\pi\zeta\delta f_{tot}}{\sigma_\varphi^2\omega_n 2\zeta - 3e\omega_n^2/8RP_C - \pi\delta f_{tot}} \qquad (5.25).$$

Expressing the result in this form allows a ready computation of the required front end bandwidth, assuming a particular carrier power penalty, to be made. Alternatively, it may be useful to evaluate the necessary carrier power if it is required that the amplifier bandwidth

should be restricted in some manner. Thus

$$P_c = \frac{-3e\omega_n X}{\pi\delta f_{tot} 8R(2\zeta + X)/\omega_n + 8R\sigma_\varphi^2(1 - 2\zeta X)} \quad (5.26).$$

These solutions are of greater practical value when expressed in a general form that accomodates for variation in the beat linewidth and natural frequency as the data rate is increased. Some progress towards this aim can be made if the solutions are normalised to the data rate as follows.

The theoretical minimum received power for a particular BER can be written in terms of the effective signal to noise ratio, Q, as,[10]

$$P_{SL} = eQ^2B/(4R), \quad (5.27)$$

where B denotes the data rate in hertz. Using this approximation the effective carrier power expression is modified to,

$$P_C = K_S K_C eQ^2B/(4R). \quad (5.28).$$

If the beat linewidth and the loop natural frequency are now normalised to the data rate, then the front end to loop natural frequency ratio X may be re-expressed as

$$X = \frac{\sigma_\varphi^2\omega_n' + 2\pi\zeta\delta f'_{tot}}{2\sigma_\varphi^2\omega_n'\zeta - 3\omega_n'^2/2K_C K_S Q^2 - \pi\delta f'_{tot}} \quad (5.29).$$

where the prime denotes the normalisation. This normalisation also allows equation 5.23 to be rewritten as

$$\sigma_\varphi^2 = \left[\frac{\pi\delta f_{tot}'(1 + 4\zeta^2)}{2\zeta^2 Q^2 K_S K_C} \right]^{1/2} \quad (5.30).$$

Thus an expression has been derived which allows an estimate of the carrier power penalty, in terms of K_S and K_C, for any linewidth to bit rate ratio, to be obtained. The following example will illustrate the use of these evaluations. The assumption that it is permissable to assume that the front end amplifier has an equivalent bandwidth to

the data rate can also now be examined.

The total power in a data transmission can be described

$$P_T = K_S(1 + K_C)P_{SL} \qquad (5.31).$$

This equation provides information of how much power is allocated to the data, $K_S P_{SL}$ (which specifies how far away from the shot noise limit the receiver is operating) and also, the power which is sacrificed in carrier transmission (to provide the required phase matching between the transmit and local oscillators). For a system operating 1 dB away from the theoretical minimum the constant K_S will be, by definition, 1.258. If the additional carrier power penalty is to be limited to 0.5 dB then the carrier coefficient K_C will be 0.122 giving the $K_C.K_S$ product of 0.153. With a variance in the phase tracking of 0.03 rads^2, Q = 36, a carrier power of this magnitude requires that the data rate to linewidth ratio be (from 5.30) approximately 1900.

This figure has been arrived at without consideration of the front end amplifier. It is a common practice to neglect the effect of this amplifier in PLL design and simply assume that it will be limited to the data rate. To assess whether or not this assumption is reasonable the power penalty to be paid, when the amplifier phase shift is considered, must be calculated.

A data rate to linewidth ratio of 1900 is equivalent to an X factor of approximately 12.8. The normalised expression of 5.26 is

$$K_s K_c = \frac{-3X\omega_n'^2}{2Q^2(\pi\delta f'_{tot}(2\zeta + X) + \omega_n'\sigma_E^2(1 - 2\zeta X))} \qquad (5.32).$$

For an X factor of 12.8, the necessary value of $K_S.K_C$ is 0.196 and hence $K_C = 0.156$. The power penalty due to the front end is

$$\frac{P_{Tnew}}{P_t} = \frac{1.258(1 + 0.156)P_{SL}}{1.258(1 + 0.122)P_{SL}} \qquad (5.33).$$

which corresponds to an increase in total power of 0.13 dB, that is a total transmission power of -57.57 dBm.

In this particular instance therefore, the additional power penalty incurred as a result of having a finite receiver bandwidth is almost insignificant and the assumption that the front end can be limited to the data rate is reasonable. It is reasonable however, to assume that this assumption will not be valid under all sets of circumstances. In order that it may be decided when the assumption is not valid, some basis for making this decision must be established. This problem is made easier with a graphical presentation of equation 5.32. This is given in Figure 5.9.

Figure 5.9 represents the carrier power penalty that is paid when a consistent phase tracking performance is maintained while the front end amplifier bandwidth is varied. The figure shows two independent traces. The dashed curve represents the power penalty which is incurred as a result of the phase shift in the feedback signal introduced by the receiver amplifier cut off frequency. This power penalty is expressed as an additional carrier power over that which would be required if the amplifier bandwidth was infinite. The solid curve represents the power penalty that arises as a result of the phase noise on the transmitter and the receiver oscillators. This phase noise, or linewidth, is normalised to the data transmission rate for convenience. While the data rate to linewidth ratio is high, the assumption that the front end bandwidth is equivalent to the data rate may be considered fair because the additional carrier power required to compensate for the amplifier phase shift, is small in comparison to the power penalty associated with source linewidth. However, as the data rate is reduced, this condition is not upheld and, at normalised data rates of less than 800, the additional carrier power required to compensate for errors in the phase tracking becomes significant. In a situation therefore, where the data rate was limited to that of existing channels, the effect of the front end amplifier must be carefully considered. In a coherent system operating a data rate of 565 Mbits/sec with a source beat linewidth of 1 MHz, the data rate to linewidth ratio is such that a substantial additional amount of carrier power would be sacrificed if the front end amplifier were limited to

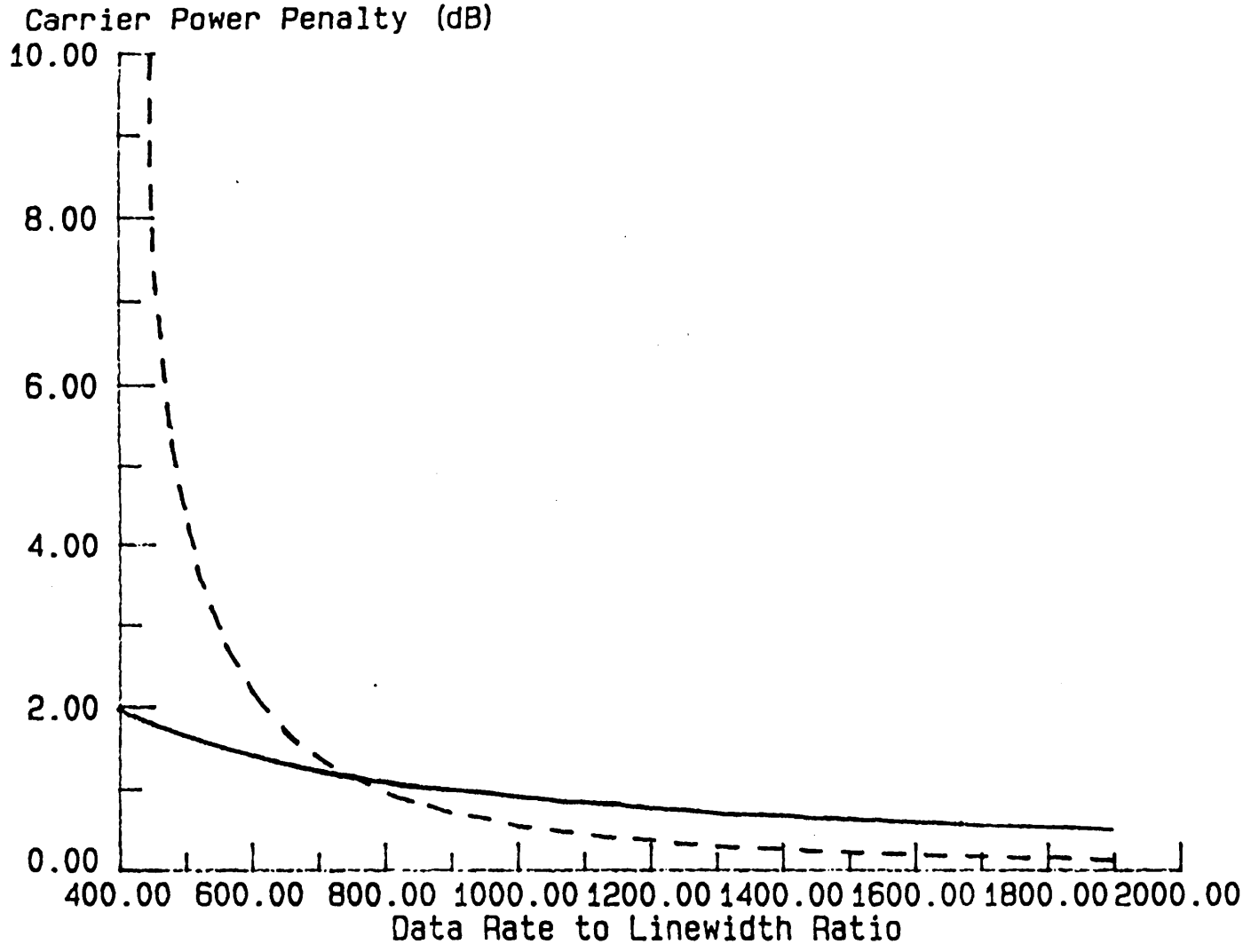

Figure 5.9

Carrier Power Penalty versus Front End Amplifier Bandwidth (Data Rate).

the data rate.

The final aspect of the front end analysis that remains to be performed is the comparison of this analytical solution with the numerically calculated loop bandwidth integrals of the propagation delay. To a first approximation the delay can be modelled as a low pass filter. The significant difference is that the pure delay does not modify the amplitude of the feedback signal, it simply alters the phase. In the situation of the OPLL since the bulk of the delay is the optical path it was felt that a pure delay was the more appropriate description. To test this hypothesis the analytical solution to the noise bandwidth integrals were displayed in a similar manner to the time delay solutions (see Figure 5.10).

Figure 5.10 shows that the single pole approximation of the loop delay results in a degradation of the phase tracking properties of the OPLL which is similar in form to that observed under the more rigorous analysis presented earlier. However the two situations are significantly different as the following figures, Figure 5.11−13, demonstrate. Figure 5.11 shows the estimated optimum natural frequency variation with loop propagation delay. The upper of the two curves shows the optimum loop natural frequency as calculated when the delay is approximated as a single pole filter, the lower of the two traces displays the more rigourous numerical solution. It is clear that the analytical solution differs significantly from the numerical solution, especially at large valus of delay. The following graph, Figure 5.12 displays the calculated optimum achievable phase error variances, for both sets of calculations. It can be seen from this graph that the analytical approximation of the delay predicts a phase tracking performace which is optimistic for all delay values. In order that a clearer measure of the difference between the two approaches to the problem can be obtained, Figure 5.13, showing the relative percentage difference between the two sets of calculations (normalised to the numerical solution), was evaluated. It is clear from this figure that the analytical approximation of the propagation delay is insufficiently accurate to be of use in calculating the effect of loop delay in situations where the delay bandwidth product is likely to be significant, that is for OPLLs constructed using sources with a beat linewidth of

FIGURE 5.10: OPLL Phase Variance Versus Natural Frequency.

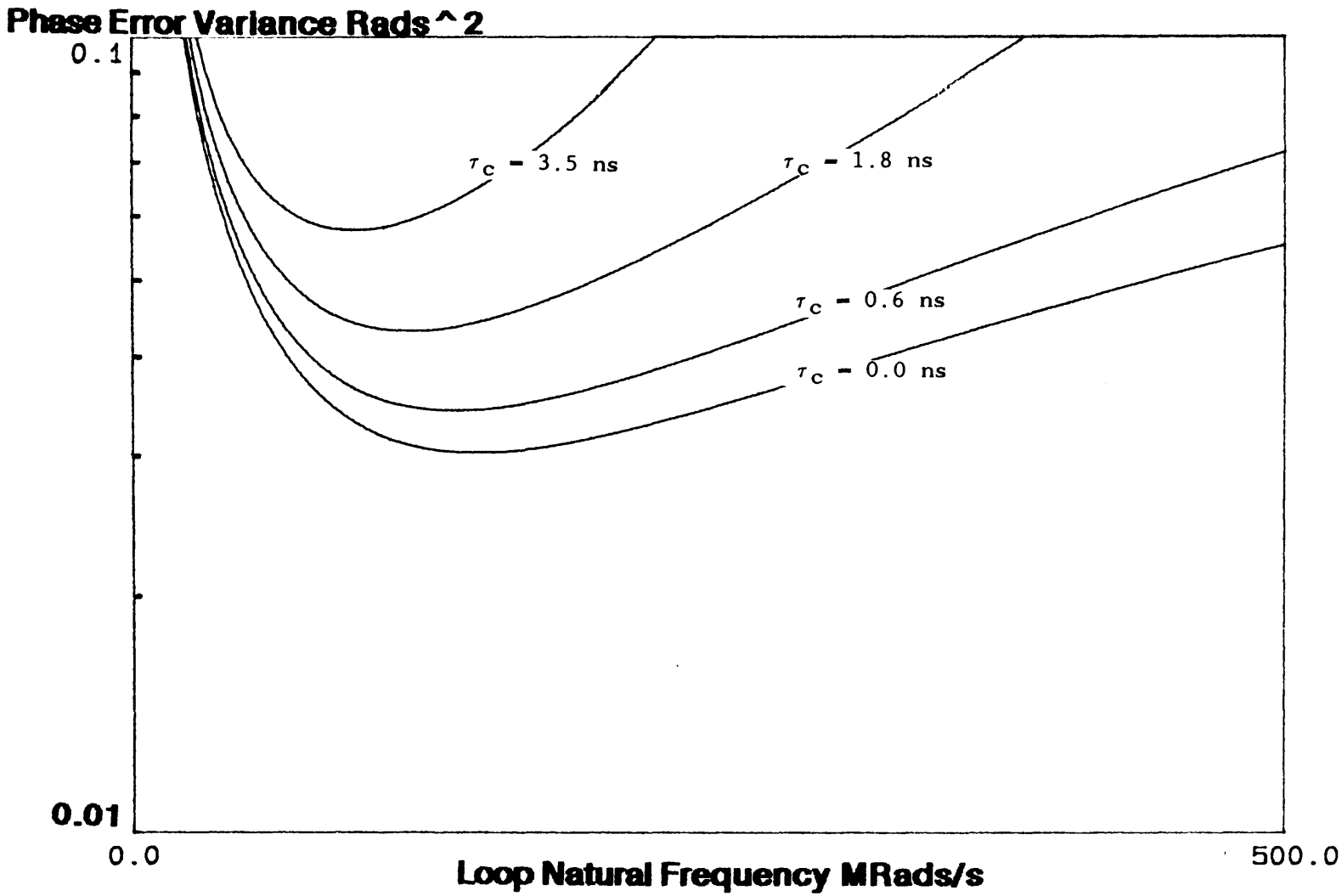

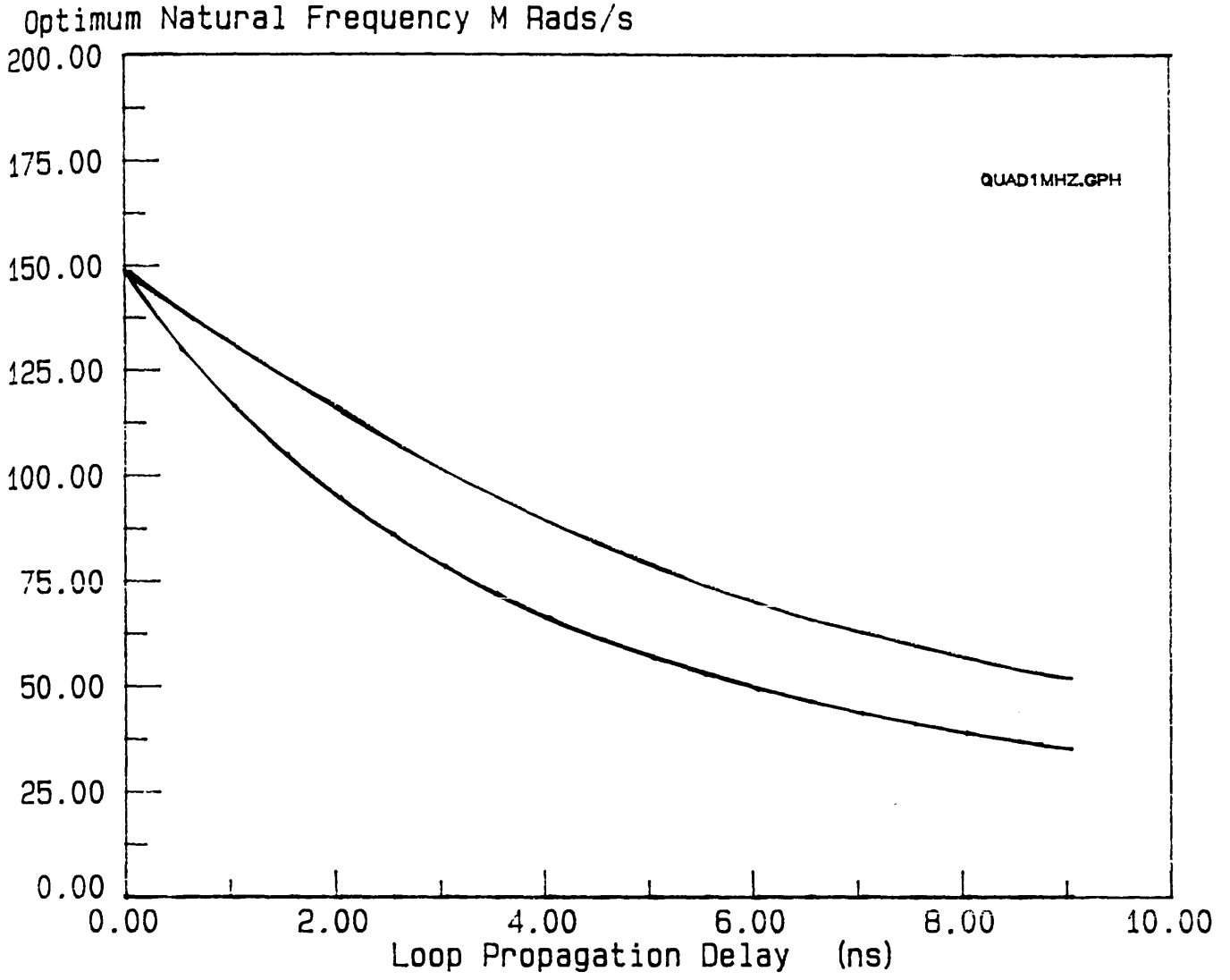

Figure 5.11.

Optimum Loop Natural Frequency for OPLL with Significant Loop Propagation Delay.
Lower Trace shows Results of Numerical Computation.
Upper Trace Shows Approximate Analytical Solution.

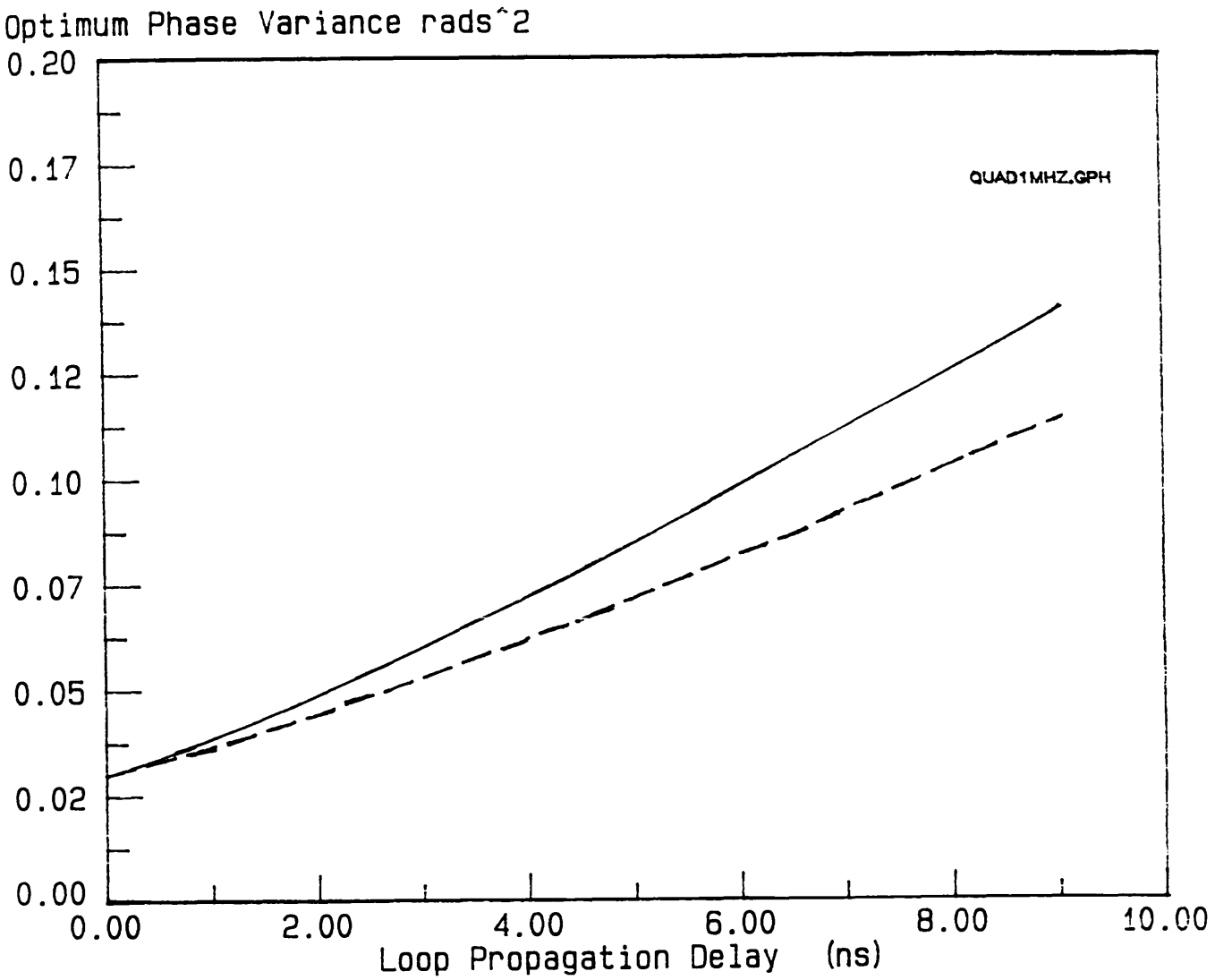

Figure 5.12.

**Phase Error Variance for OPLL with Significant Propagation Delay.
Loop Natural Frequency Optimised for Each Delay Value.
Lower Trace shows Results of Numerical Computation.
Upper Trace Shows Approximate Analytical Solution.**

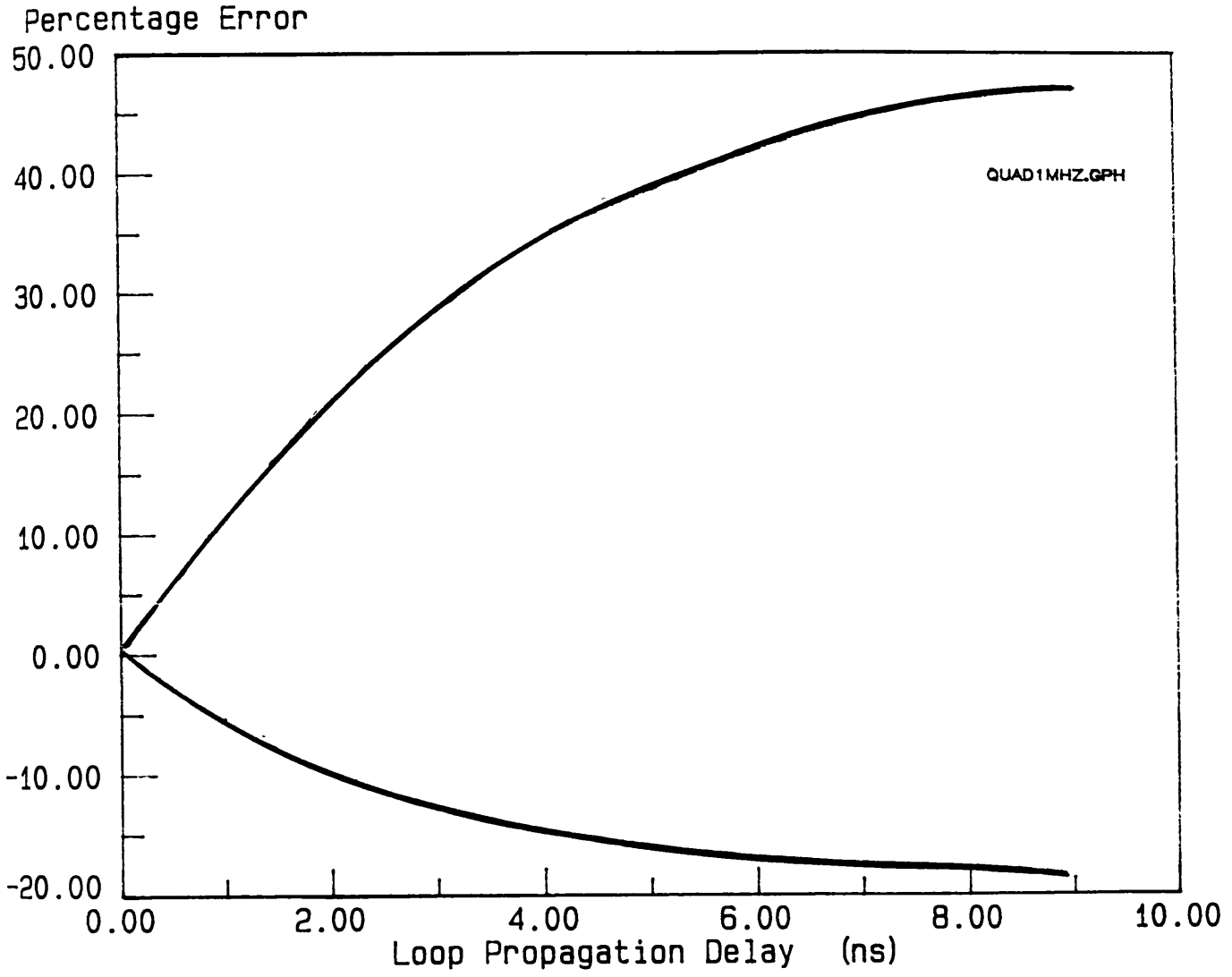

Figure 5.13.

Percentage Difference Between the Analytical and Numerical Solutions to the Loop Bandwidth Integrals. Upper Trace Shows Percentage Error in Natural Frequency. Lower Trace Shows Percentage Error in Phase Error Variance. Both Curves are Normalised to the Numerical Result.

greater than 1 MHz. Under these conditions, for a delay value of 1 nanosecond, the error in the estimation of the loop natural frequency is greater than 10 % and the analytical model predicts a Phase Error Variance which is 7.5 % less than the true value. (In practice the estimated phase tracking performnnce would be more than 7.5 % worse than this value because the analytical solution also returns a value of loop natural frequency which is greater than the optimum value). The situation is seen to further degrade as the propagation time is increased and therefore it is concluded that in such situations as these, where the tolerances in loop design are so critical, this magnitude of error would not be acceptable.

4.5.1. Conclusions to Front End Amplifier Analysis.

The effect of the front end filter bandwidth on the performance of an optical phase–locked loop has been evaluated for the condition where the loop propagation delay is assumed to be negligible. Equations have been derived which describe the effect of the front end bandwidth on the phase tracking performance and these have been normalised for the general case of a given beat linewidth to data rate. It has been concluded that if the necesary additional carrier power is to be limited, to that which would already be occurred as a result of the system linewidth (or less), then the data rate to linewidth ratio of approximately 800 must be achieved. The effect of the front end amplifier bandwidth was compared to that of the propagation delay however the two conditions were found not to be sufficiently similar that the analytical expression could be used as an approximate solution. In an OPLL the loop propagation delay may be dominated by optical path delay (the delay in the coupling of the local oscillator to the incoming source) and thus the pure delay is the more appropriate model.

5.6 Conclusions.

The analysis of the performance of the OPLL has been extended to account for the effect of loop propagation delay and the effect of the front end amplifier cut off frequency. This analysis has shown that a significant performance penalty results for propagation delays which

* The data rate to linewidth ratio required to limit the power penalty at the decision circuitry to 0.5 dB is 2000. This implies that an OPLL operating with a beat linewidth of 1 MHz would require a data rate of 2Gbits/s. While this is true it must be borne in mind that an OPLL operates as one receiver component in a communications system and therefore power allocated to the carrier synchronisation must be included in the final calculation of receiver performance. In the present example the necessary carrier power penalty (in the absence of effects of loop transport delay) would be 2.5 dB. In contrast the required carrier power for a 20 kHz beat linewidth is only 0.04 dB.

are small in comparison to the loop bandwidth. The particular case of a loop designed with sources of beat linewidth 1 MHz was examined. In this instance, a time delay of only 1.8 ns was shown to be sufficient to downgrade the performance of a binary PSK transmission incorporating this loop, such that a BER of 10^{-9} is not possible. The corresponding figure for a similar loop with a 15 MHz linewidth was found to be 0.12 ns.

A substantial number of publications describing the effect of laser phase noise on the performance of PLLs are available in the open literature [2,5,8,10]. These publications conclude that phase locking with sufficient stability for a binary PSK transmission is possible with sources of Megahertz linewidth and PLL's of wide bandwidth *. However, in these analysis no attempt was made to consider the effect of the propagation delay. This present work has shown that this consideration is significant.

In general, the analyses of the OPLL behaviour have neglected the effect of the bandwidth of the photo-diode/amplifier combination on the OPLL performance, assuming that it can be limited to the system data rate. The validity of this assumption was investigated and was found to be true only for situations where the data rate was 800 times the source beat linewidth. At data rates of less than this value the phase shift due to the front end amplifier would be sufficient to compromise the phase tracking performance such that a substantial amount of carrier power would be sacrificed to maintain a constant phase tracking performance. This is not a point only of academic interest: coherent transmission systems may be required to operate alongside existing IM/DD systems and under such circumstances it is not unreasonable to assume that the transmission bandwidth may be restricted. Careful consideration must therefore be paid to the effect that the front end amplifier will have on the loop performance. If the performance of the overall system is not to be affected then this bandwidth must not be reduced to less than 800 time the source beat linewidth.

The front end amplifier analysis was presented in a similar manner to the earlier work on the propagation delay in order that a comparison between the two could be made. It was concluded that, in

situations where the loop bandwidth is high, the effect of the propagation delay is critical and it would not be suitable therefore to approximate the effect of the delay as equivalent to that of the amplifier because of the magnitude of the error involved. It is considered that, especially in situations where largeloop bandwidths are considered, the propagation delay is the most difficult problem to eliminate. Furthermore, where delays of the order of nanoseconds are significant, it is likely that a substantial proportion of the delay will be composed of optical path length. Pure optical delays are arguably as close an approximationto a pure delay as it is possible to achieve therefore in these circumstances the model of the OPLL with a pure delay is the most appropriate model.

References.

1. V.K.Prabhu 'PSK Performance with an Imperfect Carrier Phase Recovery.' IEEE Trans. on Aero. ans Elect. Syst. Vol– AES 12(2) 1976. pp275– 286.

2. T.G.Hodgkinson 'Phase– Locked Loop Analysis for Pilot Carrier Coherent Optical Receivers' Elect. Lett. vol 21 1985. pp1202– 1203.

3. J.J.Stiffler 'Theory of Synchronous Communications' Prentice– Hall Inc. 1971.

4. W.C.Lindsey 'Synchronous Systems in Communication and Control' Englewood Cliffs, NJ: Prentice Hall, 1972.

5. L.G.Kazovsky 'Balanced Phase– Locked Loops for Optical Homodyne Receivers: Performance Analysis, Design Considerations, and Laser Linewidth Requirements' J. Lightwave. Technol. vol LT– 4(2) 1986. pp182– 194.

6. F.M.Gardner 'Phaselock Techniques' New York: Wiley, 1979.

7. A.Blanchard 'Phase– Locked Loops. Application to Coherent Receiver Design.' New York: Wiley, 1976.

8. L.G.Kazovsky 'Decision– Driven Phase– Locked Loop for Optical Homodyne Receivers: Performance Analysis and Laser Linewidth Requirements' J. Lightwave Technol. vol LT– 3(6) 1985. pp1238– 1247.

9. J.P.Costas 'Synchronous Communications' Proc. IRE, vol 44, 1956. pp1713– 1718.

10. T.G.Hodgkinson 'Costas Loop Analysis for Optical Receivers' Elect. Lett. vol 22(7) 1986. pp394– 396.

CHAPTER 6.

The Dynamic Responce of the Optical Phase Locked Loop.

6.1 Introduction.

The previous two chapters have presented a performance analysis of the OPLL from the point of view of determining the optimum natural frequency and hence phase tracking performance of the loop. The optimum natural frequency was found by evaluating the loop bandwidth integrals. While the effect of system imperfections, such as propagation delay, can be observed from this analysis no physical interpretation of these effects has so far been presented. The present chapter will attempt to provide this description. Use will be made of a standard frequency response technique, the root locus construction, and a digital simulation, to describe the behaviour of the loop in the time domain. When the time domain response is considered, the effect of the propagation delay and the front end amplifier cut off frequency can be more fully understood.

6.2 Root Locus Construction.

The closed loop response of a system can be predicted, for a given set of input conditions, by examining the position of the roots of the open loop transfer in the Laplace domain [1,2,3]. If a particular system parameter is varied, and the position of the poles evaluated as a function of this parameter, then a locus of the system roots can be drawn up. This allows the variation of the system performance to be evaluated as a function of the chosen parameter. It is generally required that the system behaviour is described for a number of different gain conditions and hence the range of gains, over which the system is stable, can be evaluated. In this instance the gain is a convenient parameter since the square of the natural frequency is proportional to the gain. The root locus constructions, corresponding to the OPLL conditions displayed in Chapter 5, Figure 5.3, were calculated in order that an explanation for the form of these figures could be obtained. The method of construction will now be described.

The Root Locus plot is obtained from the open loop transfer function which, for the OPLL, can be written thus,

$$W_o(s) = \frac{K.F(s).\exp(-s\tau_D)}{s^2(1 + s\tau_C)} \qquad (6.1.)$$

As in previous chapters, a standard active filter configuration is assumed for the loop filter F(s) allowing 6.1 to be re-written

$$W_o(s) = \frac{(\omega_n^2 + 2\zeta\omega_n s)\exp(-s\tau_D)}{s^2(1 + s\tau_C)} \quad . \qquad (6.2.)$$

The closed loop transfer function H(s) can be described as

$$H(s) = \frac{W_o(s)}{1 + W_o(s)} = \frac{K.G(s)}{1 + K.G(s)} \qquad (6.3.)$$

where K is the overall loop gain and G(s) accomodates for all other filtering aspects of the loop. The poles of the closed loop systen occur at values for which $1 + K.G(s) = 0$ or

$$\begin{aligned} &\text{mod}[K.G(s)] = 1 \\ &\text{arg}[K.G(s)] = (2n+1)\pi \qquad n = 0,1,2.... \end{aligned} \qquad (6.4)$$

The presence of the complex exponential term describing the propagation delay makes the construction of the locus more difficult than it would otherwise be. Numerical techniques were therefore used. The form of the Locus is indicated in figures 6.1 to 6.3. Note that only the positive components of the locus have been displayed, the locus is symmetrical about the σ, or real, axis. Arrows are used to denote ω_n increasing.

Figure 6.1 displays the condition where the propagation delay is insignificant. In this instance, the loop is stable for all values of natural frequency. At the designed natural frequency (ω_n = 148 Mrads/sec) the loop response can be seen to be dominated by a pair

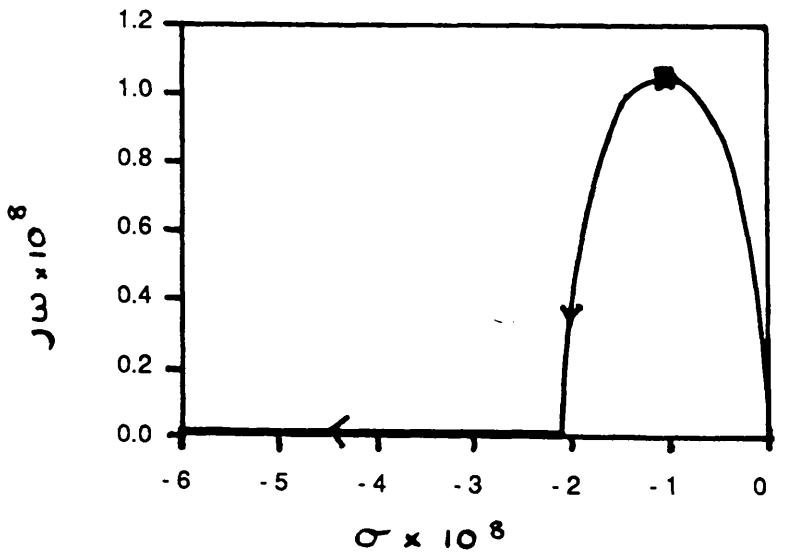

Figure 6.1

Root Locus Construction for OPLL with Negligible Propagation Delay.

Arrows Indicate Increasing Natural Frequency.

Legend Denotes ω_n = 148 MRads/s

of complex conjugate poles with equal real and imaginary parts. Thus the loop will respond to a step disturbance from equilibrium with a single damped overshoot in the phase error consistent with a damping factor of $1/\sqrt{2}$. Increasing the natural frequency, while maintaining all other parameters constant, causes the loop response to become increasingly more damped. In the final instance the loop, while wholly stable, is completely inactive.

The following two figures (Figure 6.2 and Figure 6.3) demonstrate how the propagation delay modifies the locus. Increasing the delay causes the locus to depart from the real axis at high values of gain. For low levels of delay (see Figure 6.2) the situation is not critical: the loop will remain in a stable condition even with relatively large parameter variations. In the example displayed in Figure 6.2 an increase in the loop natural frequency by a factor of ten would be permissible before the loop would lose lock. The transient behaviour of the loop would however be significantly altered and the aquisition time may be such that it would make locking less probable, never the less, the overall system is stable and therefore there is still a possibilty of lock being achieved. In the following figure (Figure 6.3) the time delay has been increased to such an extent that sensitivity of the loop to parameter fluctuations presents a greater problem. An increase in the loop natural frequency, from the designed value, would have the effect of pushing the loop closer towards an unstable state. A reduction in the damping factor, coupled with an increase in the loop gain, would be observed. This would greatly reduce the probability of solid locking being achieved.

Figure 6.4 depicts the effective reduction in the loop damping factor as the delay– bandwidth product is increased. This shows clearly how the steady move towards instability will take place.

It is of interest to compare the loop damping factor with the optimum natural frequencies as predicted for the specific values of delay and beat linewidth in Figure 5.3. Evaluation of the delay– bandwidth products corresponding to the optimum values of ω_n, for the given set of delays under consideration, allows Figure 6.5 to be constructed. This graph displays an assymptotic rise in the phase

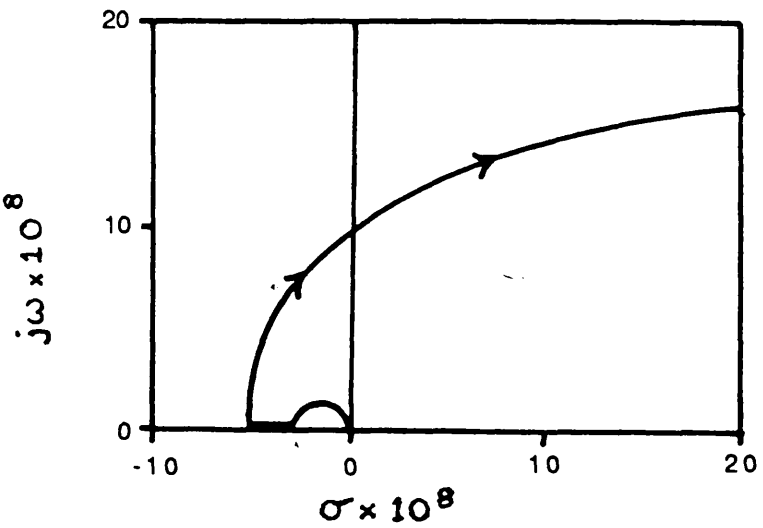

Figure 6.2
Root Locus Construction for OPLL with Propagation delay of 1.5 nano seconds.
Arrows indicate increasing Natural Frequency.

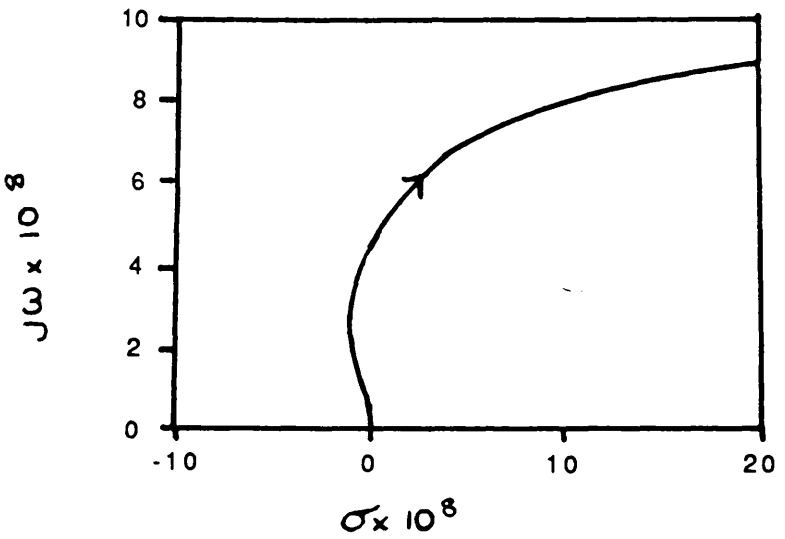

Figure 6.3
Root Locus Construction for OPLL with Propagation delay of 3.0 nano seconds.

Arrows indicate increasing Natural Frequency.

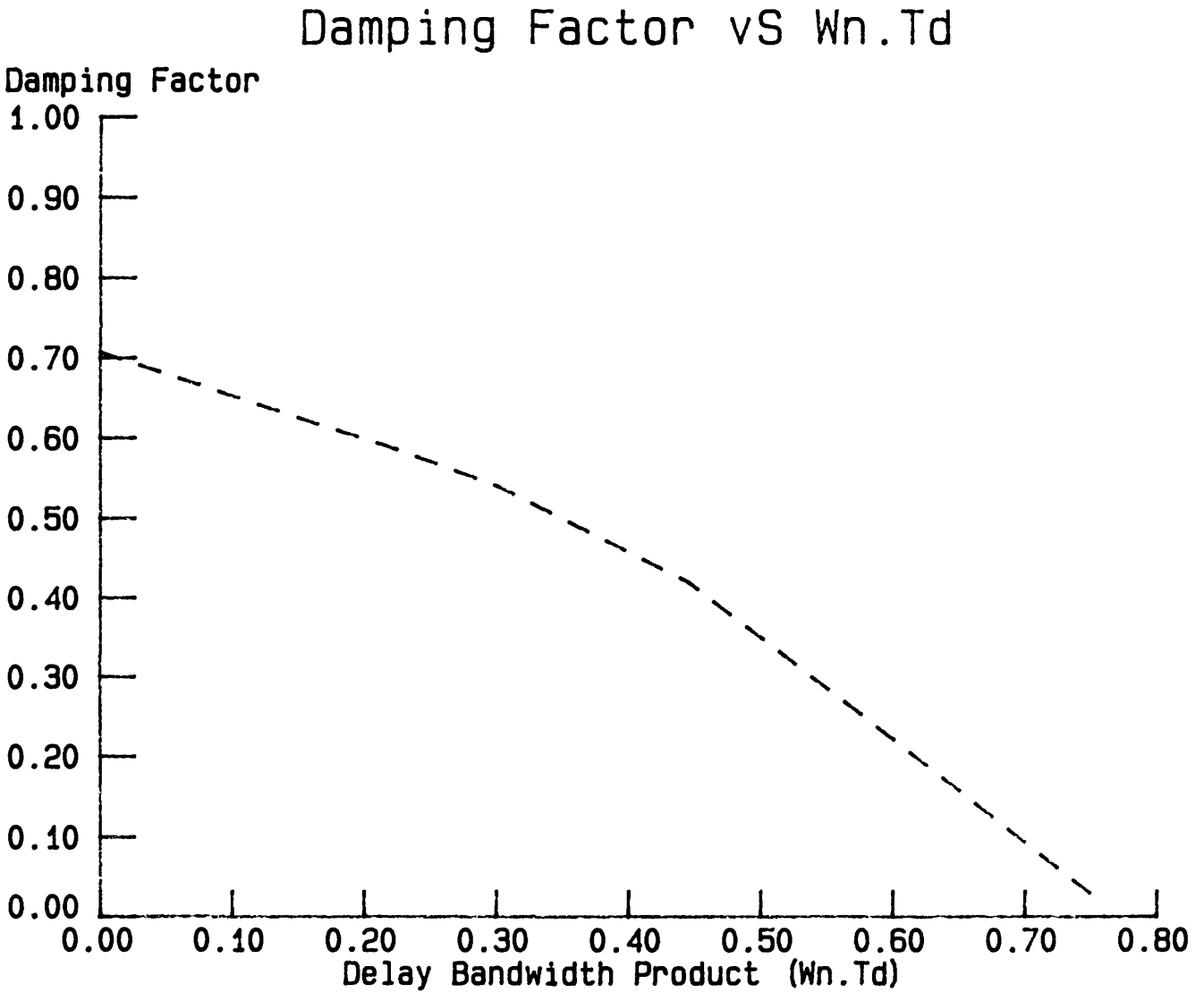
Damping Factor vS Wn.Td
Damping Factor
1.00
0.90
0.80
0.70
0.60
0.50
0.40
0.30
0.20
0.10
0.00
0.00
0.10
0.20
0.30
0.40
0.50
0.60
0.70
0.80
Delay Bandwidth Product (Wn.Td)

Figure 6.4

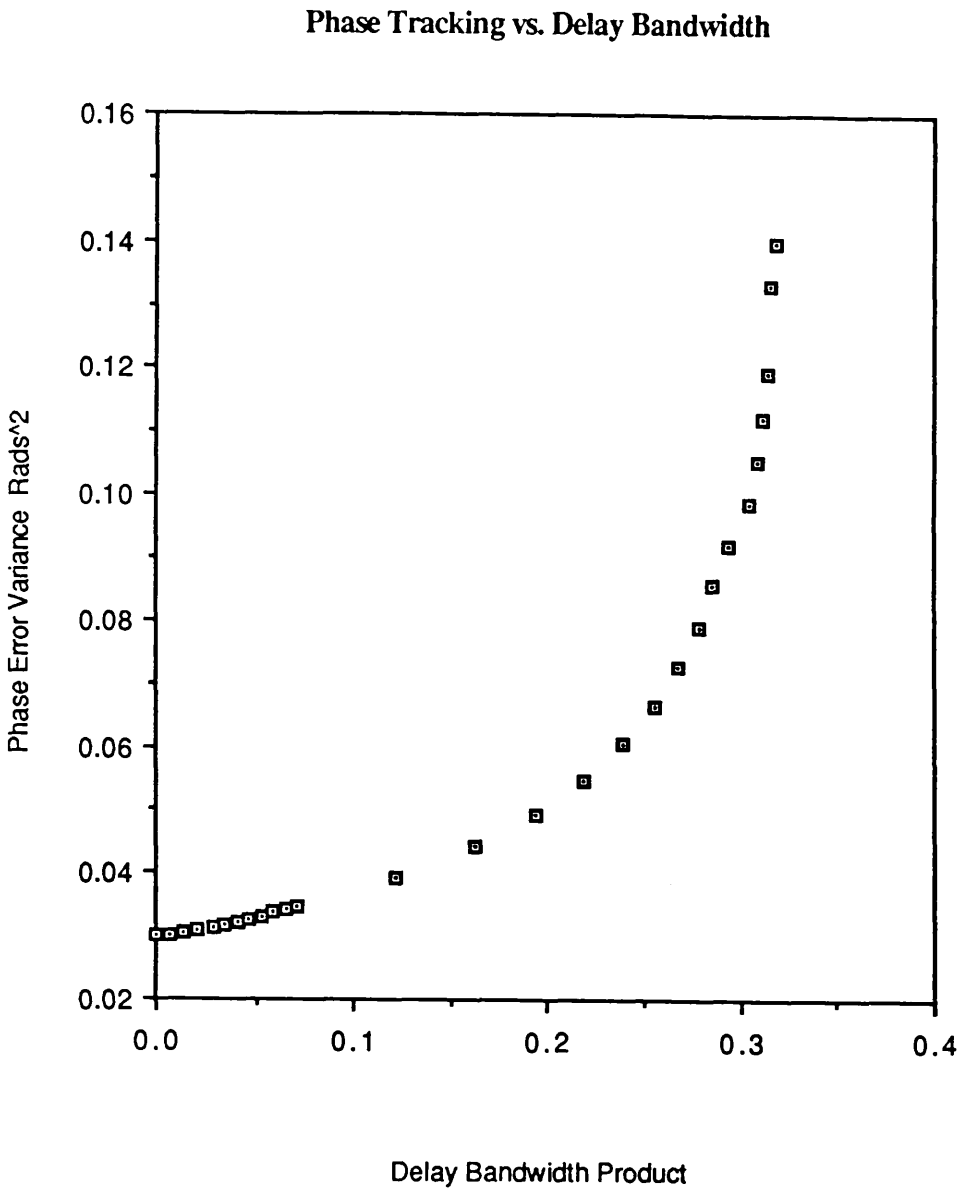

Figure 6.5
Loop Tracking Performance (Phase Variance) versus Delay Bandwidth Product.

Data Taken from Optimum Natural Frequency As displayed in Figure 5.5.

error variance as the delay– bandwidth product rises above the value of 0.32 which corresponds to a loop damping factor of less than 0.5. This suggests that for values of ζ of less than 0.5, the major cause of performance degradation is not the noise contributions but the inherent instability of the loop itself. Therefore the loop optimim bandwidth, for significant delay values, is a compromise, between the 1/f type phase noise and sufficient loop damping.

The following figures, Figure 6.6 and Figure 6.7, describe the root locus variation for delay values ranging between 0 and 5 ns. In this set of plots, the front end amplifier cut off frequency has been included in the description of the loop. In order that the effect of the amplifier would be observed, an amplifier cut of which would have a significant influence was chosen. This cut of frequency was set equal to six times the loop natural frequency. The analysis of Chpater 5 has shown that, in the absence of any significant propagation delay, the phase shift associated with a cut off frequency of this value would be sufficient to incurr a 1 dB carrier power penalty to restore the loop tracking performance to that obtained under ideal conditions.

The locus is shifted under the influence of the delay towards the imaginary axis and instability. The markers indicate pole positions for constant gain (equal to that for 148 Mrads/s natural frequency). The presence of an additional pole, due to the front end amplifier can be observed. The position of this pole is significant in that it can be used as an indicator to show the range of conditions where the second order description of the phase– locked– loop is accurate. It is generally accepted that, if the magnitude of the real part of this pole is greater than ten times that of the real parts of the conjugate poles, then the influence which it exerts on the system performance will be minimal[3]: the system response can be assumed to be essentially second order and dominated by a pair of complex conjugate poles. In situations where this condition is not met, the second order description of the system becomes inadequate. The position of the real pole associated with the front end amplifier can be seen, for delay– bandwidth products of greater than 0.2, to be sufficiently close to the real axis as to invalidate the second order definitions of loop natural frequency and damping factor.

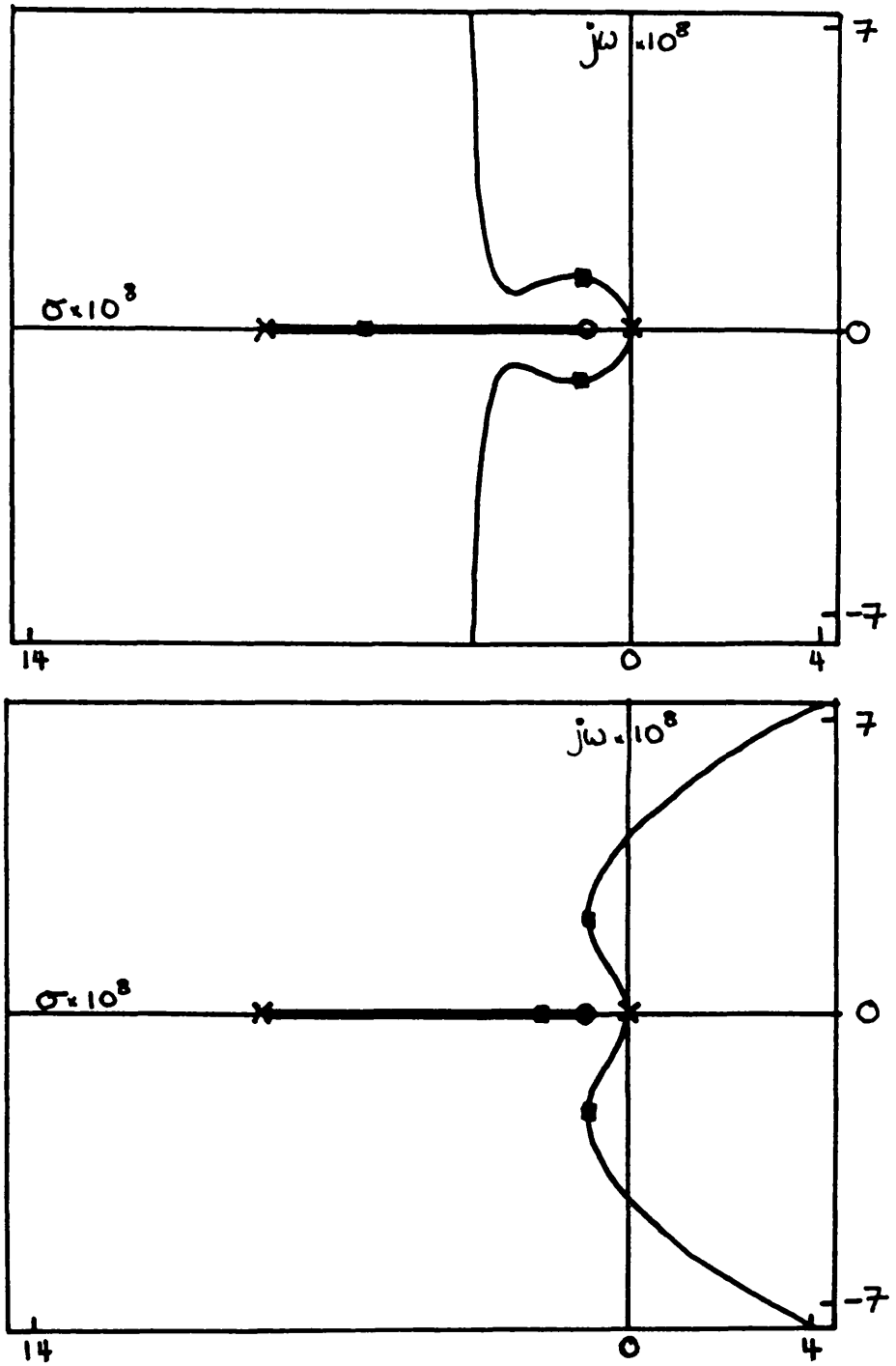

Figure 6.6

Root Locus Construction for OPLL.

Receiver Bandwidth is Restricted.

Upper Trace Propagation Delay is Negligable.

Lower Trace Propagation Delay of 2 ns.

Legends Denote Pole Positions for ω_n = 148 Mrads/s

Receiver Cut Off Bandwidth = 6. ω_n

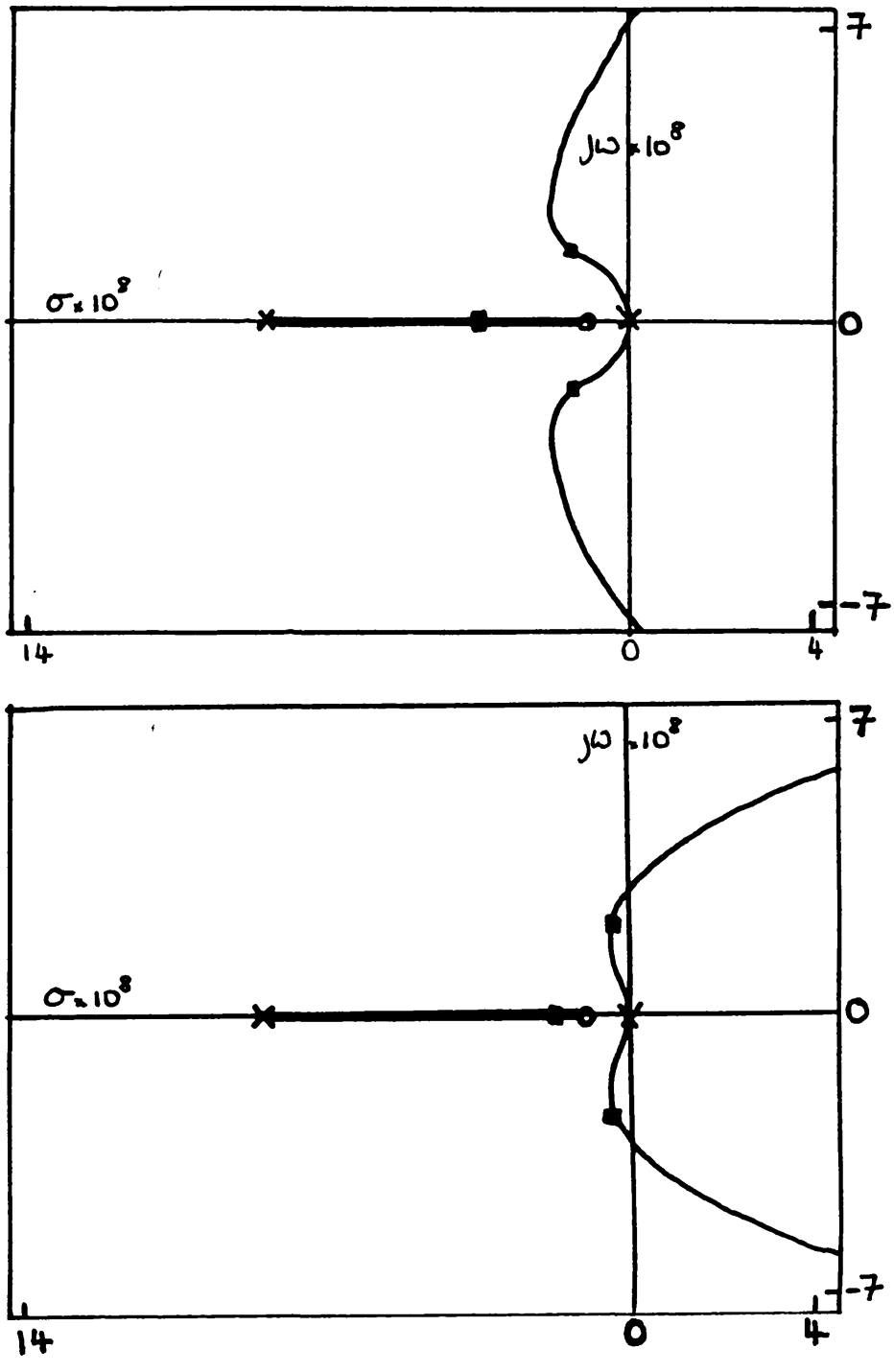

Figure 6.7

Root Locus Construction for OPLL.

Receiver Bandwidth is Restricted.

Upper Trace Propagation Delay is 4 ns.

Lower Trace Propagation Delay is 5 ns.

Legends Denote Pole Positions for ω_n = 148 Mrads/s

Receiver Cut Off Bandwidth = 6.ω_n

6.2.1 Root Locus Construction: Conclusions.

The OPLL has been investigated with the use of the Root Locus Construction technique in order that effect of the phase shifts in the feedback signal, introduced by imperfect amplifier design, may be interpreted. The Root Locus plots have shown that, as the propagation delay is increased, the loop has a tendency to become unstable. Increasing the delay– bandwidth product reduces the loop damping factor from the designed value. The loop therefore oscillates when perturbed from the equilibrium condition under the influence of the noise inputs. For large values of delay the loop will also become more sensitive to parameter variations. At delay– bandwidth products of less than 0.3, increases in the loop gain will tend to be accompanied by an increase in the damping factor. At delay values of greater 0.3 the damping factor will be reduced with increasing gain. This situation is more likely to produce an unstable response and consequently the probability of the loop maintaining solid lock are reduced. It is interesting to note that the optimum values of the loop natural frequency, as predicted for a range of delays, are limited to those which maintain the delay– bandwidth product less than approximatley 0.32.

The Root Locus construction for the OPLL with a non– infinite front– end amplifier cut off frequency was drawn up for a number of different delay values. A similar loop transient beahviour can be expected for this type of loop as the propagation delay is increased. However, the Root Locus construction indicates that the second order loop description of the OPLL is inadequate when the effect of the propagation delay becomes significant. In the following section a digital simulation of the OPLL will be discussed. The use of the digital simulation enables the effect of increasing delay to be observed in real time and therefore a better judgement over whether or not the definitions of the loop natural frequency are valid can be made.

6.3 Digital Simulation of an OPLL

The OPLL was simulated on an IBM PC– AT personal computer. A block diagram showing the digital implimentation of the PLL

model is shown in Figure 6.8. The integration method used in the simulation was the trapezoidal rule: the modelling algorithm is given in Appendix 6A1. Later versions of the simulation make use of files of randomly generated signals to simulate the phase noise and the shot noise in the OPLL. For the moment however attention will be restricted to the loop performance in the absence of noise. The loop parameters in the following figures have been allocated to correspond to those values of the optimised PLL with zero propagation delay. The removal of the noise corruptions allows the transient response to a step input in phase to be observed.

It is known from Chapter 5 that an increase in the propagation delay will result in an increase in the phase error variance. The Root Locus plots indicate that this will be the result of an under damping of the system response. Increasing the time delay in the simulation allows this effect to be observed in the time domain. The sampling period of the simulation is 0.1 ns.

Figure 6.9 shows the loop step response with zero delay. The single overshoot observed is consistent with a damping factor of $1/\sqrt{2}$. Figure 6.10 demonstrates that an increase in the propagation delay, in this instance to 3.6 ns, results in an increase in the oscillation frequency and number of overshoots. This is consistent with a reduction in the loop damping factor. The critical delay for the OPLL with an infinite front end bandwidth, and a natural frequency of 148 MRads/sec, is approximately 4.97 ns. This corresponds to the situation where the delay–bandwidth product is 0.736. Figure 6.11 displays this condition and the associated virtually undamped oscillation.

If attention is returned to the Figure 6.9 (where the delay is 3.6 nanoseconds) then a comparison can be made between the effect of the delay on the transient response and the phase error variance, as predicted in Chapter 5. In a system where the loop parameters were set considering $\tau_D = 0$, a performance degradation will be observed as the delay value is increased. Furthermore, the operating conditions for the loop will be non–optimal for any delay value other than $\tau_D = 0$. Optimum performance is recovered by adjusting the loop gain such that the natural frequency is reduced. A new optimum natural

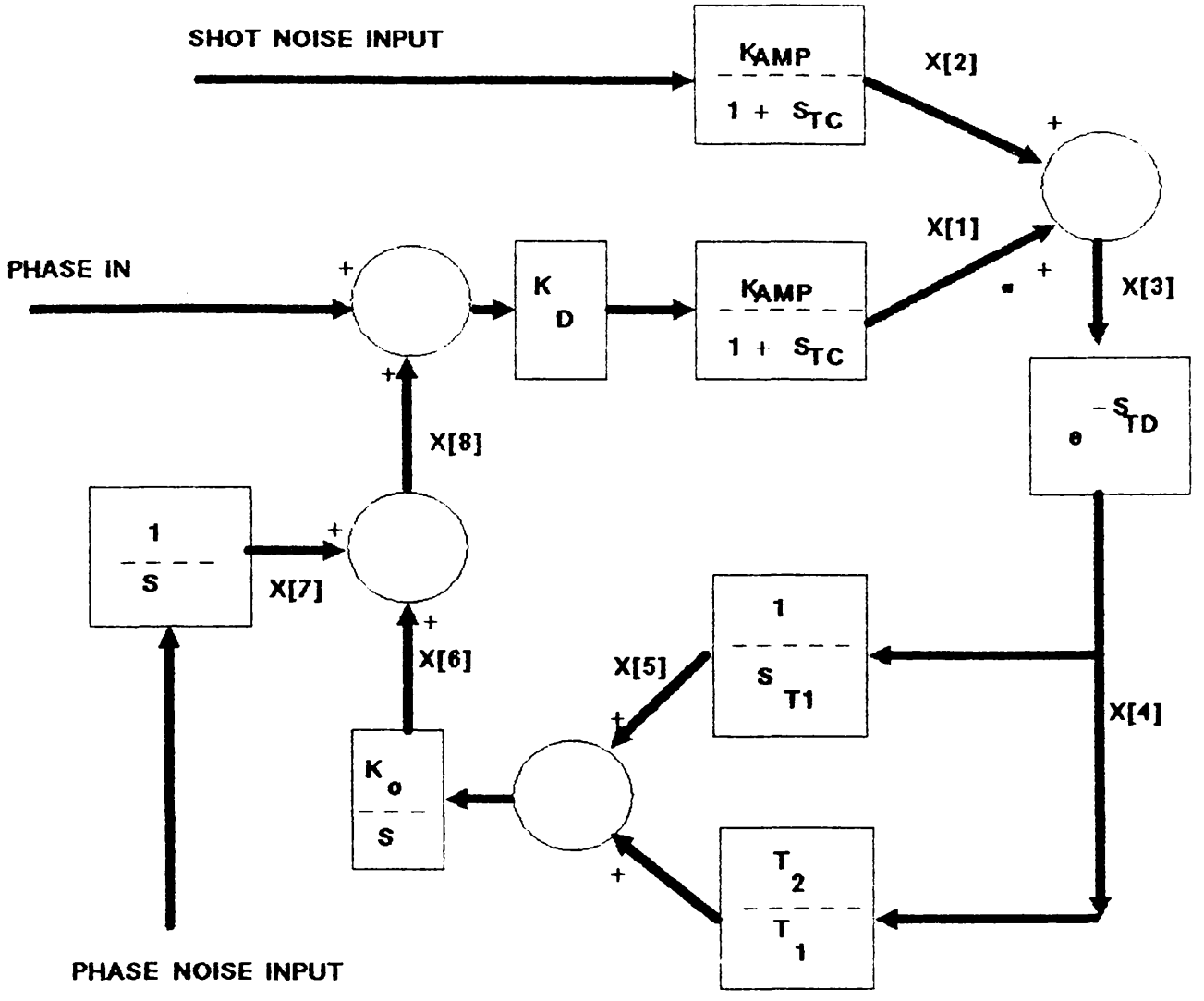

FIGURE 6.8
PHASE LOCKED LOOP SIMULATION

FIGURE 6.9: Natural Frequency 148 MRads/s: Delay 0.0 ns.

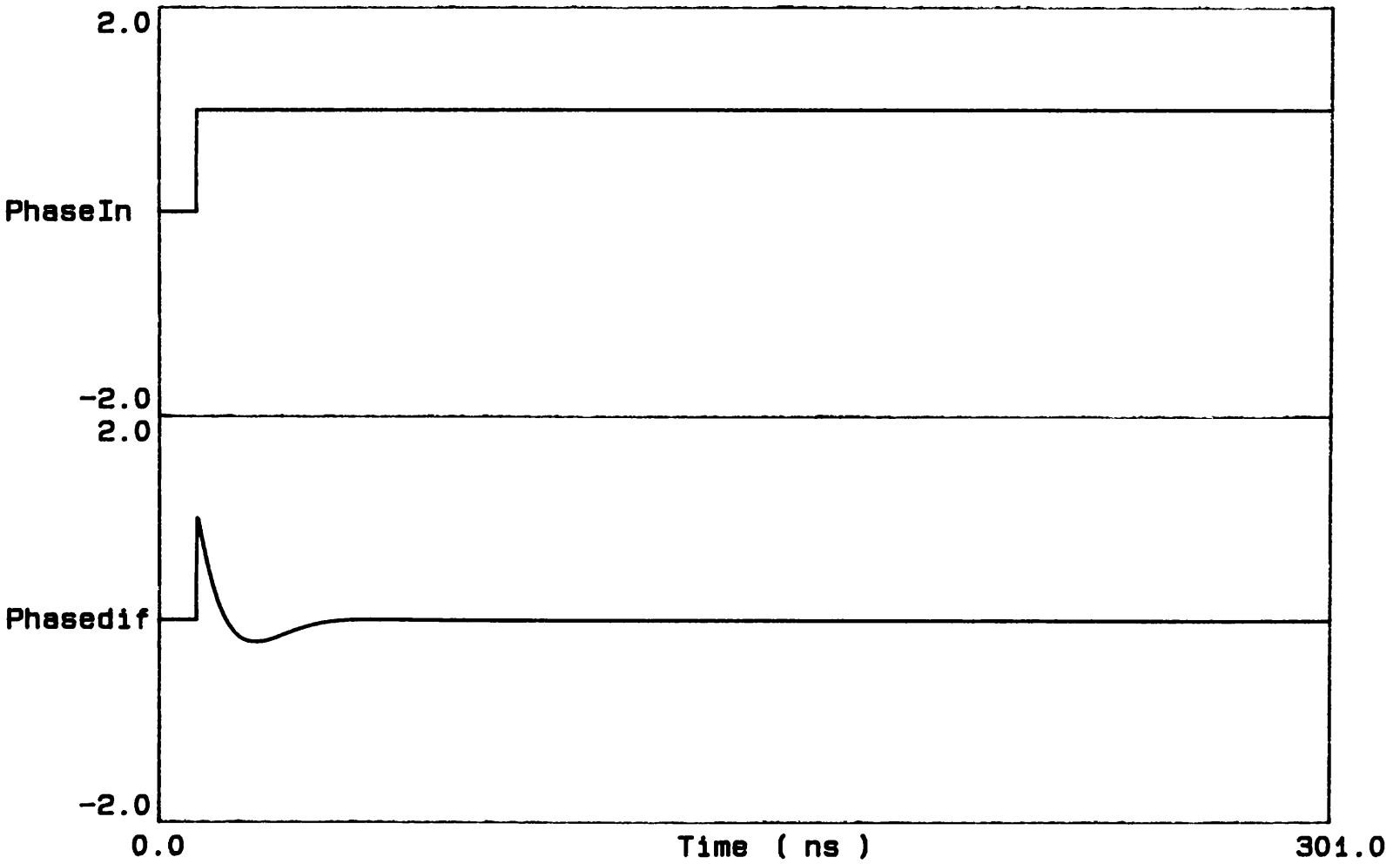

FIGURE 6.10: Natural Frequency 148 MRads/s: Delay 3.6 ns.

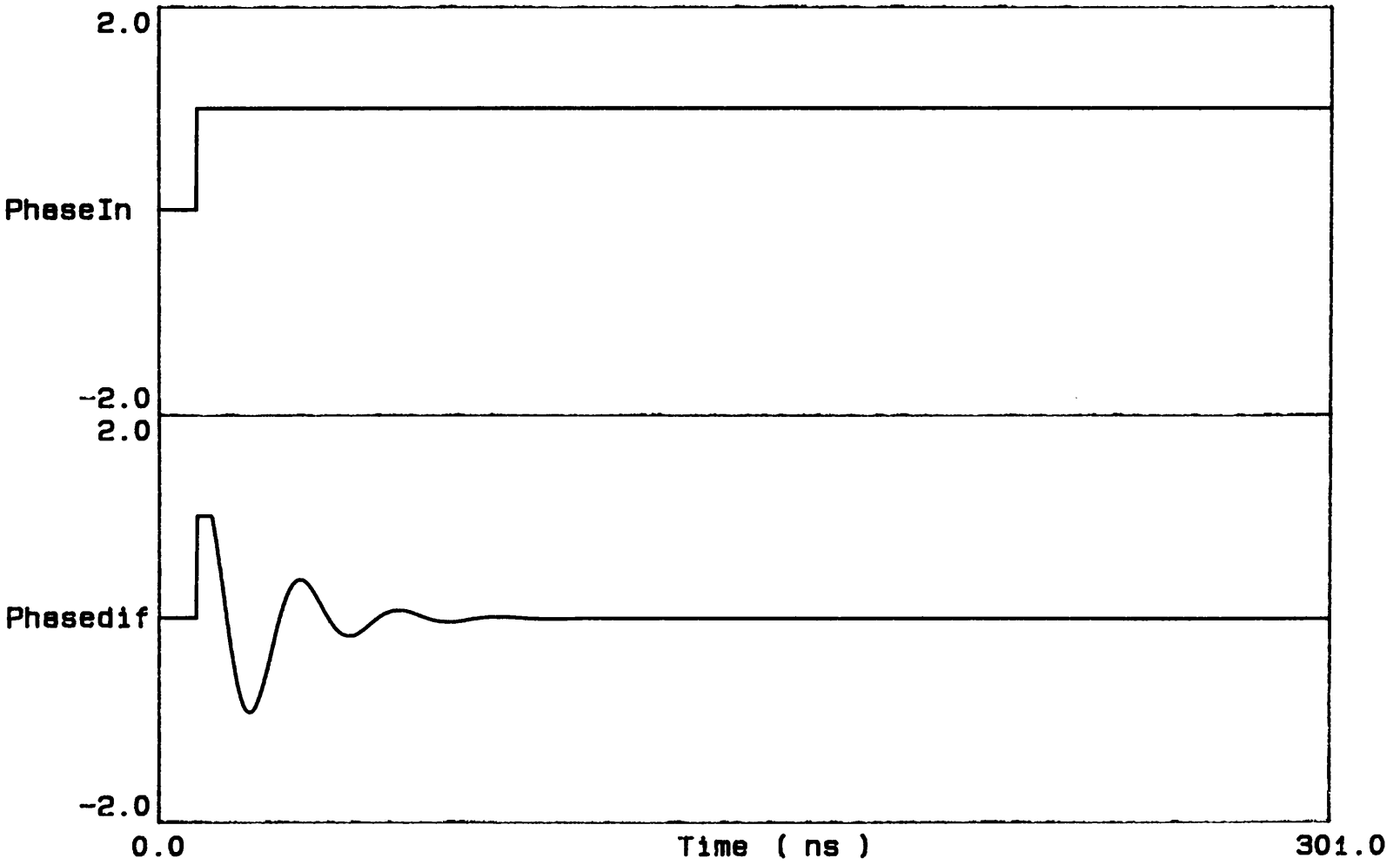

FIGURE 6.11: Natural Frequency 148 MRads/s: Delay 0.0 ns.

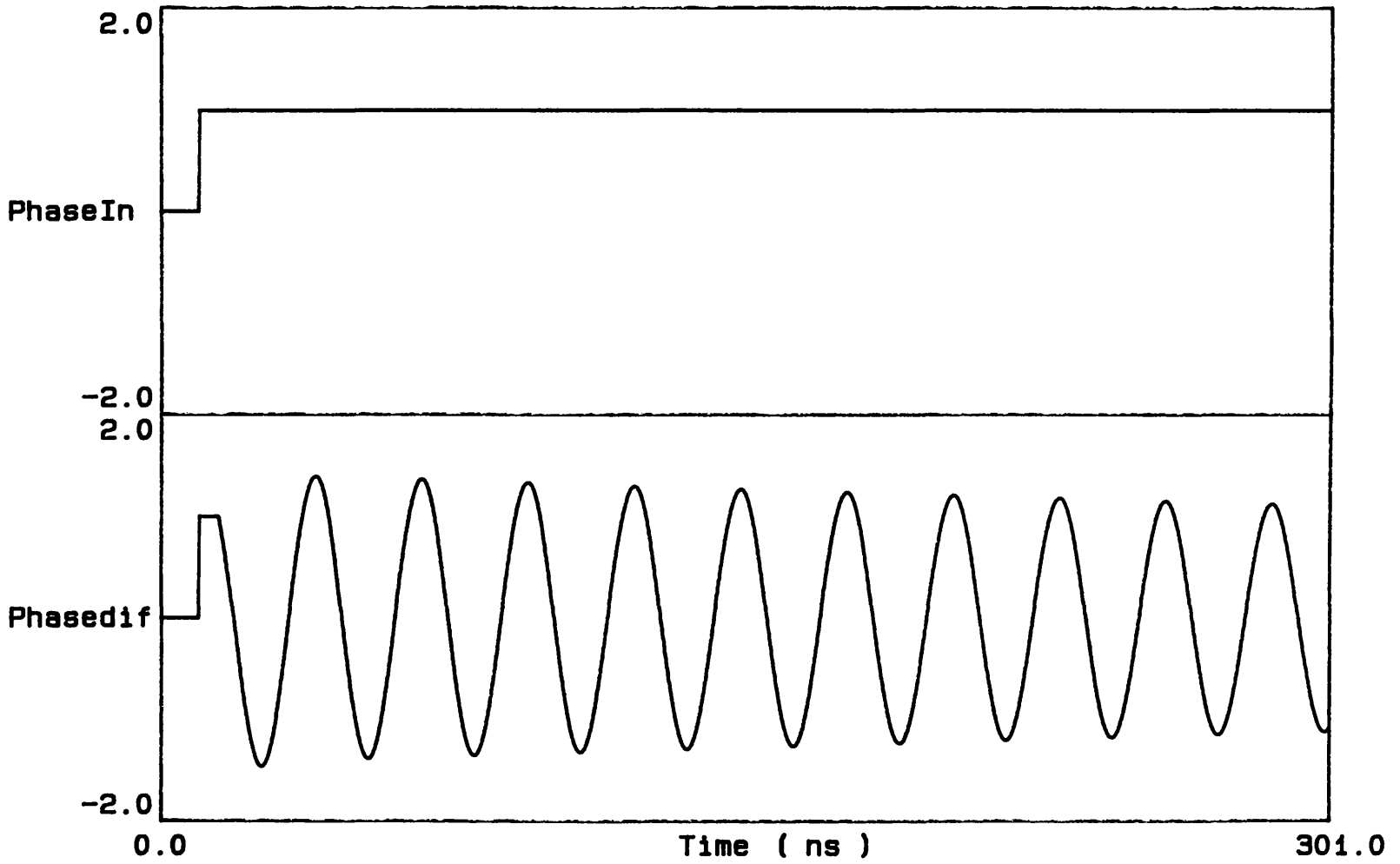

frequency (ω_n = 67 MRads/s) is then arrived at which accounts for the propagation delay. This value of ω_n was substituted into the simulation and the effect is shown in Figure 6.12. The reduced value of natural frequency has restored the loop response to a single damped overshoot for a step input. Thus the optimum value of ω_n may in fact be that value which restores the loop response to as close as possible to the critically damped situation.

If the frequency of the phase oscillations is measured then it is seen that this frequency grows as the effective damping factor is reduced. This is not unexpected because, as the damping factor diminishes, the dominant pole position moves closer to the imaginary axis and the associated oscillation would be expected to grow in frequency until the point where it is equal to ω_n. However it is surprising that the observed oscillation frequency outgrows the loop natural frequency. This is shown graphically in figure 6.13. In a truly second order system this phenomenon would not be observed. The key to the explanation of this effect lies in the root locus plots of Figures 6.6– 7. The higher values of propagation delay indicate the presence of a real root whose magnitude is comparible with the real parts of the conjugate roots. Under these conditions the second order description of the loop becomes invalid. That is, the description of the loop natural frequency must be revised. Therefore there is no reason to assume that the oscillation frequency must be restricted to less than what was previously known as ω_n. The reduction of the gain restores the loop to a stable position where the original definitions may be applied.

6.3.1 The OPLL in the Presence of Noise.

The present section describes the addition, to the simulated OPLL, of the noise sources that will be present under normal operating conditions. The noise is represented by a file of randomly generated numbers with a Gaussian distribution. This noise file is added to the phase error signal to emulate the effect of a naturally ocurring random noise voltage. In order that the laser lineshpe may be approximated, a similar Gaussian file is integrated to produce the 1/f type distribution.

FIGURE 6.12: Natural Frequency 67 MRads/s: Delay 3.6 ns.

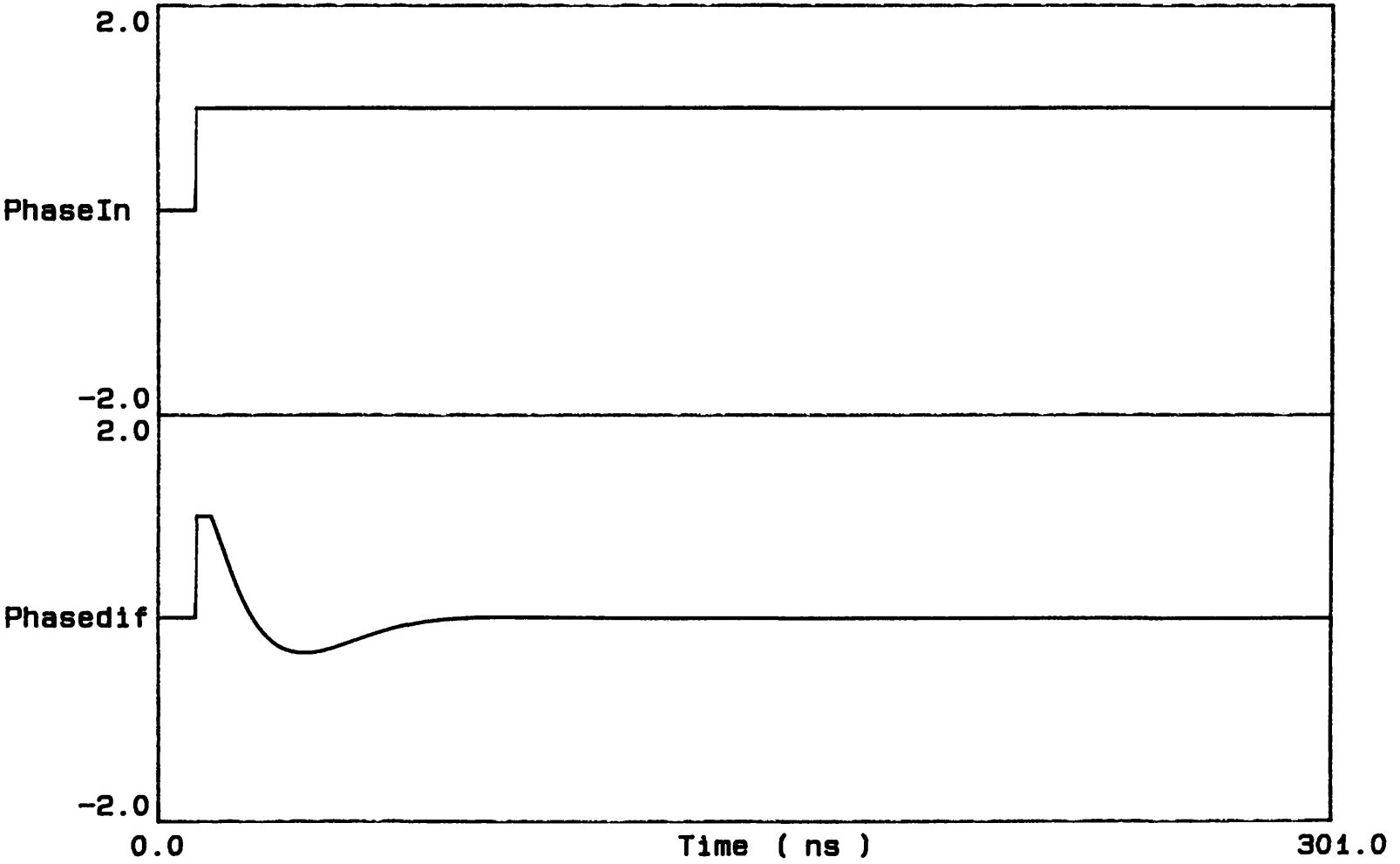

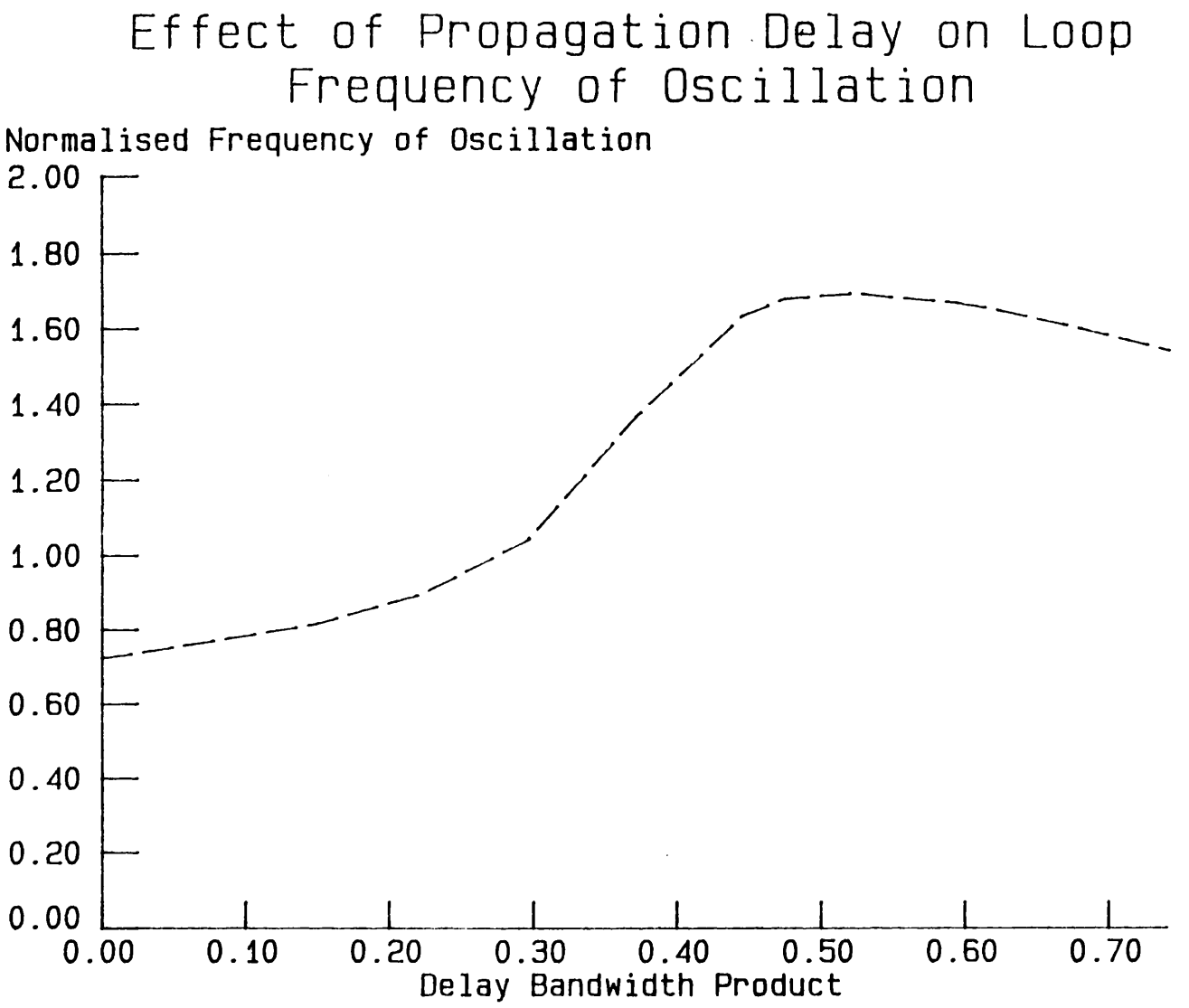
Effect of Propagation Delay on Loop Frequency of Oscillation
Normalised Frequency of Oscillation
2.00
1.80
1.60
1.40
1.20
1.00
0.80
0.60
0.40
0.20
0.00
0.00
0.10
0.20
0.30
0.40
0.50
0.60
0.70
Delay Bandwidth Product

Figure 6.13

The transfer of the noise representation from the frequency domain to the time domain is more difficult to simulate than any other aspect of the PLL. The laser phase noise has a 1/f type distribution. When modelling a distribution of this nature in the time domain it becomes obvious that a discontinuity exists in the dc condition. Low frequency components cannot therfore be accurately modelled because their weighting tends to infinity. The contributions must therefore be limited in magnitude to prevent aliasing problems occurring. A similar problem exists for the simple Gaussian noise representation. The shot noise component has an infinite noise bandwidth. While this is a convenient representation in the frequency domain, in the time domain a finite sample time will limit the accuracy of the simulation without a considerable amount of thought being given to windowing of the noise contributions. It is not the aim of this section to provide an exact model of the loop noise response. The main aim is to investigate whether or not the main source of synchronisation error arises due to the influence of the noise or whether it is due to the inherent instability of the loop itself. This performance penalty will exist even in low levels of noise and can be corroborated with only an approximate modelling of the noise contribution.

For the purposes of the simulation the maximum loop frequency was set at 14.8 Mrads/sec. A sample period of 0.1 ns was chosen. Under these conditions the loop was never observed to experience any effects of instability due to the integration routine. The noise bandwidth was set at $1/2T_S$, where T_S is the sample time. This corresponded to a noise bandwidth of approximately 300 times the loop natural frequency (in the worst situation).

The Gaussian random number files to be used as the noise inputs were designed to have an RMS value of unity. The were then scaled during the execution of the simulation to provide an RMS noise power of

$$P_{RMS} = eRP_{LO}B_{noise} \quad W. \qquad (6.5)$$

In this instance it is obvious that the higher frequency components of the noise input are likely to be influenced by the effects of aliasing and therefore the noise contribution will be limited in its accuracy. In order that no further errors were introduced by the noise simulation, the Gaussian representation was checked to verify its power spectral density over that range of frequencies of interset. This was carried out on the main-frame computer using Spectral Analysis routines written by Dr. D. Halliday for point process analysis. Figure 6.14 shows the graphical representation of the analysis which indicates that the noise files are indeed flat in their spectral distribution. A Spectral Analysis of the Phase Noise input is also given, in Figure 6.15, indicating the expected weighting to the lower frequency components.

The influence of the time delay on the noise response is demonstrated in the following figures (Figure 6.16 to Figure 6.18). Figure 6.16 shows the expected form of the phase error signal under the conditions of ω_n = 14.8 Mrads/sec and τ_d = 0.0. The phase error variance for this arrangement, predicted by the analysis in the frequency domain [4], is 0.03 rads^2.

Figure 6.16 shows clearly the way in which the noise contributions influence the loop response and that the low frequency off-set, introduced by the laser phase noise, is tracked out. The calculated phase variance for this simulation is 0.026 rads ^{2}. This is of the correct magnitude but is approximately 13% lower than the value which was predicted by the frequency domain analysis. It is considered that the limited accuracy of the modelling of the noise contributions are responsible for this inaccuracy. However since it is not the aim of the present investigation to obtain a rigourously accurate simultaion of the effects of the noise input, but instead to demonstrate how the changes in the loop parametres will affect the loop dynamic response, the accuracy of this limited model was assumed to be sufficient for these needs.

The simulation displayed in Figure 6.17 shows the effect of increasing the propagation delay to 40 ns. The expected increase in the phase error variance is observed as the loop experiences

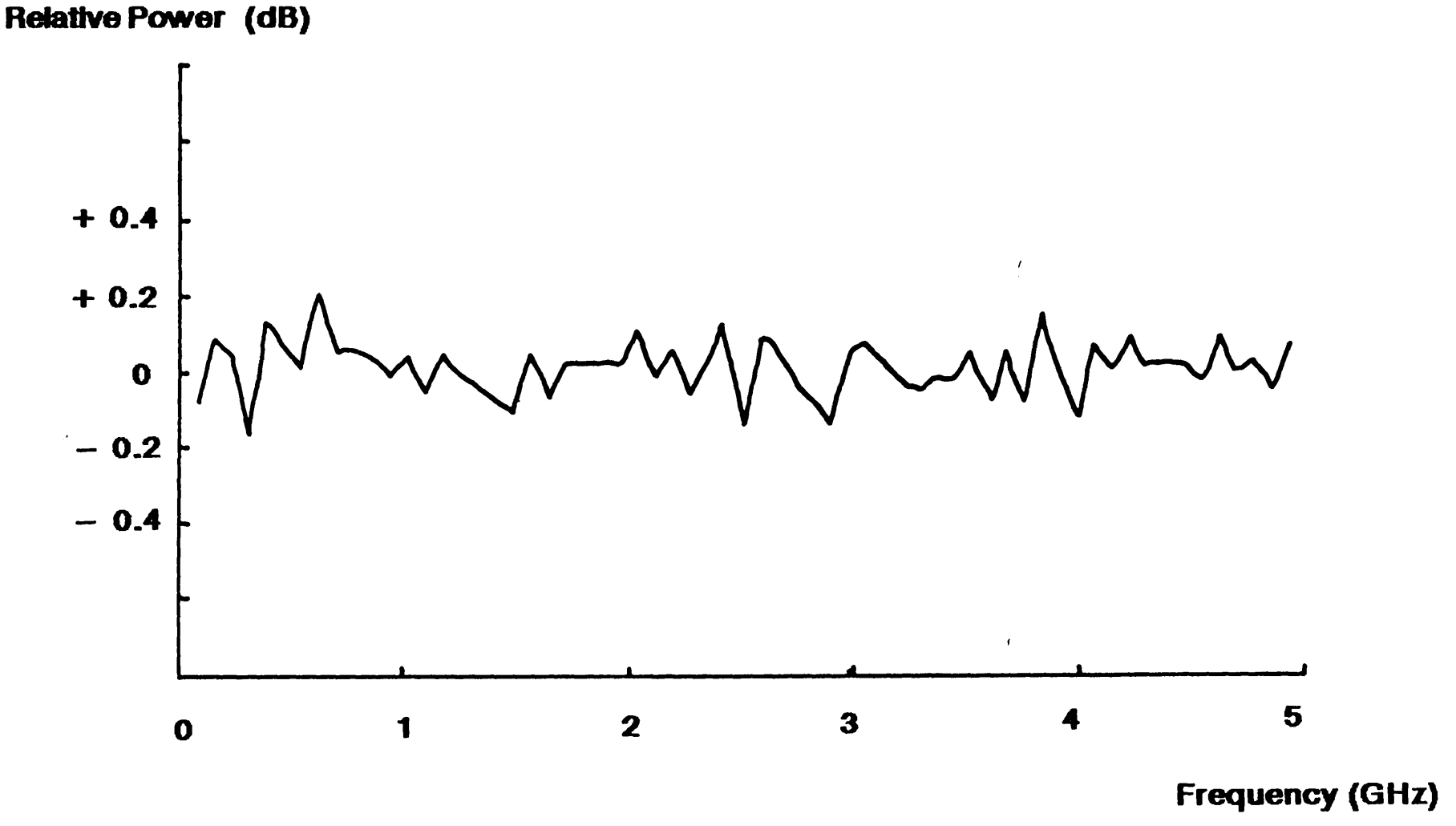

Figure 6.14 Power Spectral Density of Simulated White Noise.

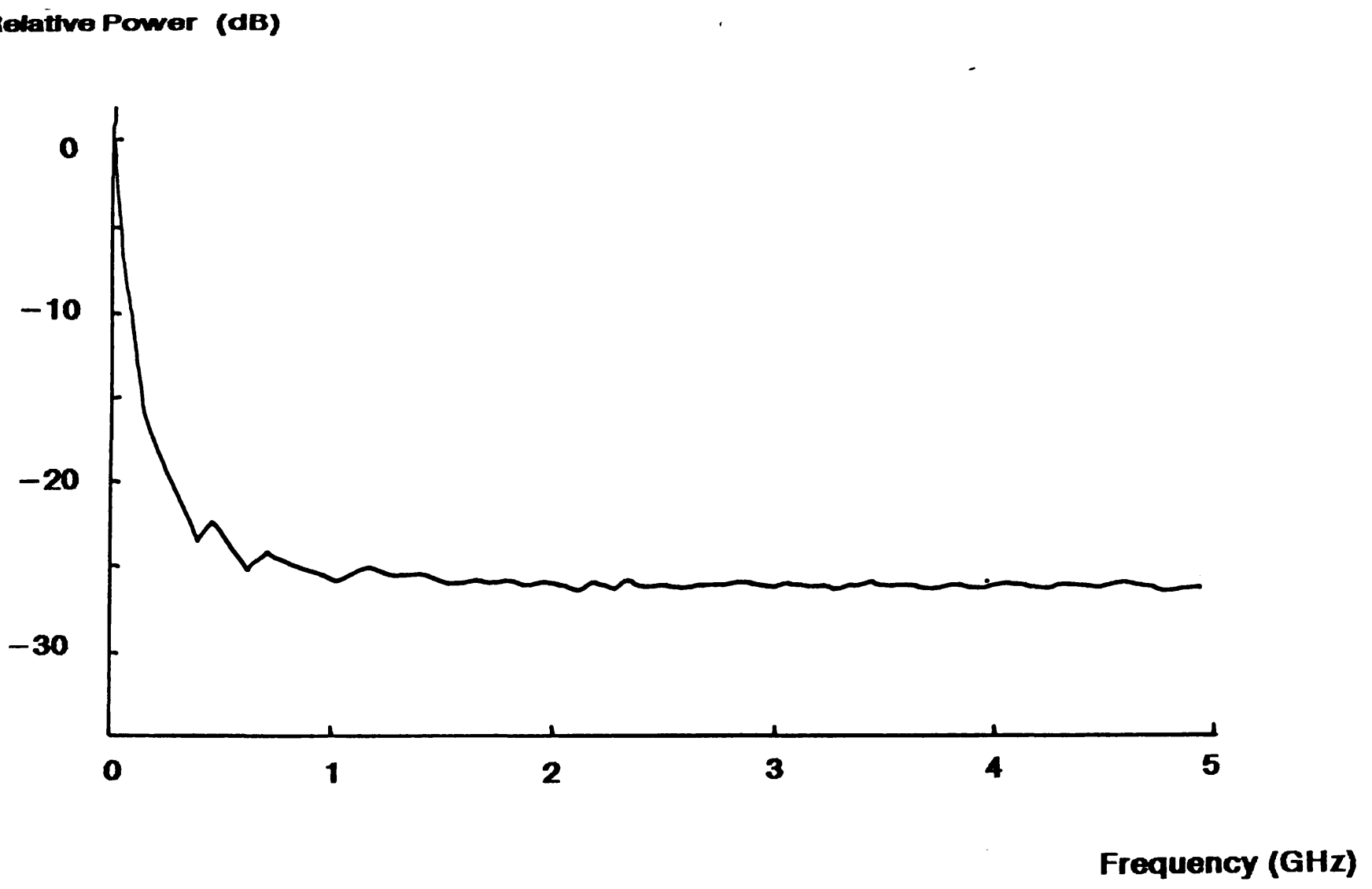

Figure 6.15: Power Spectral Density of Simulated Phase Noise.

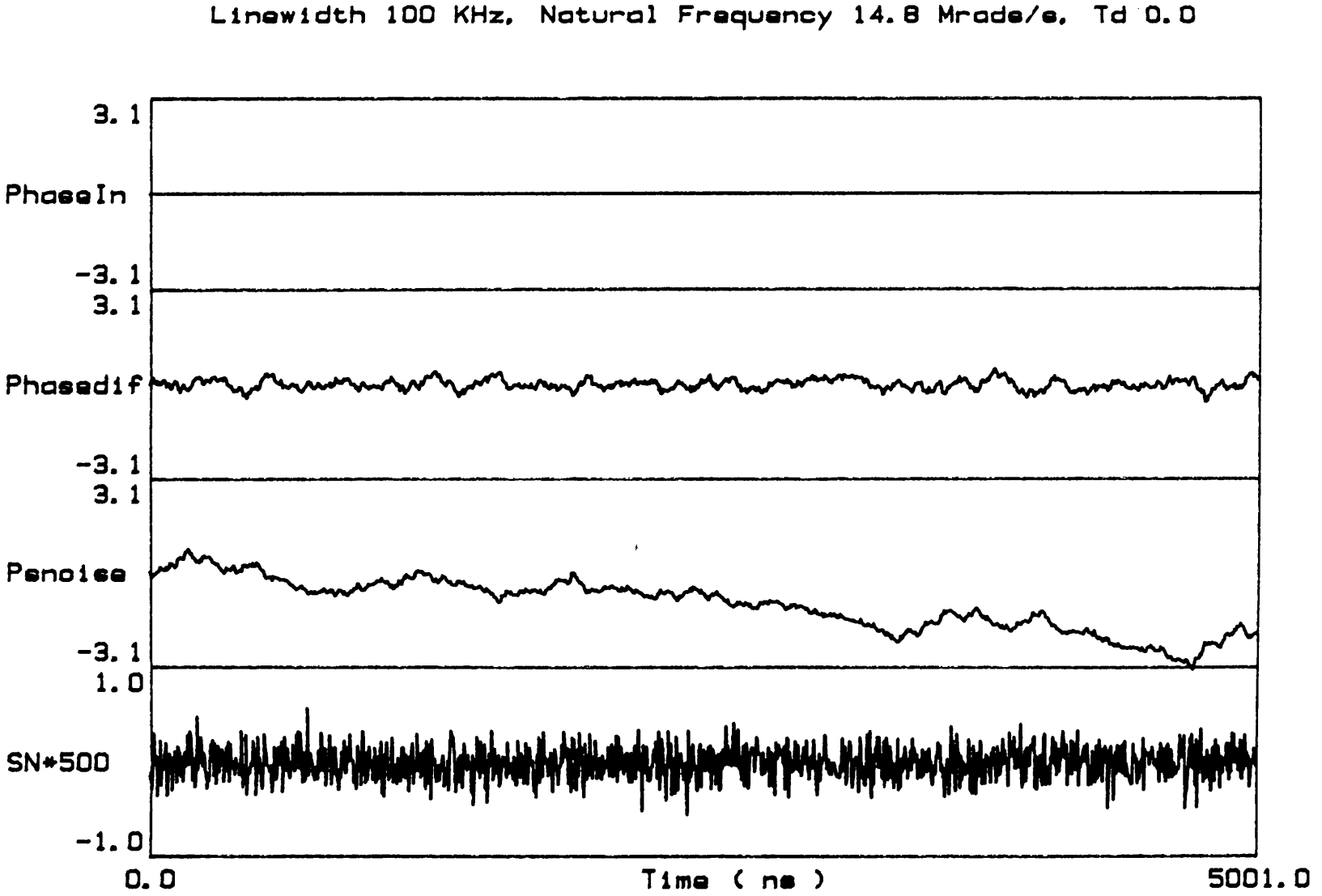
Linewidth 100 KHz, Natural Frequency 14.8 Mrade/s, Td 0.0
3.1
PhaseIn
-3.1
3.1
Phasedif
-3.1
3.1
Pnoise
-3.1
1.0
SN*500
-1.0
0.0
Time (ns)
5001.0

Figure 6.16

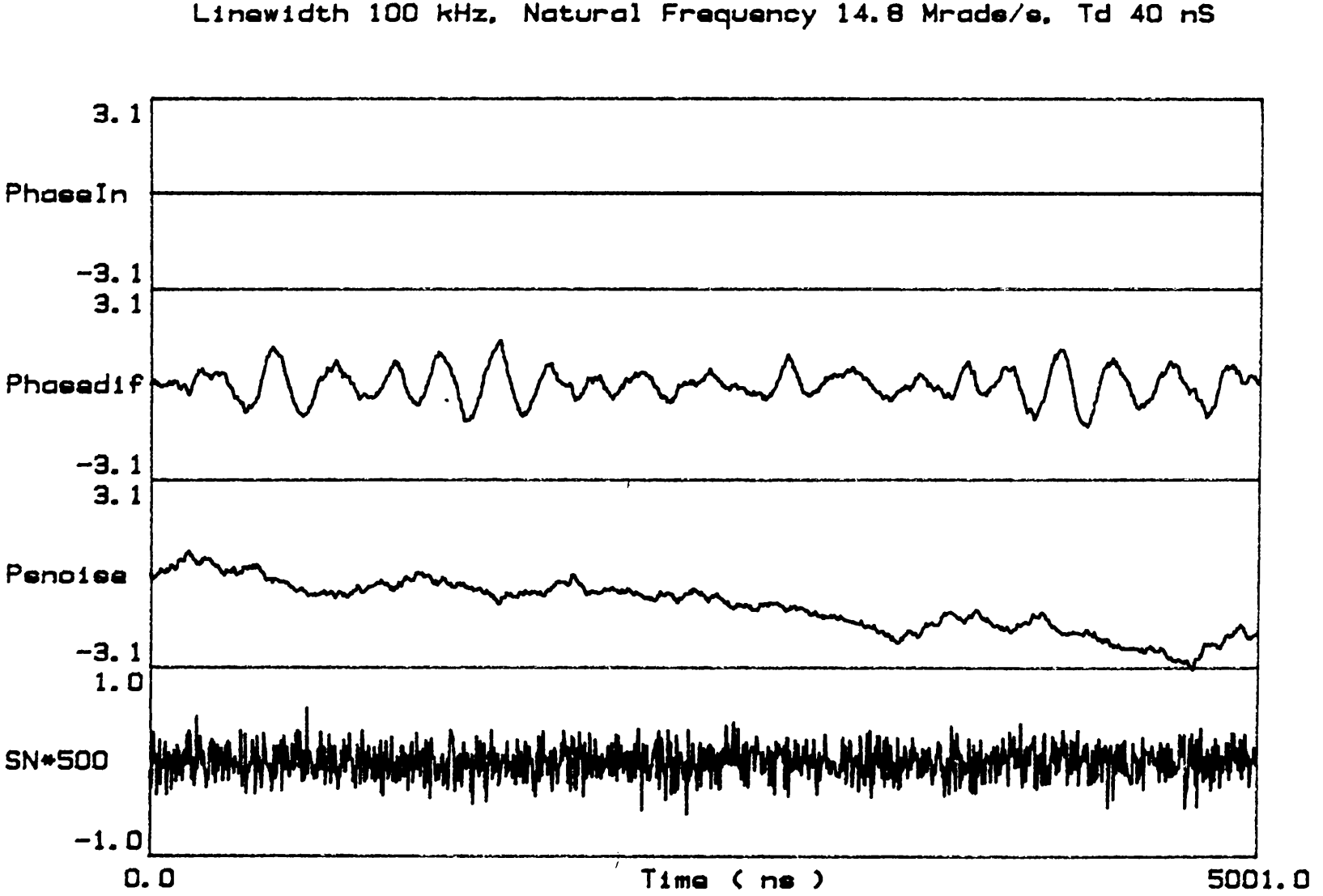
Linewidth 100 kHz, Natural Frequency 14.8 Mrade/s, Td 40 nS
3.1
PhaseIn
-3.1
3.1
Phasedif
-3.1
3.1
Penoise
-3.1
1.0
SN*500
-1.0
0.0
Time (ns)
5001.0

Figure 6.17

underdampded oscillations when it is disturbed, by the noise, from its equilibrium condition. The simulation returns a value for the phase variance value of 0.253 rads ^{2}. Reducing the loop natural frequency to that value predicted as optimum for the given delay (ω_n = 67 Mrads/sec) has the effect shown in Figure 6.18. The loop is seen to exhibit a more stable reponse and a corresponding reduction in the phase variance observed (in this instance to 0.058) which differs from the expected value [4] of 0.07 rads^2 by approximately 17%.

The simulation has demonstrated the effect of the loop propagation delay on the phase error variance. Increases in the phase variance were observed as the delay increased. While the modelling of the noise contributions is only approximate, sufficient accuracy can be assumed to allow a clearer physical understanding of the loop behaviour to be developed. The relative magnitudes of the noise components can be estimated and the assumption that the loop performance, when the delay is significant, is degraded by the reduction in phase margin was confirmed. Reduction in the loop natural frequency in order that the transient response of the loop is restored produces the condition of optimum phase tracking.

The simple analysis of the dynamic response of the OPLL discussed here will be tested against the experimental findings of another investigator in the following section. This comparison will show that there is good agreement between the simulated dynamic behaviour of the OPLL and the dynamic behaviour observed under experiment.

6.4 Experimental Phase Error Investigation.

In the work presented in this thesis so far, a theoretical description of the behaviour of an OPLL has been presented. A further analysis of the loop transient response and the effect of time delay on this response has been carried out in the present chapter with the use of a root locus construction and a digital simulation of the OPLL. It would be useful to test the validity of both of these investigations against an experimental appraisal of the OPLL. Unfortunately insufficient experimental data is available for a thorough

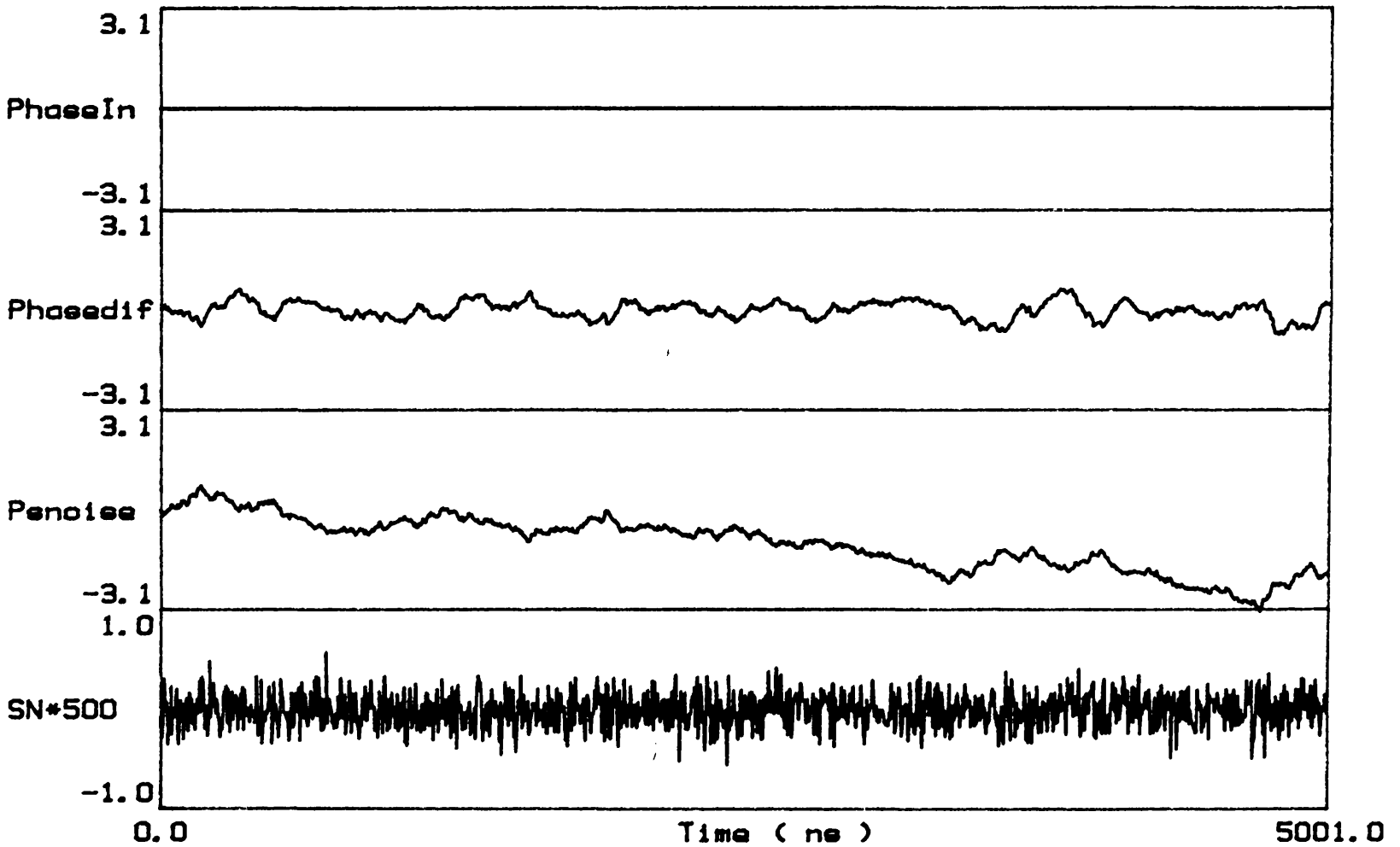
Linewdith 100 KHz, Natural Frequency 6.7 Mrade/s, Td 40 nS
3.1
PhaseIn
-3.1
3.1
Phasedif
-3.1
3.1
Penoise
-3.1
1.0
SN*500
-1.0
0.0
Time (ns)
5001.0

Figure 6.18

comparison, between experiment and analysis, of the effect of propagation delay and/or the filtering effects of the receiver amplifier on the phase error variance to be made. However, in a previous examination of the OPLL, carried out by R.C.Steele [4], sufficient experimental data on the loop transient behaviour was collected to allow an examination of the validity of the modelling of the loop dynamic response to be made. The present section of work will document this examination.

In order that a suitable comparison between the experimental investigation and the theoretical study can be carried out, the variables in the loop construction, the beat linewidth of the sources, the propagation delay and the loop natural frequency must first of all be estimated .

The OPLL constructed by Steele made use of two semiconductor laser diodes in coupled cavity configurations. The expected beat linewidth from two such diodes can range in width from 300kHz to around 10 MHz (depending on the diode and the alignment and the level of feedback [5-8]). Low frequency jitter can result in a much wider spectrum, in the order of tens of MHz being observed on a spectrum analyser trace. Figure 6.19 shows such a trace of the beat note obtained with the two diodes used by Steele in his experiment. The measured 3dB power point of this spectrum indicates that the diodes had linewidths approaching 5-10 MHz. Since no temperature control was used in the experiment, this measurement of the beat spectrum linewidth is likely to be high, however the order of magnitude of the laser beat linewidth would be such that a high loop bandwidth (tens of MHz) would have been required to achieve lock.

The propagation delay in the loop constructed by Steele was estimated, from a description given in reference 4, to be between 6 and 10 ns. For the purpose of this analysis a compromise value of 8 ns will be assumed.

Figure 6.20 shows the reduced beat linewidth of the lasers when the phase-locked condition was achieved. The loop bandwidth can be estimated from the 3 dB point in this figure as being less than 10

10 dB/div

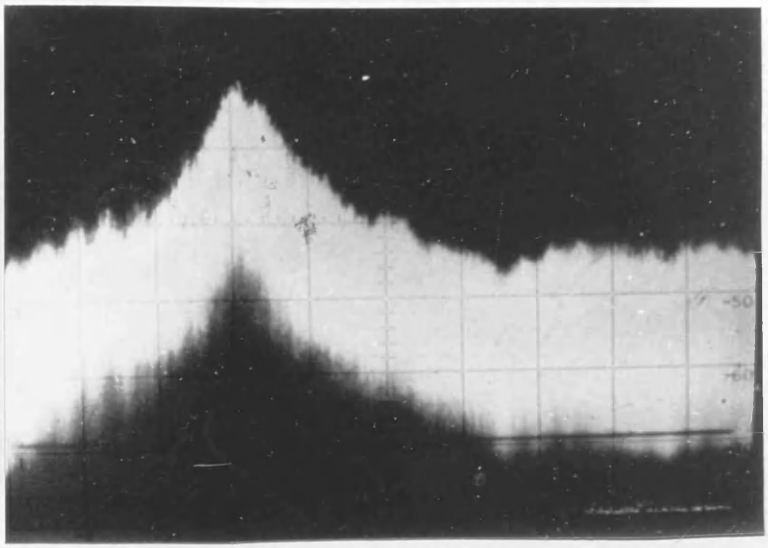

Free Running Laser Beats.
Linewidth < 100 MHz.

10 dB/div

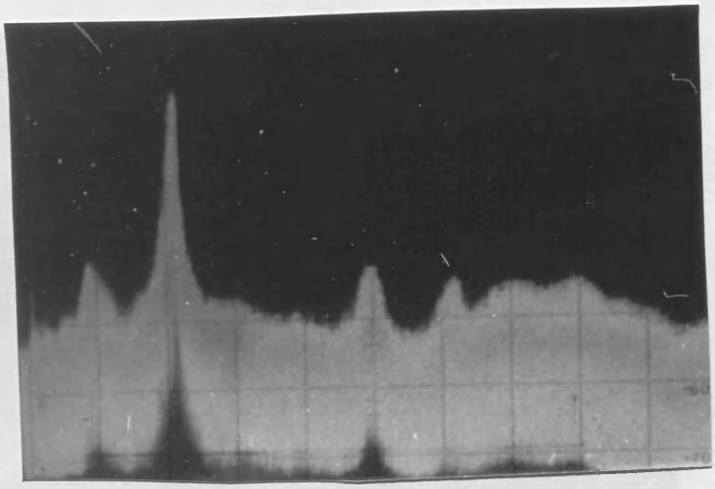

0 – 1250 MHz

Coupled Cavity Laser Beats.
Linewidth < 10 MHz.

Figure 6.19

Heterodyne Beat Spectrum of Laser Diodes [5].

10 dB/div

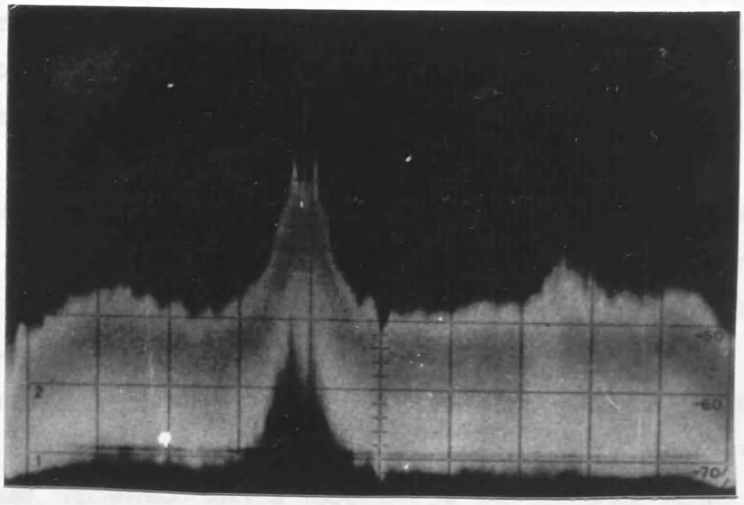

0 – 1250 MHz

10 dB/div

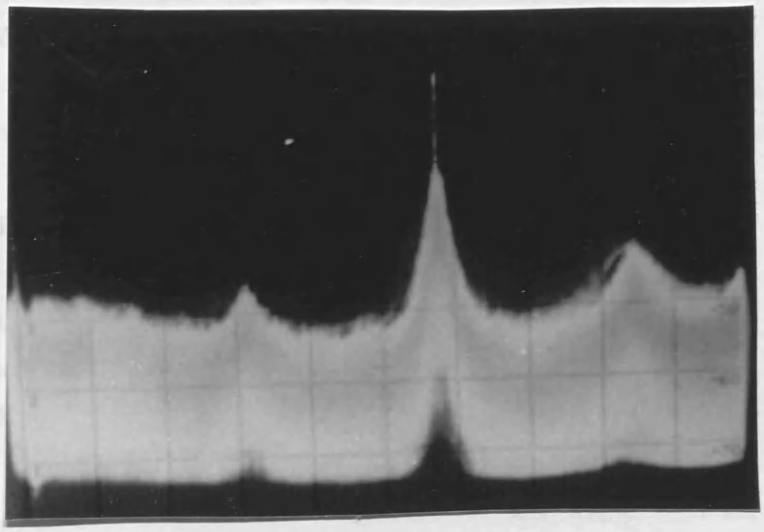

0 – 1250 MHz.

Figure 6.20

Laser Beat Spectrum When Phase Locked [5].

MHz. Figure 6.21, shows the signal fed to the local oscillator laser under the locked condition. From examination of this figure the loop bandwidth can be estimated to be around 5−6 MHz.

These estimates of loop delay and loop bandwidth (or natural frequency) yield an approximate value for the delay−bandwidth product of 0.25. Delay−bandwidth figures of this magnitude, while being well within the requirements for absolute stability, are known to cause a performance degradation [5]. The simulation and root locus analysis has shown that significant damped oscillation in the loop phase response, consistent with a reduction in the damping factor to around 0.5, would be observed under these conditions. The following section investigates this phenomenum.

While the loop was in the locked condition the response to a step input in phase was investigated by Steele. Figure 6.22 shows the arrangement used in this experiment. It is important the the mechanism whereby the phase step was achieved is given careful consideration. The failure of this apparatus to produce a leading edge in the phase shift which was sufficiently fast to be approximated as an instantaneous step change, within the timescale of the loop response, is significant in aiding the understanding of the measurements made.

The phase step input was introduced with the use of a bulk modulator and the associated drive circuitry, shown also in Figure 6.22. To achieve a $\pi/2$ step in phase the modulator required that the modulator be driven with a step input of approximately 300 V. Fast switching of voltages levels of this magnitude is not easily achieved and as a consequence of this, the phase step had a rise time of approximately 0.1 μs. This makes the correlation of the theory with the experiment slightly more involved. The phase step, with a rise time of this magnitude, presents itself to the OPLL as a finite phase ramp (the OPLL natural frequency being comparible with the rate of change of the input).

Figure 6.23 displays an experimental measurement of the loop response to this input. The oscillation frequency, with a period of approximately 6MHz is clearly visible. The corresponding simulated

10 dB/div

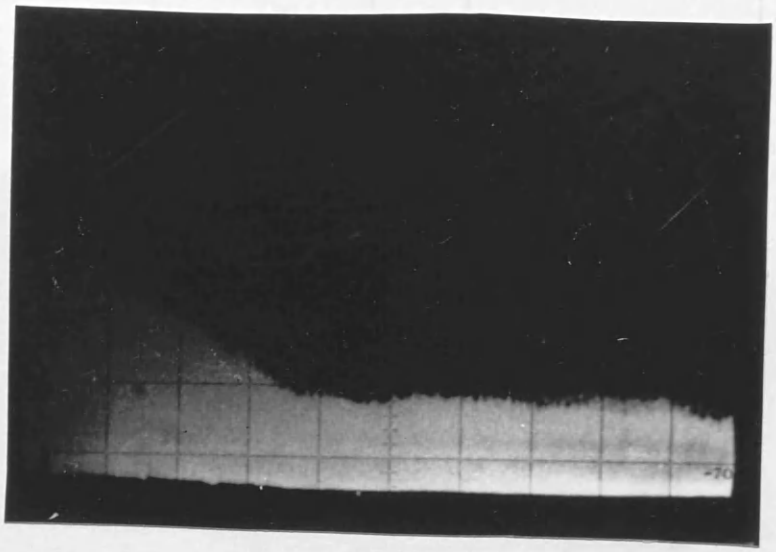

0 – 100 MHz

Figure 6.21

Frequency Spectrum of Error Signal Fed Back to Laser when Lasers are Phase – Locked [5]. Loop Bandwidth estimated 5 – 6 MHz.

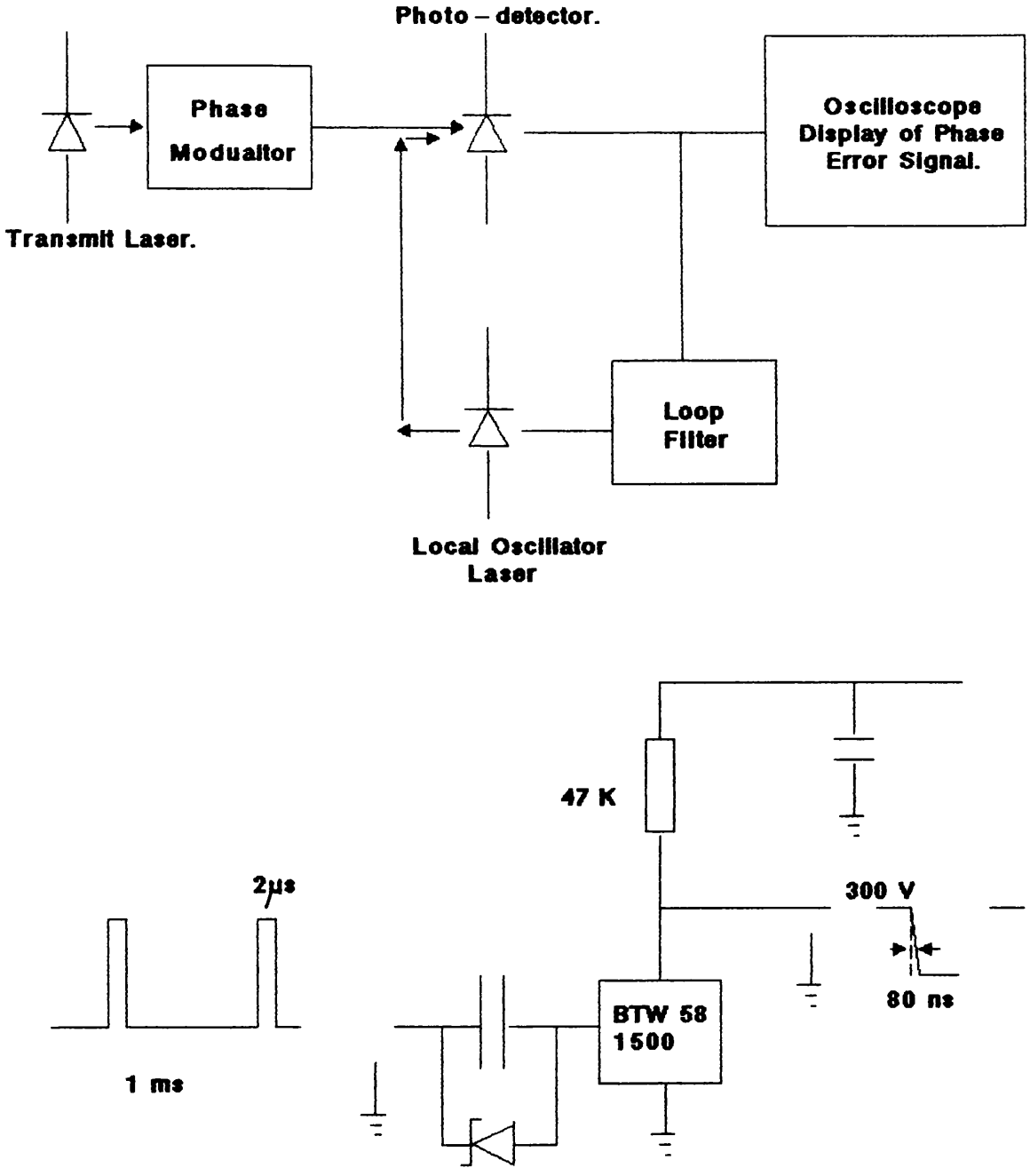

Figure 6.22

Phase Error Step Response Measurement and Phase Step Generation Ciruitry

Amplitude
Arbitrary Units

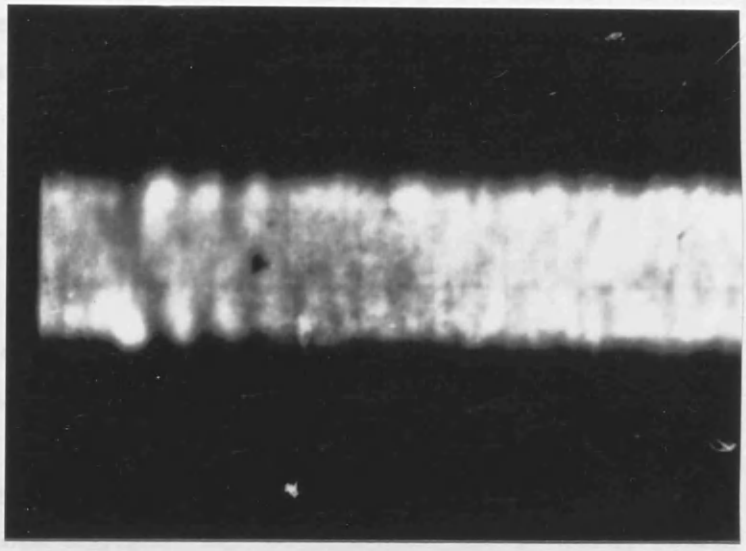

0.2 microsecond/div

Figure 6.23

**Phase Error Response to Step Input.
Evidence of Under – damped Oscillation Present.**

output is displayed in Figure 6.24. The simulation parameters for this simulation were

$$\omega_n = 6 \text{ MHz},$$
$$f_C = 1/\tau_C = 100 \text{ MHz},$$
$$\tau_D = 8 \text{ ns}.$$

The oscillation in the phase error signal (as displayed in Figure 6.23) is attributed, by Steele, to the non–linear variation of the FM response of the local oscillator laser. This is predicted to introduce a reduction in the system phase margin. To compensate for this response, a network (with a frequency response equivalent to that shown in figure 6.25) was inserted immediately before the local oscillator. The insertion of this network was effective in restoring the loop transient response to that shown in Figure 6.26: near critical damping.

While the insertion of the network was successful in achieving the desired effect, elimination of the oscillations in the phase error signal, it is the authors own opinion that the design considerations were incorrect. The oscillation of the phase error in the OPLL can be directly attributed to the phase shift arising from the propagation delay and the front end amplifier cut off frequency. The correcting action, while provided by the compensation network, was not achieved by linearising the diode FM response. It is known (see Chapter 3) that the laser diode exhibits a nonlinear FM characteristic. A shift in phase can also be observed at modulation frequencies corresponding to the cross over point between the thermal modulation effect and the carrier concentration effect. However in the above experiment, the phase lead introduced by the correcting filter affects frequency components which are greater than the loop bandwidth and therefore would not produce the effect observed. The reduction in the loop damping factor in this experiment can be attributed to the fact that the passband gain was reduced by 10 dB. A reduction of the loop natural frequency by a factor of $\sqrt{10}$ to 1.8MHz would therefore be observed. The corresponding delay–bandwidth product was therefore reduced and the damping factor restored to its original value.

FIGURE 6.24: Natural Frequency 6 MHz: Delay 8 ns.

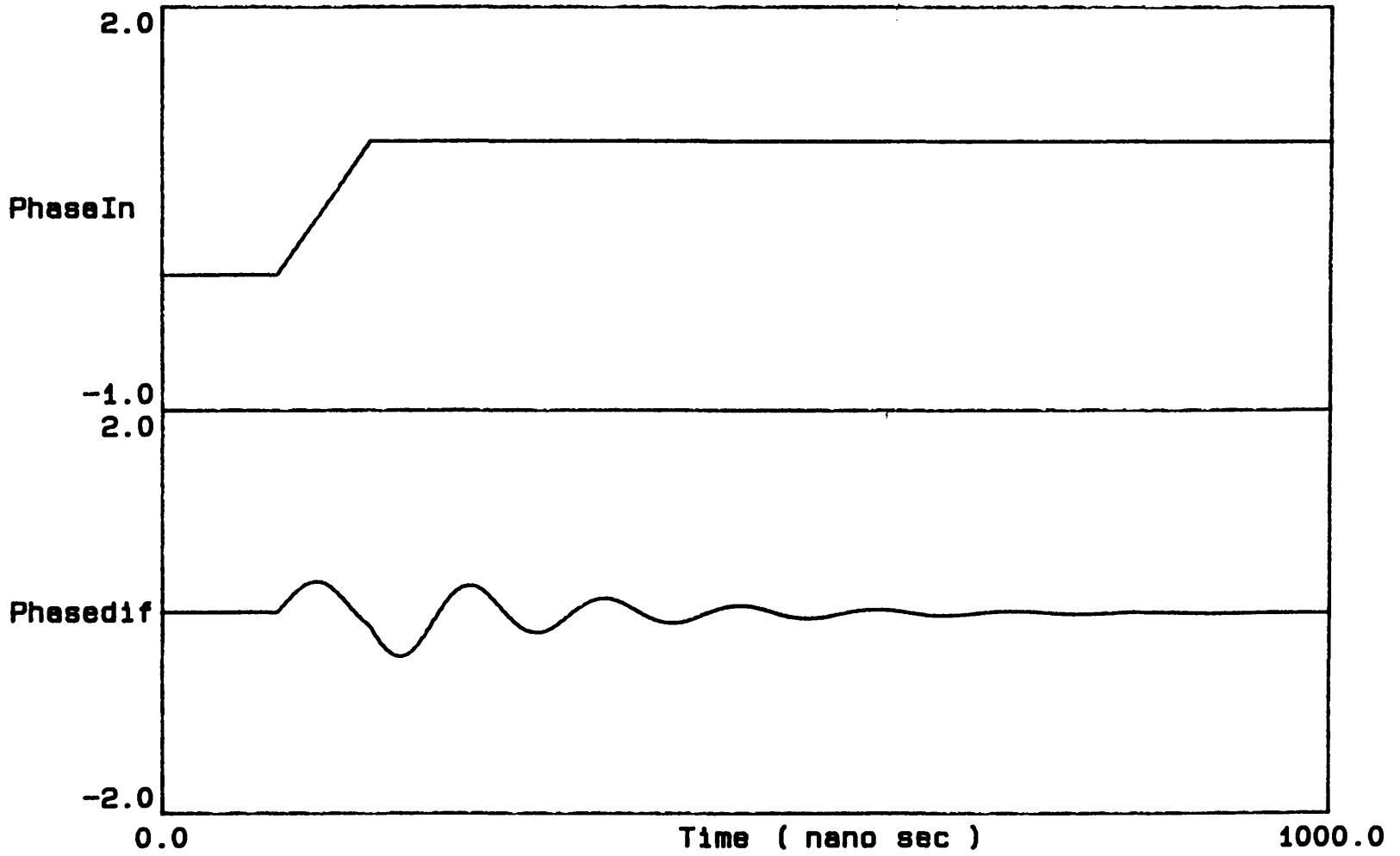

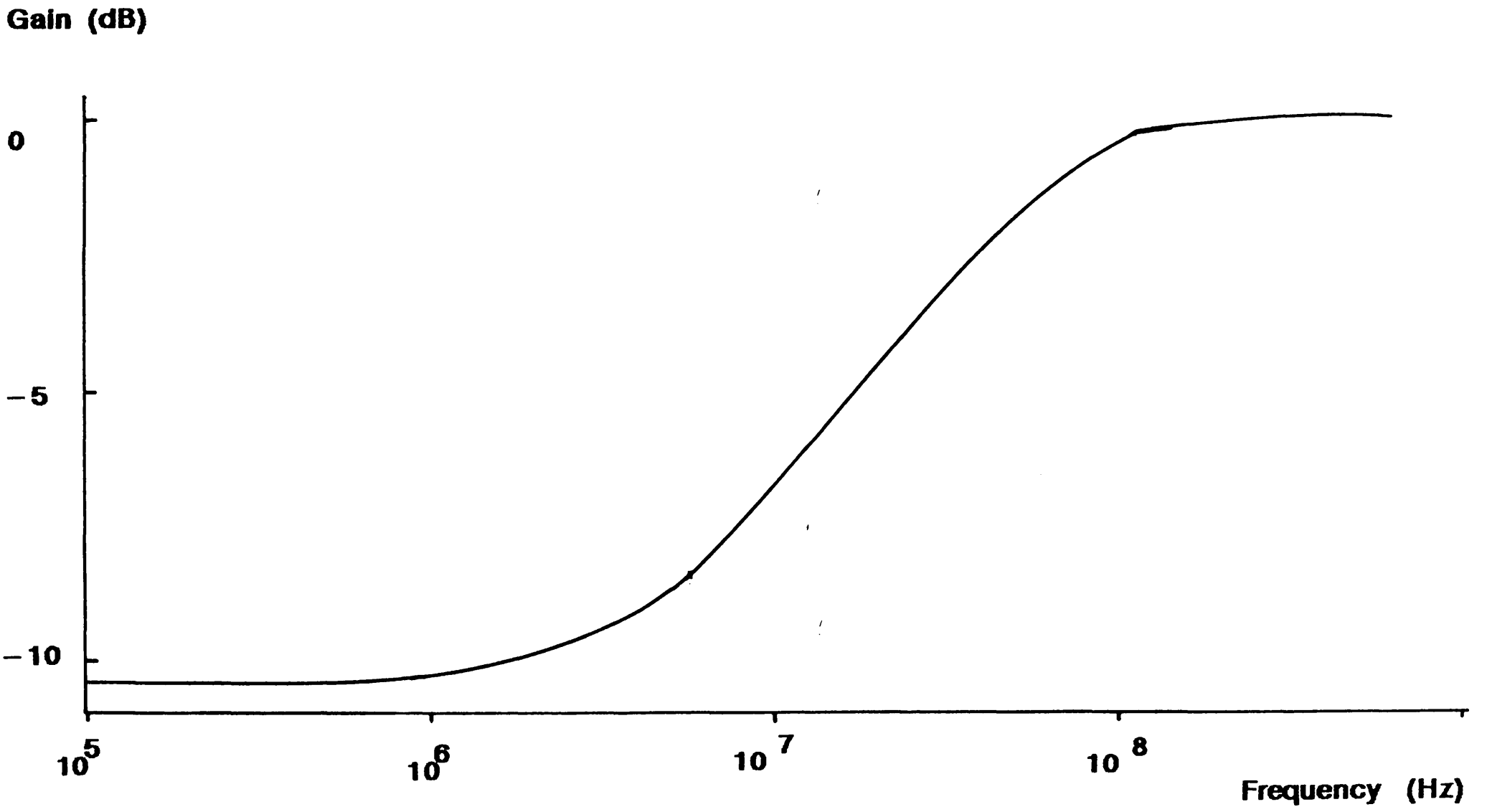

Figure 6.25: Frequency Response of Phase Compensation Network.

Amplitude
Arbitrary Units

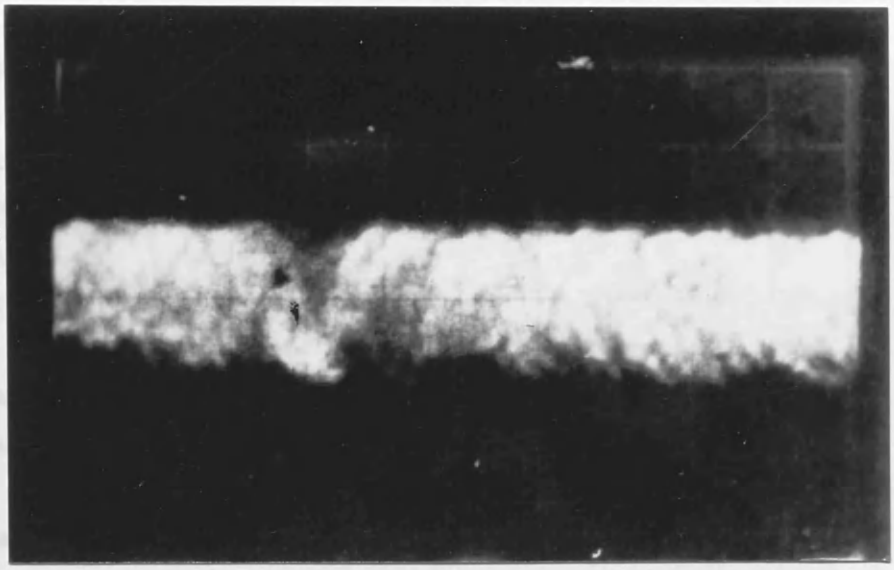

0.1 Microsecond/div

Figure 6.26

Phase Error Response to Step Input. Compenstaion Network has Restored Near Critical Damped Condition.

To test this hypotheis the loop natural frequency was reduced in the simulation. The corresponding step (or phase ramp) response is shown in Figure 6.27. This response is in good agreement with the measurement made by Steele. Agreement between the theory and the experiment has therefore been achieved except for one point. Examination of Figure 6.26 reveals that the apparent frequency of oscillation remains to be around 6 MHz. The explanation for this corruption lies in the failure of the experiment to realise a perfect phase step input.

The ramp accelaration is comparible with the loop natural frequency. The phase error therefore shows a delay followed by an attempt to track out the phase ramp. The result is that the phase ramp error signal appears rounded, and hence similar to an oscillation: confusion between the two is easily made. What appears to be an oscillation of a frequency of 6 MHz is in fact a ramp error of 10 MHz followed by an almost critically damped loop recovery response of a much lower frequency. The simulation of the effect is seen to uphold this description.

6.4.1 Conclusions.

The operation of the Optical Phase Locked Loop in the time domain has been investigated with the use of a Root Locus construction and a digital simulation. The deterioration of the phase tracking performance under the influence of propagation delay, as predicted in the analysis of Chapter 5, has been verified. The present analysis has shown that this performance degradation results from a steady movement of the OPLL, under the influence of the delay, towards a condition of instability. For delay– bandwidth products of greater than 0.32 it has also been seen that the optimum loop natural frequency is no longer a compromise between compensating for the 1/f type laser phase noise and introducing an excessive shot noise contribution, but between tracking out sufficient amounts of the laser phase noise and restricting the loop bandwidth such that the loop stability is preserved.

A departure from the second order behaviour has been observed

FIGURE 6.27: Natural Frequency 1.8 MHz: Delay 8 ns.

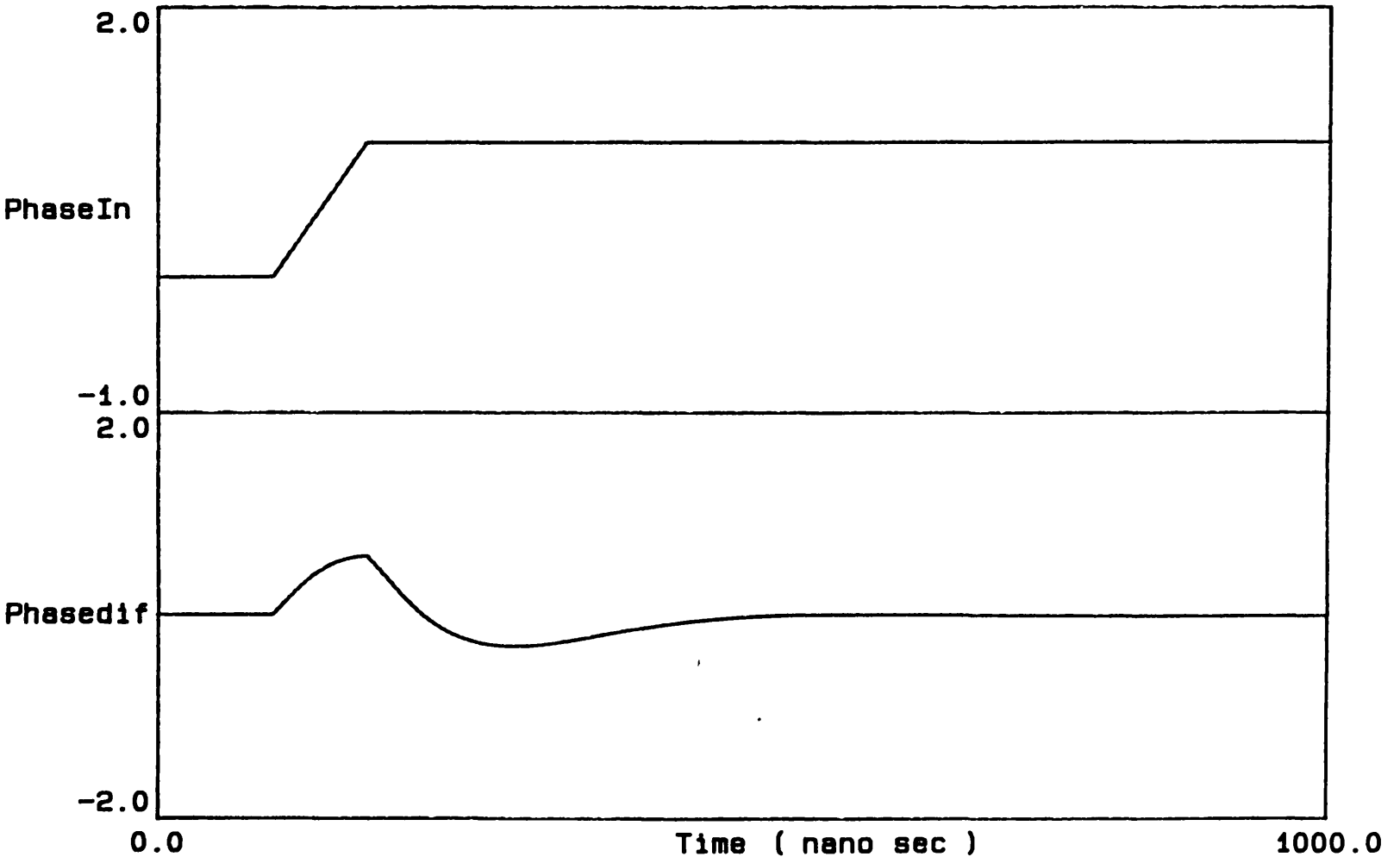

for relatively small values of delay. This suggests that loop models, common in relevant literature [9–11], are not sufficiently accurate to describe the OPLL when the loop bandwidths reach tens of Mega–Hertz. The specific instance of an OPLL with a front end amplifier bandwidth of six times the loop natural frequency was considered. Under these conditions the carrier power penalty was shown, in Chapter 5, to be 1 dB if a phase error variance of 0.03 rads^2 was to be obtained. The introduction of propagation delay into this loop was found to increase the probability of instability, as was expected, however the associated oscillations in the loop error signal were found to exceed the natural frequency of the OPLL. This is directly attributable to the fact that the second order description of the OPLL is inadequate in conditions where the propagation delay is significant. Compensation for the effect of the delay, with a reduction in the loop natural frequency, was however found to sufficient to allow the second order approximations to be used.

The reduction of the loop damping factor predicted by the root locus examination and by the simulation has been examined against experimental data collected by a previous worker [5]. While the simulation was limited in its accuracy, in that approximate values of the loop parametres were used in the model, a reasonable correlation between the experimental findings and the model of the OPLL were obtained. The simulation showed that the loop would undergo a series of damped oscillations when perturbed from the equilibrium state by a phase step input. This was confirmed in the experiment. It was also predicted that the reduction of the loop bandwidth by a factor of $\sqrt{10}$ would restore the loop respose to having a single damped overshoot and this was found to be in good agreement with the experimental findings of reference 5.

The OPLL has therefore been analysed in both the frequency domain and the time domain. The analysis in the frequency domain has been found to be beneficial in that the noise contributions can be conveniently modelled in terms of their power spectral densities. Thus an accurate measure of the loop performance under the effects of these noise contributions can be gained. In conjunction with this analysis the simulation of the OPLL in the time domain has been

shown to add support to the findings of the frequency domain analysis while providing a more convenient interpretation of the effect that system perturbations have on the overall loop performance. The conclusion that can be drawn from both analysis is that the descriptions of the OPLL commonly found in the open literature [9–11] are not of sufficient accuracy to describe the loop behaviour when then beat linewidth of the sources used exceeds 1 MHz. The analysis provided here has therefore a significant place in the design of OPLLs with free running laser diode sources.

APPENDIX 6.1 : OPLL SIMULATION ALGORITHM.

```
47: {MAIN PHASE LOCKED LOOP SIMULATION ALGORITHM}
48: Procedure Model;
49: Var
50:  II:Integer;
51: Begin
52:   If (Time=0.0) Then Init;                { INITIALISATION PROCEDURE CALL }
53:   If (Time)0E-9) Then PhaseIn:= stepchange
54:   Else PhaseIn:=0.0;                      { ALLOWS FOR STEP DISTURBANCE }
55:
56:   PhaseDiff:=PhaseIn-X[8];                { X8 REPRESENTS LOCAL OSCILLATOR INSTANTANEOUS PHASE}
57:   Phaseerror[count] := PhaseDiff;
58:
59:  If Tc>0.0 Then                             {**}
60:       Dx[1]:=((Kamp*Kd*PhaseDiff)-X[1])/Tc  {**}
61:       Else                                  {**}
62:          Begin                              { LOW}
63:              X[1]:=Kamp*Kd*PhaseDiff;       { PASS }
64:              Dx[1]:=0.0;                    { FILTERING OF }
65:         End;                                { PHASE ERROR}
66:              noise:= shotnoise[count]/Kd;      { + SHOTNOISE }
67:              X[2]:=Kamp*shotnoise[count];   {**}
68:              Dx[2]:=0.0;                    {**}
69:              shotout[count]:=x[2];          {**}
70:
71:   X[3] := X[1]+ X[2];
72:   X[4]:=Delay(1,X[3],Td,0.0,h);             { INCORPORATING TIME DELAY }
73:
74:   Dx[5]:=X[4]/T1;
75:   Dx[6]:=Ko*(x[5]+x[4]*T2/T1);               { LOOP FILTER}
76:
77:   Dx[7]:=Txnoise[count];                     { INTEGRATING WHITE NOISE INPUT }
78:   phasenoise[count]:=x[7];                   { TO SIMULAT LASER 1/f NOISE }
79:
80:   X[8] :=  X[6] + X[7] ;                     { TOTAL LOCAL OSCILLATOR SIGNAL }
81:
82:   For II:=1 to N Do
83:    Begin                                    { INTEGRATION OF ALL VARIABLES }
84:     Temp[II]:=h*dx[II];
85:     X[II]:=X[II]+Temp[II];
86:    End;
87:
88:   PlotVar[1]:= Phasein;                     { ASSIGN VARIABLES OF INTEREST TO }
89:   PlotVar[2]:= Phasediff;                   { SCREEN/PLOTTER DRIVERS }
90:   PlotVar[3]:= phasenoise[count];
91:   PLotVar[4]:= shotout[count]*500;
92:  End;
```

References.

1. S.A. Marshall 'Introduction to Control Theory.' Macmillan Press Ltd 1978.

2. R.C. Dorf 'Modern Control Systems.' 3rd Edition. 1980 Addison– Wesley Publishing Company Inc., Reading Massuchusettes.

3. R.J. Richards, 'An Introduction to Dynamics and Control.' Longmans, London 1979.

4. M.A.Grant, W.C. Michie, M.Fletcher 'The Performance of Optical Phase– locked Loops in the Presence of Non– negligible Loop Propagation Delay.' Journ, Lightwave Technol. vol LT– 5(4) 1987 pp592– 597.

5. R.C.Steele, 'Ph.D. Thesis.' University of Glasgow 1983.

6. T.P.Lee *et.al.* 'Characteristics of Linewidth Narrowing of a 1.5 μm DFB Laser with a short GRIN– rod External Coupled Cavity.' Elect. Lett. 21(15) 1985. pp655– 656.

7. F,Favre, D,LeGuen, J.C.Simon 'Optical Feedback Effects on Laser Diodes Oscillation Field Spectrum.' IEEE J.Quant. Electron. QE– 18(10) 1982 pp1712– 1717.

8. E,Patzak. 'Semiconductor Laser Linewidth in Optical Feedback Configurations.' IEE Electron. Lett. 1983 19(24)

9. L,G,Kazovsky 'Balanced phase– locked Loops for Optical Homodyne Receivers: Performance Analysis, design considerations and Linewidth requirements.' Journal Lightwave Technol. LT– 4(3) 1986, pp182– 195.

10. L.G.Kazovsky 'Decision– Driven Phase– Locked Loops for Optical Homodyne Recievers: Performance Analysis and Laser Linewidth Requirements.' J.Lightwave Tech. LT3(6) pp 1238– 1247 1985.

11. T.G Hodgkinson 'Costas Loops Analysis for Optical Recievers'

Elect. Lett. vol. 22(7) 1986. pp394–396.

12. T.G.Hodgkinson 'Phase–Locked Loop Analysis for Pilot Carrier Coherent Optical Recievers' Elect. Lett. vol 21 1985 pp1202–1203.

CHAPTER 7.

Heterodyne OPLL Experiments.

7.1 Introduction.

The previous three Chapters have provided an extensive analysis the OPLL. It was shown that the loop operation is governed mainly by the loop bandwidth and that the choice of this bandwidth is a compromise between compensating for the effect of the laser phase instability and introducing an excessive amount of shot noise into the system. Additional system imperfections, such as the phase shift in the feedback signals (resulting from a signal propagation delay and/or from the filtering effect of the front–end amplifier) were introduced into the analysis. These perturbations were seen to have a further degrading effect on the phase tracking: moving the loop closer towards instability. In Chapter 6 the analysis of the transient response of the OPLL was compared with the experimental findings of a previous worker [1] and good agreement between this analysis and the experimental data collected was found. The aim of this present Chapter is the construction of an OPLL in order that a fuller experimental evaluation of the theoretical findings can be carried out. Prior to making any attempt to phase–lock two sources, it is necessary first of all to find two sources which are sufficiently well matched in wavelength that a beat note between the two may be detected electrically. The following section documents the experimental program undertaken to achieve this goal.

7.2 Detection of a Heterodyne Beat Spectrum Between Independent Semiconductor Lasers.

Any two semiconductor laser diodes, matched in wavelength such that tuning ranges overlap, can in principle be tuned in frequency to sufficiently close proximity to allow an electrical beat note to be detected. This is the aim of this present section of work. The experimental arrangement used to achieve this goal is presented in schematic form in Figure 7.1.

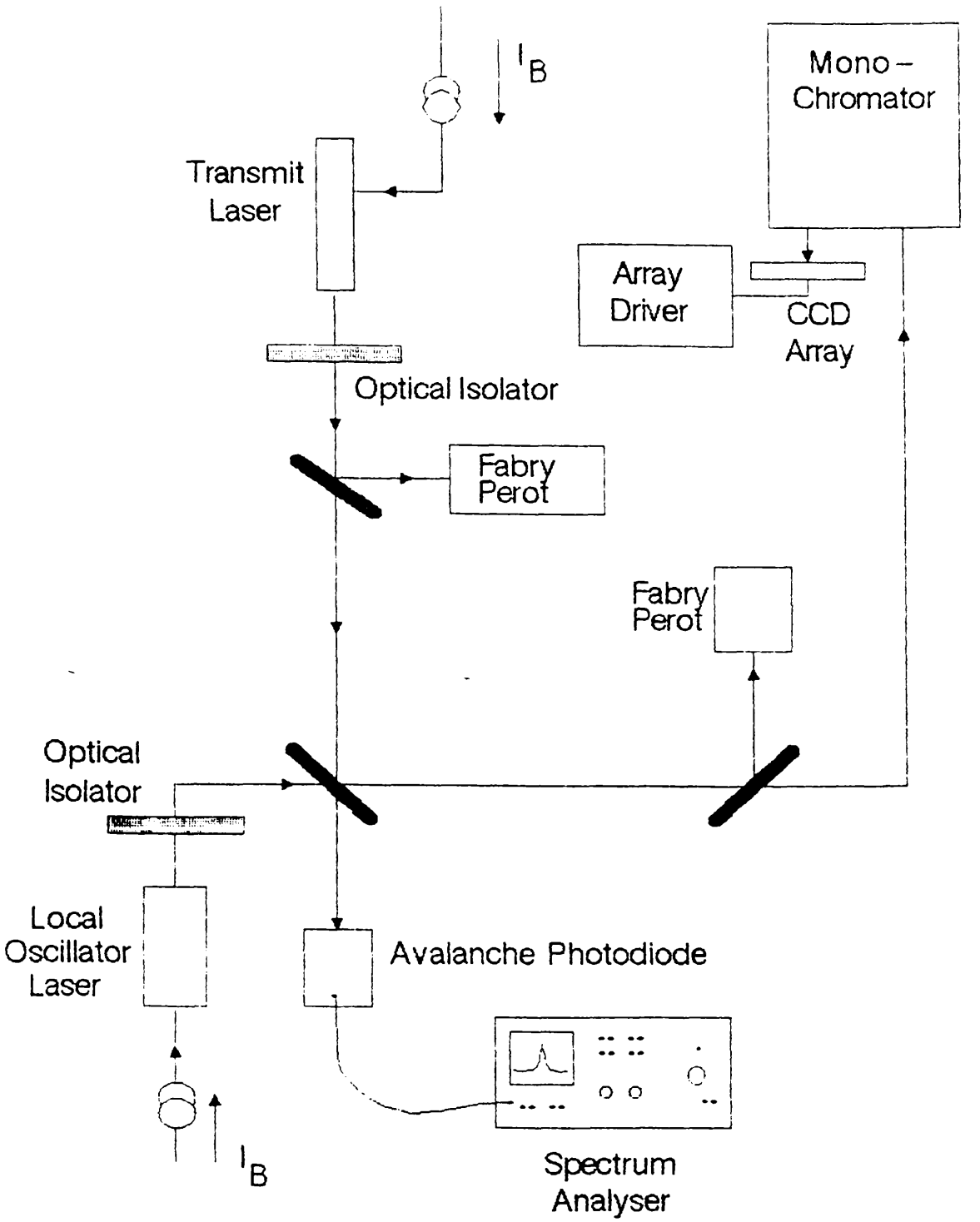

Figure 7.1 Experimental Arrengement for Obtaining Beat Spectra.

The emission from both diodes was collimated and the beams combined on a 50/50 beam–splitter/combiner. The reflected portion of the beams was then focussed onto a reverse–biased BPW 128 avalanche photo–diode in order that the electrical beat note could be displayed on a Spectrum Analyser. The throughput beams from the beam–splitter were coupled into a monochromator and detected on a charge–coupled array (as described in Chapter 3) to enable a measurement of the individual wavelengths to be made. A knowledge of the relative separation in frequency of the two sources was required in order that they could be tuned towards each other. The resoulution of the monochromator measurement was approximately 0.1 nanometers (43 GHz at 820 nm) and the bandwidth of the APD was approximately 2.5 GHz. Therefore, there existed a 40 GHz range in which it was not possible to monitor the tuning of the individual diode wavelengths. However, this was not found to cause any significant impediment to the execution of the experiment. A portion of both beams was coupled into a scanning Fabry–Perot Interferometer in order that the power and frequency stability of the diodes could be monitored at all times.

All lasers used in this experiment were matched to within 0.3 nanometers. This is well within the specified diode tuning range (nominally 5 nanometers to 10 nanometers [2]) and therfore it was expected that a beat note could be obtained, between any two of these sources, without the need for excessive temperature or current differentials. In practice this was not found to be true.

The current–wavelength measurements, of which Figure 7.2 provides a typical example, demonstrate that the tuning ranges of these diodes are non–linear: the characteristic is broken up by discontinuous jumps in the operating frequency (see Chapter 3 for fuller details). Tuning curves of this nature present considerable problems when it is attempted to tune two independent sources to the same frequency. The discrete jumps (mode hops) are unpredicatable and may occur in such a way that the laser frequencies never exactly coincide. A similar non–linear relation between the operating wavelength and the operating temperature was found to exist. More specifically, it was observed that the current–wavelength tuning

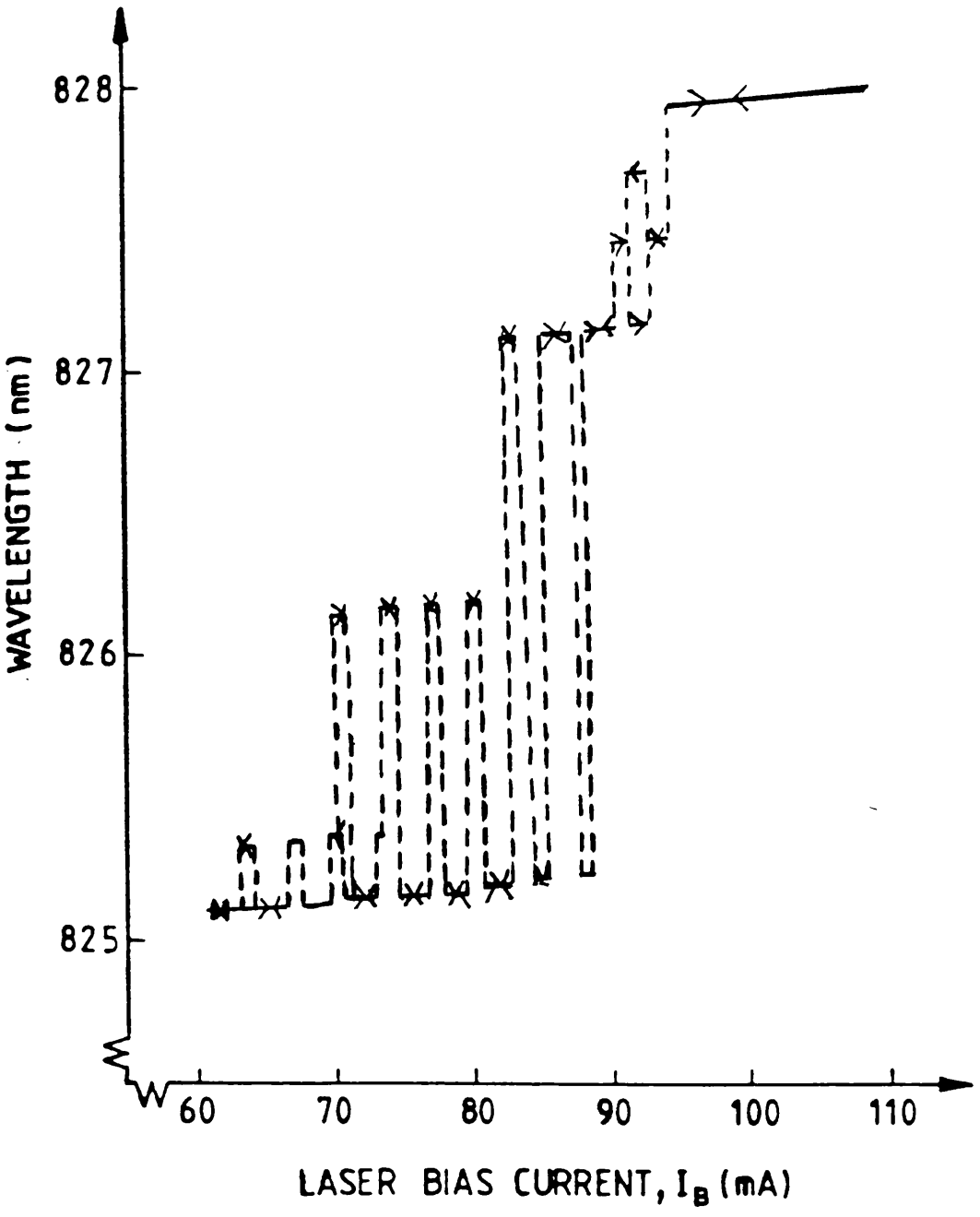

Figure 7.2

Wavelength versus Injection Current Characteristics for HLP 1400 no. 5E3070 Operating Temperature = 290.8 K.

characteristics could not be translated in wavelength (to centre around a new operating point) by causing a change in the operating temperature. Thus it was not possible to make effective use of the operating temperature of the laser diode to fine tune the wavelength of two diodes whose characteristics differed by a small amount. Small changes in temperature (of less than a degree) could completely alter the form of the tuning curves.

Discrete hops in the wavelength tuning characteristics of the laser diode are not an unusual phenomenon and have been reported by other workers [1,3]. However, in the absence of external optical feedback, these 'mode hops' should occur in one direction and should be consistant with changes in the injection current. The frequency of lasing is determined by the position of the Fabry–Perot cavity modes relative to the peak in the gain profile [4,5]. As the laser injection current is tuned, the carrier concentration (and hence refractive index of the active region) changes and the diodes wavelength tunes correspondingly. The change in carrier concentration is also reflected in a change in position of the gain profile. If the gain profile is shifted (in wavelength) by a sufficient amount that a new Fabry–Perot mode is closer to the peak, then this mode will compete with the exisiting mode and will eventually become the dominant mode. At this point the laser will undergo a mode–hop. It is possible for the wavelength jump, during a mode hop, to be greater than the separation frequency of one or more Fabry–Perot mode spacings however, these jumps should always occur in integral multiples of the cavity mode spacing and the shift in wavelength should always be consistant with the direction of current tuning. Figure 7.2 shows that in the present experiment these characteristics are not displayed. The laser frequency can be seen to jump in steps which do not always correspond to an integral number of cavity modes (0.3 nanometres) and furthermore, the direction in which the jumps occur is not always consistant with the direction of current tuning. These factors indicate that the behaviour of the laser has been influenced by external reflections.

The influence of optical feedback on the laser emission spectrum and centre frequency is well known [6,7,8]. Therefore, in order that the

laser diodes behaviour was not complicated by unwanted reflections from the optical alignment apparatus, attempts were made at all times to ensure that the probability of unwanted reflections reaching the laser were minimised. An optical isolator, consisting of the series combination of a polarising filter, aligned coincident with the state of polarisation of the laser light, and a $\lambda/4$ plate rotated at 45 degrees to the polarisation axis, was kept in position immediately following the collimating lens at all times during experiments. This provided approximately 14 dB of isolation. Isolation of this amount is insufficient to protect the laser from the effect of feedback [16] therefore a slight misalignment was introduced to the beam guiding optics in order to reduce the possibility of stray refelctions returning to the diode. No evidence of influence from back scatter from the alignment apparatus was observed on the scanning fabry perot monitor of the laser beams however, Figure 7.2 shows that the laser behaviour has clearly been influenced by optical feedback. It was deduced therefore, that the most likely cause of these reflections was the collimating lens. The wavelength current tuning characteristics, shown in Figure 7.2, are those of an early laser mount which made use of a GRIN lens to collimate the laser emission. This particular lens construction is difficult to antireflection coat because of the refractive index variation across the lens profile. Thus it is probable that this lack of efficient antireflection coating, coupled with the fact that the focal length of the lens was sub–millimetre, would result in a significant amount of optical feedback being directed into the diode from this lens. Later diode mounting arrangements made use of a Newport Corporation FLA–40 lens which had a longer focal length (4.5 mm) and was antireflection coated. Use of this lens eliminated the substructure in the laser tuning characteristics.

7.3 Beat Spectra Lineshape.

After a considerable amount of experimental time, beat spectra were obtained between almost all of the diode pairs. However, the stability and repeatability of these beats was found to be variable. Certain diode pairs required significant temperature differences (5 to 10 degrees) between in order to extract a beat note: the beat spectra

thus obtained were generally found to be unstable. Diodes which were sufficiently well matched to allow a beat note to be obtained with little difference in the operating conditions were found to produce beat spectra which were more stable (lasting several hours) and repeatable. It was concluded from this observation that the temperature control of the diode arrangement was inadequate. Figure 7.3 exhibits a sample photograph of a 'stable' beat spectrum, obtained between modules 5E3072 and 5E3060. The estimated linewidth of the beat is approximately 100 MHz.

The magnitude of linewidth of the beat spectrum shown in the above measurement is in excess of what was expected from the experimental results of Chapter 3, where the free running linewidths were measured to range between 5 and 15 MHz. Furthermore, it is evident that the beat spectrum is not Lorentzian. These observations add support to the conclusion that the temperature control of the laser mount was inadequate. Low frequency jitter of the laser beat spectrum, results in beat spectrum being detected at a number of positions during the Spectrum analyser scan. Thus an apparently wide, and non Lorentzian shaped, spectrum is observed. Thermal instability has been reported as being responsibe for causing a departure from the Lorentzian lineshape in self–heterodyne linewidth measurements [9]. In an experiment where two independent sources are heterodyned the effect is magnified.

With the use of the diode pair 5E3072 and 5E3060, beat spectra were obtained on a daily basis. However, spectra were never found to exhibit a narrower linewidth than the one displayed in Figure 7.3. The ambient temperature, and background noise, within the laboratory were found to exert a considerable influence over the stability of the beat:the laboratory floor could be felt to vibrate with pedestrian traffic in the corridor and this was found to upset the beat spectrum stability. Beat notes were found to be more stable at night, when the movements within the Rankine building were less obtrusive. It was expected that, with the obvious lack of stability of the laser beat, phase–locking experiments would be unlikely to be sucessful. Steps were therefore taken to improve the lase mount design and improve the temperature stability and accoustic isolation. It was expected

Reference Level

Marker Freq.

Horiz. Scale MHz/div

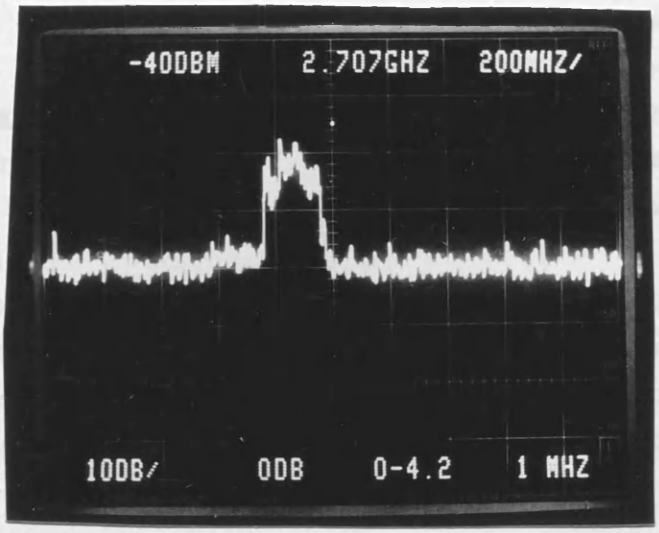

Vertical Scale dB / Div

Input Attenuation.

Freq. Span GHz

Resoultion Bandwidth

Figure 7.3

Free Running Laser Diode Beat Spectrum
Linewidth Approximately 100 MHz.

however that this would take several weeks to accomplish and therefore attempts to phase lock two diodes were continued, despite magnitude of the instabilites present in the experiment.

7.4 Experimental Attempts at Phase Locking.

The theoretical discussion given in Chapters 4 and 5 indicated that the requirements on a communications system were sufficiently strict (assuming a BER of 10^{-9} to be a reasonable performance stipulation) to exclude the possibile use of an OPLL, employing unmodified present day semiconductor lasers, as a feasable receiver component. A typical beat linewidth of 15 MHz would require a loop bandwidth of 160 MHz and would permit a maximum allowable loop propagation delay of 0.12 ns. Design criterea such as these would be too strict to be implemented without recourse to large scale integration techniques. However, if the system requirements are relaxed to 'having a reasonable probability of obtaining lock' then the engineering restrictions become less severe and it should be possible to phase–lock two diodes in a laboratory environment. This was the aim of the present section of work. In order to assess, first of all, the feasability of such an experiment an estimate of the necessary loop parametres was made.

The optimum beat linewdidth which could be expected from two free running HLP 1400 diodes lies between 10 MHz and 30 MHz (according to the individual linewidth measurements made in Chapter 3) if the effect of low frequency jitter is minimised. Phase–locking of sources with such linewidths is possible however careful account must be made of the propagation delay [10]. The expected propagation delay in a laboratory experiment was assessed as follows.

The length of the laser mount was approxmately 15 cm, including the refecting mirror positioning stage for linenarrowing. Taking into account the optical isolator, the aligning mirrors and the combining beam splitter, the expected optical path length from the laser to the detector was estimated to be between 3 nanoseconds and 5 nanoseconds. The delay introduced from the photo–diode amplifier combination was estimated to be in the region of 2 nanoseconds to 3

nanoseconds and a further 1 to 2 nanoseconds was allowed to account for the double balanced mixer required to convert the detected beat signal down to baseband and the cabling back to the local oscillator diode. Thus the delay in the OPLL was estimated to be in the region of 6 nanoseconds and 10 nanoseconds. According to the analysis of Chapter 5, delays of this magnitude would permit loop natural frequency of approximately 70 Mrads/s to 115 Mrads/s. Under these conditions phase−locking of sources with linewidths of 10 MHz −15 MHz should be possible.

The initial requirement of the experiment was the construction of the photo−diode amplifier combination. The construction and packaging of this device was carried out in house because it was necessary to restrict the overal dimensions of the device in order that the propagation delay could be limited. The initial amplifier construction employed a hybrid UHF amplifier (OM361) and a Telefunken avalanche photo−diode (BPW 26). When irradiated with an effective wideband white noise source from an LED, this amplifer photo−diode combination was seen to provide a measured gain of approximately 20 dB from a low frequency cut off of 1 MHz to an upper limit 1150 MHz.

The combined propagation delay of the photo−diode and amplifier was estimated by injecting a sinusoidal signal at the photo diode input and measuring the delay on a Tektronix 1100 sereies oscilloscope. The delay was estimated by measuring the excess delay that the amplifier contributed when inserted in line with length of coaxial cable. The amplifier diode combination was thus measured to be 2.1 ns, to within the resolution of the experiment (0.1 ns).

The output of the amplifier was coupled into a wide band double balanced mixer (Mini−circuits ZFM−54). This allowed the IF signal to be converted to baseband by multiplication with an rf oscillator. The insertion loss of the mixer, at maximum rf drive level (+7dBm), was −7dB. A minimum rf drive level of −20 dBm was required to operate the mixer however, the insertion loss at this level of drive was approximately −50 dB. The experimental arrangement for attempting the heterodyne OPLL is given in Figure 7.4.

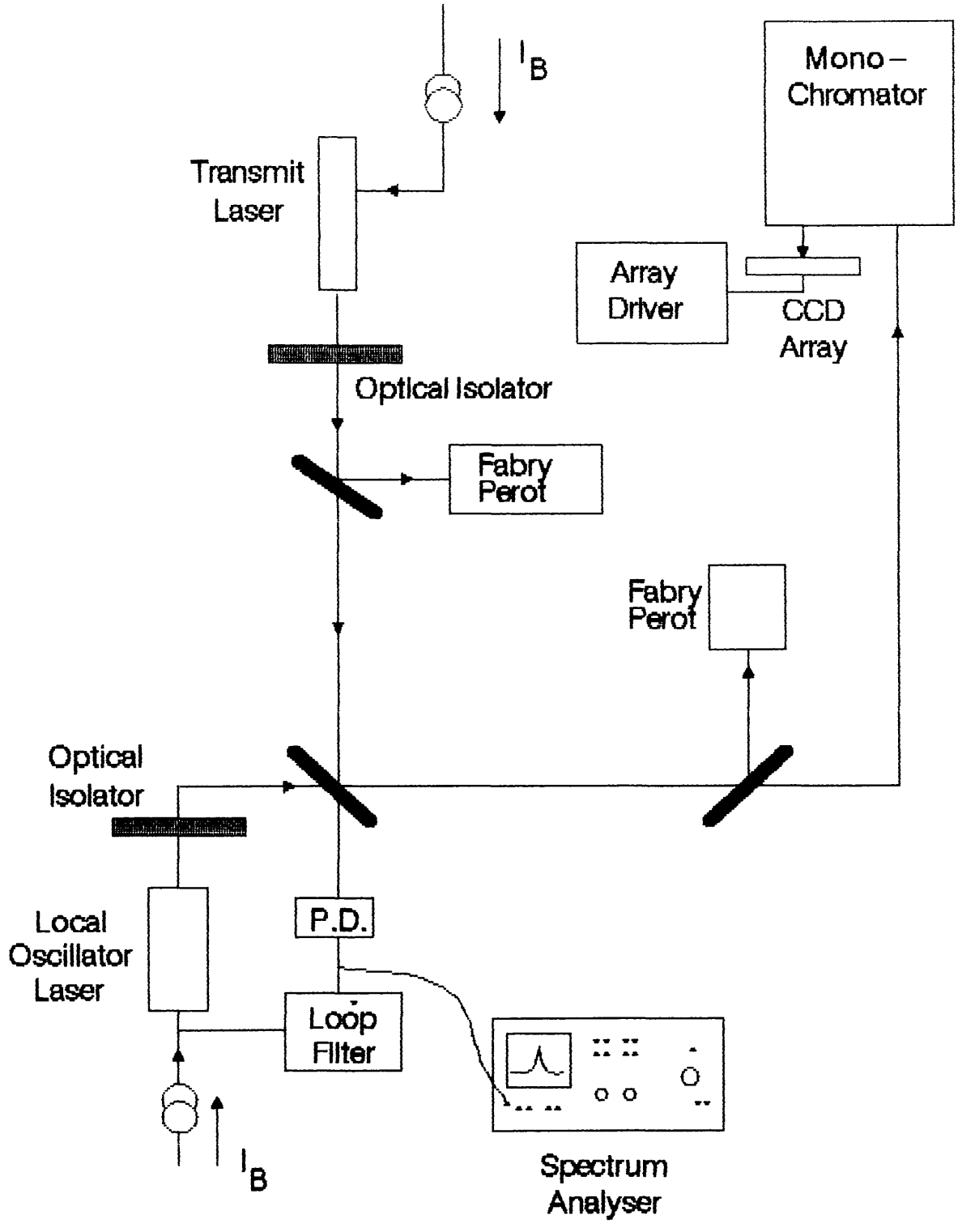

Figure 7.4 : Heterodyne OPLL Schematic.

7.4.1 Loop Filter Requirements.

Two diode modules (Module 5E3072 and 5E 3060) were used as these were found to be the most closely matched pair and, using these diodes, beat spectra could be repeatably obtained. Although the spectrum obtained displayed considerable evidence of low frequency jitter (evident in the excessive beat linewidth), an attempt to phase–lock the two diodes was considered to be a worthwhile excercise. It was felt that practical experience in attempting to phase–lock would be useful.

The loop propagation delay of between 6 nanoseconds and 10 nanoseconds limited the choice of maximum natural frequency to be between 70 Mrads/s and 115 Mrads/s [10]. The uppermost of these frequencies is optimistically high, representing the limit of stability as determined by the Nyquist criterea discussed in Chapter 5 therefore it was decided therefore to construct the loop in such a way that the natural frequency could be tuned within the region of 10 Mrads/s to 65 Mrads/s. Thus the loop filter requirements were established as follows.

The analysis of Chapter 4 showed that the loop natural frequency is determined by the closed loop gain and the choice of filter components (see Figure 4.2) as follows.

$$C = \frac{2.Resp.K_{amp}.K_o.K_m/(P_t P_{lo})}{R_1 \omega_n^2} \quad F \quad (7.1)$$

If the value of R_1 is set at 1 KΩ (an arbitrary value) then the choice of filter capacitance is set by examining the likely range of input powers for the required loop natural frequency. In the present experiment the maximum loop natural frequency was limited to 65 Mrads/s and the beat spectra powers ranged from −30dBm to −60dBm. Thus, for a local oscillator gain, K_o, of 3 GHz/mA and a mixer efficieny K_m of 50% the value of capacitance required in the loop filter ranges between 6.4 nF (at −60 dBm) and 6.4 μF (at −30) dBm. In the loop construction a value of 47 nF was used which permitted a maximum bandwidth of 32 MRads/s at −60 dBm beat

power levels. For higher beat power levels the loop natural frequency could be reduced by lowering the loop gain via the rf drive level.

The procedure of attempting to phase lock was as follows. The transmitter laser, or the local oscillator laser (or both) was tuned until a stable beat frequency was obtained. The rf oscillator (− 50 dBm power) was then tuned to this frequency and gradually incremented in amplitude until evidence of some effect upon the beat spectrum was observed. Sufficient power in the beat spectrum was always obtained for the feedback signal to have an obvious effect upon the beat spectrum, however there was not any occasion where evidence of locking was observed. At high levels of feedback power (+ 7dBm local oscillator power) the beat spectrum was observed to collapse. This was interpreted as system instability resulting from an excessive delay− bandwidth product in the loop [10]. At lower levels of power (around 0 dBm) the beat could be observed to tune away from the from rf drive frequency. The beat spectrum tuning away from the rf oscillator in this way is consistant with frequency pushing (or false lock) which arises when the phase shift round the loop is excessive for the magnitude of the loop natural frequency [11,12]. Further reduction in the rf oscillator power removed all influence on the beat spectrum. This was interpreted as being the result of a reduction in loop bandwidth to the extent that the loop capture range was smaller than the magitude of the frequency jitter, thus locking would not take place.

It was expected that the low frequency noise and the high laser linewidth would prevent a situation of solid− locking from being attained. However, it should have been possible, with the above parameters, to phase− lock temporarily. A temporary locked condition would have been observed as a momentary reduction in the beat linewidth. However this phenomenon was not observed during any of the experiments indicating the locking did not take place.

It was attempted to improve the system stability and sensitivity to temperature fluctuations by coupling the oscillation of the transmitter laser to an external cavity. Linewidth measurements (see Chapter 3) had indicated that this particular mount had a linewidth of around 700

kHz when operated in this mode. However, the mechanical sensitivity of this mount made experimentation unpractical and therefore it was decided to re-design the laser mount construction and temperature control.

7.5 OPLL with Free Running Laser Diodes: Conclusion.

The components for an OPLL were assembled and an attempt to phase-lock two free running laser diodes was made. The theoretical analysis of the previous chapters had indicated that such an OPLL, with sources of a beat linewidth of at least 10 MHz, was possible however, the chances of maintaining a solid-locking condition were not high. During attempts to lock two sources evidence of false-locking was observed as the beat frequency was tuned away from the rf oscillator frequency. False lock is normally the result of an excessive loop propagation delay for a given natural frequency [11]. The loop gain was therefore reduced in an effort to reduce the natural frequency however this resulted in all influence on the beat spectrum being lost. This was interpreted as being the result of an insufficient loop capture range for the magnitude of the frequency instabilities in the system.

The major obstacles to obtaining a locked condition were considered to be inadequate temperature control of the laser diode and also insufficient isolation from accoustic disturbance. A re-design in both the laser temperature control and accoustic isolation was therefore undertaken. The main component providing the isolation from vibration was the optical bench which was mounted on a cushion of hairlock matting and concrete slabs. It was decided that the hairlock matting arrangement should be replaced by air filled tyre inner tubes. In addition to this modification it was decided that the laser mount should be completely recontructed. A significant amount of the accoustic sensitivity of the device resulted from the mechanical instability of the lens positioning equipment (a goniometric three way positioner). It was decided that this should be replaced by a Microcontrol XYZ positioning stage. The mirror positioner was also replaced by a Physik-Instrumente PZT controlled XYZ stack in order that more accurate positioning may be obtained.

7.6 The Narrow Band OPLL.

The decision to re-design the laser mount prompted the further consideration of the external cavity diode laser in addition to the coupled cavity mounts. Excellent results in terms of wavelength tunabilty and linewidth had been achieved at 1.5 μm with these devices in other experiments [6]. Indeed an OPLL had been constructed which made use of such a device as a local oscillator and effected the tuning of the local oscillator via an intra cavity phase modulator [13].

Receipt was taken of six new diodes and three were (after verification of their current power characteristics, see Chapter 3) sent for antireflection coating. Three were sent initially so that experimental progress could continue with the remaining three diodes in the coupled cavity arrangements.

The use of diodes in an external cavity arrangement reduces the effective local oscillator gain and therefore it was necessary to compensate for this reduction by increasing the electrical gain. Construction of a new detector amplifier was therefore undertaken. This design employed three Watkins and Johnson amplifiers in cascade. A total gain of 55 dB at a bandwidth of 900 MHz was achieved. The reduction in amplifier bandwidth was not seen to be a major obstacle to obtaining a detectable beat frequency. Furthermore, the linewidths of the coupled cavity and external cavity laser diodes were one to two orders of magnitude lower than the free running lasers (see Chapter 3) and therefore the loop natural frequency could be correspondingly reduced; under these conditions the influence of the front end amplifier bandwidth and loop propagation delay should not be significant [10]. The delay through the photo-diode amplifier combination was estimated using the same technique as before to be 2.1 ns. An improvement in the board layout had allowed an increased gain to be achieved for a similar value of delay.

7.6.1 Coupled Cavity Beat Spectra.

The improvements in laser mount design were found immediately to be beneficial. Beat spectra were obtained which were significantly more stable. The new diode modules used a collimating lens specifically designed for laser diodes (Newport Corporation FLA−40). Reflections from this lens were quoted as being less than 3%. This anti−reflection coating, coupled with the fact that the lenses had a longer focal distance (4.3 mm), provided significant improvements to the ease of working with the diodes: adjustments could be made to the lens position without upsetting the modal stability of the mount. External reflectors (supplied by Comar Ltd.), flat to within $\lambda/10$ across the entire surface, with a 4% reflectivity on the mirror side and an antireflection coating on the other were positioned using piezoelectric controllers such that the reflected light was directed into the lasing medium.

The quality of the beat spectra obtained using the above arrangement is displayed in Figures 7.5 and 7.6. The estimated beat linewdiths of the two traces are 800 kHz and 250−300 kHz respectively. This indicates that individual linewidths of 125 −400 kHz were being achieved which is comparible with the individual linewidth measurements reported in Chapter 3. The width of the laser oscillation was dependent upon the critical alignment of the reflecting mirror. While an element of the low fequency jitter is still evident in these spectra, the obviously more Lorentzian lineshape was encouraging.

With beat linewidths of less than 1 MHz it should have been possible to achieve solid−locking with loop bandwidths of similar magnitude to those attempted earlier [10]. Attempts were made therefore to phase−lock the two diodes in the manner described in section 7.4. These attempts did not, however, meet with success.

The coupled cavity arrangements, although stable in their free running condition, were found to be unstable under the influence of electrical feedback. This is contrary to what was found by Steele [1]. Initially it was suspected that the instability was caused by imperfect alignment of the external reflector. However, examination of the

Reference Level

Marker Freq.

Horiz. Scale MHz/div

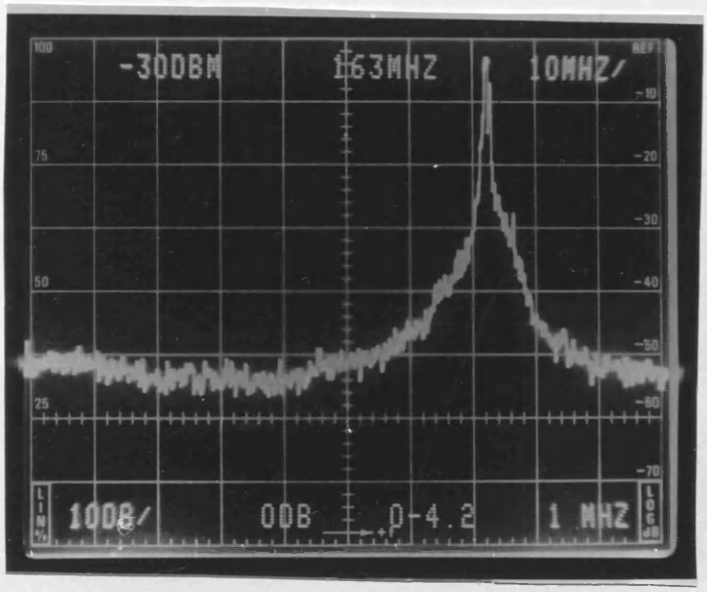

Vertical Scale dB / Div

Input Attenuation.

Freq. Span GHz

Resoultion Bandwidth

Figure 7.5

Coupled Cavity Beat Spectrum.
Individual Linewidth 400 kHz.

Reference Level

Marker Freq.

Horiz. Scale MHz/div

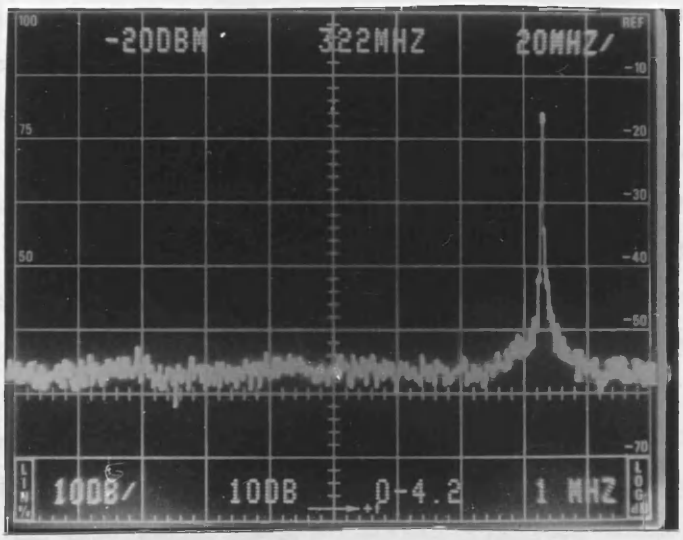

Vertical Scale dB / Div

Input Attenuation.

Freq. Span GHz

Resoultion Bandwidth

Figure 7.6

Coupled Cavity Beat Spectrum.
Individual Linewidth 100 kHz.

modal substructure revealed that additional modes, at the cavity length spacing, were reduced in power by 20 dB to 30 dB with respect to the main mode, indicating that the cavity mirror was well aligned. The explanation for the difference between the two experiments lies in the optical feedback levels.

Analysis of the coupled cavity laser diode by Goldberg *et.al.*[15] has shown that the mirror reflectivity is critical in maintaing a single mode operation (as well as having a strong influence on the laser linewidth). In order that the single mode operation, in a coupled cavity laser diode arrangement, can be gauranteed over a wide range of phase de−tuning conditions (bias−currents), Goldberg predicts that it is necessary for the effective mirror reflectivity to be less than 0.005 percent (−43 dB). For effective reflectivities of greater than 0.12 % (−30dB) single mode operation can be achieved however the stability will be dependant upon the amount of phase detuning of the optical feedback. (Similar calculations have more recently been performed by Tkach and Chraplyvy which indicate that the region of stable operation is limited to the range of feedback powers between −45dB to −55 dB). In the present experiment the mirror reflectivity was 4% and it was estimated that a substantial proportion (up to 50%) of this power could, under optimal alignment conditions, be fed back to the laser diode. Feedback of this magnitude would allow three or more modes could compete for domination and small amounts of phase detuning could easily provoke a multi−moded condition. Although the mirrors used in reference 1 were also of 4 % reflectivity, the above explanation for the laser instability is consistant with Steele's experiment when then collimating lens is taken into consideration. Experience with the GRIN lens collimator, as used in reference 1, showed that these lenses were not efficiently antireflection coated. The numerical aperture aperture of the GRIN lens was also found to be lower than that of the FLA−40 (0.2 versus 0.3). Therefore, it is likely that power was not coupled efficiently from the mirror back into the laser diode in the diode mounts used by Steele. Thus, the effective mirror reflectivity could be much reduced to a level which would allow the diodes to remain stable under a wider range of bias currents than was observed above. It would have been possible to attempt to reduce the reflectivity of the mirrors in the

above experiment, however it was decided that a better course of action would be to reduce the reflectivity of the laser facet and operate the laser in an external cavity. This arrangement had been used by other workers and had been shown to allow tuning via the injection current of up to 30% of the diode mode separation before instability was encountered[14].

On receipt of the coated diodes the shift was made to the external cavity arrangement and the remainder of the diodes sent for coating. The use of a diffraction grating to provide the feedback and influence the operating wavelength allowed these diodes to be tuned over an operating range of approximately 16 nanometres (see Chapter 3). Beat spectra obtained with these devices are shown in Figures 7.7 and 7.8. The estimated single linewidth of these devices is around 50 kHz. This estimate is likely to be pessimistic due to the fact that accoustic interference causes an amount of apparent line broadening to be observed in these spectra.

Attempts to lock these external cavity diode lasers proved once more to be unsuccessful. Although the diode beat spectra were seen to exhibit a much improved stability over those of the original mounts, there was still considerable evidence of a low frequency jitter, resulting in frequency excursions of the beat note ranging between 10 MHz and 100 MHz. This magnitude of frequency jitter was outwith the capture range of the loop which is approximately equal to one and one half times the loop natural frequency (5−10MHz) [11]. An attempt was made therefore, to improve the IF stability of the system with the use of a frequency control loop.

7.7 Intermediate Frequency Control.

The construction of a frequency stabilisation loop would substantially increase the probability of lock being achieved, provided that the IF signal could be controlled to within the loop aquisition range. The following section describes the construction of such a loop.

The central component in a frequency stabilisation network is the frequency discrimination device. In the present experiment this function

Reference Level

Marker Freq.

Horiz. Scale MHz/div

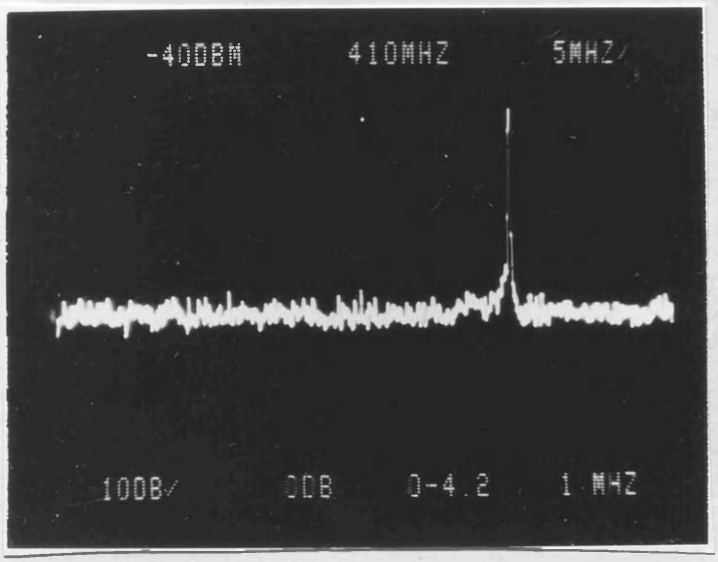

Vertical Scale dB / Div

Input Attenuation.

Freq. Span GHz

Resoultion Bandwidth

Figure 7.7

External Cavity Beat Spectrum.
Individual Linewidth 50 kHz.

Reference Level

Marker Freq.

Horiz. Scale MHz/div

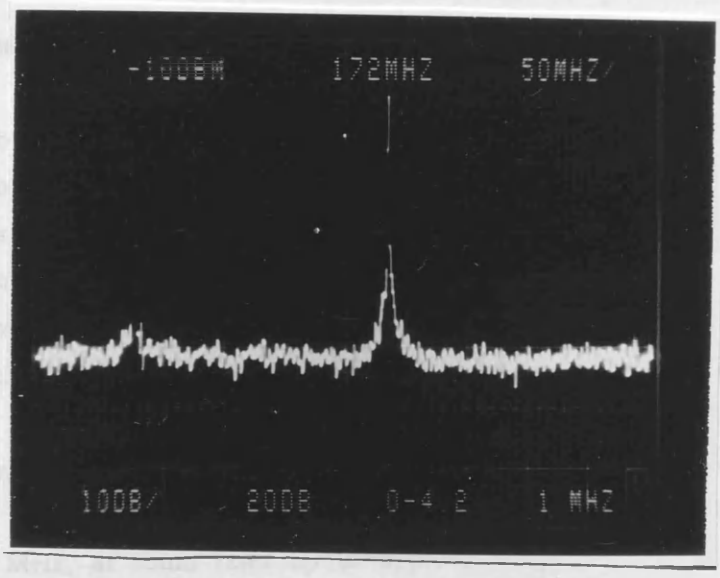

Vertical Scale dB / Div

Input Attenuation.

Freq. Span GHz

Resoultion Bandwidth

Figure 7.8

External Cavity Beat Spectrum.
Individual Linewidth 50 kHz.

was performed with the use of a double balanced mixer and delay line. The characteristic of the device (Figure 7.9) shows a range of operation of 70 MHz (tunable by varying the length of delay). The output of the mixer was filtered and amplified to produce a voltage swing of ± 15V (variable). This output was further amplified, dc level shifted to drive between 30 and 130V, and used to provide a feedback signal to drive the local oscillator longitudinal PZT transducer. This allowed the IF frequency to be stabilised by controlling the cavity length of the local oscillator laser while the main phase–locking signal could be fed back to the injection current.

7.7.1. Laser Frequency Instability.

To obtain a measure of the frequency of the laser instabilities, and therefore an idea of the required bandwidth of the feedback loop, a beat spectrum was obtained and the IF signal amplified and sent to the discriminator. The typical output from the discriminator, as observed on a storage oscilloscope, is displayed in Figure 7.10. The vertical scale of the trace represents the frequency deviation (20 MHz/cm) and the horizontal scale displays the time scale of the measurement 10 ms/cm. The IF instability can be seen to comprise of essentially low frequency components, causing frequency excursions of up to 80 MHz, at audio rates up to approximately 500 Hz. In order that these components could be accommodated within the bandwidth of the feedback loop, the amplifier cut–off frequency was set to be approximately 1 kHz.

The oscilloscope trace of the discriminator output indicates that, at certain positions, saturation occurs. This implies that frequency excursions of greater than the discriminator operating range (approximately 70 – 80 MHz) were present. This was consistant with observations of the beat note on the Spectrum Analyser which indicated that frequency stability was approximately 100 MHz (± 50MHz).

The magnitude of the frequency instabilities observed between the two laser diodes can be related to changes in the cavity length as follows. Fluctuations in the mirror position, would alter the diode

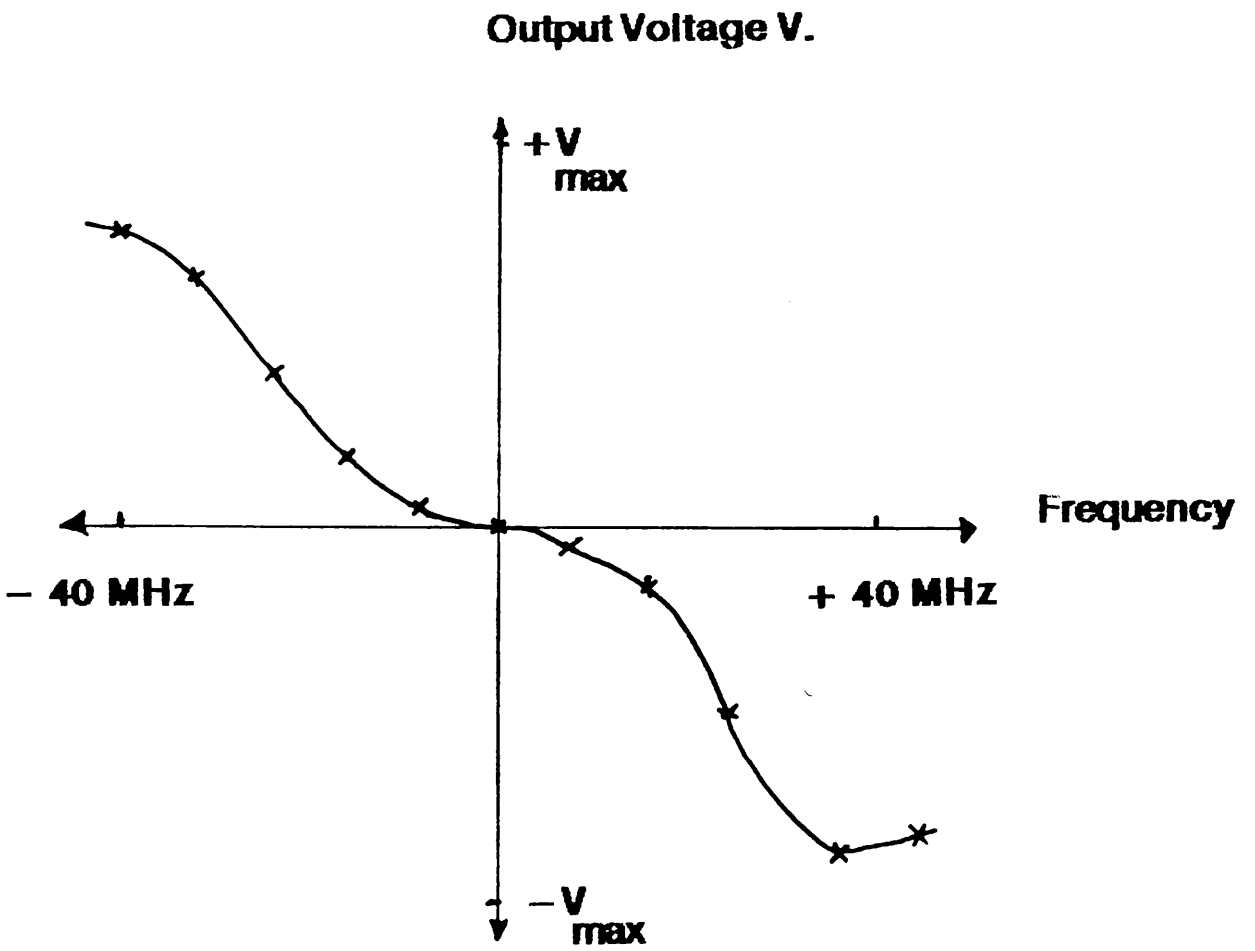

Figure 7.9

Discriminator Characteristic.

Frequency

20 MHz/cm

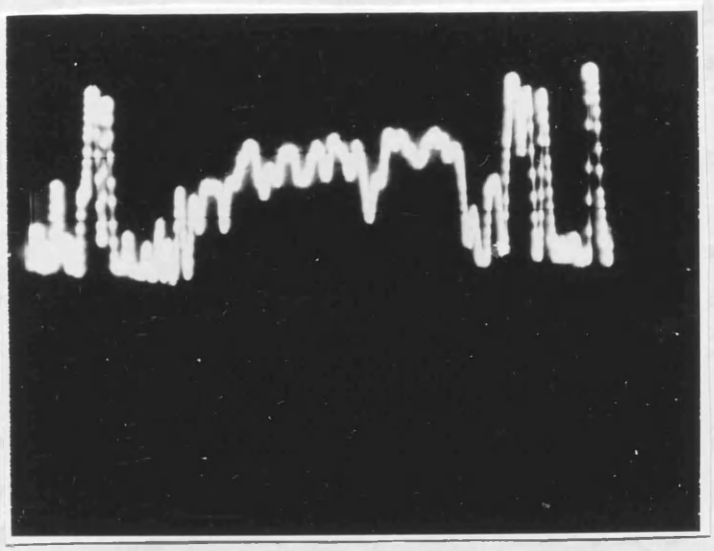

Time 10 ms/cm.

Figure 7.10

IF Discriminator Output: Open Loop Configuration.

centre frequency, δf, by an amount given by,

$$\delta f = - (f/L)\,\delta L \quad \text{Hz.} \qquad (7.1)$$

where L is the cavity length and f the oscillation frequency.

For a 12 cm cavity, a 100 MHz (± 50 MHz) frequency deviation around a centre frequency of oscillation of 825 nm, corresponds to a fluctuation in cavity length of 33nm. This was attributed to mirror displacements of ± 16 nm on each diode. This was initially suspected as being an excessively large figure for mirror vibrations however further investigation revealed that this may not the case. The average vibration on a 'quiet' concrete floor at ground level is estimated to be in the region of 1 nanometer [17]. In a building such as the Rankine building, six floors up from the ground level, under the excitation of a large number of noisey machines and air conditioning plants, the level of vibration, even allowing for the fact that an accoustically isolating table was used in the experiment, is likely to be much higher. When the control signal was fedback to the local oscillator the magnitude of the IF frequency excursion was seen to be reduced (see Figure 7.11). The average frequency excursion in Figure 7.11 is of the order of 20 MHz (± 10 MHz). This frequency stability could be achieved for a number of minutes however low frequency drift within the system was always sufficient to move the frequency separation to outwith the range of the control loop. This drift in the centre frequency was attributed to thermal expensions in the laser mount.

The laser diodes were controlled in temperature to within 0.01 K however the mounts were not controlled. Significant fluctuations in the temperature of these mounts were therefore almost certain to be present and these could cause a substantial shift in the laser operating frequency. The frequency stabilisation circuitry was observed to hold the loop within a range of ± 10 MHz for periods of several minutes until the control loop integrator output saturated. The time scale of this control cycle was consistant with the expected time duration of temperature fluctuations expected from the aluminium mount. The maximum range of control of the cavity length was 500 nanometers (the expansion coefficient of the PZT transducer was 5μm/1000 V and

Frequency

10 MHz/cm

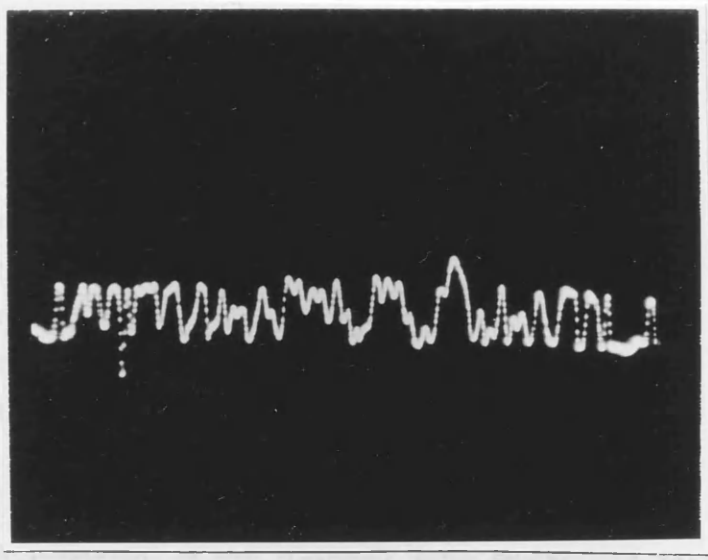

Time 10 ms/cm.

Figure 7.11

IF Discriminator Output: Closed Loop Configuration.

the dynamic range of the controller was 100 V). The thermal coefficient of expansion for Aluminium is 25.10^{-6} K^{-1} m^{-1} therefore a temperature change of 0.3 K (in a 15 cm cavity) would be sufficient to saturate the feedback the feedback signal and therefore render the control system ineffective. Temperature fluctautions of this magnitude were comparible with what would be expected over a normal working period: the temperature of the laboratory would change by several degrees Celcius over the period of one day.

Within the frequency stabilised region, frequency jitter excursions of ± 5 MHz to ± 10 MHz were present. The sensitivity to mirror position of a 12 cm long mount operating at 820 nm can be calculated from equation 7.1 as 3MHz frequency shift per nanometre movement. Thus frequency jitter, of the order described above, was concluded to be due to mirror movements of around 2 nm to 3 nm. It was suspected that insufficient regulation of the feedback controller power supply could be responsible for this effect (1V ripple would be sufficient to produce a 4 nm excursion). However measurements indicated that the supply was regulated to better than 5 mV at the operating current of the control loop.

If the discriminator output, Figure 7.11, is examined closely, then a significant proportion of the frequency jitter components appear to be discrete events, or jumps. It was suspected that a possible cause of this was hysterisis in the mechanical couplings associated in the PZT position arrangement. Inspection of the manufacturers data on the PZT controller revealed that the hysteris on the PZT stack could be as much as 0.75 nm. This would contribute significantly to the limitations in the control of the mirror position achieved by the feedback circuitry however this would not be sufficient to account for all of lack of precision achieved. However hysteresis could have been present in the mechanical mountings of the transducer and it likely that any such hysteresis would be of an order of magnitude comparible to the frequency jitter observed here. It is common practice to counteract the effects of hysteresis in any system by introducing a dither signal [19,20]. However, because absoulute frequency stability was required in this operation, this course of action was not available. It was concluded therefore that further stabilisation

of the device, without a complete redesign of the laser cavity, was unlikely to be successful. Experiments at this time were being carried out to stabilise the centre frequency of an external cavity mount to the peak of the discrimination curve of a Fabry Perot interferometer (see Chapter 3). Similar limitations were experienced in this arrangement.

7.7.2 Laser Instability Due to Coherence Collapse.

The cause of the instability in the laser centre frequency has so far, in the present discussion, been attributed to mechanical fluctuations in the laser mirror position. While this mechanism offers one possible explanation to the observed instability of the laser mounts, there are many factors which influence the laser behaviour and the above explanation may be incomplete.

An experimental investigation of laser behaviour under different amounts of external feedback has been published by Tkach and Chraplyvy [16] which shows that, in a semiconductor diode laser, several distinct regeimes of operation are possible depending upon the levels of feedback. Feedback levels ranging from -45 dB to -55 dB have been shown [16] to produce more than one stable region of operation and furthermore, a mode hopping effect between these regions would be observed over a period of time. These mode hops were found to take place with microsecond duration. The magnitude of the frequency excursions (± 100 MHz) was noted to be of a similar magnitude to those observed above. Over a limited range of feedback powers (-39 dB to -45 dB) a region of total stability was observed. Further increase in the feedback levels resulted in spectral broadening of the laser diode and multi-moded operation up to the point of total coherence collapse, however at feedback levels of greater than -8 dB, the laser oscillation was found to be totally stable and single moded.

The findings of Tkach and Chraplyvy can be related to the work carried out in the present experiment. Feedback to the external cavity diode laser was achieved using a diffraction grating blazed for an operating wavelength of 780 nm. This grating was approximately 80 %

efficient at the operating wavelength of 820 nm therefore, depending upon the efficieny of the coupling to the laser diode, the entire range of operating conditions, examined by Tkach and Chraplyvy, should have been attainable in the present experiment.

Initial experiments with the local oscillator diode showed that this diode was single–moded and stable for long periods of time. The onset of external cavity oscillation was achieved from a condition of total coherence collapse and was accompanied by an increase of around 14 dB in output power. The oscillation was never observed to be dual moded at any time. The centre frequency of the diode was tunable by adjusting the length of the cavity and furthere more, stable oscillation was maintained even with substantial fluctuations in mirror position. Figure 7.12 shows the movement in the centre frequency of the diode, as measured using a Fabry–Perot in non–scanning mode, following a firm blow with a fist to the optical bench. The device was clearly affected by this disturbance however single mode operation was maintained. These properties are all consistant with a diode operating in a true external cavity with a feedback level of greater than -8 dB. The antireflection coating placed upon this diode was efficient to better than 0.9 % and thus it is reasonable to assume that sufficient power could be returned to the diode to achieve this condition.

In experiments where lasers with an antireflection coating of around 2–5% were used. The alignment of the external reflector was found to be more critical before external cavity operation would take place. These lasers were also found to be more susceptable to accoustic interference: a disturbance of a similar magnitude to that shown in Figure 7.12 would be sufficient to cause the diode oscillation to collapse. However these diodes were not, at any point, found to be dual moded. The implication of these findings is that the diodes with this less efficient coating were being operated in an external cavity however the level of feedback was only marginally sufficient to produce single moded operation.

The discriminator traces shown in Figure 7.11 could be interpreted as being the result of a rapid mode hopping, between modes separated by 10 MHz, of one of the diodes. This would imply

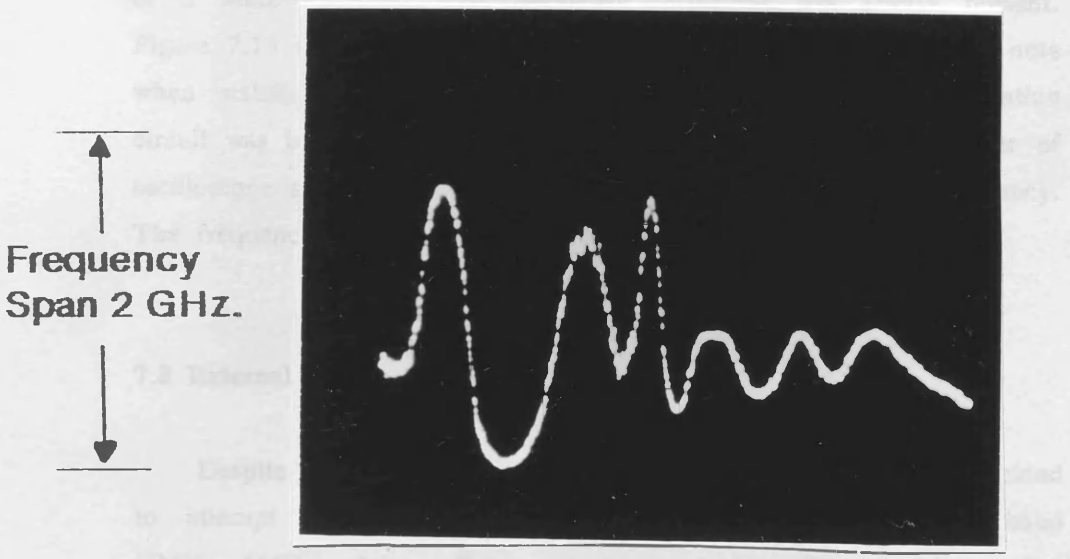

Figure 7.12

Frequency Excursion of External Cavity Diode Laser following Large Mechanical Disturbance of Optical Bench.

however that the dio de was operating in region two (as described in reference 26) with a feedback level of around −50 dB. In the present experiment, it is more probable that the diode was not operating in this region but was operating the true external cavity region of high power feedback (greater than −8dB). Although a poor coupling efficiency between the external mirror and the diode cavity could reduce the amount of power fedback to the diode it is unlikely that the feedback power were reduced by 40 dB. The logical conclusion of this argument is therfore that the laser instabilities were truly mechanical in nature.

Attempts to control the IF frequency of the laser were only partially successful. The beat spectrum could be controlled to stabilities of 5 MHz however the frequency instability was always present. Figure 7.13 shows a typical spectrum of the the heterodyne beat note when stabilised. This signal was obtained while the IF stabilisation circuit was in operation. The photograph was taken over a number of oscilloscope scans as no storage facility was available at this frequency. The frequency jitter of the beat note is clearly evident.

7.8 External Cavity Phase Locked Loop.

Despite the discouraging evidence presented above it was decided to attempt to lock the two diode lasers using a narrow band (3MHz− 6MHz) loop. Two reasons underlay this decision. The spectrum could, at particularly quiet periods, be seen to stabilise sufficiently that the jitter was within the lock bandwidth and, more importantly, the laser diode was beginning to exhibit signs of spectral degradation. It was becoming increasingly more difficult to align the module such that stable external cavity operation would result. It was felt therefore that an attempt to lock the two diodes had to be made before the stability of the diodes further deteriorated. A similar process as described previously was therefore undertaken in an attempt to lock the two diodes.

The rf oscillator was tuned through the IF spectrum centre frequency and the locking procedure was attempted as previous. It was

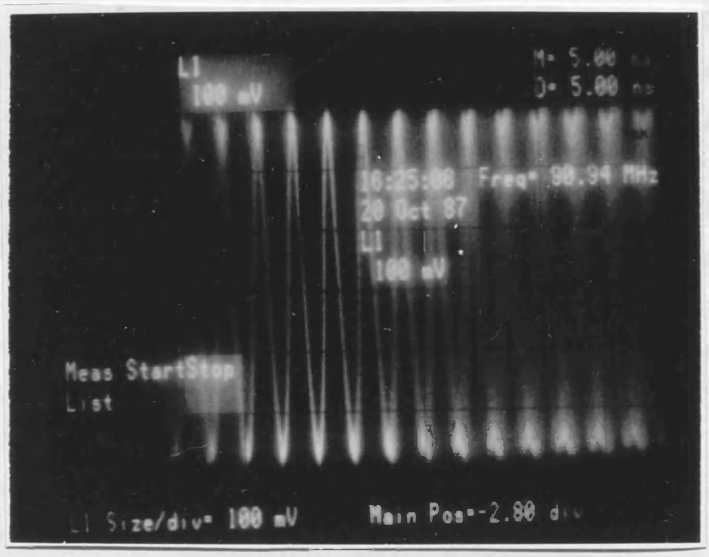

Figure 7.13

Heterodyne Beat Note in Time Domain.

observed once more that high levels of electrical feedback could cause a collapse in the beat spectrum. The magnitude of the frequency excursions that could be tolerated by the external cavity device were comparible with those that could be caused by the feedback signal. Therefore it was concluded that an excessive delay bandwidth product was causing instability. Lower levels of electrical feedback did not produce an unstable condition and, at the more stable periods during the experiment, the laser beat note and the rf oscillator could be seen to remain coincident for some seconds. It was not possible however, to conclude from this that lock was aquired. The magnitude of the frequency instability was always sufficient to shift the beat note such that it was obvious that lock was not achieved. Locking may have been accomplished instantaneously however no evidence of a reduction in the beat spectrum linewidth was ever observed. This is not surprising however since the linewidth of the beat is less than 100 kHz ,however without evidence of this phase noise reduction, or an obvious solid locking situation, it was not possible to conclude that locking was taking place.

As the experimental work continued it became increasingly more difficult to obtain stable beat spectra with the external cavity laser diodes and more difficult to align the cavity such that a stable operation would result. It was apparent that the diodes, although less than six months old, were showing signs of spectral ageing. This was not expected as experience with diodes of this type had shown them to be reliable and have an operational life time of a number of years. Examination of the individual laser diodes was therefore carried out to see if evience of damage could be observed. Inspection of the facet under an optical microscope did not reveal any unusual features.

The lack of stability of the laser operation in an external cavity could also be attributed to a reduction in the efficiency of the AR coating. A reduced efficiency in the AR coating would present difficulties in attempts to obtain sufficient levels of feedback to gaurantee stable, single moded, operation. The laser would therefore be readily upset by changes in the injection current resulting from the electrical feedback and may be forced into a condition of coherence collapse. Tracings were therefore made of the spontaneous emission

profile in order to see if this might reveal any information on the cause of the performance deterioration. The profile of laser 2203 as measured immediately after coating is shown in Figure 7.14. Figure 7.15 shows a measurement of the spontaneous emission after a few months of use. This spectrum is typical of the spectra obtained with any of the AR coated diodes after a few months use. Examination of these traces shows that, in addition to the expected Fabry–Perot modulation from the diode cavity ends, a further modulation corresponding to a reflection from a much shorter distance (approximately 30 μm) is evident. The cause of this modulation is not known and, to the authors knowledge, has not been reported in the open literature. It was thought that the antireflection coating may have diffused into the active layer however it would not be expected that it would migrate to this distance. It is possible that damage has been caused to the diode crystal lattice from localised heating effects, resulting from excessive optical power densities returning to the diodes from the focussed reflected beam. The exact mechanism of the degrading is not understood however all diodes used in external cavity operation under went this change. The sensitivity of the laser diodes, where the additional modulation on the gain profile was present, to accoustic disturbance and electrical feedback made experimentaion with these diodes impractical. Since no more lasers were available for further experimentation the conclusion that phase–locking attempts were unsucessful was drawn.

7.9 Phase Locked Loop: Conclusions.

The components for construction of an OPLL were assembled and a number of attempts made to lock two diodes in phase were made. Early attempts using free running sources were unsucessful due to the magnitude of the low frequency thermal noise present as a result of inadequate temperature control. Improvements in the quality and stability of the beat spectra were obtained with the redesign of the laser mount. Beats were obtianed with both external cavity and compound cavity arrangements which indicated individual laser linewidths of 50–100 kHz. Attempts were made to improve the frequency stability of the laser source and this was succesful up to the point where the mechanical limitations of the mount prevented further

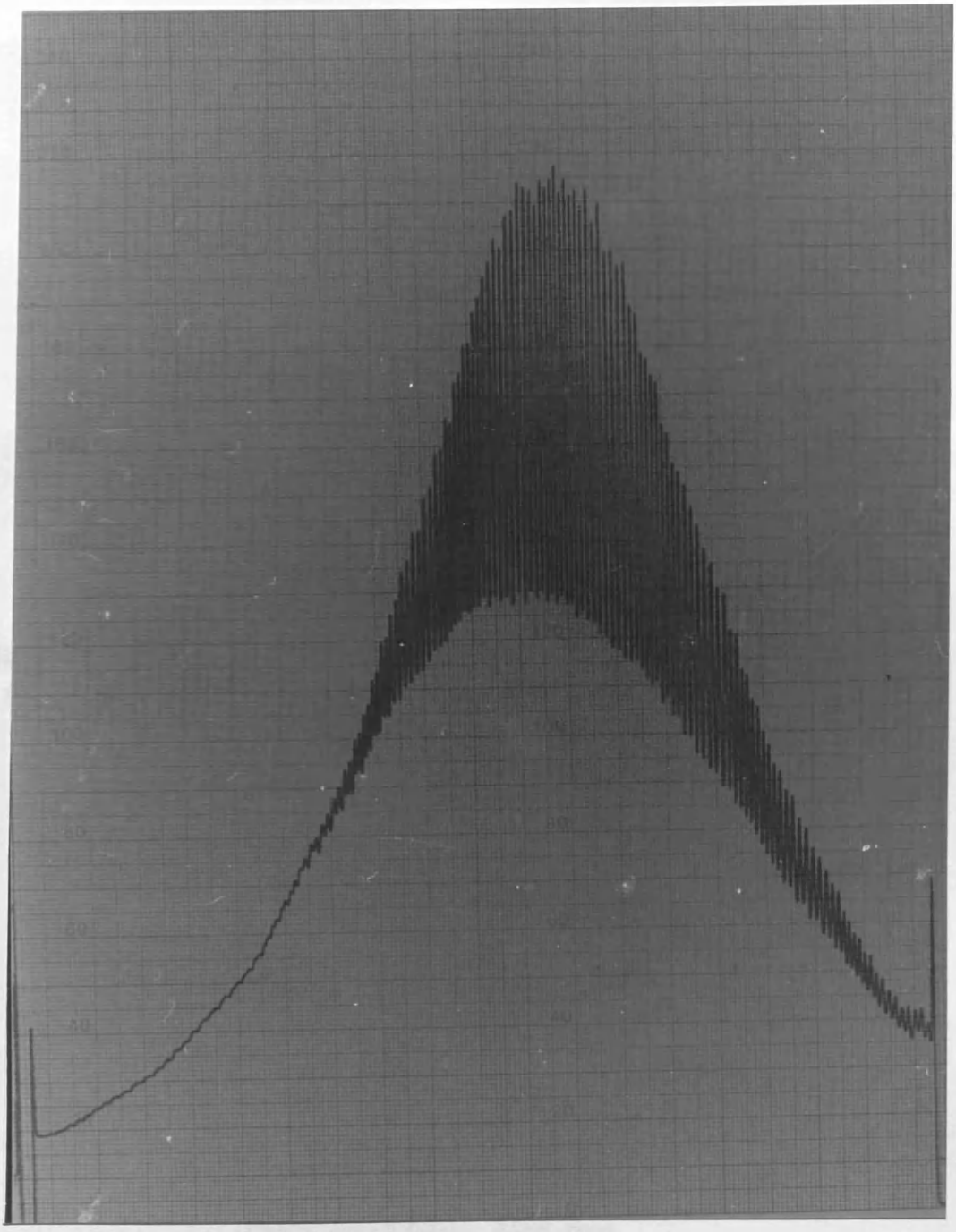

Figure 7.14

Spontaneous Emission Profile of Laser 2203.
Measurement made immediately after Coating.
Facet Reflectivity 0.6 %.
Wavelength Scan 800 – 852 nm
Peak in Profile at 834 nm.

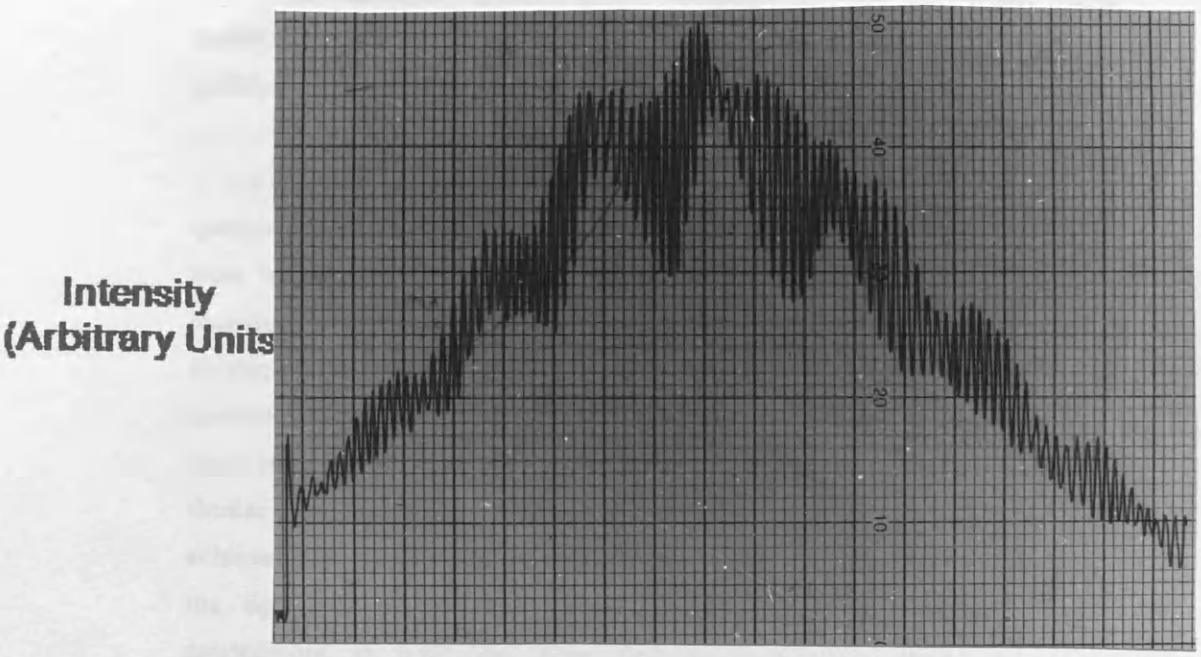

Wavelength Scan 820 – 850 nm

Peak in Profile 834 nm

Figure 7.15

Spontaneous Emission Profile of Laser 2203.
Measurement made after 3 months experimental use.

improvement.

A number of beat spectra were obtained that were found to remain for seconds at the same frequency of the rf oscillator in the heterodyne OPLL arrangement however, at no point could it be said that lock had been achieved. The spectral purity of the sources used would have made it extremely difficult to ascertain that lock had been aquired unless a stable lock situation was reached. This was never found to happen. Experimental attempts at phase–locking were therefore concluded to have been defeated by failure to relaise sufficient frequency stability of the the laser diode.

Considerable improvements were made in the stability of the beat spectra over the course of the project however, the final conditions were of insufficient steadiness to allow locking to take place: the magnitude of the frequency instability was comparible with the maximum allowable natural frequency. The frequency stability of the sources used in this experiment is not as good as the best values that have been achieved by other workers who have constructed similar arrangements [6]. However the performance improvements achieved by these workers is significantly influenced by the fact that the operating wavelength is 1.52 μm wheras the current work was carried out at 0.82 μm. The first external cavity diode laser was reported by Wyatt and Devlin [14] and this arrangement had a cavity length of 20 cm and displayed a frequency jitter of ± 1.5 MHz. This corresponds to fluctuations in the cavity length of ± 1.5 nanometres. The long term stability of the diode was improved mounting it on a silica plate with a low thermal sensitivity and packaging and thermally stabilising the entire arrangement [8] and by solid bonding of the refective grating (with epoxy) into position. Short term accoustic vibrations causing a 5 MHz deviation were however still evident [6]. This corresponds to fluctuations of 1.3 nm over the 5 cm cavity length. This is the most impressive published result to date and is significantly better than what was achieved in this experiment. Similar experiments with external cavity laser diodes, from AT&T Bell, have reported stabilities of ± 20 MHz reduced to ±5Mhz with IF stabilisation [21,22]. The former figure corresponds to mechanical fluctuations of 25 nanometres (for the 25 cm length of cavity used in

the experiment) and the latter corresponds to 5 nm (for a 20 cm cavity) which is comparible with what has been achieved in the present experiment. In attempting to implement a control loop which maintains the position of a mirror to within nanometer or subnanometer tolerances, problems due mechanlical hysteresis in the positioning equipment become evident. This particular limitation in the postioning resolution was concluded to have been responsible for limiting the frequency stability achieved in the present experiment. The problem of hysteresis in the control of the mirror position could perhaps have been aleviated with the use of a dual PZT controlled positioning system driven differentially. This would have meant a complete redesign of the laser mount arrangement however and this was not possible within the time scale of the project.

The phase–locking experiments described here were concluded to have been unsuccesful. The main cause of the failure was the lack of stability of the centre frequency of oscillation of the sources used in the experiment. Substantial improvements were made to the mechanical stability of the diode arrangements however these were found to be insufficient for the operating wavelength. The levels of stability obtained were comparible with those obtained by other workers and may have, with continued experimentation and possibly a change in laboratory location to a more stable location, yielded a temporary locked condition. It was found however that, during the course of the experimental work program, the laser diodes used in the external cavity arrangement deteriorated in stability with use. Investigation of the spontaneous emission profile revealed evidence of material defects in the laser structure. Experimental progress was terminated as a result of this deterioration in the device performance: the stability of the operation of the external cavity diode laser became sufficiently degraded to make experimentation unpractical.

References.

1. R.C. Steele, 'Ph.D. Thesis.' University of Glasgow 1983.

2. Hitatchi Diode Data Book.

3. W. Liddell 'Optical Phase–Locked Loop.'IEE Colloquim on Advances in Coherent Optic Devices and Technologies, Savoy Place, London GB, March 1985.

4. R. Lang, K. Kobayashi 'External Optical Feedback Effects on Semiconductor Injection Laser Properties' IEEE J.Quant. Elect. QE–16(3) 1980. pp347–355.

5. O'Shea, Callen, Rhodes 'An Introduction to Lasers and their Applications.' Addison Wesley Publishing Company, California, 1978.

6. M.R. Mathews, K.H. Cameron, R. Wyatt, W.J. Devlin 'Packaged Frequency–Stable Tunable 20 kHz Linewidth 1.5 μm InGaAsP External Cavity Laser' Elect. Lett. 21(3) 1985. pp113–115.

7. F. Favre, D. LeGuen 'Emission Frequency Stability in Single Mode Fibre Optical Feedback Controlled Semiconductor Lasers' Elect. Lett. 19(17) 1983. pp 663– 665.

8. F. Favre, D. Leguen, J.C. Simon 'Optical Feedback Effects on Laser Diode Oscillation Field Spectrum' IEEE J.Quant. Elect, vol QE–18(10) 1982 pp1712–1717.

9. K. Kikuchi, T. Okoshi 'Dependence of Semiconductor Laser Linewidth on Measurement Time: Evidence of Predominance of 1/f Noise.' IEE Elect. Lett. 1985 vol.21. no.22. pp1011–1012.

10. M.A. Grant, W.C. Michie, M. Fletcher 'The Performance of Optical Phase–locked Loops in the Presence of Non–negligible Loop Propagation Delay.' Journ, Lightwave Technol. vol LT–5(4) 1987 pp592–597.

11. F.M. Gardner 'Phaselock Techniques' New York: Wiley, 1979.

12. A. Blanchard 'Phase–Locked Loops. Application to Coherent Reciever Design.' New York: Wiley, 1976.

13. D.J. Malyon 'Digital Fibre Transmission using Optical Homodyne Detection.' Elect. Lett. vol. 20(7) 1984. pp281–283

14. R. Wyatt, W.J. Devlin '10 kHz Linewidth 1.5μm InGaAsP External Caivty Laser with 55nm Tuning Range.' Electronics Lett. No.19 1983 pp110–112.

15. L. Goldberg *et.al.*'Spectral Characteristics of Semiconductor Lasers with Optical Feedback.' IEEE J.Quant. Electron. vol QE–18(4) 1982.pp555–564.

16. R.W. Tkach, A.R. Chraplyvy 'Regeimes of Feedback Effects in 1.5μm Distributed Feedback Lasers.' IEEE J.Lightwave Technol. JLT–4(11) 1986 pp 1655–1661.

17. F.E. Goodwin 'A 3.39 μm Infrared Optical Heterodyne Communcations System.' IEEE Journ. Quant. Electron. QE–3(11) 1967 pp524–531.

18. 'CRC Handbook of Chemistry and Physiscs.' 1984–1985, 65th Edition, CRC Press Inc., Florida.

19. S.A. Marshall 'Introduction to Control Theory.' Macmillan Press Ltd 1978.

20. R.C. Dorf 'Modern Control Systems.' 3rd Edition. 1980 Addison–Wesley Publishing Company Inc., Reading Massuchusettes.

21. R.A. Linke *et.al.*'Coherent Lightwave Transmission over 150km fibre lengths at 400 MBits/s and 1 GBits/s data rates using Phase Modulation.' Elect. Lett 22(1) 1986 pp30–31.

22. A.H. Gnauk *et.al.* 'Coherent Lightwave Transmission at 2 GBits/s over 170 km of Optical Fibre Using Phase Modulation.' IEE Elect.

Lett. 23(6) 1987 pp286– 287.

CHAPTER 8.

Conclusions.

8.1 Introduction.

The work presented within this thesis has been concerned with evaluating the feasibility of using an Optical– Phase– Locked– Loop as a receiver component for coherent optical detection systems. Many of the conclusions reached during the course of this project have been stated at the end of each chapter. This present chapter will restate much of what has already been said, in a summarised form, in order that a broad overview of the project may be presented and conclusions, relating to the investigation, drawn.

In Chapter 2 an analysis of receiver sensitivities for a number of transmission formats was presented. It was shown that, in a binary transmission system, coherent detection schemes offer an increase in sensitivity of 7– 12 dB over the IM/DD format [1–4]. In addition to this performance improvement, coherent detection schemes also provide the potential of allowing the transmission bandwidth of optical fibre to be exploited [5]. However, while these coherent receivers are readily implemented at microwave frequencies, the required level of phase stabilty of the optical source makes a direct transfer of these methods to the optical domain difficult.

Much of the impetus behind the drive towards coherent systems has arisen from the success of the semiconductor laser in IM/DD networks. Present day, state of the art, diode lasers are however generally of insufficient temporal coherence to be of use in phase sensitive detection schemes, where the greatest receiver sensitivity is to be obtained [3]. If the semiconductor laser diode, in its free running form, is to be considered as the only feasible source for transmission networks, then it is likely that only such detection formats as heterodyne FSK, heterodyne ASK transmissions will be practically realisable within the near future. Restricting the design of coherent transmission systems to those which are not sensitive to the absolute phase of the carrier need not however necessarily result in a limitation

in system performance [6,7]. In the final sections of Chapter 2 an analysis of multi-level orthogonal signalling schemes was presented which showed that, if a sufficient number of signalling levels are chosen, a BER performance which exceeds that of Binary PSK can be achieved with a transmission scheme which is less sensitive to the absolute phase of the incoming signal. In particular, an 8-ary FSK transmission scheme, operating with a receiver phase error of 0.19 rads and 10^{-9} BER, would require an average receiver power level of approximately 7 photons per bit, while the corresponding binary PSK transmission would require 9 photons per bit under ideal, noiseless, conditions [1].

It must be observed however that, while the multi-level signalling format offers an improvement in receiver sensitivity over binary PSK transmissions, the success of such a system lies in achieving a similar phase tracking performance to that necessary for a PSK transmission. An analysis carried out by Jeromin *et.al.*[34] indicates that an incoherent M-ary FSK transmission scheme operating with sources of tens of Megahertz linewidth would incurr high receiver power penalties. In such instances the so called 'weakly coherent' transmission schemes may better serve the communications system requirements.

8.2 Modification of the Laser Diode Properties.

The discussion presented so far has assumed that it would only be practical to employ free running laser diodes in coherent transmission systems. While this is a desireable goal it may also be, in certain cases, an unnecessary restriction. Much of the success which

the semiconductor diode laser has enjoyed can be attributed to the fact that it has excellent compatibility with optical fibre communications systems. In its free running form, the diode laser is small (typically hundreds of microns in length) and has a radiative area and beam divergeance compatible with efficient launching into optical fibre. It has low power consumption (hundreds of milliampere drive current at 1.4 V forward bias voltage) and can be mounted in a fibre pigtailed package which is resilient to mechanical disturbance. In contrast, gas lasers are more bulky than diode lasers (typically tens of centimetres in length), they require power supplies which are capable of delivering hundreds of volts at hundreds of milliampere current, and must be isolated from the effects of mechanical disturbance [9]. Gas lasers are however notably advantaged over diode lasers in that their emission spectra can be restricted to tens of kilohertz in linewidth [10,11]. This narrow linewidth is of particular interest in coherent communications systems design. In order to reduce the linewidth of semiconductor diode lasers, a substantial amount of research has been carried out into examining the effect of coupling the diodes emission to an external cavity [12–18]. Using this technique, linewidths of less than ten kilohertz and tuning ranges of 50 nanometres have been achieved using semiconductor diode lasers [13,14]. One of the main concerns where the use of an external cavity laser source is considered, is the mechanical stabilisation of the external reflector and the isolation of the package from accoustic shock from the working environment. However, it has been demonstrated that such sources can be constructed with sufficient mechanical integrity to withstand the rigours of a field environment such that a stability level suitable for certain coherent transmission schemes can be maintained [19]. Although these sources may be less suited to environments where access for the maintainence worker is restricted, for example undersea systems, this does not exclude their use from such schemes. External cavity sources could be operated, for example on land based points, and the less mechanically vulnerable free running laser sources used as optical amplifiers in locations where access is not possible.

In the context of the present work, it was felt that the inherently large linewidths of the commercially available diode laser sources

would prove to be a considerable barrier to the successful construction of an OPLL [20]. Therefore an investigation was carried out into a number of the more common linenarrowing techniques. An outline of a some of these schemes is presented in Chapter 3, along with a report on the experimental investigation of some of the methods. In the work undertaken in this project, weak coupling of the diode emission to an external cavity provided significant reductions in the laser operating linewidths from between 5 MHz and 10 MHz down to 200 kHz. However, diodes in such arrangements were found to be extremely sensitive to accoustic disturbance. Experimental observations, and theoretical analysis performed by other workers has confirmed that diodes in such arrangements are highly sensitive to the phase of the optical feedback: selection of stable single moded operation is limited to a narrow range of feedback conditions [21,22]. As a consequence of this sensitivity, the diode can be forced into a state of partial or total coherence collapse by small movements in the reflecting mirror position. Furthermore, the tuning of the laser frequency, via the injection current, is effective only over a limited range, approximately equal to one tenth of the cavity free spectral range. In the present experiment it was found that the range of uninterupted tuning of the coupled cavity diode laser was approximately 10 MHz to 20 MHz. The performance of the coupled cavity diode laser is therefore not well suited to the requirements of a coherent tranmsission system thus it was decided to investigate an alternative means of linewidth reduction.

Substantial successes, in terms of linewidth reduction and wavelength tunability, have been achieved by other workers by using high values of optical feedback (> -10dB) [13,14]. It was decided therefore, that this approach should be adopted and a number of such diode sources were constructed for use in an experimental OPLL system. Construction of an external cavity diode laser permitted linewidth reductions to less than 50 kHz to be achieved. Furthermore, the use of a diffraction grating to provide the optical feedback, enabled sufficient frequency selectivity to attain a 16 nm tuning range: these figures are comparible with what has been achieved by other workers [13,14]. Although diodes in this arrangement were found to outperform diodes weakly coupled to external cavities in almost all

considerations, one of the disadvantages of using such a scheme is that it is necessary for at least one facet of the laser diode to be antireflection coated. It was not possible for the deposition of an antireflection coating layer to be carried out within the department and therefore diodes had to be sent out to be coated. This proved to be a source of some concern during the construction of the external cavity devices because the coating process was found to be both time consuming and variable in quality. Measurements made of the facet reflectivity of various diodes returned from the coating company revealed facet reflectivities ranging from 0.3% to 32%. Investigation of the coating process was beyond the scope of this project and no satisfactory explanation for the range of coating reflectivities were provided by the manufacturers. Although diodes, both weakly and strongly coupled to an external etalon, required rigid stabilisation of the reflecting element, it was found that diodes which were operated in an external cavity with strong feedback levels were less sensitive to fluctuations in mirror position. Fluctuations in mirror position, of nanometre magnitude, could provoke a total coherence collapse in the coupled cavity laser: similar mirror positional variations in the external cavity laser were evident simply as frequency instability of tens of Megahertz magnitude.

8.3 The Optical– Phase– Locked– Loop (OPLL).

The subsequent chapters, Chapters 4,5 and 6, have presented a theoretical discussion of the OPLL. Chapter 4 described the necessary background of the OPLL operation, compiled from a number of published discussions [22–25]. These analyses indicated that phase– locking, with sufficient accuracy for a binary PSK system to be implemented, was possible with lasers having linewidths of Megahertz magnitude if sufficient power is allocated to the carrier. It was calculated that, in order to obtain a phase error variance of 0.03 $rads^2$ (sufficient to incurr a 0.5 dB power penalty in a binary PSK transmission at 10^{-9} BER) with sources of a combined beat linewidth of 1MHz, a loop natural frequency of 148 Mrads/sec and a carrier power penalty of 1.5 dB would be required. The equivalent loop natural frequency and carrier power penalty was found to be 2.22 Grads/sec and 8.5 dB if the beat linewidth was extended to 15 MHz. In comparison, the carrier power penalty for a 20 kHz linewidth beat was found to be 0.04 dB. While this analysis is useful in that it provides an understanding of the manner in which the laser phase

noise and the shot noise of the detection process influence the loop behaviour, it has failed to consider the fact that control bandwidths of these magnitudes are likely to be influenced by phase shifts in the control signal resulting from the propagation delay round the loop. This perturbation to the loop model was incorporated in Chapter 5 and it was shown that, an OPLL operating with a source beat linewdith of 1 MHz could tolerate no greater than 1.8 ns propagation delay before the phase tracking performance was degraded to such an extent that a 10^{-9} BER becomes unobtainable [20]. For a 15 MHz beat linewidth the corresponding allowable delay value was found to be 0.12 ns. Although it is not surprising that the loop propagation delay affects the phase synchronisation of the loop, it is surprising that such a small delay, 1.8 ns in a bandwidth of 23.5 MHz (148 Mrads/s), should have such a significant effect upon the performance of the overall communications system.

The analysis of Chapter 4 had also assumed that the receiver amplifier bandwidth was infinite. Since the effect of the time delay was found to be significant it was felt that it would be probable that the filtering effect of the front-end amplifier bandwidth would similarly influence the loop behaviour. This perturbation was also given attention in Chaper 5. A common standpoint of communications systems analysis is the assumption that, where the receiver amplifier bandwidth is finite but unknown, it can be assumed to be limited to the data rate. Restricting the bandwidth in this way, in a system incorporating an OPLL, was found to be justified only over a limited range of data rates. If the additional error in the phase synchronisation is to be limited in magnitude to that of the tracking error caused by the laser instability, then a data rate of approximately 800 times the beat linewidth was found to be necessary. Thus for the system considered above, with a 1 MHz beat linewidth, a data rate of 800 Mbit/s would be necessary before the power penalty due to the front end anplifier bandwidth becomes smaller than the penalty arising from the source linewidth. Transmission rates at present are commonly 140 Mbit/s and 565 Mbit/s [8] therfore the incorporation of an OPLL in such systems would require more careful consideration of the receiver amplifier than might be expected.

The findings of the above analyses are not purely of academic interest. At the outset of this project sources with beat linewidths of tens of Megahertz represented the best that were commercially available. Using such sources, the construction of an OPLL in a laboratory environment is possible but requires careful consideration of the loop propagation delay. It is probably not possible to reduce the overall propagation delay in an OPLL to less than 1 nanosecond and therefore it is likely that such OPLLs would not be of use in a practical working system. However, recent publications have indicated that DFB sources can be produced which display linewidths of 1 MHz or better [26,27]. Source linewidths of this magnitude would substantially improve the probability of constructing a PLL which maintains solid lock over extended periods of time (hours as opposed to minutes).*

To provide a physical explanation for the results of the theoretical work presented in Chapter 5, an analysis of the OPLL in the time domain was presented in Chapter 6. This investigation made use of the root locus construction technique to obtain a measure of the stability margin of the OPLL as a function of the delay– bandwidth product. The phase shift in the feedback signal, resulting from the loop transport delay, was found to pull the loop closer towards the boundary of instability resulting in a significant reduction in the loop damping factor, accompanied by ringing in the phase error, thus degrading the loop phase tracking performance. This analysis also revealed that the optimum delay– bandwidth product for any loop delay limited to 0.32. This suggests that, when the delay bandwidth product exceeds this value, the improvement in carrier tracking, achieved by encompassing a greater amount of the phase noise spectrum, is negated by the reduction of the loop phase margin.

The analysis of the time domain response of the OPLL was continued with the use of a digital simulation which presented a clear

visual display of the effect of under damping in the loop response. This under damped behaviour of the loop, which was evident as a series of converging oscillations, was seen to be directly related to the magnitude of the phase shift present in the loop. It was also found that the optimum loop natural frequency, for each value of propagation delay, was that which reduced the ringing in the loop transient response and restored the loop to the near critically damped condition. Under operating conditions where the loop propagation delay, or receiver bandwidth, had a significant effect, it was found that the second order definitions of the loop parameters were inaccurate. Oscillations in the loop phase error, resulting from an under damping in the loop transient response, were found to exceed the second order definition of the loop natural frequency by a factor of approximately 1.4. This is a significant observation in that it underpins the fact that the second order loop models, as presented in Chapter 4, do not adequately describe the OPLL constructed using semiconductor diode laser sources. Reduction of the loop bandwidths, to the extent that a near critically damped response to a step disturbance was restored, was found to be a sufficient stipulation to allow the second order definitions of loop behaviour to be applied.

During the work of a previous worker, an experimental investigation of the transient response of the OPLL was investigated[28]. Sufficient data was available from this experiment to allow a comparison between the experimental results and the simulation of the loop response to be obtained. The natural frequency, of the OPLL constructed by Steele, was estimated to have been 6 MHz and the propagation delay was thought to be around 8 ns: giving a probable delay– bandwidth product of approximately 0.3. The simulation and Root Locus analysis had predicted that an OPLL with these parameters would exhibit under damped oscillations in the phase error signal. These oscillations were observed in the experimental investigation of Steele and also displayed in the simulation. The simulation, and theoretical analysis, also predicted that a reduction of the loop natural frequency, by a factor of $\sqrt{10}$, would remove the oscillations in the phase error signal and restore the loop to a critically damped condition. This was seen to be in good agreement with the experimental findings where a reduction in the loop gain by one order

of magnitude was found to be necessary to restore the loop operation to the near critically damped condition.

The final aspect of this work to be presented within this thesis was the attempted construction of an OPLL. Loop components, which would in theory allow free running laser diodes to be locked, were assembled and an attempt to phase lock made. Numerous attempts were carried out to lock two sources however these attempts were not successful. One of the main causes for the failure of this experiment was instability of the centre frequency of the laser sources, resulting from inadequate thermal stabilisation of the laser mount. Beat spectra between free running diodes measuring hundreds of Meghertz were obtained. This value of beat linewidth is much in excess of what was expected following the individual linewidth measurements of Chapter 3 where the diode sources were found to have linewidths of between 5MHz and 10 MHz. The excessive beat linewidth resulted from the beat note being inadequately stabilised and chirping in frequency during the spectrum analyser scan time. An attempt was made to improve the stability of the beat note by coupling the oscillation of one of the sources to an external cavity, however this was ineffective due to the mechanical instability of the mirror positioning arrangement. Attempts to phase lock were abandoned until the diode mounting arrangement was improved.

Later experiments, with a re–designed laser mount, and a move to the external cavity mode of operation showed substantial improvements in the stability of the laser oscillator. Beat notes of better than 50 kHz were observed between external cavity laser diodes however attempts to phase lock these diodes continued to be frustrated. While the beat notes were seen to be significantly more stable than in the previous experiments, evidence of an audio rate frequency jitter causing frequency jumps of up to ± 50 MHz was observed. Frequency jitter of this magnitude was greater than the loop aquisition bandwidth (approximately 5MHz) and therefore it would not have been possible for lock to take place. In an attempt to improve the frequency stability of the laser beat note, a frequency control loop was constructed. Long term stability of this control loop arrangement was limited by thermal expansion of the laser mount. However, over periods of minutes, short term stability of ± 5 MHz was obtained.

The short term frequency instability was attributed to accoustically induced displacements of 3 nanometres magnitude in the position of the reflecting grating. Control of the mirror position to better than this value was not achieved as a result of hysteresis in the positioning equipment. Approximately 0.75 nanometres backlash was present in the PZT transducer [29] and an additional amount of hysteresis will have almost certainly been present in the mechanical couplings of the laser mount. The combined effect of both of these influences was concluded to have been a significant factor in limiting the performance of the frequency stabilisation circuitry. Similar limitations in devices of this construction have been reported by other workers, however reasons for this limitation was not presented [13,14,30,31].

It should have been possible, with diode sources of the above construction, for aquisition of lock to have been attained. However there was not at any time evidence of improved stability of the beat note which would indicate that lock had been aquired. It is possible that, with a sufficient number of experimental attempts, phase–locking could have been achieved. Experimental progress was however limited by the eventual deterioration of the laser source. The external cavity diode laser sources could be observed to become more difficult to align, and become progressivley less stable as the experimental work program continued. Examination of the spontaneous emission profile of diodes used in the experiment showed evidence of modulation superimposed upon the profile (this modulation was in addition to the expected modulation due to the residual Fabry–Perot effect from the cavity ends). This additional modulation was consistant with a reflection from a point some 30 μm within the diode cavity and may have been the result of crystal dislocations, possibly due to excessive heating in the diode caused by greater than normal optical power densities when the diode was operated in an external cavity arrangement. The exact cause of this effect is unkown. However, all diodes used in an external cavity arrangement were seen to degrade in stabilty with use, and were found to display additional modulation on the spontaneous emission profile as described above. A recent publication has indicated that the migration of crystal defects in semiconductor materials takes place at a faster rate than has been previously suggested under conditions of high carrier concentration [32].

It is also suggested that such defects tend to migrate towards, and associate within, the active layer of LED sources. These observations may provide a key to understanding the degradation of the sources used within this experiment. However all sources experienced this degrading effect, making experimental progress increasingly more difficult, therefore the attempts to construct an OPLL were concluded to have been unsuccessful.

8.4 Further Work.

The continued drive to implement an OPLL which is insensitive to mechanical disturbance is a worthy goal. Loops have been successfully constructed using sources coupled to external cavities, however these loops have not been shown to be of sufficient stability to be of use in a practical working environment[28]. Improvements in the semiconductor laser source technology now being reported [26,27] are such that the most obvious route to implementing a workable OPLL would be to use sources such as those described in references 26 and 27 in conjunction with hybrid packaging techniques to reduce the loop propagation delay. Miniturisation of the OPLL in this way will undoubtably be the most successful means of constructing an OPLL which is insensitive to mechanical disturbance. Future generations of the device may be refined with the use of large scale integration techniques. Loops constructed in this way would be significantly smaller than OPLLs designed around the bulky external cavity sources and therefore would be more likely to be accepted as a standard communications system component. While the large scale integrated circuit OPLL may be some years away from production the components exist at present for a hybrid packaged version of the OPLL, using narrow linewidth DFB laser sources, to be constructed.

Although the OPLL would be an extremely useful component in a coherent transmission system, the future of coherent communications is not totally dependent upon its successful development. The discussion of Chapter 2 revealed that multi−level FSK transmissions could provide a receiver sensitivity which would outperform that of perfect binary PSK transmission. With adequate provision of thermal stabilisation, the linewidths of present day sources are adequate for

the development of such schemes and, although such receivers would be costly in terms of receiver bandwidth, the available bandwidth of present day fibre systems immense and could easily accommodate such schemes. To the authors own knowledge only a limited amount of experimental work has been carried out in this sphere to date [33]. The development of semiconductor laser sources will not only aleviate the burdens on the construction of binary coherent signalling schemes but will also make easier the investigation of multi– level systems.

References.

1. Y.Yammamoto 'Recoever Performance Evaluation of Various Digital Optical Modulation－Demodulation Systems in the 0.5－10μm Wavelength Region.' IEEE J.Quant.Electron. 16(11) 1980. pp1251－1259.

2. K.Kikuchi *et.al.* ' Degradation of the BER in Coherent Optical Communications Due to the Spectral Spread of the Transmitter and the Local Oscillator.' J. Lightwave Technol. 2(6), 1984. pp1024－1033

3. T.Okoshi *et.al.* 'Calculation of the Bit Error Rate of Various Heterodyne and Coherent Type Optical Comminication Schemes.' J.Opt. Commun. vol. 2(3) 1983. pp89－96.

4. S.Saito, Y.Yammamoto, T.Kimura 'S/N and Error Rate Evaluation for an Optical FSK Heterodyne Detection System Using Semiconductor Lasers.' IEEE J.Quant. Electron. 19(2) 1983. pp180－193.

5. O.E. Delange 'Wide Band Optical Communication Systems: Part 2－ Frequency Division Multiplexing' Proc. IRE, vol, 58, no.10,pp1683－1690 1970.

6. C.E.Shannon. ' The Mathematical Theory of Communication.' Bell Syst. Techn. Journ. 1948 vol.27 pp379－423,623－656.

7. A.J.Viterbi 'On Coded Phase－Coherent Communications.' IRE Trans. on Space and Telem. March 1961 pp3－14.

8. J.E. Midwinter 'Current Status of Optical Communications Technology.' Journal Lightwave Technol. LT－3(5) OCt. 1985 pp927－930.

9. T.Fujita *et.al.* 'Narrow Spectral Linewidth Characteristics of Monolithic Integrated Passive Cavity InGaAsP/InP Semiconductor Lasers' Elect. Lett. 21(9) 1985. pp374－376.

10. A.L.Schawlow, C.H.Townes 'Infrared and Optical Masers' Phys.

Rev. voll 112, 1958. pp1940–1949.

11. O'Shea, Callen, Rhodes 'An Introduction to Lasers and their Applications.' Addison Wesley Publishing Company, California, 1978.

12. C.Park *et.al.* 'Single Mode Behaviour of a Multimode 1.55μm Laser with a Fibre Grating External Cavity'. IEE Elect. Lett 22(21), pp1132–1134 1986.

13. R.Wyatt, W.J.Devlin '10 kHz Linewidth 1.5 μm InGaAsP Laser with 55nm Tuning Range' Elect. Lett. 19(0) 1983 pp110–112.

14. M.R.Mathews, K.H.Cameron, R.Wyatt, W.J.Devlin 'Packaged Frequency–Stable Tunable 20 kHz Linewidth 1.5 μm InGaAsP External Cavity Laser' Elect. Lett. 21(3) 1985. pp113–115.

15. F.Favre, D.LeGuen 'Emission Frequency Stability in Single Mode Fibre Optical Feedback Controlled Semiconductor Lasers' Elect. Lett. 19(17) 1983. pp 663– 665.

16. F.Favre, D.leguen, J.C.Simon 'Optical Feedback Effects on Laser Diode Oscillation Field Spectrum' IEEE J.Quant. Elect, vol QE–18(10) 1982 pp1712–1717.

17. H.Olesen *et.al* 'Solitary Spectral Linewidth and its Reduction with External Grating Feedback for a 1.55μm InGaAsP BH Laser.' Jap. Journ. Appl. Phys. vol.22 no.10 1983 pp L664–L666.

18. J.H.Osmundsen *et.al.* 'Experimental Investigation of Stability Properties for a Semiconductor Laser with Optical Feedback.' IEE Elect. Lett. vol.19 no.25 pp1068–1070 1983.

19. Creaner M.J. *et.al.* 'Field Demonstration of 565 Mbit/s DPSK Transmission over 176 km of installed fibre.' Electron. Lett. vol.24(22) Oct. 1988 pp1354–1356.

20.. M.A.Grant, W.C.Michie, M.Fletcher 'The Performance of Optical Phase–Locked Loops in the Presence of Nonnegligible Loop

Propagation Delay' Journ. Lightwave Technol. vol LT−5, no.4 1987 pp 592−597.

21. L. Goldberg *et.al.*'Spectral Characteristics of Semiconductor Lasers with Optical Feedback.' IEEE J.Quant. Electron. vol QE−18(4) 1982.pp555−564.

22. R.W. Tkach, A.R. Chraplyvy 'Regeimes of Feedback Effects in 1.5μm Distributed Feedback Lasers.' IEEE J.Lightwave Technol. JLT−4(11) 1986 pp 1655−1661.

23. L.G. Kazovsky 'Balanced Phase Locked Loops for Optical Homodyne Recievers: Performance Analysis, Design Considerations, and Laser Linewidth Requirement Analysis.' J. Lightwave Tech. LT−4(2) pp182−194 1982.

24. L.G. Kazovsky 'Decision−Driven Phase−Locked Loops for Optical Homodyne Recievers: Performance Analysis and Laser Linewidth Requirements.' J.Lightwave Tech. LT3(6) pp 1238−1247 1985.

25. T.G. Hodgkinson 'Costas Loops Analysis for Optical Recievers' Elect. Lett. vol. 22(7) 1986. pp394−396.

26. Y.Kondo *et.al.*'Extremely Narrow Linewidth (1MHz) and High Power DFB Lasers Grown by MOVPE.' Electron. Lett. 25(3) Feb.1989 pp175−176.

27. J.J. Boonzaaier *et.al.* 'Narrow−linewidth AlGaAs/GaAs Multpile Quantum Well Distributed Feedback Lasers.' Electron. Lett.25(3) Feb.1989 pp240−241.

28. R.C. Steele, 'Ph.D. Thesis.' University of Glasgow 1983.

29. Physik Instrumente Data Sheet.

30. R.A. Linke *et.al.*'Coherent Lightwave Transmission over 150km fibre lengths at 400 MBits/s and 1 GBits/s data rates using Phase Modulation.' Elect. Lett 22(1) 1986 pp30−31.

31. A.H. Gnauk *et.al.* 'Coherent Lightwave Transmission at 2 GBits/s over 170 km of Optical Fibre Using Phase Modulation.' IEE Elect. Lett. 23(6) 1987 pp286–287

32. J.Salzman *et.al.* 'Material Evolution and Gradual Degradation in Semiconductor Lasers and Light Emitting Diodes.' Electron. Lett. 25(3) Feb.1989 pp244–245.

33. K. Nakanishi, K. Iwashita' Optical 4–ary FSK Modulation and Demodulation Experiment.' Electron. Lett. 24(21) Oct. 1988 pp1310–1311.

34. L.L. Jeromin, V.W.S. Chan 'M–ary FSK Performance for Coherent Optical Communications Systems Using Semiconductor Lasers.' IEEE Transactions on Communications COM–34(4) 1986 pp275–381.